

A Thesis Submitted for the Degree of PhD at the University of Warwick

Permanent WRAP URL:

<http://wrap.warwick.ac.uk/162233>

Copyright and reuse:

This thesis is made available online and is protected by original copyright.

Please scroll down to view the document itself.

Please refer to the repository record for this item for information to help you to cite it.

Our policy information is available from the repository home page.

For more information, please contact the WRAP Team at: wrap@warwick.ac.uk

Biophysical And Biochemical Studies of Penicillin Binding Proteins And Novel PBP3 Inhibitors

Hector Newman

A thesis submitted in partial fulfilment of the requirements for the degree
of Doctor of Philosophy

University of Warwick

Department of Life Sciences

June 2021

Table of Contents

List of Tables	8
List of Figures and Schemes	9
Acknowledgements	13
Declaration	14
Abstract	16
Abbreviations	17
List of Chemical Structures	21
Chapter 1. Introduction	23
1.1 Antimicrobial Resistance	23
1.1.1 A Brief History of Antimicrobial Drug Discovery	24
1.2 Challenges of Antibiotic Resistance	25
1.2.1 A Tripod of Socio-economic Challenges	25
1.2.2 Regulatory Challenges	27
1.2.3 Scientific Challenges	28
1.2.3.1 Big Pharma in a post-golden age	28
1.2.3.2 Novel Compounds and Novel Targets	29
1.2.3.3 The membrane challenges	30
1.2.3.4 Clinical Considerations	31
1.2.3.5 Molecular Mechanisms of Antibiotic Resistance	31
1.2.3.6 Methods to Slow Resistance	33
1.3 Approaches to finding new antibiotics	33
1.3.1 Whole cell vs Target-based methods	33
1.3.2 Library Selection	34
1.3.3 Fragment Based Drug Discovery (FBDD)	35
1.4 PBPs and β-lactams	36
1.4.1 Functional Role	36
1.4.2 PBP3	40
1.4.2.1 Functional Role of PBP3	40
1.4.2.2 Topology	40
1.4.2.3 Crystallography of the Transpeptidase Domain	41
1.4.3 β -lactams	43
1.4.3.1 Kinetics	45
1.4.3.2 Crystallographic Interactions with β -lactams	46
1.4.3.3 Physiological Effect of β -lactam Inhibition of PBPs	48

1.4.4 Resistance to β -lactams	49
1.4.1 Penetration-efficiency-mediated Resistance to β -lactams	49
1.4.2 Target-mediated Resistance to β -lactams	49
1.4.3 β -lactamase-mediated Resistance to β -lactams	49
1.4.5 Non- β -lactam compounds	51
1.4.6 PBP Assays	57
1.5 Conclusions	63
1.6 References	64
Chapter 2. Feasibility Studies of a Surface Plasmon Resonance system for PBPs	83
2.1 Introduction	83
2.1.1 Biophysics of SPR	84
2.1.2 Instrumentation	86
2.1.3 Coupling and Regeneration	87
2.2 Methods	88
2.2.1 Instrument	88
2.2.2 Buffers	88
2.2.3 Reagents	89
2.2.4 Procedure for preparation of activated thiol PaPBP3	90
2.2.5 Reference Surfaces	90
2.2.6 DMSO Calibration Curves	91
2.2.7 Analysis	92
2.3 Results and Discussion	92
2.3.1 CAPture System	92
2.3.2 Thiol-based System	94
2.3.3 Streptavidin coupling	97
2.3.4 Amide Coupling	99
2.3.5 Analyte Binding	99
2.3.5.1 Clinical β -lactams	99
2.3.5.2 Nitrocefin	102
2.3.5.3 Benzoxaborole	104
2.3.5.4 Reasons for Unresponsiveness	106
2.3.5.5 Non-specific Binding and Alternate Reference Surface	106
2.3.5.6 Buffer Screen	108
2.3.6 Comparisons with López-Pérez et al. (2021)	109
2.4 Future Work	110
2.5 Conclusions	111

2.6 References	112
Chapter 3. Design and Optimisation of a High-Throughput Antimicrobial Screening Platform	116
3.1 Introduction	116
3.2 Methods	117
3.2.1 Antimicrobial Assays	117
3.2.2 Inocula	117
3.2.3 Antibiotics Stocks	118
3.2.4 Gonococcal (GC) media	118
3.3 Results and Discussion	119
3.3.1 Optimisation of Growth Rates	119
3.3.2 Z-factor	122
3.3.3 Robotic Liquid Handling	123
3.3.4 DMSO	124
3.3.5 Data Processing	125
3.3.5.1 Workflow	125
3.3.5.2 Determining the MIC	127
3.3.6 Screening Boronates	133
3.3.7 Synergy Studies	134
3.3.8 Growth of Other Organisms	135
3.3.9 Case Studies	137
3.3.9.1 Repurposing Screens	137
3.3.9.2 Synergy Screens	137
3.4 Conclusion	138
3.5 References	138
Chapter 4. Target-Mediated Resistance in PBP3: Role of Loop Flexibility	142
4.1 Introduction	142
4.1.1 Mapping the Locations of Mutations	142
4.1.2 β 2 region	143
4.1.3 β 3- β 4 loop	145
4.1.4 β 5- α 11 loop	145
4.1.5 α 10- β 3 loop	146
4.2 Methods	146
4.2.1 Ensemble refinement	146
4.2.2 RMSDs	147
4.2.3 B factors	147

4.2.4 PDBFlex	147
4.3 Results and Discussion	148
4.3.1 Assessing Backbone Flexibility with Crystallography	148
4.3.2 Novel Ligands Generate Novel Conformations	153
4.3.2.1 Conformations of the β 5- α 11 Loop	153
4.3.2.2 Conformations of the α 10- β 3 Loop	155
4.3.2.3 Networks of Coupled Promoting Motions	157
4.4 Future Work: Beyond Cryo-Crystallography	158
4.4.1 Room Temperature Crystallography	158
4.4.2 Tryptic Digestion	159
4.4.3 NMR	159
4.4.4 Molecular dynamics	159
4.5 Conclusions	161
4.6 References	162
Chapter 4.S. Supplementary Information for Chapter 4	170
Chapter 5. Boron-based Inhibitors of PBP3: Benzoxaboroles with Novel Binding Modes	174
5.1 Introduction	174
5.2 Methods	177
5.2.1 Proteins and Crystallography	177
5.2.2 BOCILLIN FL Assays	178
5.2.3 S2d Assay	179
5.2.4 Nitrocefin Assay	180
5.2.5 Antimicrobial Assays	181
5.2.6 Chemoinformatics	181
5.2.7 Synthetic Chemistry	182
5.2.7.1 General Protocol 1: amide coupling	183
5.2.7.2 General Protocol 2: Synthesis of 9, 10 and 11 (Scheme 5.2A)	186
5.2.7.3 Synthesis of 12 (Scheme 5.2A)	188
5.3 Results	189
5.3.1 X-ray Fragment Screen	189
5.3.2 Fragment Hit Examples	191
5.3.3 Hit Expansion: Design and Synthesis	193
5.3.4 Vaborbactam	197
5.3.5 Inhibition Assays	198
5.3.6 Microbiology	203
5.4 Discussion	204
5.4.1 Boron Binding Modes	204

5.4.2 Structural Views	208
5.5 Future Work and Conclusions	211
5.6 References	213
 Chapter 5.S Supplemental Information for Chapter 5	 219
5.S1 Fragments Screened	219
5.S2 Crystallography Statistics	221
5.S3 Further Crystallography Views	224
5.S4 Computational Chemistry	228
5.S5 LC-MS traces	229
5.S6 References	234
 Chapter 6. Double Reaction of Nitrocefin with PBP3	 235
6.1 Introduction	235
6.1.1 Simple Saturation and Substrate Inhibition Kinetics	236
6.2 Methods	238
6.2.1 Protein Expression and Purification	238
6.2.2 Kinetics Assays	239
6.2.3 BOCILLIN FL Stained Gels	240
6.2.4 Denaturing Mass Spectrometry	240
6.3 Results	241
6.3.1 Crystal Structures	241
6.3.2 Substrate Inhibition Kinetics	245
6.3.2.2 Nitrocefin Turnover by gram-negative class B PBPs	245
6.3.2.3 CENTA turnover by PaPBP3	248
6.3.3 Reactions with BOCILLIN FL	248
6.3.4 Denaturing Mass Spectrometry	249
6.3.5 Tryptic Digest Mass Spectrometry	252
6.4 Discussion	253
6.4.1 Structural Analysis	253
6.4.2 Nitrocefin Kinetics	254
6.4.3 β -lactam Kinetics Beyond Gram-Negative Class B PBPs	254
6.4.4 Kinetics Models	255
6.4.5 S294A and S349A Mutants	256
6.4.6 The Tyr409Ala Mutant	257
6.4.7 Mass Spectrometry	259
6.4.8 Hypotheses on the Observation of Two Nitrocefin Molecules	260
6.4.9 Future Work	262
6.5 Conclusion	263

6.6 References	263
Chapter 6.S Supplemental Information for Chapter 6	268
6.S1 Structural Views	268
6.S2 Kinetics	268
6.S2.1 Derivation of Equation 6.3	268
6.S2.2 More Complex Models	270
6.S3 Tryptic Digest Mass Spectrometry	270
6.S3.1 Sample Preparation Methods	270
6.S3.1.1 Protocol I	270
6.S3.1.2 Protocol II	271
6.S3.1.3 Protocol III (in-gel digest)	272
6.S3.2 Proteomic Mass Spectrometry Methods	272
6.S4 Protein Crystallography Methods	272
6.S5 References	273
Chapter 7. Concluding Remarks	275
Appendix: Publications by the author	277

List of Tables

Table 1.1. Non-β-lactam PBP binding small molecules previously reported	53
Table 1.2. Assays used for the identification and classification of Class B PBP binding agents	58
Table 3.1. Details of the models investigated for determining the MIC in the automated pipeline	130
Table 4.1. Mutants observed in the class B PBPs of three species of gram-negative pathogens cluster in various regions	143
Table 4.2. R values of different refinement methods	148
Table 4.S1. Local flexibility of active site residues	172
Table 5.1. Crystallography shows boronates can form a number of interesting and high valency complexes	176
Table 5.2. Electrophilic fragments screened against PaPBP3	190
Table 5.3. Activity profiles of 1-16 and vaborbactam	200
Table 5.4. Inhibition of various class B PBPs by 13	201
Table 5.5. Minimum inhibitory concentrations for selected compounds against a panel of gram-negative bacteria	203
Table 5.S1. Fragments screened by crystallography	219
Table 5.S2. Crystallography Statistics	221
Table 5.S3. PaPBP3 crystal pH	223
Table 6.1. Kinetics of nitrocefin and CENTA turnover	247
Table 6.2. Screens to identify tryptic digestion mass spectrometry conditions for stable adduction	252

List of Figures and Schemes

Figure 1.1. Summary of the various challenges related to antimicrobial resistance	25
Figure 1.2. Functional role of the PBPs with the periplasm.	39
Figure 1.3. Sequence alignments of five clinically important class PBPs from gram-negative pathogens	42
Scheme 1.1. β -lactams and β -lactamase inhibitors	44
Scheme 1.2. Reaction pathway of β -lactams interacting with PBPs	45
Figure 1.4. Structural views of class B PBPs	47
Figure 1.7. Chemical probes for the behaviour of PBPs	61
Figure 2.1. The fundamental components of a Biacore SPR instrument.	85
Figure 2.2. Generalised coupling and regeneration methods.	87
Figure 2.3. Preparation of activated thiol PaBP3.	90
Figure 2.4. A typical Solvent Correction Curve.	92
Figure 2.5. Route A regeneration: CAPture coupling system.	93
Figure 2.6. Simplified reactions of thiols used for the preparation of the thiol-coupled chip.	94
Figure 2.7. Route A regeneration: thiol coupling.	96
Figure 2.8. Thiol coupling sensorgrams.	97
Figure 2.9. Route B regeneration: streptavidin coupling system with biotinylated protein.	98
Figure 2.10. Route B regeneration: amide coupling system.	100
Figure 2.11. β -lactam binding to various chip surfaces	101
Figure 2.12. Investigation of nitrocefin binding.	103
Figure 2.13. Investigation of benzoxaborole binding.	105
Figure 2.14. Binding of benzoxaborole 13 corrected with a MreC reference.	107
Figure 2.15. Buffer Screening.	109

Figure 3.1. Antibiotic source and destination plates.	119
Figure 3.2. Optimisation of Growth Conditions.	121
Figure 3.3. Variation due to starting inoculant.	122
Figure 3.4 Liquid handling methods to transfer solutions between 96 well and 384 well plates and generate concentration series.	123
Figure 3.5. Sensitivity of <i>E. coli</i> Δ TolC to DMSO.	125
Figure 3.6. Overview of the workflows used to prepare a report of a set of MICs	126
Figure 3.7. Dose responses of <i>E. coli</i> Δ TolC to different compounds	128
Figure 3.8. Results generated by each model (A-D) when analysing MICs of novel compounds. Models: (a) A; (b) B; (c) C; (d) D.	132
Figure 3.9. Histogram of MICs of boron-containing compounds screened.	133
Figure 3.10. Synergy Studies.	135
Figure 3.11. Growth curves of clinically relevant species.	136
Figure 4.1. Plotting locations of clinical mutants on the class B transpeptidase domain.	144
Figure 4.2. Investigation of loop movements of PaPBP3 and NgPBP2.	150
Figure 4.3. Loops on the “back” face of PaPBP3.	152
Figure 4.4. Boronate binding can affect the conformation of the β 5- α 11 loop in PaPBP3.	154
Figure 4.5. The structure of PaPBP3:13 shows two alternate conformations of the α 10- β 3 loop.	155
Figure 4.6. Boronate binding can affect the conformation of the α 10- β 3 loop in PaPBP3.	156
Figure 4.S1. Comparisons between two structures of the transpeptidase domain of NgPBP2 from strain FA6140	170
Figure 4.S2. Comparison of <i>apo</i> and piperacillin reacted PaPBP3 crystal structures	171
Figure 4.S3. TEM-1 was found to have a cryptic allosteric site between the α 11 helix and the α 10- β 3 loop	173

Figure 5.1. Boron mimicry of transition states on the transpeptidation and penicillin catalysis pathways of PBPs.	175
Scheme 5.1. The model used to determine K_i in Kintek Global Explorer.	179
Scheme 5.2. Synthesis of benzoxaborole derivatives	183
Figure 5.2. Properties of the fragments screened.	189
Figure 5.3. Tri-covalency is observed in the reaction between boronic acids 1 and 2 and PaBPB3	191
Figure 5.4. Benzoxaborole fragments form di-covalent complexes with PaBPB3.	193
Figure 5.5. Binding modes of piperacillin and benzoxaboroles 12 (predicted) and 8 (observed) complexed with PaBPB3.	194
Figure 5.6. PaBPB3 complex with C-3 acid group containing benzoxaboroles (13, 14 and 16) and 15.	196
Figure 5.7. The PaBPB3:vaborbactam complex.	197
Figure 5.8. Progress curves of boronate inhibition.	199
Figure 5.9. The effect of 2-fold dilution on the PaBPB3 pIC ₅₀ of 13 and ceftazidime.	202
Figure 5.10. Three distinct binding modes of complexes of PBPs with boron-containing compounds.	205
Figure 5.11. Overlay of various benzoxaborole conformations as observed in complex with PaBPB3.	206
Figure 5.12. Comparisons between PaBPB3 reacted with meropenem and 13 reveal similar conformations for the β_3 strand, unlike that of the piperacillin reacted structure.	209
Figure 5.13. Comparisons between PaBPB3 reacted with piperacillin (black, PDB code: 6R3X) and 14 (orange)	210
Figure 5.14. Phenyl groups of the benzoxaboroles were designed to engage the hydrophobic wall, but do not do so.	211
Figure 5.15. The hybridisation state transition of benzoxaboroles.	213
Figure 5.S1. Benzoxaboroles engage β -lactamases (AmpC) and PaBPB3 differently.	224
Figure 5.S2. Comparison of the interactions of reacted piperacillin and 1 with PaBPB3.	225

Figure 5.S3. Crystal structure views and Newman projections of Ser294 reacted with boron-containing inhibitors and piperacillin.	226
Figure 5.S4. β -lactams piperacillin, ceftazidime, amoxicillin and aztreonam make a consistent hydrogen bond with Thr487.	227
Figure 6.1. Chemical structure of nitrocefin.	235
Scheme 6.1. Schemes of the simple saturation reaction pathway (a) and the substrate inhibition pathway (b).	236
Figure 6.2. Simulations of substrate inhibition kinetics by plotting equation 6.3 with different values of K_{SI} and V_{max} .	237
Figure 6.3. Crystal structure of nitrocefin-reacted PaBPB _{Y409A} .	242
Figure 6.4. Electron density of nitrocefin-reacted PaBPB _{3wt} (a) and comparison of the active sites of crystal structures of PaBPB _{3wt} and PaBPB _{Y409A} reacted with nitrocefin (b), including the positions of serine residues (c-f).	244
Figure 6.5. Change in absorbance at 482 nm due to nitrocefin turnover.	245
Figure 6.6. The kinetics of nitrocefin and CENTA turnover by PBPs.	247
Figure 6.7. BOCILLIN FL (a) and coomassie (b) staining of an SDS-PAGE gel.	248
Figure 6.8. Denaturing mass spectrometry of the reaction of PaBPB _{3wt} (a-d) and PaBPB _{3Y409A} (e-h) with nitrocefin.	249
Figure 6.9. Denaturing mass spectrometry of the reaction of PaBPB _{3S294A} (a and b) and PaBPB _{3S394A} (c and d) with nitrocefin.	251
Figure 6.10. Waters near to the active site serine.	258
Figure 6.11. Di-covalently binding benzoxaboroles may mimic a transition state in a nitrocefin serine transfer mechanism.	261
Figure 6.S1. Tyr409 conformational flexibility in PaBPB ₃ .	268
Scheme 6.S1 Alternative schemes (a-b) and rate equations (c-d) for substrate inhibition.	270

Acknowledgments

Thank you to Diamond Light Source and the University of Warwick for providing me with the opportunity and funding to complete this PhD. I am hugely grateful to my supervisors Chris Dowson, Katherine McAuley and Neil Paterson for their assistance and encouragement throughout this project. I would like to thank Chris for giving me his constant support and trust to allow me to explore new ideas. You have given me so many opportunities and opened so many doors.

Thank you to all those who have taught me the skills necessary to write this thesis, in particular: Adrian Lloyd from whom I have learnt everything about kinetics and many topics besides and Joe Eyermann for bringing me into the world of medicinal chemistry and supporting me in South Africa and beyond. To the Dowson Roper Lloyd group: with a special thank you to Abby Henney, Chris Graham, Julie Todd, John Moat, Anita Catherwood and Dom Bellini, I have learnt so much from you all.

I am indebted to my collaborators: from the University of Cape Town and H3D, Grant Boyle, Sandeep Ghorpade and Kelly Chibale; from the University of Oxford, Alen Krajnc, Jürgen Brem, Anthony Tumber and particularly Chris Schofield who has given me so much of his valuable time. Thank you to Gemma Harris, Sarah Bennett, Claire Shepherd and Richard Napier.

To my friends and family who have listened, encouraged and supported me throughout: I could not have done this without you. Thank you so much.

Declaration

This thesis is submitted to the University of Warwick in support of my application for the degree of Doctor of Philosophy. It has been composed by myself and has not been submitted in any previous application for any degree.

The work presented (including data generated and data analysis) was carried out by the author except in the cases outlined below:

- Dom Bellini (LMB, Cambridge) prepared PBP3 proteins used in Chapter 2 and Chapter 5; Chris Graham (University of Warwick) provided MreC protein (Chapter 2); Julie Todd (University of Warwick) provided some proteins used in Chapter 6.
- Sarah Bennett (University of Warwick) operated the liquid handling system during antimicrobial assays (Chapter 3).
- Mukesh Gangar (University of Cape Town) synthesised Compound **16** (Chapter 5). Robert Lesniak (Stanford University) synthesised **S2d** (Chapter 5).
- Dom Bellini crystallised and collected data for all crystal structures in Chapter 5, but these were refined by the author. Dom Bellini crystallised, collected data and refined (with input from the author) crystal structures in Chapter 6. All other crystal structures are taken from the protein data bank (PDB code referenced in the text).
- Joe Eyermann (University of Cape Town) generated the docked model of a PBP:**12** complex (Chapter 5).
- ¹³C NMR for compounds in Chapter 5 were collected and assigned by Alen Krajnc (University of Oxford). High resolution mass spectra were collected by Thomas Corner (University of Oxford).
- Mass Spectrometry of PBP:nitrocefins complexes (Chapter 6) was performed by Alen Krajnc and Anthony Tumber (University of Oxford).

- Proteomic Mass Spectrometry was performed by Warwick Proteomics Research Technology Platform (sample preparation was performed by the author).

Parts of this thesis have been published by the author:

Bellini D*, Koekemoer L*, Newman H*, Dowson CG. Novel and Improved Crystal Structures of H. influenzae, E. coli and P. aeruginosa Penicillin-Binding Protein 3 (PBP3) and N. gonorrhoeae PBP2: Toward a Better Understanding of β -Lactam Target-Mediated Resistance. J Mol Biol. 2019 Aug 23;431(18):3501–19. **Joint first authors*

This work formed the basis for Chapter 4 and is summarised in section 4.1.

Kidd SL, Fowler E, Reinhardt T, Compton T, Mateu N, Newman H, et al. Demonstration of the utility of DOS-derived fragment libraries for rapid hit derivatisation in a multidirectional fashion. Chem Sci. 2020 Oct 14;11(39):10792–801.

The author contributed structural activity relationship input to this work, discussed in section 1.3.3 and published two crystal structures (PDB: 6Y6U and 6Y6Z)

Newman H, Krajnc A, Bellini D, Eyermann CJ, Boyle GA, Paterson NG, et al. High-Throughput Crystallography Reveals Boron Containing Inhibitors of a Penicillin Binding Protein with Di- and Tri-covalent Binding Modes. J Med Chem. *Accepted.*

Chapter 5 was modified and submitted for publication: it was accepted, reviewed, revised and is currently returned to the reviewers for their approval (as of 11th June 2021). As part of this, 10 crystal structures (5.S2) were published on the PDB.

All three papers are included in the appendix.

Abstract

Antimicrobial resistance presents a worrying and growing threat to modern medicine. Combatting this challenge requires the discovery of new antimicrobial compounds, which are insensitive to current resistance pathways. One of the most important classes of antibiotics, β -lactams, target penicillin binding proteins (PBPs), a family of enzymes that synthesise the bacterial cell wall. In most clinically important gram-negative bacteria, PBP3 is a ubiquitous and essential drug target, whose inhibition can prevent the growth of bacterial cells. Novel mode of action inhibitors of PBPs are needed to combat rising resistance to β -lactams, but finding such inhibitors requires improved understanding of these proteins and new discovery methods.

This thesis describes the development of two tools for inhibitor discovery: biophysical methods (surface plasmon resonance) in an attempt to characterise the interactions of PBP3 with its ligands; and a high throughput microbiology platform designed to provide low cost, low volume, rapid screening of early stage compounds.

PBP3 mutation-mediated resistance mechanisms have been investigated by analysing structural data to provide insight into how mutations distal to the active site may lower the susceptibility of PBPs to β -lactams. Novel compounds are used to show the indirect link between the active site and these distant regions.

A crystallographic fragment screen, and follow up medicinal chemistry, was used to identify benzoxaboroles as inhibitors of PBP3 with a novel, di-covalent binding mode, engaging two highly conserved serines in the active site. Studies with a non-clinical probe β -lactam, nitrocefina, also appear to show an unprecedented binding mode involving engagement of two serines. These results introduce benzoxaboroles and other compounds as warheads that can bind both serine residues, thereby opening up new avenues for research in the pursuit of non- β -lactam PBP inhibitors.

Abbreviations

2,2-DTP	2,2'-Dithiodibispyridine
$A_{XXX\text{ nm}}$	Absorbance at the specified (XXX) wavelength
ABC	Ammonium Bicarbonate
AbPBP3	Acinetobacter baumannii PBP3
AMR	Antimicrobial resistance
ATCC	American Type Culture Collection
$\alpha N/ \beta N$	Notation for secondary structure of proteins; α : alpha helices; β : beta strands. N refers to its index (in order N-C terminal). Two codes separated by a dash e.g. $\alpha 11\text{-}\beta 5$ indicates the loop between these structures
caMHB	Cation-adjusted Mueller-Hinton broth 2
CDI	1,1'-carbonyldiimidazole
CENTA	((6R,7R)-3-(((3-carboxy-4-nitrophenyl)thio)methyl)-8-oxo-7-(2-(thiophen-2-yl)acetamido)-5-thia-1-azabicyclo[4.2.0]oct-2-ene-2-carboxylic acid
CLSI	Clinical & Laboratory Standards Institute
CFU	Colony forming units
DHFR	dihydrofolate reductase
DMF	N,N-dimethylformamide
DMSO	Dimethyl Sulphoxide
DNA	Deoxyribonucleic acid
DOS	Diversity orientated synthesis
DTNB	5,5-dithio-bis-(2-nitrobenzoic acid)
DTT	Dithiothreitol
EC50/90	Effective concentration at which 50/90 % of the growth is inhibited

EcPBP3	Escherichia coli PBP3
EDC	1-ethyl-3-(3-dimethylaminopropyl)carbodiimide
EDTA	Ethylene diamine tetraacetate
equiv.	Equivalents
ER	Ensemble refinement
ES(I)	Electrospray (ionisation)
FA	Fluorescence Anisotropy
FBDD	Fragment based drug discovery
FIC(I)	FIC(I): fractional inhibitory concentration (index)
g	Gravitational Force
GC	Gonococcal
GSK	GlaxoSmithKline
GT	Glycosyltransferase
HiPBP3	Haemophilus influenzae PBP3
HMM	High molecular mass
HPLC	High Performance Liquid Chromatography
HRMS	High resolution mass spectrometry
IPTG	Isopropyl β -d-1-thiogalactopyranoside
K_i	Kinetic constant: defined in Scheme 5.1.
K_M	Kinetic constant: defined in equation 6.S5
K_{SI}	Kinetic constant: defined in equation 6.S6
k_{cat}	Enzyme turnover number: defined in equation 6.S7
k_x	Rate constant for the indicated step
LB	Lysogeny broth
LB agar	Lysogeny broth agar
LC	Liquid chromatography
LCMS	Liquid chromatography mass spectrometry
LMM	Low molecular mass
M	Species mass (in the context of mass spectrometry)
MCA	Multichannel arm

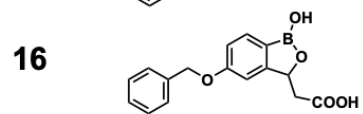
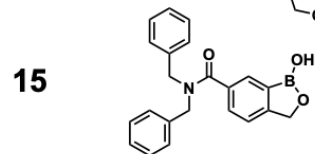
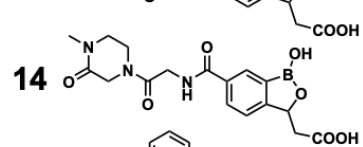
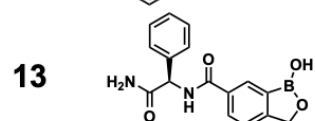
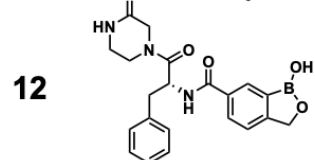
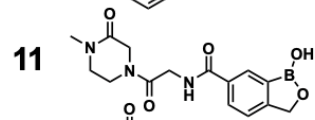
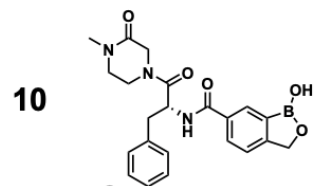
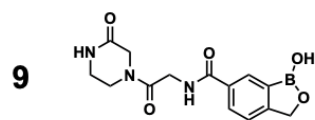
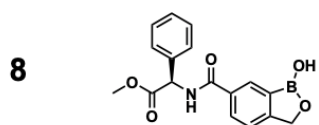
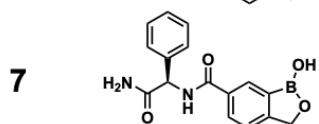
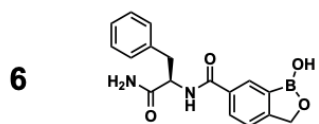
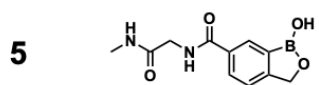
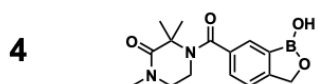
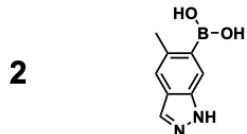
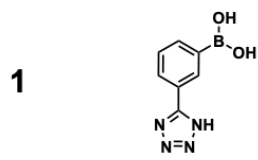
MD	Molecular dynamics
MIC	Minimum inhibitory concentration
MS	Mass spectrometry
MR	Relative molecular mass,
MRSA	Methicillin-resistant <i>Staphylococcus aureus</i>
NCTC	National Collection of Type Cultures
NgPBP2	<i>Neisseria gonorrhoeae</i> PBP2
NHS	N-hydroxysuccinimide
NMR	Nuclear magnetic resonance
OD ₆₀₀	Optical density at 600 nm
PaPBP3	<i>Pseudomonas aeruginosa</i> PBP3
PBP	Penicillin binding protein
PDB	Protein data bank
PDEA	2-(2-pyridinyldithio)ethaneamine hydrochloride
pI	Protein isoelectric point
pIC ₅₀	Negative logarithm of half maximal inhibitory concentration
pK _a	Negative logarithm of the acid dissociation constant
SA	Streptavidin (an SPR Chip)
SDS PAGE	Sodium dodecyl sulphate polyacrylamide gel electrophoresis
SMILES	Simplified molecular-input line-entry system
SOC	Super optimal broth with catabolite repression
SPR	Surface plasmon resonance
TCEP	Tris(2-carboxyethyl)phosphine
TFA	Trifluoroacetic acid
TG	transglycosylation
TLS	Translation/libration/screw - a refinement parameter

TOF	Time of flight
TP	Transpeptidation
Tris	Tris(hydroxymethyl)aminomethane
RA	Residual activity
	Theoretical maximal amount of analyte
R_{\max}	that can be bound to the chip. Defined in equation 2.2
R_{xxx}	Response of an SPR detector. XXX refers to the binding species
UDP	Uridine diphosphate
UMP	Uridine monophosphate
UPLC	Ultra Performance Liquid Chromatography
rpm	Revolutions per minute
rt	Room temperature
V_{\max}	Maximal velocity of an enzyme- substrate interaction
RMSD	Root-mean-square deviation
RoMa	Robotic manipulator arm
RU	Response units
v/v	Volume to volume ratio
wt	Wild type
w/v	Weight to volume ratio
Other notation	
[XXX]	Concentration of XXX

Amino acid substitutions are referred to as e.g. S349A: meaning the substitution of a serine residue for an alanine residue at the indicated (numerical) position.

In chapter 6 subscripts are used to indicate the substitution mutations (or wt) of a protein: e.g.: PaBPB_{3S349A} is the S349A substitution mutation of PaBPB3

List of Chemical Structures



“[W]e shall therefore continue to labour under discouragement so long as we are faced with the bugbear of drug resistance.”

Sir Charles Harington, 1957

Chapter 1. Introduction

1.1 Antimicrobial Resistance

Antimicrobials have been described as the “Fire extinguishers of medicine” ¹, in an analogy that elegantly captures their role: mundane and overlooked yet essential. Their use allows for the safe undertaking of surgery ² and cancer treatment ³ as well as treatment of all types of infections within the community ⁴. Their ubiquity in modern health systems has led to rising cases of resistance, with bacteria evolving mechanisms which reduce the efficacy of antibiotics ^{5,6}.

Resistance to antibiotics is an ancient ⁷⁻⁹ and inevitable ¹⁰ phenomenon, resulting from the historical co-evolution of antibiotic-resistant organisms alongside antibiotic-producing ones. Before the widespread use of antibiotics, it was predicted (by Fleming himself) that their “underdosage” would lead to the proliferation of resistance. It is not possible to prevent the development of resistance in the long-term and at the moment the only strategy against it has been to innovate with new drugs at a faster rate than the development of resistance to the current therapies. During the “golden age” of antimicrobial discovery (1930-1962) this was successful, with 20 classes of antibiotic discovered. Since then only 2 new classes of antibiotics have been marketed¹¹. As drugs discovered more than 60 years ago become increasingly ineffective, a serious and growing lack of treatment options are emerging. The lack of new drugs within the antimicrobial sector is not a problem encountered across the rest of the pharmaceutical industry, which continues to discover drugs of all classes at a high rate ¹².

The combined challenges of low discovery rate and the development of resistance are creating a “slow tsunami” ¹³ of untreatable infections. Both of these topics shall be discussed briefly below, but they are interlinked. The continual development of resistance creates the imperative for novel drug discovery, and resistance slows discovery efforts by introducing barriers rarely encountered in other areas of pharmaceutical discovery science. Before investigating these twin issues, it is worth considering how our current antibiotics were discovered.

1.1.1 A Brief History of Antimicrobial Drug Discovery

Perhaps the first modern antimicrobial screen was that of Paul Ehrlich in 1910 in his efforts to discover an effective treatment for syphilis by *in vivo* screening of syphilitic rabbits ^{14,15}. In the 1930s, *in vivo* screening of mice with streptococcal sepsis was similarly used to discover prontosil ^{15,16}, an antibiotic prodrug and the first in class of the sulfonamide “sulfa” drugs, of which many derivatives were later made ¹⁷ such as the essential medicine sulfamethoxazole ¹⁸.

The most famous of the early antibiotics was penicillin ^{19,20}. Whilst the antimicrobial activity of moulds was known, from 1928 onwards Fleming studied them systematically and quantitatively, by streaking bacteria over penicillin-spiked agar ¹⁹. The successful extraction of penicillin in 1940 ²⁰ and subsequent “public-private” partnership established to mass produce it during the second world war stimulated the US pharmaceutical industry ^{21,22} and led to the start of the “golden age” of antibiotic discovery. During this period, almost all current classes of antibiotics ²³, as many as 250 individual compounds ²¹ were marketed as systematically administratable products. Many of these compounds came from screening soil samples to identify active compounds, beginning with the work of Hotchkiss and Dubos ²⁴ who discovered gramicidin and tyrocidine and later works using *actinomyces* species to extract streptomycin ²⁵ (notable for being the first effective treatment for tuberculosis ^{26,27}). Waksman, the Nobel prize-winning inventor of streptomycin, in fact coined the term antibiotic in 1941. In this period (1949-1962), chloramphenicol, tetracyclines, aminoglycosides, macrolides then glycopeptides, streptogramins and quinolones were discovered in quick succession ²⁸. Only quinolones were fully synthetic, discovered (apparently serendipitously) as a byproduct of chloroquine production ^{29,30}. In 2000, following a chemical screening program at Du Pont ³¹, oxazolidinones were released as the first novel class of inhibitors in 40 years. These represent the third class of synthetic antibiotics, with the rest all coming from natural product origins ³².

In summary, the antibiotics we have today benefited in their discovery from government investment, a lack of competing compounds on the market, and readily available natural products produced by soil microorganisms, which could be developed into drugs relatively quickly by medicinal chemistry techniques. Often, as is the case with penicillin, the intracellular target was discovered many years later ³³

and the fundamental biochemistry was not considered important for the drug discovery efforts ^{34,35}.

1.2 Challenges of Antibiotic Resistance

In contrast, the past few decades have yielded few compounds with genuinely novel mechanisms of action and the pipeline of upcoming drugs remains empty ³⁶. The challenges of antimicrobial resistance are three-fold: **socio-economical**, **regulatory** and **scientific** (Figure 1.1).

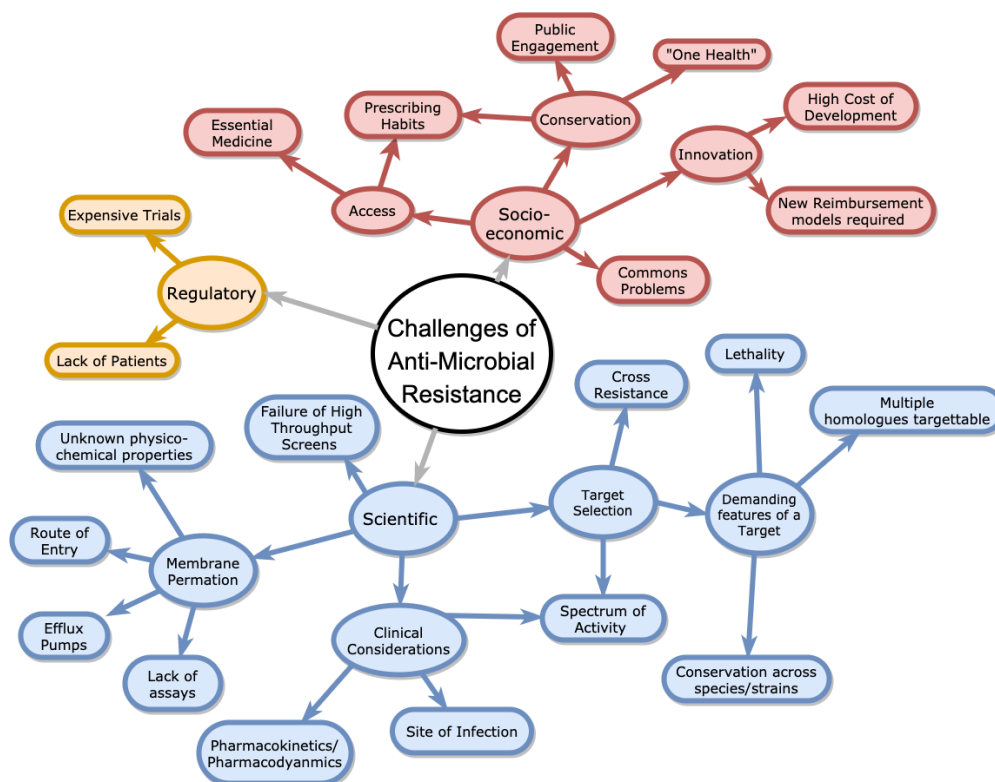


Figure 1.1. Summary of the various challenges related to antimicrobial resistance

1.2.1 A Tripod of Socio-economic Challenges

Steven J. Hoffman and Kevin Outterson have described antimicrobial resistance as a tripod of three intersecting and mutually supporting pillars, each representing an individual challenge within the overarching AMR crisis ³⁷. These pillars are: access,

innovation and conservation. Solutions to AMR will require that each of these challenges is addressed: access is necessary to ensure that these essential medicines can be used by all: currently more people are killed by antibiotic-treatable infections than from resistant organisms ^{38,39}. It would be unethical and counterproductive ⁴⁰ to address AMR in rich countries without simultaneous work to lower the burden of infectious disease as a whole. Conservation and appropriate use of antibiotics will ensure that resistance is kept at a minimum level to allow successful cycles of drug development to keep pace with drug resistance in the clinic. In this way, public-awareness and a “One Health” approach to antibiotics, which encompasses limitations on their use in veterinary practice ^{38,41}, and better control of their end of life in wastewater treatment plants ^{38,42} become crucial to ensuring innovation efforts are not wasted.

In their use of the tripod analogy, Hoffman and Outtersen ³⁷ recognised that a singular focus on any of the three issues in isolation would be insufficient to prevent the rising antibiotic crisis leading us to a post-antibiotic world. Whilst the majority of this thesis is focussed on the technical aspects of the “innovation” leg of the tripod, it is worth briefly covering the other two to put the need for (and limits of) innovation in context.

Stymying attempts to challenge each of these three pillars is the fact that each has characteristics of a “commons” problem, one in which individuals can benefit in the short term by acting selfishly but that over the long term has severe negative effects on all stakeholders ⁴³. For example, in antimicrobial conservation a single prescriber can inappropriately prescribe antibiotics, driving resistance, with the consequences spreading outside their community whilst they benefit by quickly getting the patient out of the consulting room and higher patient satisfaction ⁴⁴. In this example the “prescriber” could be a single hospital with insufficient guidelines, or entire nations failing to correctly regulate antibiotic use, thereby spreading resistance across the globe.

Within innovation there is a similar problem. Antibiotic development, as with typical drug development, is very expensive; the “all-in” cost of bringing a modern drug to market is estimated at around \$1.7 billion ⁴⁵. Given that a new antibiotic should be carefully regulated in its use, a novel compound may struggle to recoup this cost before exclusivity rights expire ^{38,46,47}. In the majority of cases antibiotics are only prescribed for short periods (~ weeks) compared to drugs for chronic conditions

which may require treatment over years or for the rest of the patient's life. This reduces the sales volume and may drive pharmaceutical companies to different therapeutic areas ³⁸. Poor sales after release have led to the recent failures of companies launching new antibiotics: Melinta ⁴⁸ and Achaogen ⁴⁹. As such, new models are needed to “delink” the relationship between drug sales and payments to the drug developers. Multiple models have been proposed to do this ^{50–53}.

Fundamentally, a model must recognise the value of antibiotics to society and finance the developers appropriately ⁵⁴. The social value of an antibiotic for the treatment of hospital acquired/ventilator associated bacterial pneumonia antibiotics for example, is estimated to be worth \$12 billion ⁵⁴. In this context, the development cost of a new compound is justifiable.

Even in the event of public money being used for antimicrobial drug development, global access could still be a commons problem as only rich countries can afford to pay but all countries will need access to the new drugs as resistance spreads without recognition of borders ^{43,55}. Policy makers and the public will need to understand that this apparent altruistic and ethical behaviour is actually essential to slow the spread of resistance globally ⁴⁰.

Commons problems must be addressed through well designed and well managed ^{56,57} international agreements with buy-in from all nations ⁴³. Politicians and the public must be engaged with these challenges now. Lessons in this can be learned from the concurrently burgeoning commons problem of the climate crisis ⁵⁸.

1.2.2 Regulatory Challenges

Companies now face an increasing burden of regulation by the approval agencies (greater patient size and increasingly stringent non-inferiority trials) and postmarketing obligations ⁵⁹. The cost of these expensive trials cannot be recouped by drugs that are 3 times less profitable than cancer drugs and 11 times less profitable than musculoskeletal drugs ⁶⁰, so corporate policy has shifted budgets towards these more profitable areas. In addition to the cost, recruiting patients to trials can be difficult as those with the most intractable and drug-resistant infections are rare and often critically ill, but trials must start as soon as the patient is admitted to hospital and before they receive other treatments ^{61,62}.

1.2.3 Scientific Challenges

1.2.3.1 Big Pharma in a post-golden age

Following the “golden age” of antibiotic discovery (see *A Brief History of Antimicrobial Drug Discovery* above) new chemical matter to fill the pipeline began to become increasingly rare and the first wave of scaling back by the pharmaceutical industry began ⁶². Advances in high throughput biochemical screening from the 1980s onwards ⁶³ using largely synthetic “robotically mass produced” chemical libraries and the start of the “genomic era” (following the publication of the first complete genome sequence of *Haemophilus influenzae* in 1995 ⁶⁴), failed to bring in a new wave of antibiotic discoveries. After a decade of Big Pharma efforts, it appeared a new golden era would not be forthcoming ⁶⁵, and a second wave of exits occurred ⁶².

Researchers at Merck noted in the 1990s that antibiotic drug discovery was unlike other therapeutic areas the company worked in. There was not a simple relationship between the inhibition of the isolated biochemical target and “the alleviation of the disease state” ³². They were able to find potent inhibitors of bacterial proteins which could not be used to inhibit activity at the cellular level. GlaxoSmithKline (GSK) have estimated that even in target based screens antibiotic drug discovery success rate “was four- to five-fold lower than for targets from other therapeutic areas”, a fact that made their pursuit of antibacterial drugs financially unviable ⁶⁶. Similarly, detailed analysis by AstraZeneca ⁶⁷ of their screens of hundreds of thousands of compounds revealed hit rates far lower than required to sustain these expensive projects. Despite a large increase in the size of chemical libraries available and the use of modern automated technologies ⁶⁸, high throughput methods on very large compound libraries failed to deliver for antibiotic discovery as it has for other targets (compounds in many pharma chemical libraries are focussed upon entry into mammalian cells and do not possess the properties required for entry into bacteria, especially gram-negative pathogens for which there is a particular dearth of new inhibitors). Now just 6 large pharmaceutical companies remain in the anti-infectives field ⁵¹ and only recently have increasing numbers of small and medium sized companies begun developing antimicrobials ⁶⁹.

1.2.3.2 Novel Compounds and Novel Targets

Finding a new molecular target for antibiotics and then screening against this seemed like an attractive prospect in the genomic era. Genomics, it was hoped, would allow essential, but previously untargeted, genes to be identified which would lack any cross resistance to current antibiotics. GSK's analysis ⁶⁶ of their antibiotic discovery efforts is illustrative of the challenges faced when trying to find new targets for antibiotic treatment:

- They identified targets that were effective in *in vivo* infection models, but which did not inhibit bacterial growth *in vitro*.
- High throughput screens for the new target would fail to yield any tractable hits.
- They would find hits but then could not develop these hits into leads as activity could not be increased.
- Of the 67 high throughput screens on different bacteria protein targets, only 5 led to a lead, the majority of which eventually proved fruitless.

Discovery efforts by other companies appeared to face similar issues ⁶⁵, severely slowing the rate of antibiotic innovation. The failure of high throughput screens has since been the focus of further work, for example it has been noted ^{66,70–73} that antibacterials seem to have different physicochemical properties to non-antibiotic chemicals, and this may be the source of the challenges in identifying hits. Interestingly, AstraZeneca had fewer issues identifying hits, but still failed to convert these into leads ⁶⁷.

Novel targets remain elusive. A potential target must fulfil many criteria. In addition to being lethal when inhibited, any effective new target must be well conserved amongst bacteria to ensure a sufficient spectrum of activity ⁷⁴. A few hundred such targets might exist ^{35,66,74,75}. A target which is essential and non-circumventable and has multiple individually essential homologues within the cell, will experience a lower rate of development of resistance ⁵. It has been suggested that selecting single enzymes as targets during the genomic era led to a more rapid onset of resistance ^{35,76}. Penicillin binding proteins (PBPs), the focus of this thesis, make excellent targets of chemotherapy, partly due to the fact so many homologues exist in the cell that can be targeted by the same warhead. As a result, for some bacterial species (such as *Escherichia. coli*), target-mediated resistance is relatively uncommon. In contrast, attempts by GSK to inhibit a single aminoacyl tRNA

synthetase lead to the rapid development of resistance *in vivo*⁷⁷, which may not have occurred had the compound been able to inhibit multiple tRNA synthetases. Multi-targeting should be high on the list of important criteria.

The majority of current antibiotics for systemic therapy target either the cell wall (Figure 1.2); or DNA, RNA and protein production centres of the bacteria^{74,78}, and were all identified in the pre-genomic era. The challenge of finding new targets led GSK to instead focus on finding new chemical matter to target these well validated centres⁶⁶, and almost all antibacterial compounds in the current pipeline are focussed towards them too³⁶. Whilst known to be effective in killing bacteria when modulated, an over reliance on these few mechanisms of inhibition may increase cross-resistance and speed the rate of resistance to a new agent.

1.2.3.3 The membrane challenges

Any compound aiming to inhibit an intracellular (or periplasmic) protein must accumulate near the target in sufficient quantities for sufficient time. This requires a balance in favour of the flow of the drug in rather than out of the cell. Drugs can enter the cell via passive diffusion or through porins⁷¹ and are removed by efflux pumps⁷⁹. In addition to its on-target affinity, a compound must be optimised with properties that maximise influx whilst avoiding efflux. A particular challenge in the discovery of novel drugs to target gram-negative pathogens is their outer membrane, which makes chemical permeation much more challenging by providing orthogonal filters that exclude potential drugs⁷¹. Methods to study the ability of compounds to enter cells are being developed⁸⁰, but the rules about what chemical features are needed to ensure access have not been elucidated^{71,73,81–84}. Without such rules, phenotypic screening has been used to probe the effect of knocking in porins⁸² and knocking out outer membrane efflux pumps⁸³ and porins⁸⁵ to understand their internal logic.

Factors distinguishing between an effective gram-negative agent from an exclusively gram-positive one appeared to be low molecular weight (<600 Da) and higher polarity^{70,73,86}. The need for polarity may be a reason for the lack of success of large library high throughput screens, as these libraries are biased towards lipophilic molecules which are easier to synthesise⁷². Recently, assays for determining whether a compound was able to accumulate in *Escherichia coli* identified rigidity, globularity, amphiphilicity and the presence of an amine group as

contributing to increased accumulation ⁸¹. The simple addition of amine groups onto known compounds was demonstrated to increase their accumulative properties ⁸⁷.

With these complex demands for new molecules, an optimal strategy may be to use high throughput assays to find compounds that can permeate the membrane and add antimicrobial properties to them afterwards ⁶⁶. Gram-negative membranes have thus been described as presenting additional drug targets to optimise towards, on top of that of the inhibited protein, essentially doubling the challenge ³².

1.2.3.4 Clinical Considerations

The clinical demands on antibiotics are also significant. As with all drugs, the compound must be designed with tolerable pharmacokinetic and pharmacodynamic properties which allow it to reach sufficient concentrations at the site of infection for long enough to kill the bacteria ^{88,89}, whilst being non-toxic to humans. For certain diseases, this is made even more challenging by particular pathologies, for example the inaccessibility of *Pseudomonas aeruginosa* in the lungs of cystic fibrosis patients ^{90,91}. Unlike other areas of medicine, further consideration must be made of the consequences of the dosing regime selected, as suboptimal dosing can result in increased resistance ⁹²⁻⁹⁵.

Certain infections, such as those causing sepsis, require such rapid treatment that broad spectrum agents are necessary, whilst for others a narrow spectrum antibiotic coupled to a strain-identifying diagnostic is sufficient, and avoids deleterious effects on gut bacteria ⁷⁸.

Any putative antibiotic must then fulfil many scientific requirements whilst being discovered on a budget by the few remaining scientists still dedicated to this area of research. This is a huge challenge.

1.2.3.5 Molecular Mechanisms of Antibiotic Resistance

Resistance can develop by horizontal transfer of existing determinants or *de novo* mutations that arise by chance ⁵. If conditions are correct, mutations of a gene in a single cell can increase its fitness sufficiently to allow the cell line to become the dominant strain ⁹⁶. This mutant gene can then be passed onto a plasmid and be transmitted rapidly around the globe, as demonstrated recently in the spread of resistance to the last-resort antibiotic colistin ^{97,98}. In this way, a single incidence of

resistance development in one locale can, within a few years, become a global challenge.

Horizontal transfer can occur between different species⁹⁹, and the natural competency of species such as *Neisseria gonorrhoeae* allows them to drive their resistance to “superbug” status¹⁰⁰. High-level resistance is unlikely to arise from a single point mutation, but instead requires complex changes in cellular biochemistry, which is unlikely to occur in a single patient¹⁰¹. Combining resistance elements from many species is often necessary for high level resistance¹⁰¹.

On a molecular level, bacteria can become resistant to an antimicrobial through 3 main mechanisms:

- I. Bacteria can modify the active compound to reduce its activity¹⁰². Examples of this mechanism include β -lactamases which hydrolyse the amide of β -lactam antibiotics¹⁰³ or the enzymatic adenylation, acetylation or phosphorylation modifications of aminoglycosides¹⁰⁴.
- II. The drug target can be altered to change compound affinity. This can occur as a resistance mechanism against penicillin binding proteins (PBPs), the targets of β -lactam antibiotics (see below)^{105,106}, vancomycin¹⁰⁷, trimethoprim¹⁰⁸ as well as rifampicin¹⁰⁹.
- III. Bacteria can use efflux pumps and changes to membrane permeation to prevent entry or prevent build up of inhibitory compounds^{71,81,110}. Penetration into gram-negative bacteria which have two lipidic membranes with orthogonal “sieving properties”¹¹¹ is particularly challenging, and it is these organisms which top the World Health Organisation’s priority pathogens list¹¹².

The first two mechanisms are mostly specific to a single class of antibiotics: for example, β -lactamase induction may be effective against penicillin but will not affect the efficacy of vancomycin. In contrast, the third mechanism has been recognised to be a significant source of cross resistance as the induced efflux pumps can have broad specificity to many drugs¹¹³. Such cross resistance is concerning as it leads to organisms resistant to many families of antibiotics.

1.2.3.6 Methods to Slow Resistance

Many mechanisms of resistance will be associated with a fitness cost ¹¹⁴. If the fitness cost presents too high a burden for the organism under conditions of low selective pressure, reversion to the wildtype (non-resistant) may occur, alternatively, compensatory mechanism by further mutation may lower the burden ^{115–117}. If reversion is possible, it has been suggested to use cycling of antibiotics to periodically revert the population and keep resistance low, although more evidence for the effectiveness of this is required ^{118,119}.

Another method suggested to slow the development of resistance is to use more than one antibiotic concurrently ¹²⁰. This can reduce mortality rates compared to a monotherapy ¹²¹ and reduces the probability of emergent resistance phenotypes. Certain combinations of drugs have synergistic interactions, making combinations more effective than the sum of their individual effects ¹²². However, many possible combinations of drugs and their relative doses exist and high throughput methods are required to determine the optimal strategy¹²³. Whilst methods like this will likely be of benefit to the slowing of resistance, new molecular entities are required.

1.3 Approaches to finding new antibiotics

1.3.1 Whole cell vs Target-based methods

As mentioned above (section 1.1.1), many of the classes of drugs we use today were found by screening soil samples for molecules with antimicrobial activity. Generally, modern attempts to revisit these methods often only end up finding the same compounds ¹²⁴. An exception to this trend was found by screening uncultured species leading to the discovery of a novel, gram-positive active compound: teixobactin ^{125,126}.

Whole cell screening may identify compounds with antimicrobial activity but without providing insight into the mechanism of action. Additionally, without having control over the target selected, either non-specific (and potentially toxic) hits or the same, known biological targets may end up being continually re-selected ⁶⁵. Finding the mechanism of action is a significant hurdle, especially if a screen identifies thousands of compounds with distinct activities ^{66,127}. New methods are

being developed that can accelerate this process ^{127,128}, or the whole cell screen itself can be designed to detect inhibitors for a particular target of interest ^{65,124,129,130}. An additional advantage of whole-cell screening is that (if the correct bacterial strains are chosen) any hits will *a priori* have the necessary properties to permeate the cell, removing the need to add this property after the fact (which may be necessary for target-based screening), and which can be very challenging.

Alternatively, a purified enzyme (or an entire substrate pathway ⁶⁵) can be the target of a screen (as was the case for many of the screens attempted by GSK for example⁶⁶). If the target has previously been well characterised and found to be amenable to inhibition, then this method has the advantage of not needing the challenging mechanisms of action studies of a whole cell approach. In addition to the challenges discussed above (section 1.2.3.2), ignoring more complex aspects of the protein's role in the cell (e.g. the formation of protein complexes) or simplifications made to assay the target's activity (e.g. artificial substrates) may lead to a mismatch between the compound's on-target affinity and its cellular activity. On the other hand, subsequent cellular assays may demonstrate a compound has a broader inhibitory profile than anticipated, which would require mechanism of action studies to investigate.

1.3.2 Library Selection

Once the screening method has been devised, a library of chemicals needs to be found to screen against. As pharmaceutical companies and their large libraries were broadly unsuccessful ⁶⁶, other methods to provide chemical diversity are needed. Natural product libraries represent one such pool of molecules and have been used to identify leads ¹²⁴, as they were used in the 20th century. Others have noted that high throughput screening libraries are enriched in achiral and apolar molecules, properties unlike natural products. Their lack of these properties is a potential reason for the failure of high throughput screens ¹³¹.

Diversity Oriented Synthesis (DOS) can be used to generate molecules more like natural products ¹³², where properties of structural complexity and diversity of a library are the objectives as opposed to a specific chemical pharmacophore. However, even using diversity methods, very few of the possible arrangements of atoms (the "chemical space") have been synthesised. The number of organic

molecules with up to 17 heavy atoms has been enumerated at 1.6×10^{10} , but only 6×10^6 compounds (including those with >17 heavy atoms) have reportedly been synthesised ¹³³. If, as some have suggested, there exists a small molecule that can inhibit each druggable protein target ¹³⁴, we need methods to more completely search chemical space and find that lead. Fragment-based drug discovery offers a solution to this challenge ¹³⁵.

1.3.3 Fragment Based Drug Discovery (FBDD)

The use of smaller chemical molecules: “fragments” allows a larger chemical space to be covered with fewer experiments because the chemical space is smaller at lower molecular weights ¹³³. Fragments are small, partially drug-like compounds, which have few functional groups but conform to the rule of three (similar to Lipinski’s famous rule of 5 ¹³⁶): <300 Da, three or fewer hydrogen bond donors and acceptors, cLogP <3 ¹³⁷. Simpler molecules make better starting points for lead optimisation and may have a larger probability of binding to a target as they lack non-binding groups that reduce the overall affinity ¹³⁸.

Conversely however, if a hit is found its affinity is likely to be lower affinity as it has few opportunities to make interactions with the protein. This typically requires assays capable of detecting low affinity for protein-drug interactions. One method is to use X-Ray crystallography, which allows for very high concentrations of ligands to be used and non-specific interactions to be filtered out as the binding site can be seen in the model. In order to be used for screening many of the stages of typical X-ray crystallography required optimisation to increase their throughput. The XChem technology, developed at Diamond Light Source, has done this ^{134,139}. Proteins are crystallised then soaked with fragments from a series of libraries before high throughput (400 crystal per run) crystallography is used to screen the crystals for any binding fragments. In order to identify low occupancy fragments, “PanDDA” software is used to find a background for the unligated structure and then this is compared to the new structure to identify any differences in electron density ¹⁴⁰.

In a recent example, via collaboration with the University of Cambridge we screened a DOS library of ~1,300 compounds against PBP3 crystals and identified a single hit. We then used the crystal structure to identify vectors in which the fragment could be “grown” to access further regions of the active site, although we were not able to

determine detectable inhibition in assays ¹⁴¹. Where two or more fragments are found within the active site, they can be “linked” or “merged” to increase in their potency ¹³⁵.

FBDD has become increasingly popular since its initial description ^{142,143}, against antimicrobial targets ^{144,145}. This thesis describes an attempt to use FBDD against PBPs, which resulted in the identification of benzoxaboroles as PBP inhibitors with a novel binding mode (Chapter 5).

In actuality, a balance between screening specific targets and whole cell screening to find previously undiscovered modes of action which can then be further elucidated by mode of action studies has been recognised as the best approach ³². This work also covers the design of a high throughput screen for whole cell screening at the University of Warwick.

1.4 PBPs and β -lactams

PBPs, particularly PBP3, are the focus of the target-based methods described in this thesis. As the name suggests, PBPs are the target of penicillin, and all other members of the β -lactam class of antibiotics (section 1.4.3). Since they were found to be the targets of this important drug class ^{34,35}, they have been relatively well characterised ¹⁴⁶ and well validated as a drug target. The β -lactams, through bacterial evolution and rational medicinal chemical design satisfy many of the requirements for antimicrobial drugs described above, and are the most frequently prescribed antibiotic in primary care ¹⁴⁷. This section will describe the structure and function of PBPs and their interactions with β -lactams.

1.4.1 Functional Role

The bacterial cell wall is a component of the bacterial envelope, which bacteria use to protect and isolate themselves against the external environment ¹⁴⁸. The cell wall must be constantly maintained to withstand turgor pressure upon the cell, to determine cell shape and accommodate cell division. One component of the cell wall; peptidoglycan, is a strong, elastic and adjustable biopolymer which wraps around the cell ¹⁴⁹. The chemistry of the peptidoglycan is broadly similar in both gram-positive and -negative bacteria although it is thicker in the former ¹⁴⁹.

Gram-negative and gram-positive bacteria both possess a number of PBPs which are used to produce and maintain the bacterial cell wall ^{146,150}. *E. coli* has twelve PBPs, but only four are essential to the cell and lethal when knocked out ¹⁵¹. Their names follow a convention from their descending order of molecular weights when run on an SDS polyacrylamide gel ¹⁵², and are typically classified as either high molecular weight (HMM) or low molecular weight (LMM). HMM PBPs are responsible for catalysing glycosyltransferase (GT) and transpeptidation (TP) reactions needed for the polymerisation of peptidoglycan, whereas LMM PBPs have roles in peptidoglycan recycling and maturation ^{146,153,154}. The PBPs can also be separated by their functions: class A PBPs have both GT and TP activity, whereas class B PBPs have only TP activity and lack a transglycosylase domain ^{146,153}. Penicillin binding proteins have different roles within the cell. For example in *E. coli*: cellular elongation is driven by the mutually redundant PBP1a and PBP1b as well as PBP2, while PBP3 is responsible for cell division at the septum ^{146,152}. Inhibition of the functional activity carried out by these enzymes is lethal to the cell.

Peptidoglycan is composed of a long glycan strand, made of alternating N-acetylglucosamine (GlcNAc) and N-acetylmuramic acid (MurNAc) amino sugars, interlinked by a short stem peptide chains (Figure 1.2a). It is synthesised from its constituent sugars in the cytoplasm by the sequential reactions of the “Mur” enzymes ^{155,156}. MurA-F append the 5-amino acid chain to a uridine diphosphate-MurNAc (UDP-MurNAc) sugar, the product of which MraY then appends to a lipid tail (undecaprenyl phosphate), with the concomitant loss of uridine monophosphate (UMP). MurG catalyses the glucoaminylation reaction of this molecule (“lipid I”) to UDP-GlcNAc to form “lipid II” ¹⁵⁷. Lipid II is “flipped” into the periplasm where transglycosylases polymerise it ¹⁴⁶ (Figure 1.2a).

Certain bifunctional PBPs, such as PBP1b from *E. coli* have the transglycosylase activity, but non-PBP transglycosylases also contribute to this activity ^{155,158–160}. Transpeptidation is then used to cross-link the peptides of adjacent glycan stands. Whilst all PBPs have a DD-peptidase domain they may not all perform transpeptidation reactions, with others performing endopeptidase and carboxypeptidase roles ¹⁴⁶. In almost all bacteria, the 4th and 5th amino acids (distal to the glycan chain) of the stem peptide are both D-alanine residues ¹⁶¹. The reaction occurring between the transpeptidation (TP) domain of PBPs and these terminal residues is shown in Figure 1.2b. The stem peptide (by convention, referred to as the “donor”) enters the active site, forming a non-covalent complex, which is

attacked by the active site nucleophilic serine to form an acyl-enzyme complex concomitant with the release of the terminal D-Ala. A subsequent attack by a second nucleophile (by convention this is the “acceptor”) de-acylates the enzyme. In transpeptidation reactions of gram-negative organisms, the acceptor nucleophile is the ϵ -amine of the meso-diaminopimelyl (DAP) residue (the 3rd amino acid in the stem peptide), but in a carboxypeptidation reaction, this role is performed by water¹⁴⁶. This chemistry is also exploited by β -lactams which, as Tipper and Strominger noted, share structural similarity with the D-Ala-D-Ala dipeptide (highlighted in orange, Figure 1.2b)¹⁶². β -lactams are recognised by this structural motif, allowing them to be acylated onto the PBP, but once acylated, their rate of de-acylation is significantly slower¹⁶³ than for the natural substrate so the β -lactam remains acylated to the PBP, resulting in a suicidal, steric inhibition. It is likely that the β -lactam’s substrate-mimicking mechanism of action and structure has contributed to their success and conservation through evolution. Serine β -lactamases exploit their structural similarities with PBPs to bind β -lactams, but are optimised for much faster de-acylation, leading to the chemical destruction of the β -lactam and resistance to β -lactams for the bacteria¹⁶⁴.

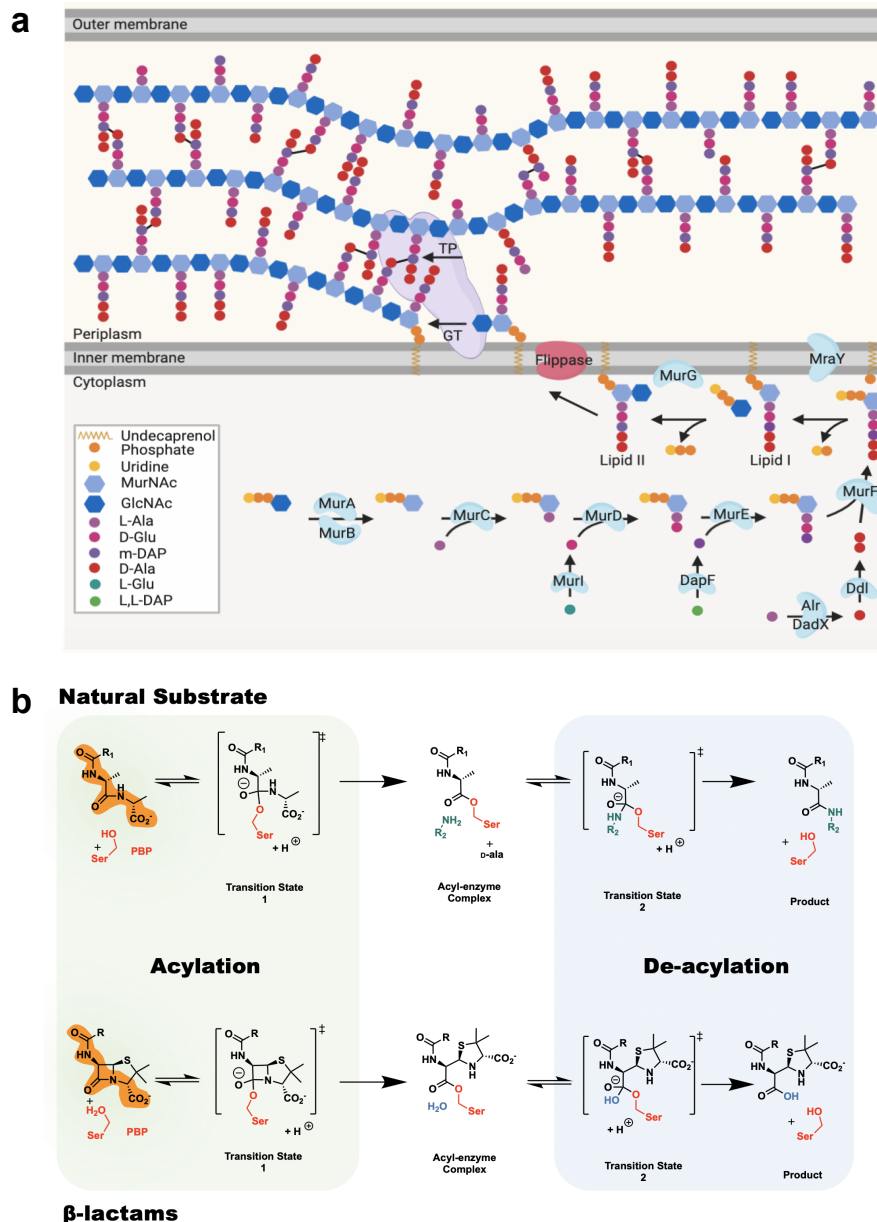


Figure 1.2. Functional role of the PBPs within the gram-negative periplasm. (a) Peptidoglycan synthesis machinery is complex and involves many enzymes¹⁵⁵. Cytoplasmically, the UDP-MurNAc is synthesised and the amino acids of the peptide pentamer are sequentially added¹⁵⁶. This molecule is then appended to a lipid tail (undecaprenyl phosphate) with the concomitant release of UMP to make lipid I and then glucoamylated with UDP-GlcNAc to produce lipid II¹⁵⁷. Lipid II is “flipped” into the periplasm where it is polymerised by the PBPs which catalyse transglycosylation and transpeptidation reactions¹⁴⁶. Figure reproduced, with permission from K. Smart. (b) Outline chemical mechanism of the transpeptidation domain. The peptide bond is acylated by nucleophilic attack from the active site serine, passing through a tetrahedral transition state to reach an acyl-enzyme complex. A second nucleophilic attack (by an amine or water molecule) de-acylates the acyl-enzyme complex, releasing the protein. The figure shows these reactions occurring with the terminal D-Ala-D-Ala of the stem peptide or with β-lactams (a generic penicillin in this example). The structural similarity between the two species is highlighted in orange.

1.4.2 PBP3

1.4.2.1 Functional Role of PBP3

Partial inhibition of PBP3 has long been known to cause an elongated *E. coli* phenotype ¹⁵², rationalised as PBP3 having a role in promoting peptidoglycan transpeptidation at the dividing cell septum. PBP3 interacts with other proteins as part of the “divisome complex”. Work using filamenting temperature-sensitive (*fts*) mutants of *E. coli* ¹⁶⁵ showed a sequential assembly of proteins at the site of division, starting with FtsZ which forms a cytoskeletal Z-ring. The *Fts* genes are all found in the “division of the cell wall” (*dcw*) gene cluster, which is conserved, in order, amongst many bacterial species ¹⁶⁶. One of the gene products to complex later in the process is FtsW, a transmembrane, non-PBP transglycosylase that itself recruits PBP3 (gene name: *ftsI*) into the divisome ^{159,167}. The binding of PBP3 to *P. aeruginosa* FtsW was shown to lead to the activation of the glycan polymerase activity of FtsW, which presumably supplies the PBP3 with the feedstocks for transpeptidation ¹⁵⁹. *In vitro* natural substrate processing by PBP3 has yet to be demonstrated, although thioester substrate-mimics can be turned over by PBP3 ¹⁶⁸. PBP3 of *P. aeruginosa* is the only PBP of that species which is genetically essential ¹⁶⁹, making it an attractive target for inhibition. Confusingly, *P. aeruginosa* also expresses a class B PBP called PBP3a (or PBP3x), but this appears to be non-essential ¹⁷⁰.

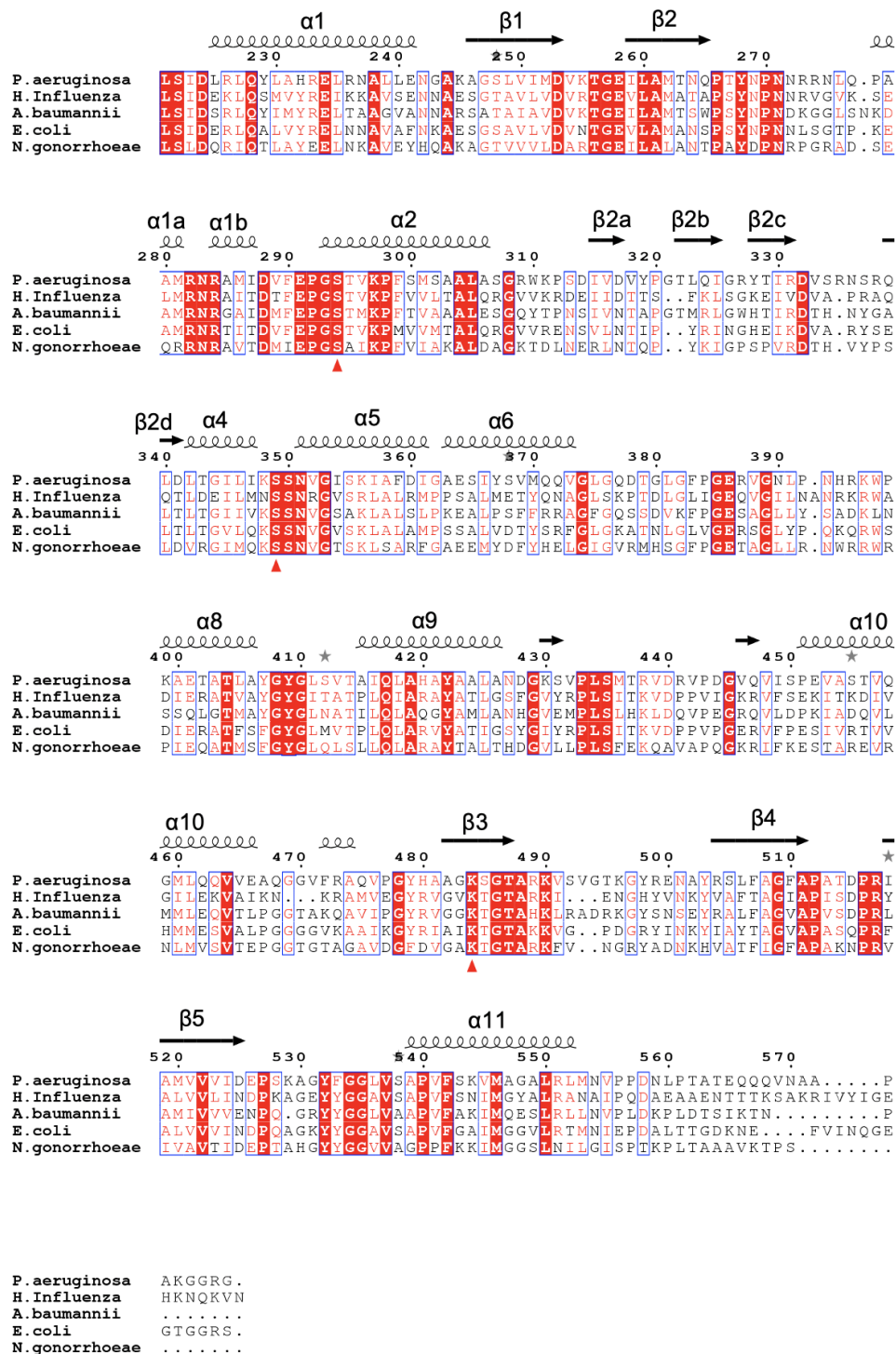
1.4.2.2 Topology

As monofunctional transpeptidases (class B PBPs), the PBP3 of gram-negative organisms such as *E. coli*, *P. aeruginosa*, *Acinetobacter baumannii*, and *H. influenzae* as well as the PBP2 of *N. gonorrhoeae* share significant structural homology ¹⁰⁵, despite low sequence identity (e.g. *E. coli* and *P. aeruginosa* share just 45.1% identity ¹⁷⁰) (Figure 1.3). These proteins have three domains, an inner membrane spanning domain, a non-penicillin binding N-terminal domain and the penicillin binding transpeptidase domain ^{154,171,172} (Figure 1.4b). The transmembrane helix spans the membrane once ¹⁷³ and is itself capable of directing the protein (or even GFP) to the septum ¹⁷⁴. The role of the N terminal domain has not been fully described but appears to mediate PBP3 interactions with other divisome proteins ^{175,176}. Interestingly, certain interactions with divisome proteins have been shown to sensitise PBP3 to acylation by cephalixin (but not other β -lactams) ¹⁷⁷, raising the possibility of allosteric regulation via the N-terminal domain.

The PBP3 C-terminal penicillin binding domain shares a common fold with many PBPs and β -lactamases in the penicilloyl-serine transferase superfamily. Members of the family align structurally and have conserved active site sequence motifs of SXXK, SXN, K(S/T)G¹⁵³ and a consistent protein fold^{178,179} (Figure 1.4). PBP3 retains β -lactam binding activity if truncated to the TP domain only^{105,180}, indicating this domain alone is sufficient for catalytic activity. Some proteins such as *P. aeruginosa* PBP3 do not tolerate this truncation¹⁷⁹ (D. Bellini unpublished observations). Crystal structures have been produced of only transpeptidation domains^{105,180} or more commonly with the transpeptidation and N-terminal domains but lacking the transmembrane domain which is removed to allow for crystallisation and aqueous solubility^{105,173,179,181–183}.

1.4.2.3 Crystallography of the Transpeptidase Domain

Crystal structures of the class B PBP transpeptidase domain reveal a highly ordered core with a wide, shallow central cleft, which has the active site serine (e.g. in *P. aeruginosa* PBP3 Ser294) at its centre^{105,178,179,181,182,184} (Figure 1.4). The fold of the transpeptidase domain is shared by all PBPs and β -lactamases of the penicilloyl-serine transferase superfamily¹⁸⁵. The core of the domain is formed by a 5 stranded β -sheet (β 1a and 1b and β 3-5), with β 3 forming the floor of the active site cleft (Figure 1.4c and d). The “jaws” of the active site cleft are formed by α 11 on the bottom and the short and consecutive β 2a-d and α 4 elements on the top (Figure 1.4b). The catalytic residues are stabilised by their location near the centre of the domain, on α 6 (the active site serine and nearby lysine in the SXXK motif), α 4 (the serine of SXN) or β 3 (lysine of the K(S/T)G motif). Mobile loops extend between the secondary structure elements and are important for binding. Notable are the β 5- α 11 loop which moves up and towards the active site upon piperacillin binding¹⁷⁹ and the β 3- β 4 loop which is poorly resolved in some structures¹⁰⁵ (Chapter 4).

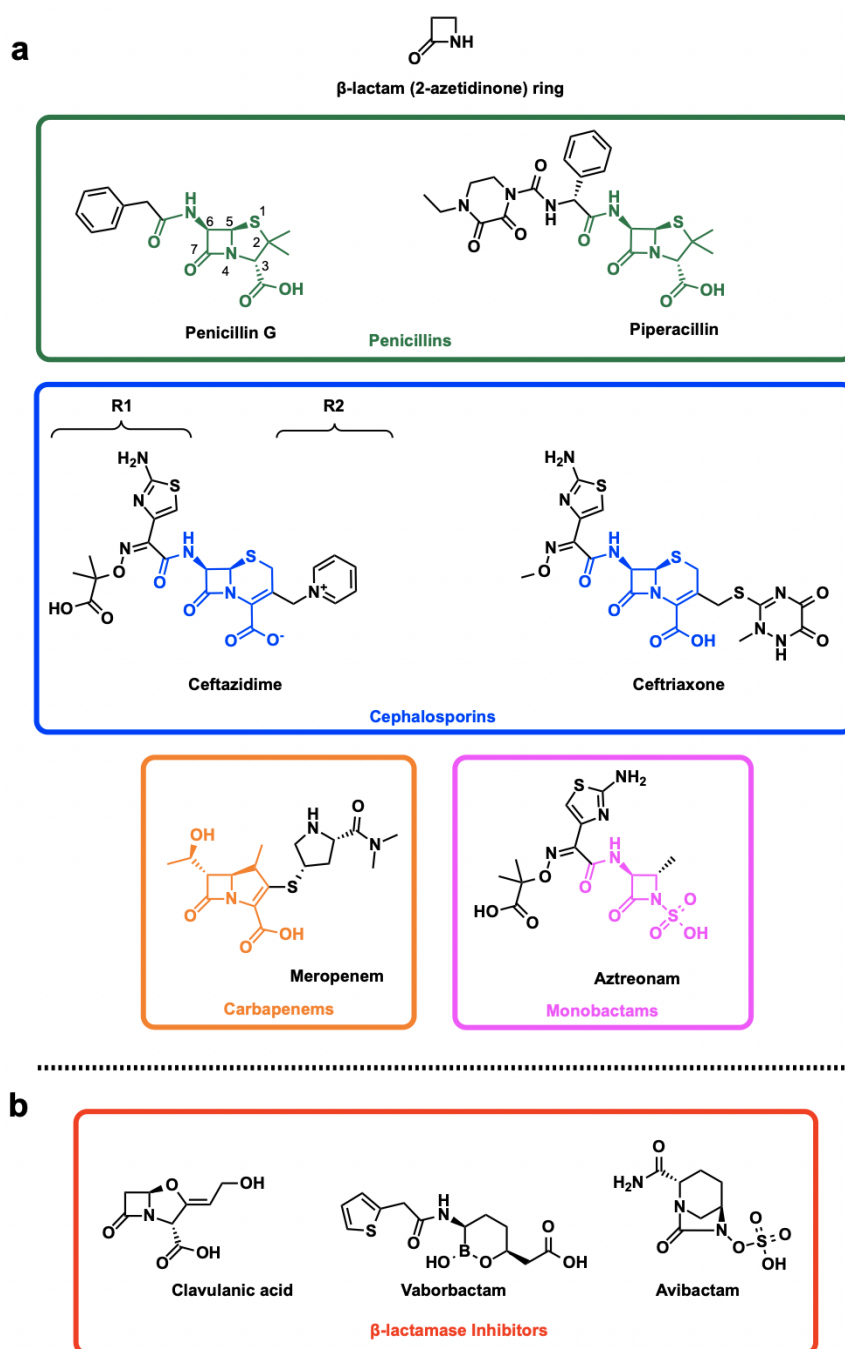


1.4.3 β -lactams

The β -lactams are a family of drugs containing a 4-membered (β) 2-azetidinone (lactam) ring. They are some of the most important antibiotics being “well tolerated, efficacious and well prescribed”¹⁰³.

The first example of each class were found from natural product screens: penicillin was identified from fungal extracts¹⁹ as were cephalosporins^{188–190}, whilst carbapenems and monobactams^{191,192}, were extracted from bacterial isolates. Many derivatives of each class have been synthesised and are used in the clinic¹⁹³, although just one example of a monobactam, aztreonam, has been marketed. Since the release of aztreonam^{191,194} in the 1980’s no further classes have been discovered although many iterations of drugs within these classes have been developed. The most recent to be released is Cefiderocol which features an iron-conjugating catechol group to drive its uptake into gram-negative bacteria^{195,196}. Other innovations have been the development of various combinations of a β -lactam and β -lactamase inhibitor (see below)¹⁰³.

Given the wide arsenal of β -lactams available (Scheme 1.1), clinical decisions on the choice of β -lactam administered depend on the pathogenic agent, route of administration, and the risk of allergic reaction^{193,197,198}.

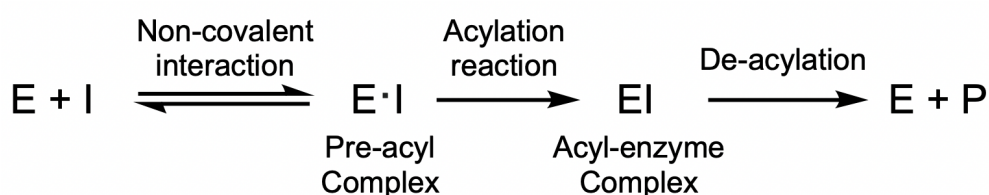


Scheme 1.1 β -lactams and β -lactamase inhibitors. (a) Example structures of four common classes of clinical β -lactam drugs. The characteristic core group for each of the classes is coloured. The R1 and R2 side chains are labelled on the structure of ceftazidime, and the numbering system of the penicillin core group is indicated. The C-3 carboxylate is the carboxylic acid at the 3-position on penicillin G (b) Selected example structures of β -lactamase inhibitors. Note the presence of a β -lactam ring in clavulanic acid.

1.4.3.1 Kinetics

When β -lactams react with PBPs they form covalent acyl-enzyme complexes with the active site serine (Figure 1.2). The steps of this reaction are summarised in Scheme 1.2¹⁹⁹. An initial non-covalent Michaelis complex ($E \cdot I$) is in rapid equilibrium with the free enzyme (E). The PBP and β -lactam composing $E \cdot I$ react to give the covalently acylated EI . This acylation step is typically considered to be irreversible^{179,200}. The acyl-enzyme complex can be hydrolysed to give the product (P , a ring-opened penicilloic or cephalosporic acid) and free enzyme. This de-acylation is typically slow ($< 0.02 \text{ min}^{-1}$)^{163,168,201,202}, thus the inhibition of a PBP is primarily sensitive to the ratio of the rate of covalent bond formation and the non-covalent dissociation constant¹⁸⁵. Chromogenic nitrocefin appears to act differently to other β -lactams, with a much higher turnover rate (up to $\sim 40 \text{ min}^{-1}$) in, a phenomenon which is discussed in more detail in Chapter 6.

The non-covalent components of the interaction are strong enough to allow several non-acylated β -lactams to be observed in crystals in the PBP3 active site^{183,203}. The cephalosporic acid of cefoperazone (but not the penicilloic acid of azlocillin) can stabilise the protein to thermal melting^{183,203}. However, thermodynamic analysis of *E. coli* PBP5 found that the noncovalent interactions of four different β -lactams did not correlate with the experimentally determined acylation rates (which includes both non-covalent interaction and the covalent bond formation). This indicates that the non-covalent component is the less important component²⁰⁴.



Scheme 1.2 Reaction pathway of β -lactams interacting with PBPs. E represents the enzyme, I the β -lactam, $E \cdot I$ is a non-covalent complex, EI is an acyl-enzyme covalent complex, P is the penicilloic acid (or equivalent) product of ester hydrolysis.

1.4.3.2 Crystallographic Interactions with β -lactams

Several important regions in the cleft contribute to β -lactam binding. Crystal structures of *P. aeruginosa* PBP3 (PaPBP3) are studied throughout this work and Figure 1.4e shows the principal residues of this protein that interact with piperacillin. The active site serine (Ser294) reacts with the β -lactam bond to form an acyl-enzyme complex. Nearby, and forming an interacting hydrogen bonding network are Ser349, Lys484 and Lys297 (blue in Figure 1.4e), which are thought to activate the Ser294 for nucleophilic attack^{205–210}. Positioned on the β 3 adjacent to Lys484 are Ser495 and Thr497 (residues in red in Figure 1.4e). These residues form an “acid binding pocket” that hydrogen bonds with the C3 carboxylate group (or equivalent in monobactams or cephalosporins) found in all β -lactams. Backbone amines of Ser294 (active site serine) and Thr487 (on the β 3 strand) hydrogen bond with the β -lactam carbonyl, creating an oxyanion hole which polarises the carbonyl, activating it during its initial acylation, and later de-acylation¹⁸⁵. Gly486 (glycine of the K(S/T)G motif - directly preceding Thr487), is apparently the key determinant of positioning of the amine of Thr487 as this residue is conserved in all members of the penicilloyl-serine transferase superfamily²¹¹.

A “hydrophobic wall”¹⁷⁹ of residues Tyr503, Tyr532 and Phe533 can form adjacent to the β -lactam phenyl group as shown in Figure 1.4e. The R1 side chain of the β -lactam is engaged by a channel formed of tyrosines (Tyr328, Tyr407, Tyr409 and Tyr498) and the β 3 strand (Arg489 side chain and several β 3 backbone amides). Asn351 is a highly conserved residue¹⁵³ which interacts with the first amide carbonyl of the β -lactam (this is another frequent motif of β -lactams). Val333 forms hydrophobic interactions with the β -lactam and the hydrophobic wall, creating the column seen spanning the active site cleft in Figure 1.4d.

The above description of interactions is generally true for simple penicillins^{105,179,183,212}, aztreonam¹⁷⁹, cefoperazone¹⁸³, ceftazidime¹⁸¹ and even β -lactams without a covalent link to the protein^{183,203}. For meropenem¹⁷⁹, β -lactams with large siderophore conjugates^{179,213–216} and ceftobiprole (a cephalosporin with a large R2 sidechain²¹⁷) many of the same regions participate but accommodation is made to fit the different groups.

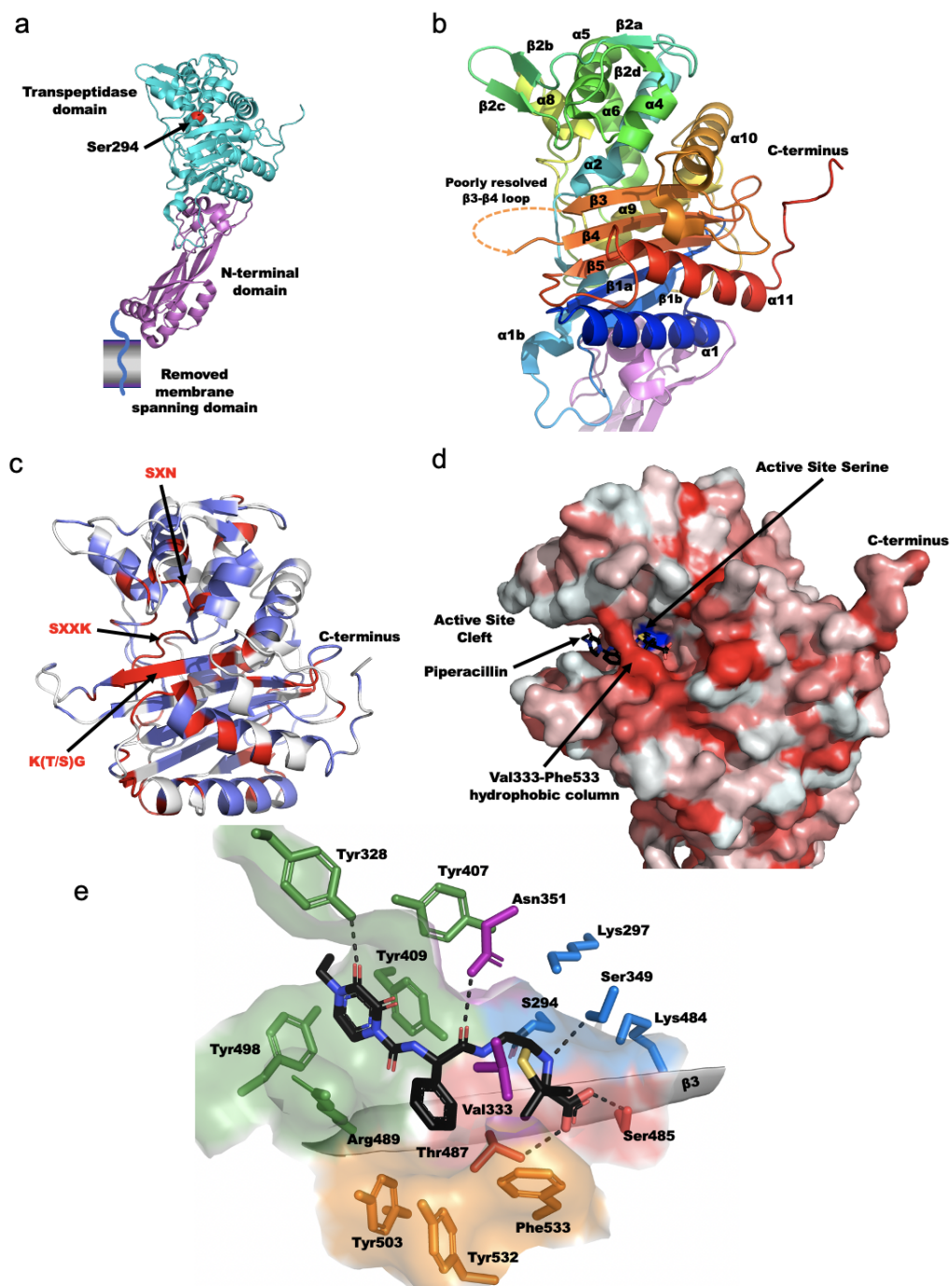


Figure 1.4. Structural views of class B PBPs. (a) Overall topology of a class B PBP (PaPBP) shown in cartoon representation. The first domain is a short, single spanning transmembrane region including a short cytoplasmic sequence. This domain has never been crystallised and is sketched only. The crystal structure of the non-penicillin binding N-terminal domain is shown in pink and the functional transpeptidase domain in cyan with the active site serine highlighted in red. (b) Secondary structure elements of the penicillin binding domain of *P. aeruginosa* PBP3 (PDB code 6HZR¹⁰⁵) following the convention from¹⁷⁸. Rendered in cartoon representation with colours in rainbow from dark blue at the N-terminal to red at the C-terminal. Sequences for these secondary structure features are shown in

Figure 1.3. Despite the high resolution of this structure, the β 3- β 4 loop is poorly resolved, likely due to its flexibility. A dotted arrow indicates the missing region. Secondary structure elements are labelled following convention ¹⁷⁸. (c) Sequence conservation of the transpeptidase domain. The same colours (red for highly conserved, blue for partially conserved and white for non-conserved) are shown for each residue on the 3D crystal structure as used in Figure 1.3. The highly conserved (across the entire penicilloyl-serine transferase superfamily) active site motifs are labeled. (d) Surface representation of the *P. aeruginosa* PBP3 reacted with piperacillin (PDB: 6R3X ¹⁰⁵), coloured according to degree of hydrophobicity ^{218,219} shows the “jaws” around the shallow cleft of the active site. A column formed by the hydrophobic interactions of Val333 and Phe533 that spans the cleft. (e) The active site of the piperacillin-acylated PBP3 shown as a transparent surface. The β 3 strand which runs parallel to the β -lactam along the floor of the active site is shown in cartoon representation. Residues interacting with the piperacillin are shown in stick representation and coloured according to binding region: catalytic residues (blue); acid binding pocket (red); hydrophobic wall (orange); R1 binding pocket (green); residues on the roof of the cleft (purple). Hydrogen bonds between piperacillin and residue side chains are shown (dashed lines).

1.4.3.3 Physiological Effect of β -lactam Inhibition of PBPs

Early microscopic observations noted that *E. coli* when treated with penicillin transformed from their typical rod shapes into protoplasts, which lyse under unfavourable osmotic conditions ^{220,221}. If osmosis was prevented by isotonic conditions and the penicillin was washed off, growth could recover ²²¹. Similarly if the *E. coli* were treated with penicillin in media that did not support growth, the drug treatment did not lead to lysis ²²⁰. These results indicate that penicillin (and β -lactams more generally) only acts indirectly through its inhibition of the cell wall synthesis. Later work showed that hydrolases play an important role in breaking down the peptidoglycan, particularly during cell division, and the disruption of the balance between production and destruction of the macromolecule at the cell septum leads to cell lysis ²²². Pneumococcal cells without autolytic hydrolases were insensitive to penicillin ^{223,224}. More recent evidence suggests that β -lactams may induce futile cycles of glycan strand production, which hastens cell death ^{225,226}.

β -lactams each have individual specificities for the various PBPs of a cell ^{227–230} and it has been shown, using β -lactams with single PBP affinity, that the inhibition of more than one PBP in *E. coli* causes rapid bactericidal effects where the inhibition of just one causes only bacteriostasis ²³¹. Thus, the relationship between target engagement and physiological effect is inexact. Additionally, each β -lactam has different membrane permeation properties and susceptibility to β -lactamase attack, further complicating this relationship ²³². Ultimately, the broad spectrum antimicrobial activity (both gram negative and gram positive) of the β -lactams as a group derives

from their diverse on-target profile, which in turn derives from their mechanistic similarity to the PBP substrate. Consequently, a β -lactam can be found with activity against most organisms.

1.4.4 Resistance to β -lactams

Resistance of bacteria to β -lactams has been observed to occur by all three of the resistance mechanisms described above (see “Mechanisms of Antibiotic Resistance”) ²³³.

1.4.1 Penetration-efficiency-mediated Resistance to β -lactams

Resistance to β -lactams in *E. coli* can occur through mutations to the OmpC and OmpF porin proteins, which are a major entry route of β -lactams into this species ^{113,234}. In *P. aeruginosa* this mechanism is less common and instead changes in the composition of the lipopolysaccharide, a layer of polymers beyond the outer membrane has been shown to influence the ability of β -lactams to enter the cell ^{235,236}. This layer contributes to the “intrinsic resistance” of *P. aeruginosa*, along with expression of efflux pumps ^{113,237}. Efflux pumps alone can lead to high levels of resistance in certain species such as *Klebsiella pneumoniae* ²³⁸.

1.4.2 Target-mediated Resistance to β -lactams

Target-mediated Resistance to β -lactams is discussed in Chapter 4. Broadly, this route appears to vary in its use significantly between species. In certain gram-positive species (e.g. methicillin resistant *Staphylococcus aureus*) acquisition and expression of a gene (e.g. *mecA*) encoding new, low affinity PBPs occurs ²³⁹, but this has not been observed for gram-negative class B PBPs. *N. gonorrhoeae* and *H. influenzae* are frequently observed to reduce the β -lactam affinity of target PBPs by generating variants in the PBP sequence. However, the exact mechanisms that lead to reduced affinity are not yet deciphered ¹⁰⁵.

1.4.3 β -lactamase-mediated Resistance to β -lactams

Perhaps the best studied resistance mechanism is β -lactamase expression. Resistance through β -lactamase expression was observed even before the widespread clinical use of β -lactams ^{240,241} and evidence suggests they have existed for millions of years ^{242,243}, likely co-evolving alongside β -lactams ¹⁹³, in a bacterial “arms race”. There exists a β -lactamase that can hydrolyse each class of β -lactam

(although not all β -lactamases can hydrolyse all β -lactams)²⁴⁴ and β -lactamases are continually evolving^{193,245}, increasing their activity and broadening their substrate specificity. New β -lactams experience β -lactamase-mediated resistance within a few years of their release²⁴³. The impact of β -lactamases is not limited to a single cell and they can serve as communal defense mechanisms, protecting susceptible cells in liquid media²⁴⁶ and in biofilms²⁴⁷.

The Ambler classification separates β -lactamases on the basis of their sequence into 4 groups A,B,C and D^{244,248,249}. A, C and D are all serine β -lactamases, with acylation and de-acylation mechanisms similar to PBPs²⁴⁴. Class B enzymes are metallo- β -lactamases, for which there are no approved inhibitors^{250,251} (although aztreonam is not effectively turned over by this class, providing a therapeutic option²⁴⁴). An alternative classification method, the Bush-Jacoby-Medeiros classification scheme separates β -lactamases by their function, which is the most important consideration for clinicians encountering a β -lactamase in a medical context^{249,252}. In this scheme group 1 contains mostly chromosomally encoded, Ambler class C cephalosporinases; group 2 (the largest group, with 12 subgroups) contains penicillinases, cephalosporinases and carbapenemases from Ambler class A and D; and group 3 is composed of metallo- β -lactamases (Ambler class B), which cannot be inhibited by clavulanic acid and tazobactam and generally have poor affinity for monobactams^{249,252}. Serine β -lactamases appear to have evolved from a primordial PBP, obtaining mutations that maintain β -lactam recognition capabilities and their overall fold, but which give them improved catalytic properties¹⁸⁵ and decreased affinity of the PBP substrate²⁵³. Genetic analysis indicates that the different classes of β -lactamase diverged from distinct ancestors, and each β -lactamase is more closely related to a PBP than to another β -lactamase¹⁸⁵. The core fold of the transpeptidase domain is thus able to support a wide array of different enzymatic functions each tuned to the enzyme's function.

Attempts have been made to counter β -lactamase resistance by using a number of different β -lactamase inhibitors to protect a co-administered β -lactam. Three examples of β -lactamase inhibitors are shown in Scheme 1.1b. The earliest of these inhibitors, clavulanic acid was discovered from natural product screens^{254,255}. The β -lactam bond undergoes the typical serine acylation reaction with class A β -lactamases (Figure 1.2), however unlike other β -lactams, this releases a reactive intermediate that forms an irreversible complex with the β -lactamase, leading to suicidal inhibition^{193,256–258}. Like most β -lactamase inhibitors, clavulanic acid lacks

antimicrobial activity and it is administered alongside a β -lactam (often amoxicillin²⁵⁹). More recent β -lactamase inhibitors classes include the diazabicyclooctanes, typified by avibactam, a reversible inhibitor of all serine β -lactamases²⁶⁰, and boron-based inhibitors such as vaborbactam (class A and C activity)^{261–263}. Whilst β -lactamase inhibitor/ β -lactam combinations have been able to restore the efficacy of β -lactams to β -lactamase expressing strains, their efficacy depends on the ability of both components to reach the site of infection at sufficient concentrations^{264,265}. A single agent, β -lactamase-resistant therapy would not have this limitation.

1.4.5 Non- β -lactam compounds

PBPs are an excellent drug target. Many attempts have been made to find non- β -lactam PBP small molecule inhibitors (reviewed in^{266–268}), with the hope of inducing the same physiological effect as β -lactams but without the liability to β -lactamase attack. These are summarised in Table 1.1. These can be broadly divided into 3 groups. (i) Those that act as suicidal covalent inhibitors of PBPs (similarly to β -lactams), (ii) those with non-covalent mechanisms of action and (iii) those that acylate the active site with a boron warhead (which forms a reversible covalent interaction). Additionally, cyclic peptides have previously been investigated for PBP and β -lactamase inhibition²⁶⁹ and are currently being investigated by Bicycle Therapeutics for PBP inhibition²⁷⁰. Unfortunately, in many cases even if a warhead has been demonstrated to engage PBPs, this can be insufficient to cause bacterial growth inhibition: this may be due to low potency, inability to reach the target, chemical instability within the cell or a combination of these factors.

Whilst a large number of pharmacophores have been investigated as PBP inhibitors, none have reached clinical medicine. The diazabicyclooctane (DBO) avibactam and the boronate vaborbactam are used as β -lactamase inhibitors and the bicyclic boronate taniborbactam (formerly VNRX-7145) is in Phase III clinical trials for combination with cefepime^{271,272}. New boron-based β -lactamase inhibitor QPX7728²⁷³ has recently entered Phase I clinical trials. The DBO literature offers hope that successful β -lactamase inhibitors may one day find use against PBPs. Avibactam has been shown to bind PBPs^{274,275} and ongoing work^{275–280} may prove DBOs to be an effective PBP-targeting therapeutic. Crystal structures show that DBOs including zidebactam, avibactam, ETX0462 and WCK 4234 can bind PBP2 and PBP3^{276,277,281} and that there is an “enhancer effect” on the activity of the

β -lactams activity PBPs^{275,277,278} when co-administered with DBOs such as nacubactam and zidebactam. Additionally, the DBOs have efficacy via direct inhibition of PBPs and β -lactamases.

The diversity of non- β -lactam covalent warheads that have been investigated indicate the unique properties of the β -lactam, benefiting from substrate analogy, active site affinity and correct chemistry of the warhead. The β -lactam bond is one of a number of privileged warheads which have reactivity towards serine, (like boronates)²⁸². The amide carbonyl of the β -lactam is destabilised by the ring strain of the 4 membered ring, making nucleophilic attack by the alcohol more likely²⁸³. The activation energy for this reaction must be low enough for the attack to be possible by serine but avoid rapid spontaneous hydrolysis²¹⁴. The energy barrier is tuned by the side chain chemistry and the type of core found in the molecule²⁸⁴. As has been noted with the novel lactivicin core²¹⁴, any new serine-binding warhead must carefully compromise between reactivity to serine attack and hydrolysis.

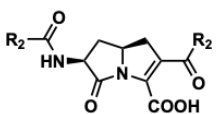
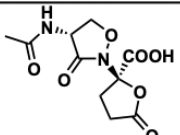
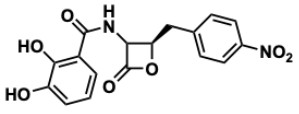
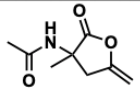
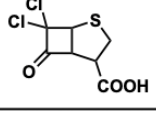
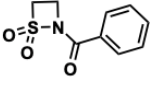
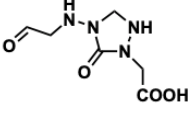
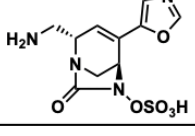
Lactivicin and γ -lactam derivatives in particular were the subject of large pharmaceutical investigations, which may eventually yield new medicines^{214,266,285–289}. Adding sidechains from β -lactams to these molecules has been used to improve their affinity and the crystal structures demonstrate that they are using many of the β -lactam-binding regions shown in Figure 1.4.

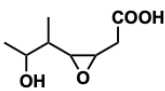
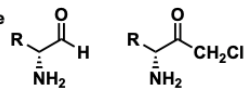
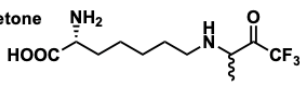
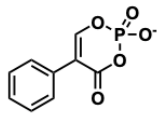
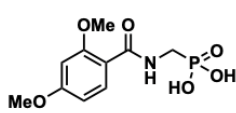
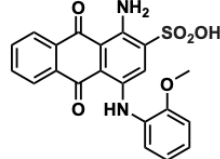
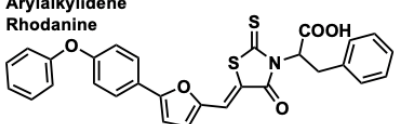
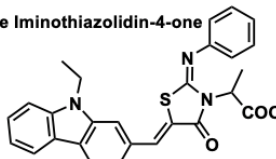
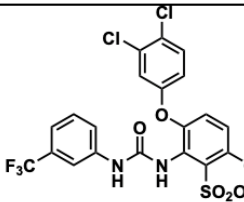
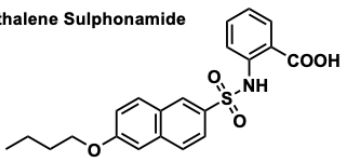
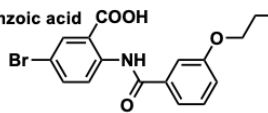
A number of different compounds apparently demonstrate non-covalent inhibition of PBPs (at least 2 of which are thought to be non-specific promiscuous binders, whose activity is ablated in the presence of detergent^{267,290}) (Table 1.1). The low μ M potency (against *P. aeruginosa* PBP3) and antimicrobial activity of the pyrrolidine-2,3-diones offers promise²⁹¹. However with all the non-covalent inhibitors, their mode of action is unclear. They have proved difficult to observe crystallographically^{291–293}, with the only successful example being found in the allosteric site of PBP2a from *S. aureus*, (a site not found in gram-negative class B PBP3s^{294–297}). Similarly, our crystallographic fragment screen of 1,300 diversity-orientated fragments against PBP3 found only a single hit (a γ -lactone) and this was *covalently* bound¹⁴¹. This is a hit rate several orders of magnitudes lower than other projects using a similar technique. Why PBPs are so difficult to crystallise with non-covalent inhibitors is unclear, and is reminiscent of the paucity of structural information about the protein-natural substrate complex (at least for HMM PBPs). Until this is understood, crystallographic FBDD screens may not be very productive.

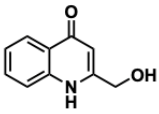
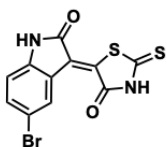
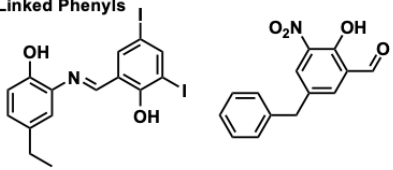
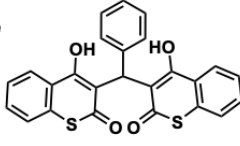
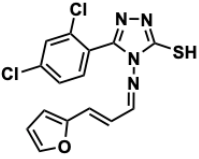
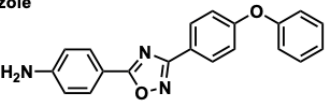
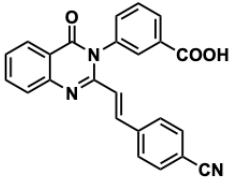
The boron-based inhibitors will be discussed in more detail in Chapter 5, but they are distinct in that they are typically considered transition state inhibitors^{210,298,299}, mimicking the transition state of the β -lactam binding cycle (Figure 1.2). Boron is uniquely able to fill this role as it can exist in both an sp^2 and sp^3 hybridisation states

300

Table 1.1 demonstrates that there is still much to understand about the behaviours of non- β -lactam inhibitors of PBPs.

Chemistry	Active Site Serine Engagement	PBP Class Investigated	Targets Gram-negative PBP3	Examples Structural data	Antimicrobial Activity	β -lactamase Interaction	Comments	References
Pyrrolidinone γ-lactam 	C	H	Y	6VOT	+ve & -ve	S	Many derivatives have been synthesised (see reviews).	A
Lactivicin 	C	H	Y	4OOL	+ve & -ve	BLI	Many derivatives have been synthesised (see reviews).	B
β-lactone 	C	H	E	ND	+ve & -ve	S	Found in a natural product screen. Poorly stable in solution. β -lactones have been used for labelling PBPs	C
γ-lactone 	C	H	Y	6Y6Z	N	ND	Found in an X-ray crystallographic screen	D
Cyclobutanone 	C	ND	ND	R	N	BLI	In equilibrium with the hemiacetal in solution and in the active site	E
β-sultam 	C	L	ND	1YQS	ND	BLI	Tested only in R61 from <i>S. Pneumoniae</i> , slow acylation of the active site is observed	F
Triazoline-3-one 	C	ND	ND	ND	N	ND	Triazoline-3-thiones were also tested, similarly inactive	G
Diazabicyclooctane 	C	H	Y	6G9S	+ve & -ve	BLI	First investigated as a β -lactamase inhibitor, with later derivatives optimised for PBP inhibition (focussed on <i>E. coli</i> PBP2)	H

Epoxide		C	ND	N	ND	N	BLI (w)	Little investigation into this group. Unstable in solution	I
Activated Alanine		C	L	N	ND	ND	ND	R is a Boc- and carboxybenzyl-protected lysine	J
Trifluoroketone		C	L	ND	3ZCZ	ND	ND		K
Cyclic Phosphate		C	L	ND	1SCW	ND	BLI	Can acylate or phosphorylate the active site serine	L
Phosphonate		C	L	ND	ND	ND	BLI	Several different phosphonates have been synthesised as inhibitors	M
Anthraquinine		PR	H	ND	ND	ND	ND	Detergent not used in activity assays, suggested to be non-specific binding.	N
Arylalkylidene Rhodanine		NC	H	Y	ND	+ve & -ve	BLI	Shows slow, reversible inhibition. Inhibition of analogues are detergent sensitive - possible promiscuous binders.	O
Arylalkylidene Iminothiazolidin-4-one		NC	H	Y	ND	+ve & -ve	BLI		
Ortho-phenoxy diphenylurea		PR	H	ND	A	ND	ND	Investigated PBP2x from Streptococcus pneumoniae: class B PBP. Found using a virtual screen. Resistant mutants were weaker binding	P
Naphthalene Sulphonamide		PR	L+H	ND	ND	+ve & -ve	ND	This pharmacophore has been identified in two separate screens	Q
Benzamidobenzoic acid		PR	L+H	ND	ND	+ve	ND	Assayed in the presence of Triton X-100 to reduce risk of promiscuous binding	R

4-Quinolone		PR	L+H	Y	ND	N	ND	Discovered in a computational docking screen against PBP5 (details not given)	S
Thiazolidine								Similarity to the core of the Arylalkylidene Iminothiazolidin-4-ones is noted. Possibility of covalent acylation though amide, but not identified in mass spectrometry experiments. MIC<IC ₅₀ *	
Linked Phenyls		PR	H	Y	ND	-ve	ND	Presence of reactive hydroxyl nitrobenzaldehyde group could be a covalent warhead. MIC<IC ₅₀ *	T
Thiochromenone								* These compounds are a selection of 28 hits identified in a screen of 50,000 compounds against PBP2 using a bocillin fluorescence anisotropy assay. Note that the MICs are significantly lower than the IC ₅₀ for PBP2, which may indicate other cellular targets.	
Triazole									
Oxadiazole		PR	H	ND	A	+ve	ND	Discovered in a computational docking screen against Methicillin-resistant <i>Staphylococcus aureus</i> PBP2a	U
Quinazolinone		PR	H	ND	4CJN	+ve	ND	Crystal structure shows binding to an allosteric site of <i>Staphylococcus aureus</i> PBP2a, as reported for a β -lactam. This causes structural re-arrangement of the active site. The authors propose that the compound's addition inhibition of PBP1 (which lacks an allosteric site) indicates active site binding is possible as well	V

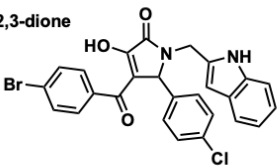
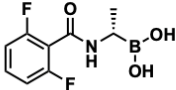
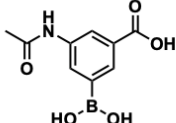
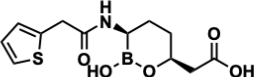
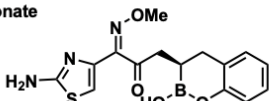
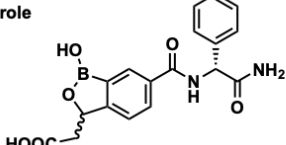
Pyrrolidine-2,3-dione 	PR	H	Y	ND	-ve	ND	Discovered by screening PaPBP3 with an S2d based assay. Compounds show low μ M activity vs <i>P. aeruginosa</i> cells and no cytotoxicity	W
Alkyl boronic acid 	C	L+H	ND	2Y2K	+ve	BLI	Investigated as a natural substrate mimic of D-ala. Can form trivalent complexes with PBPs	X
Aryl boronic acid 	C	L+H	Y	3ZVT	N	BLI	Can form trivalent complexes with PBPs	Y
Vaborbactam 	C	H	Y	7AUH	N	BLI	The first clinically used boron-based BLI. Crystal structures show remarkable conservation of binding mode with β -lactams	Z
Bicyclic Boronate 	C	L+H	Y	5J8X	+ve & -ve	BLI	Investigation by Venatorx for use as a PBP and BLI. Very encouraging results, including good MICs	AA
Benzoxaborole 	C	H	Y	7AU1	N	BLI	Subject of a large section of my work. Promising new warhead for PBPs. Investigated but later dropped by AZ as a BLI	BB

Table 1.1. Non- β -lactam PBP binding small molecules previously reported.

References: A^{266,285–287}, B^{214,266,288,289}, C^{301–303}, D¹⁴¹, E^{266,284,304,305}, F^{306–308}, G³⁰⁹, H^{260,274,276,277}, I²⁶⁸, J^{299,310}, K^{299,311}, L^{267,312}, M^{267,311,313,314}, N³¹⁵, O^{267,290}, P²⁹², Q^{316–318}, R^{316,317}, S³¹⁹, T³¹⁸, U²⁹³, V^{294–296,320}, W²⁹¹, X^{299,311,321–325}, Y^{322,326}, Z^{262,327,328} (Chapter 5), AA^{329–331}, BB^{332,333} (Chapter 5). Data listed is a summary of the properties of each class and not reflective of the individual molecule shown. Abbreviations: C: Covalent: Warhead designed to engage covalently; PR: Reduced binding of probes (S2d, BOCILLIN FL, nitrocefin, or radiolabelled penicillin to the active site but mechanism not confirmed to be competitive); NC: When probed with S2d, behaves non-competitively. L: Activity demonstrated in a LMM PBP, H: Activity demonstrated in a HMM PBP E: Elongation phenotype was observed microscopically following treatment of bacteria: indicative of PBP3 inhibition¹⁵²; R: Crystallography reported, not found in the PDB; A: Crystallography attempted, but could not determine crystal structures with the inhibitor bound; +ve: gram-positive activity; -ve: gram-negative activity; BLI: β -lactamase Inhibitor; S: β -lactamase susceptible (w) weak.

1.4.6 PBP Assays

In order to quantitatively assess the ability of a compound to bind to PBPs, assays are required. The assays reported for investigation of PBPs are listed in Table 1.2 and the structures of the probes in Figure 1.5. Early investigation of PBPs and the binding affinities of various β -lactams were typically carried out with radiolabelled analogues of important β -lactams. When run on a gel, these reagents could give a picture of the affinity of all the PBPs in a membrane preparation for a given β -lactam^{152,334}. Alternatively, the binding of a radiolabeled probe β -lactam to a purified enzyme can be used to find the kinetics of an individual protein: β -lactam interaction, and by extension the kinetics of a competing ligand³¹⁵.

Assay	β -lactam-based probe In gram-negative Class B PBPs Practicality			Methodology	Advantages	Disadvantages	References
Radio-labelled β -lactams	Y	Y	-	Radiolabelled analogues of various β -lactams are used to bind to PBPs which are then separated either on a gel and imaged using photographic paper or by filter then measured by scintillation	<ul style="list-style-type: none"> - Chemically (but not physically) identical analogues of β-lactams can be used, minimising artefacts. - Membrane preparations allow the observation of many PBPs simultaneously - Can be used in a microplate assay format 	<ul style="list-style-type: none"> - Long exposures times required (days to weeks) to develop signal - Health and safety concerns when handling radioactive substances - End point assay - Generally low throughput 	A
Nitrocefin and CENTA	Y	Y	++	Reaction of nitrocefin/CENTA with a PBP leads to a colour change that is detected in absorbance spectrophotometry	<ul style="list-style-type: none"> - Quick and easy assay - Good sensitivity of signal - Continuous assay 	<ul style="list-style-type: none"> - Non-clinical β-lactam, results may not be relevant to all β-lactams - Substrate turnover not observed for all enzymes - Coloured inhibitors can interfere 	B
Bocillin FL fluorescence anisotropy	Y	Y	++	Reaction of bocillin FL with a PBP can be measured by a change in the rate of rotation of the fluorophore, as determined by polarisation of fluorescent light	<ul style="list-style-type: none"> - Quick and easy assay - Good sensitivity of signal - Continuous assay - Most PBPs acylated - Very little protein consumed - Can observe acylation and de-acylation separately - Little interference from coloured compounds 	<ul style="list-style-type: none"> - Presence of large fluorophore may affect normal β-lactam kinetics - Assay interference if aggregation occurs - Indirect substrate-concentration relationship 	C
Bocillin-labelled β -lactams in SDS-PAGE gels	Y	Y	+	Bocillin binds to PBPs which are then run on an SDS-PAGE gel and imaged using a scanning fluorescence imager. Quantification possible by densitometry	<ul style="list-style-type: none"> - Membrane preparations allow the observation of many PBPs simultaneously - Direct substrate-concentration relationship - Less prone to interference than bocillin anisotropy 	<ul style="list-style-type: none"> - End point assay - Presence of large fluorophore may affect normal β-lactam kinetics - Quantification can be a challenge - Low throughput 	D
Biotinylated β -lactams	Y	Y	-	Biotinylated β -lactams bind to PBPs, which are then quantified using a streptavidin-conjugated horseradish peroxidase (HRP) and a fluorescent, oxidised substrate	<ul style="list-style-type: none"> - Has been developed into a high throughput assay - Good sensitivity of signal 	<ul style="list-style-type: none"> - End point assay - Presence of large fluorophore may affect normal β-lactam kinetics - Requires multiple wash steps 	E
S2d thioester substrate	N	Y	++	Thioester substrate can react with the PBP, releasing a free thiol which is detected by an absorbance or fluorescence coupling reagent	<ul style="list-style-type: none"> - Supposedly mimics the transpeptidase reaction (amino acids can be used as "acceptor substrates" to accelerate de-acylation) - Quick and easy assay - Good sensitivity of signal - Continuous assay - Non-β-lactam probe 	<ul style="list-style-type: none"> - Not all PBPs can process the substrate- some prohibitively slow 	F

Intrinsic fluorescence	N	Y	+	Changes in the electronic environment near a tryptophan caused by ligand interaction can be measured as changes in its intrinsic UV fluorescence	<ul style="list-style-type: none"> - Label free - Rapid if coupled to stopped flow apparatus 	<ul style="list-style-type: none"> - Requires a tryptophan near the active site - Requires UV fluorometer - Not suitable for high throughput - Large amounts of protein required 	G
Mass spectrometry (MS)	N	Y	--	A β -lactams are reacted with PBP's in a quenched flow system then denatured and analysed by MS	<ul style="list-style-type: none"> - Very small time step resolution possible - Can monitor acylation and de-acylation separately and quantitatively - Label free - Tryptic MS can find the location of covalent attachment 	<ul style="list-style-type: none"> - Only works for covalent binders - Large protein consumption - Expensive equipment required 	H
Surface Plasmon Resonance	N	N	--	Changes in the optical properties of a thin layer of metal are observed to change if an analyte binds to proteins which are bound to the metal's surface.	<ul style="list-style-type: none"> - Can observe acylation and de-acylation events - Microfluidics gives excellent control over timing - Sensitive to weak, non-covalent binders, anywhere on the protein - Label free 	<ul style="list-style-type: none"> - Very challenging to set up: requiring various protein coupling chemistries - Sensitive to non-specific binders 	I
Thermodynamic analysis by reversible denaturation	N	N	+	Free energies of unfolding the β -lactam-acylated or apo forms of a PBP can be used to determine the non-covalent contributions to the binding of a β -lactam. Determined using circular dichroism.	<ul style="list-style-type: none"> - Gives thermodynamic details about the hydrogen bonding network of an inhibitor and its interactions with the protein 	<ul style="list-style-type: none"> - Non-kinetic - Requires a reversibly folding protein- some PBP's appear to aggregate upon heating 	J
Thermal shift assay	N	Y	++	An environment-sensitive hydrophobic fluorescent probe, SYPRO orange is used to indicate the degree of exposure of hydrophobic regions within the protein as it is thermally denatured	<ul style="list-style-type: none"> - Quick and easy assay - Can detect binding beyond the active site 	<ul style="list-style-type: none"> - Generally non-kinetic (although complex kinetic protocols are available) - Not all ligands change the protein stability 	K
Natural substrate assays	N	N	-	Release of D-ala from the natural substrate of a PBP by the transpeptidase reaction is used generate a fluorescent signal through coupled reaction of D-ala oxidase and HRP	<ul style="list-style-type: none"> - Mimics the true functioning of PBP's - May be able to identify, non-active site inhibitors that have physiological relevance - Could be used to understand the natural functions of PBP's 	<ul style="list-style-type: none"> - Precursors for this reaction are challenging to make - Has not been reported to date for a class B enzyme, only in a class A, coupled with transglycosylation 	L

Table 1.2. Assays used for the identification and classification of Class B PBP binding agents References: A ^{152,315,335}, B ^{329,336-339}, C ^{163,318,340}, D ^{227,325,340}, E

341-343, F ^{168,200,291,321}, G ^{180,200}, H ^{179,344}, I ^{291,345,346}, J ²⁰⁴, K ^{179,347}, L ³⁴⁸. Abbreviations: Y: Yes; N: No; Practicality: a qualitative scale from challenging (-) to simple (++), which aims to encompass the cost of the equipment and reagents for the assay, technical skill required to use it, and time taken to run the assay. For example, mass spectrometry assays score "-" due to the high cost of the instrument, whilst nitrocefin scores "++" as it requires only a common benchtop plate reader and cheap, readily available reagents.

Later, fluorescent probes which are easier to handle, were developed ^{163,318,340}, which can be used to stain PBPs in membrane extracts in an analogous fashion and with similar results to the radiolabelled probes ³⁴⁰. This method does not allow for continuous observations of the reaction.

Because the fluorescence intensity does not typically change following acylation, the fluorescent anisotropy method is used to differentiate between the bound and unbound states ^{163,340}. The theory behind fluorescence anisotropy has been understood since the 1920s ³⁴⁹, but the first plate reader based instruments were only designed in the mid 1990's, leading to a "burst" of research activity, resulting in many assays exploiting this method ³⁵⁰. Figure 1.5b and c give a simplified overview of the physical aspects of the process. At the simplest level, the binding of BOCILLIN FL to a larger molecule slows its rotation and this is measured by the intensities of the parallel and perpendicular emitted light.

a

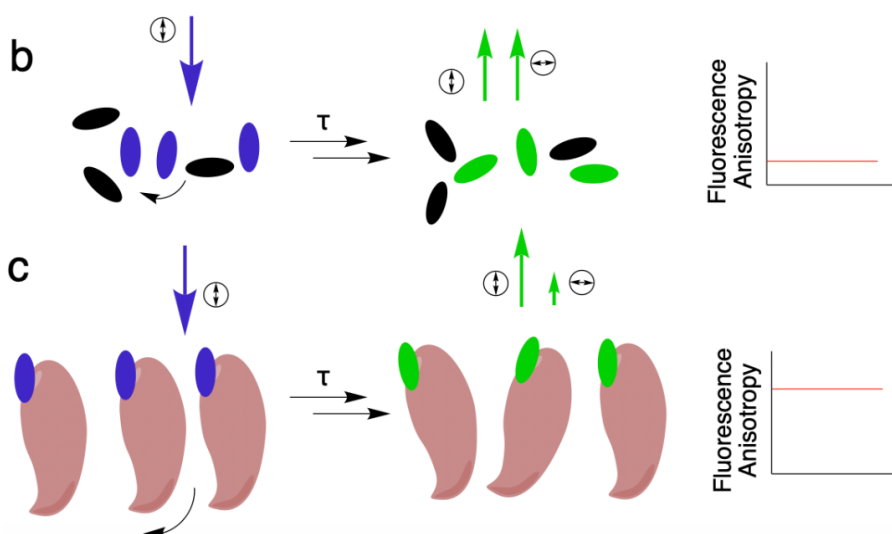
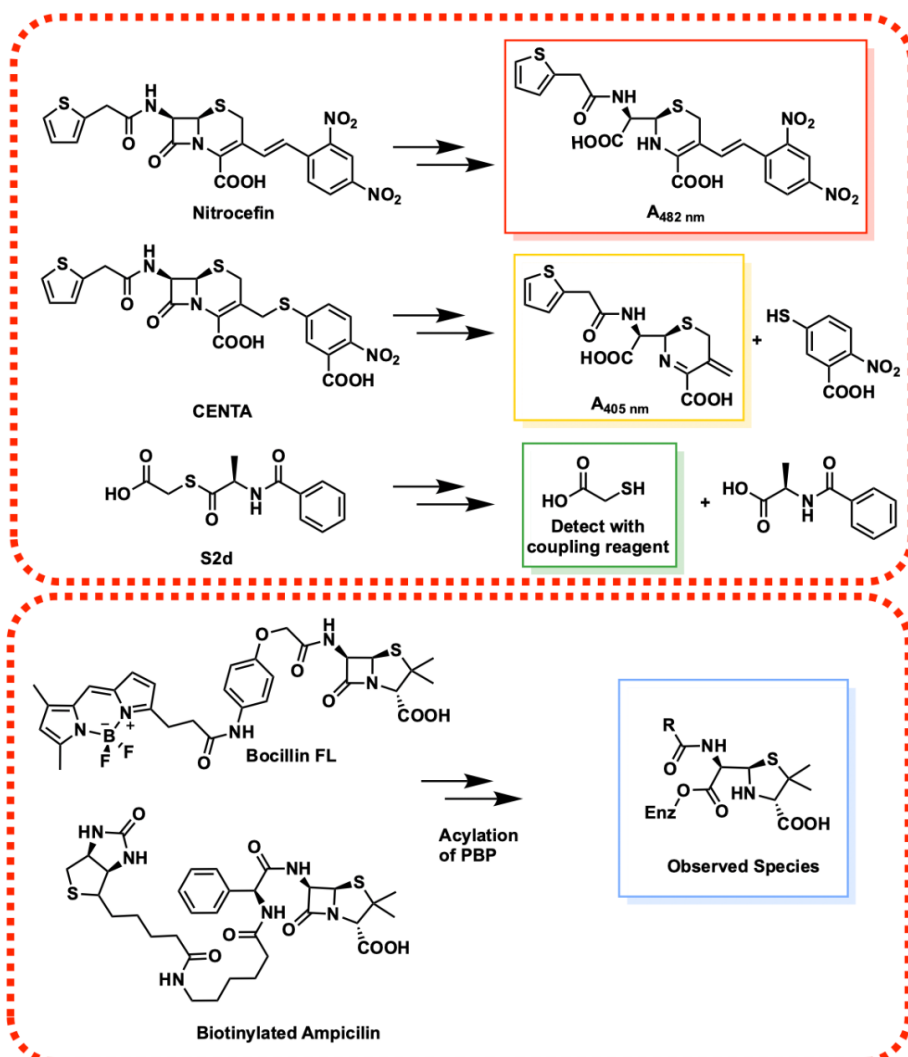


Figure 1.5. Chemical probes for the behaviour of PBPs. (a) Chemical structures of some of the probes used in Table 1.2. The reaction that produces the observable change is shown. Release of the 2-mercaptoacetic acid leaving group of S2d can be monitored by absorbance³²⁶ or fluorescence²⁹¹ of coupling agents, or by direct observation of the change in absorbance at 250 nm due to the cleavage of the thioester^{168,200}. (b and c) Simplified scheme describing fluorescence anisotropy (or fluorescence polarisation). (b) Fluorophores (ovals) are randomly orientated in solution, with those orientated parallel to the polarised incident light excited by it (cyan), those that are not parallel (black) are not excited. Excited fluorophores emit light (green) after their average fluorescence lifetime τ . After time τ the fluorophores will have randomly rotated due to Brownian motion of the solution. If the speed of rotation is much greater than τ (as it is for small BOCILLIN FL molecules) emitted light from the solution has no overall polarisation, due to the randomness of the orientations of the excited molecules. The fluorescence anisotropy of the sample is correspondingly low. (c) In this case, molecules of fluorophore are bound to a much larger molecule (as would be the case for BOCILLIN FL binding to PBP3). Only molecules starting parallel to the polarisation of the incident light are shown. Now, in the time interval τ , much less rotation of the fluorophore has occurred because larger molecules rotate more slowly due to Brownian motion. Emitted light will therefore have a larger component polarised parallel to the polarisation of the incident light and the fluorescence anisotropy signal will be greater.

Biochemically, CENTA, nitrocefin and S2d behave quite similarly. The ligand is turned over by the PBP and released to give a change in absorbance that is monitored by a spectrophotometer. The species responsible for the colour changes are shown in Figure 1.5a. PBP3 from *P. aeruginosa* turns over these substrates rapidly, faster than related class B PBPs (Chapter 6). The kinetics of nitrocefin and CENTA are discussed in more detail in Chapter 6.

There are no assays that accurately utilise the natural product of class B PBPs, leaving open questions as to its exact mechanism in nature. A recent paper investigating natural product turnover in class A PBPs showed there were few chemical recognition elements required by the donor substrate (left hand side of Figure 1.2b) and even fewer specifying the characteristics of the acceptor nucleophile (right hand side nucleophile in Figure 1.2b)³⁴⁸. Functional assays are important because assays that rely on β -lactam probes may miss novel classes of compounds with functional inhibitory activity against PBPs (i.e. can disrupt the binding of the natural substrate), but which do not affect the acylation of β -lactams (or probes like S2d).

Mass spectrometry methods can provide label free, very short time scale (if combined with quenched flow) insight into the behaviour of covalent binders of PBPs^{179,344}. This has been used to find the acylation rates of PBPs by β -lactams,

without the need for a competing substrate^{202,344}. If a protein is covalently bound to an inhibitor and then digested by proteases such as trypsin, the masses of the resultant peptides can be analysed to find the location of the acylation³⁵¹. These techniques are investigated in Chapter 6.

Chapter 2 covers SPR in more detail.

Thermodynamic methods, investigating the effect of the ligand binding on protein stability are useful for understanding the *EI* complex, but provide little kinetic information. For β -lactams, it has been shown that the non-covalent components of the active site interactions contribute little to the overall acylation efficiency²⁰⁴.

Each of the techniques shown in Table 1.2 has its own advantages and often a combination of multiple methods is the best approach, and gives the broadest insight into the problem (Chapters 5 and 6).

1.5 Conclusions

The successful use of antimicrobials allows for much of modern medicine, but antimicrobial resistance can render them useless. Like fire extinguishers, we do not appreciate the value of antimicrobials until we no longer have access to them in an emergency. Better policy and incentives are required to ensure future generations have access to these essential medicines. The threat of resistance necessitates constant discovery of new compounds whilst low sales volumes and the need to keep drugs as a “last line of defense” disincentivises companies from investing in research. At the same time, data from pharmaceutical companies appears to show that discovery of good antimicrobials is more scientifically challenging than discovery drugs for other therapeutic areas.

Inhibition of PBPs is a well-validated antibacterial approach but β -lactams, the only drugs to target them, are increasingly subject to resistance that threatens their efficacy. Other classes of compounds have been shown to bind and inhibit PBPs but none with the efficacy of the β -lactams. As such, the employment of new methods may yet lead to effective new inhibitor classes. This thesis describes the development of tools for drug discovery, insight into PBP3-mediated mechanisms of

resistance and two examples of previously undescribed PBP inhibitor binding modes.

1.6 References

- 1 Rex J. New Antibiotics Development | Newsletter by John Rex | AMR Solutions. John H Rex MD. <https://amr.solutions/> (accessed 5 Oct2020).
- 2 Bowater RJ, Stirling SA, Lilford RJ. Is antibiotic prophylaxis in surgery a generally effective intervention? Testing a generic hypothesis over a set of meta-analyses. *Ann Surg* 2009; **249**: 551–556.
- 3 Bow EJ. Fluoroquinolones, antimicrobial resistance and neutropenic cancer patients: *Curr Opin Infect Dis* 2011; **24**: 545–553.
- 4 NICE Summary of antimicrobial prescribing. Summ. Antimicrob. Prescr. Guid. – Manag. Common Infect. <https://www.nice.org.uk/Media/Default/About/what-we-do/NICE-guidance/antimicrobial%20guidance/summary-antimicrobial-prescribing-guidance.pdf>. Accessed 05/10/20.
- 5 Munita JM, Arias CA. Mechanisms of Antibiotic Resistance. *Microbiol Spectr* 2016; **4**. doi:10.1128/microbiolspec.VMBF-0016-2015.
- 6 Wright G. Mechanisms of resistance to antibiotics. *Curr Opin Chem Biol* 2003; **7**: 563–569.
- 7 D’Costa VM, King CE, Kalan L, Morar M, Sung WWL, Schwarz C *et al*. Antibiotic resistance is ancient. *Nature* 2011; **477**: 457–461.
- 8 Perry J, Waglechner N, Wright G. The Prehistory of Antibiotic Resistance. *Cold Spring Harb Perspect Med* 2016; **6**: a025197.
- 9 Kobayashi T, Nonaka L, Maruyama F, Suzuki S. Molecular Evidence for the Ancient Origin of the Ribosomal Protection Protein That Mediates Tetracycline Resistance in Bacteria. *J Mol Evol* 2007; **65**: 228–235.
- 10 Waglechner N, Wright GD. Antibiotic resistance: it’s bad, but why isn’t it worse? *BMC Biol* 2017; **15**: 84.
- 11 Coates AR, Halls G, Hu Y. Novel classes of antibiotics or more of the same?: New antibiotic classes are urgently needed. *Br J Pharmacol* 2011; **163**: 184–194.
- 12 Kinch MS, Haynesworth A, Kinch SL, Hoyer D. An overview of FDA-approved new molecular entities: 1827–2013. *Drug Discov Today* 2014; **19**: 1033–1039.
- 13 Dr Tedros Adhanom Ghebreyesus. WHO Director-General opening remarks at the AMR Action Fund Launch. World Health Organization, 2020 <https://www.who.int/director-general/speeches/detail/who-director-general-opening-remarks-at-the-amr-action-fund-launch>. Accessed 29/12/20.
- 14 Ehrlich P, Hata S. *Die experimentelle chemotherapie der Spirillosen*. Springer, 1910.
- 15 Aminov RI. A Brief History of the Antibiotic Era: Lessons Learned and Challenges for the Future. *Front Microbiol* 2010; **1**. doi:10.3389/fmicb.2010.00134.
- 16 Domagk G. Ein Beitrag zur Chemotherapie der bakteriellen Infektionen. *DMW - Dtsch Med Wochenschr* 1935; **61**: 250–253.
- 17 Connor EE. Sulfonamide antibiotics. *Prim Care Update OBGYNS* 1998; **5**: 32–35.
- 18 Organization WH. WHO model list of essential medicines, 20th list (March 2017, amended August 2017). World Health Organization, 2017.
- 19 Fleming A. On the antibacterial action of cultures of a penicillium, with special reference to their use in the isolation of *B. influenzae*. *Br J Exp Pathol* 1929;

- 10: 226.
- 20 Chain E, Florey HW, Gardner AD, Heatley NG, Jennings MA, Orr-Ewing J *et al*. THE CLASSIC: Penicillin as a Chemotherapeutic Agent: *Clin Orthop* 2005; **439**: 23–26.
- 21 Livermore DM. Antimicrobial Drugs: Chronicle of a Twentieth Century Medical Triumph. *J Antimicrob Chemother* 2009; **63**: 1086–1086.
- 22 Quinn R. Rethinking antibiotic research and development: World War II and the penicillin collaborative. *Am J Public Health* 2013; **103**: 426–434.
- 23 Gould K. Antibiotics: from prehistory to the present day. *J Antimicrob Chemother* 2016; **71**: 572–575.
- 24 Hotchkiss D, Dubos J. THE ISOLATION OF BACTERICIDAL SUBSTANCES FROM CULTURES OF BACILLUS BREVIS..
- 25 Schatz A, Bugle E, Waksman SA. Streptomycin, a Substance Exhibiting Antibiotic Activity Against Gram-Positive and Gram-Negative Bacteria.*. *Exp Biol Med* 1944; **55**: 66–69.
- 26 Hinshaw HC, Pyle MM, Feldman WH. Streptomycin in tuberculosis. *Am J Med* 1947; **2**: 429–435.
- 27 BALDRY P. *The Battle Against Bacteria. A Fresh Look*. Zeitschrift für allgemeine Mikrobiologie, 1979<http://doi.wiley.com/10.1002/jobm.19790190611>. Accessed 12/10/20
- 28 Walsh C, Wencewicz TA. *Antibiotics: challenges, mechanisms, opportunities*. ASM Press: Washington, DC, 2016.
- 29 Bisacchi GS. Origins of the Quinolone Class of Antibacterials: An Expanded “Discovery Story”: Miniperspective. *J Med Chem* 2015; **58**: 4874–4882.
- 30 Leshner GY, Froelich EJ, Gruett MD, Bailey JH, Brundage RP. 1, 8-Naphthyridine derivatives. A new class of chemotherapeutic agents. *J Med Chem* 1962; **5**: 1063–1065.
- 31 Slee AM, Wuonola MA, McRipley RJ, Zajac I, Zawada MJ, Bartholomew PT *et al*. Oxazolidinones, a new class of synthetic antibacterial agents: in vitro and in vivo activities of DuP 105 and DuP 721. *Antimicrob Agents Chemother* 1987; **31**: 1791–1797.
- 32 Silver L, Bostian K. Screening of natural products for antimicrobial agents. *Eur J Clin Microbiol Infect Dis* 1990; **9**: 455–461.
- 33 Strominger JL, Willoughby E, Kamiyo T, Blumberg PM, Yocum RR. PENICILLIN-SENSITIVE ENZYMES AND PENICILLIN-BINDING COMPONENTS IN BACTERIAL CELLS. *Ann N Y Acad Sci* 1974; **235**: 210–224.
- 34 Lewis K. Recover the lost art of drug discovery. *Nature* 2012; **485**: 439–440.
- 35 Silver LL. Appropriate Targets for Antibacterial Drugs. *Cold Spring Harb Perspect Med* 2016; **6**: a030239.
- 36 Pew Trusts. Tracking the Global Pipeline of Antibiotics in Development, April 2020. <https://pew.org/2UCFs46>. Accessed 29/12/20.
- 37 Hoffman SJ, Outtersen K. What Will it Take to Address the Global Threat of Antibiotic Resistance? *J Law Med Ethics* 2015; **43**: 363–368.
- 38 O'Neill J. TACKLING DRUG-RESISTANT INFECTIONS GLOBALLY: FINAL REPORT AND RECOMMENDATIONS. 2016.<https://amr-review.org/Publications.html>. Accessed 05/10/20.
- 39 Frost I, Craig J, Joshi J, Faure K, Laxminarayan R. Access Barriers to Antibiotics. 2019. https://cddep.org/wp-content/uploads/2019/04/AccessBarrierstoAntibiotics_CDDEP_FINAL.pdf. Accessed 12/10/20.
- 40 Daulaire N, Bang A, Tomson G, Kalyango JN, Cars O. Universal Access to Effective Antibiotics is Essential for Tackling Antibiotic Resistance. *J Law Med Ethics* 2015; **43**: 17–21.
- 41 Scott HM, Acuff G, Bergeron G, Bourassa MW, Gill J, Graham DW *et al*.

- Critically important antibiotics: criteria and approaches for measuring and reducing their use in food animal agriculture. *Ann N Y Acad Sci* 2019; **1441**: 8–16.
- 42 Baquero F, Martínez J-L, Cantón R. Antibiotics and antibiotic resistance in water environments. *Curr Opin Biotechnol* 2008; **19**: 260–265.
 - 43 Hollis A, Maybarduk P. Antibiotic Resistance is a Tragedy of the Commons That Necessitates Global Cooperation. *J Law Med Ethics* 2015; **43**: 33–37.
 - 44 Ashworth M, White P, Jongsma H, Schofield P, Armstrong D. Antibiotic prescribing and patient satisfaction in primary care in England: cross-sectional analysis of national patient survey data and prescribing data. *Br J Gen Pract* 2016; **66**: e40–e46.
 - 45 Rex J, Krause K. All-In Cost Of A New Antibiotic From Discovery To 10 Years On Market. 2021. <https://amr.solutions/2021/01/09/all-in-cost-of-a-new-antibiotic-from-discovery-to-10-years-on-market/>. Accessed 19/01/21.
 - 46 Carr A, Stringer J, Shen J. Antibiotic and Antifungal Update: January 2020. 2020.
 - 47 Rex J. Mandatory reading: Alan Carr's Jan 2020 Antibacterial and Antifungal market review • John H. Rex, MD. John H Rex MD. 2020. <https://amr.solutions/2020/01/28/mandatory-reading-alan-carrs-jan-2020-antibacterial-and-antifungal-market-review/>. Accessed 12/10/20.
 - 48 Staff R. Antibiotics maker Melinta files for Chapter 11 bankruptcy. Reuters. 2019. <https://www.reuters.com/article/us-melinta-bankruptcy-idUSKBN1YV1AT>. Accessed 16/12/20.
 - 49 Mullard A. Achaogen bankruptcy highlights antibacterial development woes. *Nat Rev Drug Discov* 2019; **18**: 411–411.
 - 50 Årdal C, Lacotte Y, Ploy M-C. Financing Pull Mechanisms for Antibiotic-Related Innovation: Opportunities for Europe. *Clin Infect Dis* 2020; : ciaa153.
 - 51 Outtersen K, Rex JH. Evaluating for-profit public benefit corporations as an additional structure for antibiotic development and commercialization. *Transl Res* 2020; **220**: 182–190.
 - 52 Crabb N, Leonard C, Jennings G, Perkins M, Glover D. subscription-based payment model. ; : 44.
 - 53 Rome BN, Kesselheim AS. Transferrable Market Exclusivity Extensions to Promote Antibiotic Development: An Economic Analysis. *Clin Infect Dis* 2019; : ciz1039.
 - 54 Analytical Framework for Examining the Value of Antibacterial Products. ASPE. 2015. <https://aspe.hhs.gov/report/analytical-framework-examining-value-antibacterial-products>. Accessed 12/10/20.
 - 55 Barlam TF, Gupta K. Antibiotic Resistance Spreads Internationally across Borders. *J Law Med Ethics* 2015; **43**: 12–16.
 - 56 Hoffman SJ, Røttingen J-A, Frenk J. International Law Has a Role to Play in Addressing Antibiotic Resistance. *J Law Med Ethics J Am Soc Law Med Ethics* 2015; **43 Suppl 3**: 65–67.
 - 57 Hoffman SJ, Ottersen T. Addressing Antibiotic Resistance Requires Robust International Accountability Mechanisms. *J Law Med Ethics* 2015; **43**: 53–64.
 - 58 Andresen S, Hoffman SJ. Much Can Be Learned about Addressing Antibiotic Resistance from Multilateral Environmental Agreements. *J Law Med Ethics J Am Soc Law Med Ethics* 2015; **43 Suppl 3**: 46–52.
 - 59 Plackett B. Why big pharma has abandoned antibiotics. *Nature* 2020; **586**: S50–S52.
 - 60 Projan SJ. Why is big Pharma getting out of antibacterial drug discovery? *Curr Opin Microbiol* 2003; **6**: 427–430.
 - 61 Wellcome Trust. Clinical Trial Networks for Antibiotic-Development Wellcome.

- <https://wellcome.org/sites/default/files/clinical-trial-networks-for-antibiotic-development-wellcome-oct16.pdf>. Accessed 03/03/21.
- 62 Projan SJ, Shlaes DM. Antibacterial drug discovery: is it all downhill from here? *Clin Microbiol Infect* 2004; **10**: 18–22.
 - 63 Pereira DA, Williams JA. Origin and evolution of high throughput screening: Origin and circumscribed history of HTS. *Br J Pharmacol* 2007; **152**: 53–61.
 - 64 Fleischmann R, Adams M, White O, Clayton R, Kirkness E, Kerlavage A *et al.* Whole-genome random sequencing and assembly of *Haemophilus influenzae* Rd. *Science* 1995; **269**: 496–512.
 - 65 Chan PF, Holmes DJ, Payne DJ. Finding the gems using genomic discovery: antibacterial drug discovery strategies – the successes and the challenges. *Drug Discov Today Ther Strateg* 2004; **1**: 519–527.
 - 66 Payne DJ, Gwynn MN, Holmes DJ, Pompliano DL. Drugs for bad bugs: confronting the challenges of antibacterial discovery. *Nat Rev Drug Discov* 2007; **6**: 29–40.
 - 67 Tommasi R, Brown DG, Walkup GK, Manchester JI, Miller AA. ESKAPEing the labyrinth of antibacterial discovery. *Nat Rev Drug Discov* 2015; **14**: 529–542.
 - 68 Lewis K. Platforms for antibiotic discovery. *Nat Rev Drug Discov* 2013; **12**: 371–387.
 - 69 Dheman N, Mahoney N, Cox EM, Farley JJ, Amini T, Lanthier ML. An Analysis of Antibacterial Drug Development Trends in the United States, 1980–2019. *Clin Infect Dis* 2020; : ciaa859.
 - 70 O'Shea R, Moser HE. Physicochemical Properties of Antibacterial Compounds: Implications for Drug Discovery. *J Med Chem* 2008; **51**: 2871–2878.
 - 71 Silver LL. A Gestalt approach to Gram-negative entry. *Bioorg Med Chem* 2016; **24**: 6379–6389.
 - 72 Mugumbate G, Overington JP. The relationship between target-class and the physicochemical properties of antibacterial drugs. *Bioorg Med Chem* 2015; **23**: 5218–5224.
 - 73 Brown DG, May-Dracka TL, Gagnon MM, Tommasi R. Trends and Exceptions of Physical Properties on Antibacterial Activity for Gram-Positive and Gram-Negative Pathogens. *J Med Chem* 2014; **57**: 10144–10161.
 - 74 Lange R, Locher H, Wyss P, Then R. The Targets of Currently Used Antibacterial Agents: Lessons for Drug Discovery. *Curr Pharm Des* 2007; **13**: 3140–3154.
 - 75 Hughes D. Exploiting genomics, genetics and chemistry to combat antibiotic resistance. *Nat Rev Genet* 2003; **4**: 432–441.
 - 76 Brotzoesterhelt H, Brunner N. How many modes of action should an antibiotic have? *Curr Opin Pharmacol* 2008; **8**: 564–573.
 - 77 O'Dwyer K, Spivak AT, Ingraham K, Min S, Holmes DJ, Jakielaszek C *et al.* Bacterial Resistance to Leucyl-tRNA Synthetase Inhibitor GSK2251052 Develops during Treatment of Complicated Urinary Tract Infections. *Antimicrob Agents Chemother* 2015; **59**: 289–298.
 - 78 Singh SB, Young K, Silver LL. What is an “ideal” antibiotic? Discovery challenges and path forward. *Biochem Pharmacol* 2017; **133**: 63–73.
 - 79 Du D, Wang-Kan X, Neuberger A, van Veen HW, Pos KM, Piddock LJV *et al.* Multidrug efflux pumps: structure, function and regulation. *Nat Rev Microbiol* 2018; **16**: 523–539.
 - 80 Cama J, Henney AM, Winterhalter M. Breaching the Barrier: Quantifying Antibiotic Permeability across Gram-negative Bacterial Membranes. *J Mol Biol* 2019; **431**: 3531–3546.
 - 81 Richter MF, Drown BS, Riley AP, Garcia A, Shirai T, Svec RL *et al.* Predictive compound accumulation rules yield a broad-spectrum antibiotic. *Nature* 2017; **545**: 299–304.

- 82 Krishnamoorthy G, Leus IV, Weeks JW, Wolloscheck D, Rybenkov VV, Zgurskaya HI. Synergy between Active Efflux and Outer Membrane Diffusion Defines Rules of Antibiotic Permeation into Gram-Negative Bacteria. *mBio* 2017; **8**: mBio.01172-17, e01172-17.
- 83 Manchester JI, Buurman ET, Bisacchi GS, McLaughlin RE. Molecular Determinants of AcrB-Mediated Bacterial Efflux Implications for Drug Discovery. *J Med Chem* 2012; **55**: 2532–2537.
- 84 Bajaj H, Acosta Gutierrez S, Bodrenko I, Mallocci G, Scorciapino MA, Winterhalter M *et al.* Bacterial Outer Membrane Porins as Electrostatic Nanosieves: Exploring Transport Rules of Small Polar Molecules. *ACS Nano* 2017; **11**: 5465–5473.
- 85 Choi U, Lee C-R. Distinct Roles of Outer Membrane Porins in Antibiotic Resistance and Membrane Integrity in Escherichia coli. *Front Microbiol* 2019; **10**: 953.
- 86 Richter MF, Hergenrother PJ. The challenge of converting Gram-positive-only compounds into broad-spectrum antibiotics: Challenges in developing broad-spectrum antibiotics. *Ann N Y Acad Sci* 2019; **1435**: 18–38.
- 87 Perlmutter SJ, Geddes EJ, Drown BS, Motika SE, Lee MR, Hergenrother PJ. Compound Uptake into E. coli Can Be Facilitated by N-Alkyl Guanidiniums and Pyridiniums. *ACS Infect Dis* 2020; : acsinfecdis.0c00715.
- 88 Craig WA. State-of-the-Art Clinical Article: Pharmacokinetic/Pharmacodynamic Parameters: Rationale for Antibacterial Dosing of Mice and Men. *Clin Infect Dis* 1998; **26**: 1–10.
- 89 Drusano GL. Antimicrobial pharmacodynamics: critical interactions of 'bug and drug'. *Nat Rev Microbiol* 2004; **2**: 289–300.
- 90 Lodise TP, Sorgel F, Melnick D, Mason B, Kinzig M, Drusano GL. Penetration of Meropenem into Epithelial Lining Fluid of Patients with Ventilator-Associated Pneumonia. *Antimicrob Agents Chemother* 2011; **55**: 1606–1610.
- 91 Ambrose PG, Bhavnani SM, Ellis-Grosse EJ, Drusano GL. Pharmacokinetic-Pharmacodynamic Considerations in the Design of Hospital-Acquired or Ventilator-Associated Bacterial Pneumonia Studies: Look before You Leap! *Clin Infect Dis* 2010; **51**: S103–S110.
- 92 DeRyke CA, Young Lee S, Kuti JL, Nicolau DP. Optimising Dosing Strategies of Antibacterials Utilising Pharmacodynamic Principles: Impact on the Development of Resistance. *Drugs* 2006; **66**: 1–14.
- 93 Zhang L, Huang Y, Zhou Y, Buckley T, Wang HH. Antibiotic Administration Routes Significantly Influence the Levels of Antibiotic Resistance in Gut Microbiota. *Antimicrob Agents Chemother* 2013; **57**: 3659–3666.
- 94 Kouyos RD, Metcalf CJE, Birger R, Klein EY, Abel zur Wiesch P, Ankomah P *et al.* The path of least resistance: aggressive or moderate treatment? *Proc R Soc B Biol Sci* 2014; **281**: 20140566.
- 95 Olofsson SK, Cars O. Optimizing Drug Exposure to Minimize Selection of Antibiotic Resistance. *Clin Infect Dis* 2007; **45**: S129–S136.
- 96 Alexander HK, MacLean RC. Stochastic bacterial population dynamics restrict the establishment of antibiotic resistance from single cells. *Proc Natl Acad Sci* 2020; **117**: 19455–19464.
- 97 Liu Y-Y, Wang Y, Walsh TR, Yi L-X, Zhang R, Spencer J *et al.* Emergence of plasmid-mediated colistin resistance mechanism MCR-1 in animals and human beings in China: a microbiological and molecular biological study. *Lancet Infect Dis* 2016; **16**: 161–168.
- 98 Poirel L, Jayol A, Nordmann P. Polymyxins: Antibacterial Activity, Susceptibility Testing, and Resistance Mechanisms Encoded by Plasmids or Chromosomes. *Clin Microbiol Rev* 2017; **30**: 557–596.
- 99 Thomas CM, Nielsen KM. Mechanisms of, and Barriers to, Horizontal Gene Transfer between Bacteria. *Nat Rev Microbiol* 2005; **3**: 711–721.

- 100 Unemo M, Shafer WM. Antimicrobial Resistance in *Neisseria gonorrhoeae* in the 21st Century: Past, Evolution, and Future. *Clin Microbiol Rev* 2014; **27**: 587–613.
- 101 Lipsitch M. The rise and fall of antimicrobial resistance. *Trends Microbiol* 2001; **9**: 438–444.
- 102 Schaenzer AJ, Wright GD. Antibiotic Resistance by Enzymatic Modification of Antibiotic Targets. *Trends Mol Med* 2020; **26**: 768–782.
- 103 Bush K, Bradford PA. β -Lactams and β -Lactamase Inhibitors: An Overview. *Cold Spring Harb Perspect Med* 2016; **6**: a025247.
- 104 Wright GD. Aminoglycoside-modifying enzymes. *Curr Opin Microbiol* 1999; **2**: 499–503.
- 105 Bellini D, Koekemoer L, Newman H, Dowson CG. Novel and Improved Crystal Structures of *H. influenzae*, *E. coli* and *P. aeruginosa* Penicillin-Binding Protein 3 (PBP3) and *N. gonorrhoeae* PBP2: Toward a Better Understanding of β -Lactam Target-Mediated Resistance. *J Mol Biol* 2019; **431**: 3501–3519.
- 106 Zapun A, Contreras-Martel C, Vernet T. Penicillin-binding proteins and β -lactam resistance. *FEMS Microbiol Rev* 2008; **32**: 361–385.
- 107 Walsh CT, Fisher SL, Park IS, Prahalad M, Wu Z. Bacterial resistance to vancomycin: five genes and one missing hydrogen bond tell the story. *Chem Biol* 1996; **3**: 21–28.
- 108 Adrian PV, Klugman KP. Mutations in the dihydrofolate reductase gene of trimethoprim-resistant isolates of *Streptococcus pneumoniae*. *Antimicrob Agents Chemother* 1997; **41**: 2406–2413.
- 109 Wehrli W. Rifampin: Mechanisms of Action and Resistance. *Clin Infect Dis* 1983; **5**: S407–S411.
- 110 Zgurskaya HI, López CA, Gnanakaran S. Permeability Barrier of Gram-Negative Cell Envelopes and Approaches To Bypass It. *ACS Infect Dis* 2015; **1**: 512–522.
- 111 Silver LL. The Antibiotic Future. In: Fisher JF, Mobashery S, Miller MJ (eds). *Antibacterials*. Springer International Publishing: Cham, 2017, pp 31–67.
- 112 Organization WH. Prioritization of pathogens to guide discovery, research and development of new antibiotics for drug-resistant bacterial infections, including tuberculosis. World Health Organization, 2017.
- 113 Nikaido H. Prevention of drug access to bacterial targets: permeability barriers and active efflux. *Science* 1994; **264**: 382–388.
- 114 Andersson DI, Hughes D. Antibiotic resistance and its cost: is it possible to reverse resistance? *Nat Rev Microbiol* 2010; **8**: 260–271.
- 115 Vincent LR, Kerr SR, Tan Y, Tomberg J, Ratterman EL, Dunning Hotopp JC et al. In Vivo-Selected Compensatory Mutations Restore the Fitness Cost of Mosaic penA Alleles That Confer Ceftriaxone Resistance in *Neisseria gonorrhoeae*. *mBio* 2018; **9**. doi:10.1128/mBio.01905-17.
- 116 Schulz zur Wiesch P, Engelstadter J, Bonhoeffer S. Compensation of Fitness Costs and Reversibility of Antibiotic Resistance Mutations. *Antimicrob Agents Chemother* 2010; **54**: 2085–2095.
- 117 Maisnier-Patin S, Andersson DI. Adaptation to the deleterious effects of antimicrobial drug resistance mutations by compensatory evolution. *Res Microbiol* 2004; **155**: 360–369.
- 118 van Duijn PJ, Verbrugghe W, Jorens PG, Spöhr F, Schedler D, Deja M et al. The effects of antibiotic cycling and mixing on antibiotic resistance in intensive care units: a cluster-randomised crossover trial. *Lancet Infect Dis* 2018; **18**: 401–409.
- 119 Brown EM, Nathwani D. Antibiotic cycling or rotation: a systematic review of the evidence of efficacy. *J Antimicrob Chemother* 2005; **55**: 6–9.
- 120 Coates ARM, Hu Y, Holt J, Yeh P. Antibiotic combination therapy against resistant bacterial infections: synergy, rejuvenation and resistance reduction.

- Expert Rev Anti Infect Ther* 2020; **18**: 5–15.
- 121 Qureshi ZA, Paterson DL, Potoski BA, Kilayko MC, Sandovsky G, Sordillo E *et al.* Treatment Outcome of Bacteremia Due to KPC-Producing *Klebsiella pneumoniae*: Superiority of Combination Antimicrobial Regimens. *Antimicrob Agents Chemother* 2012; **56**: 2108–2113.
 - 122 Barbosa C, Beardmore R, Schulenburg H, Jansen G. Antibiotic combination efficacy (ACE) networks for a *Pseudomonas aeruginosa* model. *PLOS Biol* 2018; **16**: e2004356.
 - 123 Sun W, Weingarten RA, Xu M, Southall N, Dai S, Shinn P *et al.* Rapid antimicrobial susceptibility test for identification of new therapeutics and drug combinations against multidrug-resistant bacteria. *Emerg Microbes Infect* 2016; **5**: 1–11.
 - 124 Singh SB, Young K, Miesel L. Screening strategies for discovery of antibacterial natural products. *Expert Rev Anti Infect Ther* 2011; **9**: 589–613.
 - 125 Ling LL, Schneider T, Peoples AJ, Spoering AL, Engels I, Conlon BP *et al.* A new antibiotic kills pathogens without detectable resistance. *Nature* 2015; **517**: 455–459.
 - 126 Shukla R, Medeiros-Silva J, Parmar A, Vermeulen BJA, Das S, Paioni AL *et al.* Mode of action of teixobactins in cellular membranes. *Nat Commun* 2020; **11**: 2848.
 - 127 French S, Ellis MJ, Coutts BE, Brown ED. Chemical genomics reveals mechanistic hypotheses for uncharacterized bioactive molecules in bacteria. *Curr Opin Microbiol* 2017; **39**: 42–47.
 - 128 Schenone M, Dančik V, Wagner BK, Clemons PA. Target identification and mechanism of action in chemical biology and drug discovery. *Nat Chem Biol* 2013; **9**: 232–240.
 - 129 Farha MA, Brown ED. Unconventional screening approaches for antibiotic discovery: Unconventional approaches for antibiotic discovery. *Ann N Y Acad Sci* 2015; **1354**: 54–66.
 - 130 Nozaki U, Kawashima F, Imada A. C-19393 S2 and H2, new carbapenem antibiotics. III. Mode of action. *J Antibiot (Tokyo)* 1981; **34**: 206–211.
 - 131 Lovering F, Bikker J, Humblet C. Escape from Flatland: Increasing Saturation as an Approach to Improving Clinical Success. *J Med Chem* 2009; **52**: 6752–6756.
 - 132 Schreiber SL. Target-Oriented and Diversity-Oriented Organic Synthesis in Drug Discovery. *Science* 2000; **287**: 1964–1969.
 - 133 Ruddigkeit L, van Deursen R, Blum LC, Reymond J-L. Enumeration of 166 Billion Organic Small Molecules in the Chemical Universe Database GDB-17. *J Chem Inf Model* 2012; **52**: 2864–2875.
 - 134 Bradley AR, Echalié A, Fairhead M, Strain-Damerell C, Brennan P, Bullock AN *et al.* The SGC beyond structural genomics: redefining the role of 3D structures by coupling genomic stratification with fragment-based discovery. *Essays Biochem* 2017; **61**: 495–503.
 - 135 Erlanson DA, McDowell RS, O'Brien T. Fragment-Based Drug Discovery. *J Med Chem* 2004; **47**: 3463–3482.
 - 136 Lipinski CA, Lombardo F, Dominy BW, Feeney PJ. Experimental and computational approaches to estimate solubility and permeability in drug discovery and development settings. *Adv Drug Deliv Rev* 1997; **23**: 3–25.
 - 137 Congreve M, Carr R, Murray C, Jhoti H. A 'Rule of Three' for fragment-based lead discovery? *Drug Discov Today* 2003; **8**: 876–877.
 - 138 Hann MM, Leach AR, Harper G. Molecular Complexity and Its Impact on the Probability of Finding Leads for Drug Discovery. *J Chem Inf Comput Sci* 2001; **41**: 856–864.
 - 139 Cox OB, Krojer T, Collins P, Monteiro O, Talon R, Bradley A *et al.* A poised fragment library enables rapid synthetic expansion yielding the first reported

- inhibitors of PHIP(2), an atypical bromodomain. *Chem Sci* 2016; **7**: 2322–2330.
- 140 Pearce NM, Krojer T, Bradley AR, Collins P, Nowak RP, Talon R *et al.* A multi-crystal method for extracting obscured crystallographic states from conventionally uninterpretable electron density. *Nat Commun* 2017; **8**: 15123.
 - 141 Kidd SL, Fowler E, Reinhardt T, Compton T, Mateu N, Newman H *et al.* Demonstration of the utility of DOS-derived fragment libraries for rapid hit derivatisation in a multidirectional fashion. *Chem Sci* 2020; **11**: 10792–10801.
 - 142 Murray CW, Rees DC. The rise of fragment-based drug discovery. *Nat Chem* 2009; **1**: 187–192.
 - 143 Erlanson DA, Fesik SW, Hubbard RE, Jahnke W, Jhoti H. Twenty years on: the impact of fragments on drug discovery. *Nat Rev Drug Discov* 2016; **15**: 605–619.
 - 144 Basarab GS, Manchester JI, Bist S, Boriack-Sjodin PA, Dangel B, Illingworth R *et al.* Fragment-to-Hit-to-Lead Discovery of a Novel Pyridylurea Scaffold of ATP Competitive Dual Targeting Type II Topoisomerase Inhibiting Antibacterial Agents. *J Med Chem* 2013; **56**: 8712–8735.
 - 145 Duncan LF, Wang G, Ilyichova OV, Scanlon MJ, Heras B, Abbott BM. The Fragment-Based Development of a Benzofuran Hit as a New Class of *Escherichia coli* DsbA Inhibitors. *Molecules* 2019; **24**: 3756.
 - 146 Sauvage E, Kerff F, Terrak M, Ayala JA, Charlier P. The penicillin-binding proteins: structure and role in peptidoglycan biosynthesis. *FEMS Microbiol Rev* 2008; **32**: 234–258.
 - 147 Sun X, Gulliford MC. Reducing antibiotic prescribing in primary care in England from 2014 to 2017: population-based cohort study. *BMJ Open* 2019; **9**: e023989.
 - 148 Silhavy TJ, Kahne D, Walker S. The bacterial cell envelope. *Cold Spring Harb Perspect Biol* 2010; **2**: a000414.
 - 149 Huang KC, Mukhopadhyay R, Wen B, Gitai Z, Wingreen NS. Cell shape and cell-wall organization in Gram-negative bacteria. *Proc Natl Acad Sci* 2008; **105**: 19282–19287.
 - 150 Leclercq S, Derouaux A, Olatunji S, Fraipont C, Egan AJF, Vollmer W *et al.* Interplay between Penicillin-binding proteins and SEDS proteins promotes bacterial cell wall synthesis. *Sci Rep* 2017; **7**: 43306.
 - 151 Denome SA, Elf PK, Henderson TA, Nelson DE, Young KD. *Escherichia coli* mutants lacking all possible combinations of eight penicillin binding proteins: viability, characteristics, and implications for peptidoglycan synthesis. *J Bacteriol* 1999; **181**: 3981–3993.
 - 152 Spratt BG. Distinct penicillin binding proteins involved in the division, elongation, and shape of *Escherichia coli* K12. *Proc Natl Acad Sci U S A* 1975; **72**: 2999–3003.
 - 153 Ghuysen JM. Serine Beta-Lactamases and Penicillin-Binding Proteins. *Annu Rev Microbiol* 1991; **45**: 37–67.
 - 154 Goffin C, Ghuysen JM. Multimodular penicillin-binding proteins: an enigmatic family of orthologs and paralogs. *Microbiol Mol Biol Rev MMBR* 1998; **62**: 1079–1093.
 - 155 Heijenoort J v. Formation of the glycan chains in the synthesis of bacterial peptidoglycan. *Glycobiology* 2001; **11**: 25R–36R.
 - 156 Barreteau H, Kovač A, Boniface A, Sova M, Gobec S, Blanot D. Cytoplasmic steps of peptidoglycan biosynthesis. *FEMS Microbiol Rev* 2008; **32**: 168–207.
 - 157 Bouhss A, Trunkfield AE, Bugg TDH, Mengin-Lecreux D. The biosynthesis of peptidoglycan lipid-linked intermediates. *FEMS Microbiol Rev* 2008; **32**: 208–233.
 - 158 Lovering AL, de Castro LH, Lim D, Strynadka NCJ. Structural Insight into the Transglycosylation Step of Bacterial Cell-Wall Biosynthesis. *Science* 2007;

- 315:** 1402–1405.
- 159 Taguchi A, Welsh MA, Marmont LS, Lee W, Sjodt M, Kruse AC *et al.* FtsW is a peptidoglycan polymerase that is functional only in complex with its cognate penicillin-binding protein. *Nat Microbiol* 2019; **4**: 587–594.
 - 160 Meeske AJ, Riley EP, Robins WP, Uehara T, Mekalanos JJ, Kahne D *et al.* SEDS proteins are a widespread family of bacterial cell wall polymerases. *Nature* 2016; **537**: 634–638.
 - 161 Vollmer W, Blanot D, De Pedro MA. Peptidoglycan structure and architecture. *FEMS Microbiol Rev* 2008; **32**: 149–167.
 - 162 Tipper DJ, Strominger JL. Mechanism of action of penicillins: a proposal based on their structural similarity to acyl-D-alanyl-D-alanine. *Proc Natl Acad Sci* 1965; **54**: 1133–1141.
 - 163 Shapiro AB, Gu R-F, Gao N, Livchak S, Thresher J. Continuous fluorescence anisotropy-based assay of BOCILLIN FL penicillin reaction with penicillin binding protein 3. *Anal Biochem* 2013; **439**: 37–43.
 - 164 Vu H, Nikaido H. Role of beta-lactam hydrolysis in the mechanism of resistance of a beta-lactamase-constitutive *Enterobacter cloacae* strain to expanded-spectrum beta-lactams. *Antimicrob Agents Chemother* 1985; **27**: 393–398.
 - 165 Buddelmeijer N, Beckwith J. Assembly of cell division proteins at the *E. coli* cell center. *Curr Opin Microbiol* 2002; **5**: 553–557.
 - 166 Vicente M, Gomez MJ, Ayala JA. Regulation of transcription of cell division genes in the *Escherichia coli* *dcw* cluster. *Cell Mol Life Sci CMLS* 1998; **54**: 317–324.
 - 167 Mercer KLN, Weiss DS. The *Escherichia coli* Cell Division Protein FtsW Is Required To Recruit Its Cognate Transpeptidase, FtsI (PBP3), to the Division Site. *J Bacteriol* 2002; **184**: 904–912.
 - 168 Adam M, Fraipont C, Rhazi N, Nguyen-Distèche M, Lakaye B, Frère JM *et al.* The bimodular G57-V577 polypeptide chain of the class B penicillin-binding protein 3 of *Escherichia coli* catalyzes peptide bond formation from thiolesters and does not catalyze glycan chain polymerization from the lipid II intermediate. *J Bacteriol* 1997; **179**: 6005–6009.
 - 169 Chen W, Zhang Y-M, Davies C. Penicillin-Binding Protein 3 Is Essential for Growth of *Pseudomonas aeruginosa*. *Antimicrob Agents Chemother* 2017; **61**. doi:10.1128/AAC.01651-16.
 - 170 Liao X, Hancock RE. Identification of a penicillin-binding protein 3 homolog, PBP3x, in *Pseudomonas aeruginosa*: gene cloning and growth phase-dependent expression. *J Bacteriol* 1997; **179**: 1490–1496.
 - 171 Goffin C, Fraipont C, Ayala J, Terrak M, Nguyen-Distèche M, Ghuysen JM. The non-penicillin-binding module of the tripartite penicillin-binding protein 3 of *Escherichia coli* is required for folding and/or stability of the penicillin-binding module and the membrane-anchoring module confers cell septation activity on the folded structure. *J Bacteriol* 1996; **178**: 5402–5409.
 - 172 Nguyen-Distèche M, Fraipont C, Buddelmeijer N, Nanninga N. The structure and function of *Escherichia coli* penicillin-binding protein 3. *Cell Mol Life Sci CMLS* 1998; **54**: 309–316.
 - 173 Bowler LD, Spratt BG. Membrane topology of penicillin-binding protein 3 of *Escherichia coli*. *Mol Microbiol* 1989; **3**: 1277–1286.
 - 174 Wissel MC, Wendt JL, Mitchell CJ, Weiss DS. The Transmembrane Helix of the *Escherichia coli* Division Protein FtsI Localizes to the Septal Ring. *J Bacteriol* 2005; **187**: 320–328.
 - 175 Piette A, Fraipont C, den Blaauwen T, Aarsman MEG, Pastoret S, Nguyen-Distèche M. Structural Determinants Required To Target Penicillin-Binding Protein 3 to the Septum of *Escherichia coli*. *J Bacteriol* 2004; **186**: 6110–6117.

- 176 Marrec-Fairley M, Piette A, Gallet X, Brasseur R, Hara H, Fraipont C *et al.* Differential functionalities of amphiphilic peptide segments of the cell-septation penicillin-binding protein 3 of *Escherichia coli*. *Mol Microbiol* 2000; **37**: 1019–1031.
- 177 Eberhardt C, Kuerschner L, Weiss DS. Probing the Catalytic Activity of a Cell Division-Specific Transpeptidase In Vivo with β -Lactams. *J Bacteriol* 2003; **185**: 3726–3734.
- 178 Pares S, Mouz N, Pétillot Y, Hakenbeck R, Dideberg O. X-ray structure of *Streptococcus pneumoniae* PBP2x, a primary penicillin target enzyme. *Nat Struct Biol* 1996; **3**: 284–289.
- 179 Han S, Zaniewski RP, Marr ES, Lacey BM, Tomaras AP, Evdokimov A *et al.* Structural basis for effectiveness of siderophore-conjugated monocarbams against clinically relevant strains of *Pseudomonas aeruginosa*. *Proc Natl Acad Sci* 2010; **107**: 22002–22007.
- 180 Fedarovich A, Cook E, Tomberg J, Nicholas RA, Davies C. Structural Effect of the Asp345a Insertion in Penicillin-Binding Protein 2 from Penicillin-Resistant Strains of *Neisseria gonorrhoeae*. *Biochemistry* 2014; **53**: 7596–7603.
- 181 Sainsbury S, Bird L, Rao V, Shepherd SM, Stuart DI, Hunter WN *et al.* Crystal Structures of Penicillin-Binding Protein 3 from *Pseudomonas aeruginosa*: Comparison of Native and Antibiotic-Bound Forms. *J Mol Biol* 2011; **405**: 173–184.
- 182 Sauvage E, Derouaux A, Fraipont C, Joris M, Herman R, Rocaboy M *et al.* Crystal Structure of Penicillin-Binding Protein 3 (PBP3) from *Escherichia coli*. *PLoS ONE* 2014; **9**: e98042.
- 183 Ren J, Nettleship JE, Males A, Stuart DI, Owens RJ. Crystal structures of penicillin-binding protein 3 in complexes with azlocillin and cefoperazone in both acylated and deacylated forms. *FEBS Lett* 2016; **590**: 288–297.
- 184 Houba-Hérin N, Hara H, Inouye M, Hirota Y. Binding of penicillin to thiol-penicillin-binding protein 3 of *Escherichia coli*: identification of its active site. *Mol Gen Genet MGG* 1985; **201**: 499–504.
- 185 Ghuysen J-M. Molecular structures of penicillin-binding proteins and β -lactamases. *Trends Microbiol* 1994; **2**: 372–380.
- 186 Sievers F, Wilm A, Dineen D, Gibson TJ, Karplus K, Li W *et al.* Fast, scalable generation of high-quality protein multiple sequence alignments using Clustal Omega. *Mol Syst Biol* 2011; **7**: 539.
- 187 Robert X, Gouet P. Deciphering key features in protein structures with the new ENDscript server. *Nucleic Acids Res* 2014; **42**: W320–W324.
- 188 Brotzu, G. Ricerche su di un nuovo antibiotico. *Labori Dell'Istituto Lgiene Cagliari*
<https://discovery.nationalarchives.gov.uk/details/r/3fdecee6-34b7-4b8b-9225-c3ba7a8f41d5>. Accessed 08/01/21
- 189 Crawford K, Heatley NG, Boyd PF, Hale CW, Kelly BK, Miller GA *et al.* Antibiotic Production by a Species of Cephalosporium. *J Gen Microbiol* 1952; **6**: 47–59.
- 190 Abraham EP, Newton GGF, Hale CW. Purification and some properties of cephalosporin N, a new penicillin. *Biochem J* 1954; **58**: 94–102.
- 191 Sykes RB, Cimarusti CM, Bonner DP, Bush K, Floyd DM, Georgopapadakou NH *et al.* Monocyclic β -lactam antibiotics produced by bacteria. *Nature* 1981; **291**: 489–491.
- 192 Imada A, Kitano K, Kintaka K, Muroi M, Asai M. Sulfazecin and isosulfazecin, novel β -lactam antibiotics of bacterial origin. *Nature* 1981; **289**: 590–591.
- 193 Bush K. Past and Present Perspectives on β -Lactamases. *Antimicrob Agents Chemother* 2018; **62**: e01076-18, /aac/62/10/e01076-18.atom.
- 194 Sykes RB, Bonner DP, Bush K, Georgopapadakou NH. Azthreonam (SQ 26,776), a synthetic monobactam specifically active against aerobic

- gram-negative bacteria. *Antimicrob Agents Chemother* 1982; **21**: 85–92.
- 195 Aoki T, Yoshizawa H, Yamawaki K, Yokoo K, Sato J, Hisakawa S *et al*. Cefiderocol (S-649266), A new siderophore cephalosporin exhibiting potent activities against *Pseudomonas aeruginosa* and other gram-negative pathogens including multi-drug resistant bacteria: Structure activity relationship. *Eur J Med Chem* 2018; **155**: 847–868.
 - 196 Giacobbe DR, Ciacco E, Girmenia C, Pea F, Rossolini GM, Sotgiu G *et al*. Evaluating Cefiderocol in the Treatment of Multidrug-Resistant Gram-Negative Bacilli: A Review of the Emerging Data. *Infect Drug Resist* 2020; **Volume 13**: 4697–4711.
 - 197 Lima LM, Monteiro da Silva BN, Barbosa G, Barreiro EJ. β -lactam antibiotics: An overview from a medicinal chemistry perspective. *Eur J Med Chem* 2020; : 112829.
 - 198 Mitscher, L. M., Lemke, T. A., Gentry, E. J. Antibiotics and Antimicrobial Agents. In: *Foye's Principles of Medicinal Chemistry*. Lippincott Williams & Wilkins, 2008.
 - 199 Page MI. *The Chemistry of β -Lactams*. 1992
<https://doi.org/10.1007/978-94-011-2928-2>.
 - 200 Jamin M, Damblon C, Millier S, Hakenbeck R, Frère JM. Penicillin-binding protein 2x of *Streptococcus pneumoniae*: enzymic activities and interactions with beta-lactams. *Biochem J* 1993; **292**: 735–741.
 - 201 Ghuysen JM, Frère JM, Leyh-Bouille M, Nguyen-Distèche M, Coyette J. Active-site-serine D-alanyl-D-alanine-cleaving-peptidase-catalysed acyl-transfer reactions. Procedures for studying the penicillin-binding proteins of bacterial plasma membranes. *Biochem J* 1986; **235**: 159–165.
 - 202 Lu W-P, Kincaid E, Sun Y, Bauer MD. Kinetics of β -Lactam Interactions with Penicillin-susceptible and -resistant Penicillin-binding Protein 2x Proteins from *Streptococcus pneumoniae*. *J Biol Chem* 2001; **276**: 31494–31501.
 - 203 van Berkel SS, Nettleship JE, Leung IKH, Brem J, Choi H, Stuart DI *et al*. Binding of (5 S)-Penicilloic Acid to Penicillin Binding Protein 3. *ACS Chem Biol* 2013; **8**: 2112–2116.
 - 204 Beadle BM, Nicholas RA, Shoichet BK. Interaction energies between beta-lactam antibiotics and *E. coli* penicillin-binding protein 5 by reversible thermal denaturation. *Protein Sci Publ Protein Soc* 2001; **10**: 1254–1259.
 - 205 Shi Q, Meroueh SO, Fisher JF, Mobashery S. A Computational Evaluation of the Mechanism of Penicillin-Binding Protein-Catalyzed Cross-Linking of the Bacterial Cell Wall. *J Am Chem Soc* 2011; **133**: 5274–5283.
 - 206 Shi Q, Meroueh SO, Fisher JF, Mobashery S. Investigation of the Mechanism of the Cell Wall -Carboxypeptidase Reaction of Penicillin-Binding Protein 5 of *Escherichia coli* by Quantum Mechanics/Molecular Mechanics Calculations. *J Am Chem Soc* 2008; **130**: 9293–9303.
 - 207 Hargis JC, White JK, Chen Y, Woodcock HL. Can Molecular Dynamics and QM/MM Solve the Penicillin Binding Protein Protonation Puzzle? *J Chem Inf Model* 2014; **54**: 1412–1424.
 - 208 Kumarasiri M, Zhang W, Shi Q, Fisher JF, Mobashery S. Protonation states of active-site lysines of penicillin-binding protein 6 from *Escherichia coli* and the mechanistic implications: Mechanistic Link to Active-Site Protonation in PBP6. *Proteins Struct Funct Bioinforma* 2014; **82**: 1348–1358.
 - 209 Lewandowski EM, Lethbridge KG, Sanishvili R, Skiba J, Kowalski K, Chen Y. Mechanisms of proton relay and product release by Class A β -lactamase at ultrahigh resolution. *FEBS J* 2018; **285**: 87–100.
 - 210 Dzhekheva L, Rocaboy M, Kerff F, Charlier P, Sauvage E, Pratt RF. Crystal Structure of a Complex between the Actinomadura R39 dd-Peptidase and a Peptidoglycan-mimetic Boronate Inhibitor: Interpretation of a Transition State Analogue in Terms of Catalytic Mechanism. *Biochemistry* 2010; **49**:

- 6411–6419.
- 211 Massova I, Mobashery S. Kinship and Diversification of Bacterial Penicillin-Binding Proteins and β -Lactamases. *Antimicrob Agents Chemother* 1998; **42**: 1–17.
 - 212 Sacco MD, Kroeck KG, Kemp MT, Zhang X, Andrews LD, Chen Y. Influence of the α -Methoxy Group on the Reaction of Temocillin with *Pseudomonas aeruginosa* PBP3 and CTX-M-14 β -Lactamase. *Antimicrob Agents Chemother* 2019; **64**: e01473-19, /aac/64/1/AAC.01473-19.atom.
 - 213 Murphy-Benenato KE, Dangel B, Davis HE, Durand-Réville TF, Ferguson AD, Gao N *et al.* SAR and Structural Analysis of Siderophore-Conjugated Monocarbam Inhibitors of *Pseudomonas aeruginosa* PBP3. *ACS Med Chem Lett* 2015; **6**: 537–542.
 - 214 Starr J, Brown MF, Aschenbrenner L, Caspers N, Che Y, Gerstenberger BS *et al.* Siderophore Receptor-Mediated Uptake of Lactivicin Analogues in Gram-Negative Bacteria. *J Med Chem* 2014; **57**: 3845–3855.
 - 215 Mitton-Fry MJ, Arcari JT, Brown MF, Casavant JM, Finegan SM, Flanagan ME *et al.* Novel monobactams utilizing a siderophore uptake mechanism for the treatment of gram-negative infections. *Bioorg Med Chem Lett* 2012; **22**: 5989–5994.
 - 216 Brown MF, Mitton-Fry MJ, Arcari JT, Barham R, Casavant J, Gerstenberger BS *et al.* Pyridone-Conjugated Monobactam Antibiotics with Gram-Negative Activity. *J Med Chem* 2013; **56**: 5541–5552.
 - 217 Kumar V, Tang C, Bethel CR, Papp-Wallace KM, Wyatt J, Desarbre E *et al.* Structural Insights into Ceftobiprole Inhibition of *Pseudomonas aeruginosa* Penicillin-Binding Protein 3. *Antimicrob Agents Chemother* 2020; **64**. doi:10.1128/AAC.00106-20.
 - 218 Eisenberg D, Schwarz E, Komaromy M, Wall R. Analysis of membrane and surface protein sequences with the hydrophobic moment plot. *J Mol Biol* 1984; **179**: 125–142.
 - 219 Mamoru Suzuki. PyMOL tutorial -Hydrophobicity-. <http://www.protein.osaka-u.ac.jp/rcsfp/supracryst/suzuki/jpxtal/Katsutani/en/hydrophobicity.php>. Accessed 08/01/21
 - 220 Hahn FE, Ciak J. Penicillin-Induced Lysis of *Escherichia coli*. *Science* 1957; **125**: 119–120.
 - 221 Lederberg J. BACTERIAL PROTOPLASTS INDUCED BY PENICILLIN. *Proc Natl Acad Sci* 1956; **42**: 574–577.
 - 222 Schwarz U, Asmus A, Frank H. Autolytic enzymes and cell division of *Escherichia coli*. *J Mol Biol* 1969; **41**: 419–429.
 - 223 Tomasz A, Albino A, Zanati E. Multiple Antibiotic Resistance in a Bacterium with Suppressed Autolytic System. *Nature* 1970; **227**: 138–140.
 - 224 Tomasz A. THE ROLE OF AUTOLYSINS IN CELL DEATH. *Ann N Y Acad Sci* 1974; **235**: 439–447.
 - 225 Banzhaf M, van den Berg van Saparoea B, Terrak M, Fraipont C, Egan A, Philippe J *et al.* Cooperativity of peptidoglycan synthases active in bacterial cell elongation: Bacterial peptidoglycan synthesis. *Mol Microbiol* 2012; **85**: 179–194.
 - 226 Cho H, Uehara T, Bernhardt TG. Beta-Lactam Antibiotics Induce a Lethal Malfunctioning of the Bacterial Cell Wall Synthesis Machinery. *Cell* 2014; **159**: 1300–1311.
 - 227 Kocaoglu O, Carlson EE. Profiling of β -Lactam Selectivity for Penicillin-Binding Proteins in *Escherichia coli* Strain DC2. *Antimicrob Agents Chemother* 2015; **59**: 2785–2790.
 - 228 Kocaoglu O, Tsui H-CT, Winkler ME, Carlson EE. Profiling of β -Lactam Selectivity for Penicillin-Binding Proteins in *Streptococcus pneumoniae* D39. *Antimicrob Agents Chemother* 2015; **59**: 3548–3555.

- 229 Curtis NA, Orr D, Ross GW, Boulton MG. Affinities of penicillins and cephalosporins for the penicillin-binding proteins of *Escherichia coli* K-12 and their antibacterial activity. *Antimicrob Agents Chemother* 1979; **16**: 533–539.
- 230 Sutaria DS, Moya B, Green KB, Kim TH, Tao X, Jiao Y *et al*. First Penicillin-Binding Protein Occupancy Patterns of β -Lactams and β -Lactamase Inhibitors in *Klebsiella pneumoniae*. *Antimicrob Agents Chemother* 2018; **62**: e00282-18, /aac/62/6/e00282-18.atom.
- 231 Satta G, Cornaglia G, Mazzariol A, Golini G, Valisena S, Fontana R. Target for bacteriostatic and bactericidal activities of beta-lactam antibiotics against *Escherichia coli* resides in different penicillin-binding proteins. *Antimicrob Agents Chemother* 1995; **39**: 812–818.
- 232 Nikaido H, Normark S. Sensitivity of *Escherichia coli* to various B-lactams is determined by the interplay of outer membrane permeability and degradation by periplasmic B-lactamases: a quantitative predictive treatment. *Mol Microbiol* 1987; **1**: 29–36.
- 233 Frère J-M, Joris B, Granier B, Matagne A, Jacob F, Bourguignon-Bellefroid C. Diversity of the mechanisms of resistance to β -lactam antibiotics. *Res Microbiol* 1991; **142**: 705–710.
- 234 Jaffe A, Chabbert YA, Semonin O. Role of porin proteins OmpF and OmpC in the permeation of beta-lactams. *Antimicrob Agents Chemother* 1982; **22**: 942–948.
- 235 Godfrey AJ, Hatlelid L, Bryan LE. Correlation between lipopolysaccharide structure and permeability resistance in beta-lactam-resistant *Pseudomonas aeruginosa*. *Antimicrob Agents Chemother* 1984; **26**: 181–186.
- 236 Livermore DM. Penicillin-Binding Proteins, Porins Andouter-Membrane Permeability of Carbenicillin-Resistant and -Susceptible Strains of *Pseudomonas Aeruginosa*. *J Med Microbiol* 1984; **18**: 261–270.
- 237 Nikaido H, Pagès J-M. Broad-specificity efflux pumps and their role in multidrug resistance of Gram-negative bacteria. *FEMS Microbiol Rev* 2012; **36**: 340–363.
- 238 Pages J-M, Lavigne J-P, Leflon-Guibout V, Marcon E, Bert F, Noussair L *et al*. Efflux Pump, the Masked Side of β -Lactam Resistance in *Klebsiella pneumoniae* Clinical Isolates. *PLoS ONE* 2009; **4**: e4817.
- 239 Lim D, Strynadka NCJ. Structural basis for the β lactam resistance of PBP2a from methicillin-resistant *Staphylococcus aureus*. *Nat Struct Biol* 2002. doi:10.1038/nsb858.
- 240 Abraham EP, Chain E. An Enzyme from Bacteria able to Destroy Penicillin. *Nature* 1940; **146**: 837–837.
- 241 Kirby WMM. Extraction Of A Highly Potent Penicillin Inactivator From Penicillin Resistant Staphylococci. *Science* 1944; **99**: 452–453.
- 242 Bhullar K, Waglechner N, Pawlowski A, Koteva K, Banks ED, Johnston MD *et al*. Antibiotic Resistance Is Prevalent in an Isolated Cave Microbiome. *PLoS ONE* 2012; **7**: e34953.
- 243 Hall BG, Barlow M. Evolution of the serine β -lactamases: past, present and future. *Drug Resist Updat* 2004; **7**: 111–123.
- 244 Bonomo RA. β -Lactamases: A Focus on Current Challenges. *Cold Spring Harb Perspect Med* 2017; **7**: a025239.
- 245 Petrosino J, Cantu C, Palzkill T. β -Lactamases: protein evolution in real time. *Trends Microbiol* 1998; **6**: 323–327.
- 246 Perlin MH, Clark DR, McKenzie C, Patel H, Jackson N, Kormanik C *et al*. Protection of *Salmonella* by ampicillin-resistant *Escherichia coli* in the presence of otherwise lethal drug concentrations. *Proc R Soc B Biol Sci* 2009; **276**: 3759–3768.
- 247 Amanatidou E, Matthews AC, Kuhlicke U, Neu TR, McEvoy JP, Raymond B. Biofilms facilitate cheating and social exploitation of β -lactam resistance in

- Escherichia coli*. *Npj Biofilms Microbiomes* 2019; **5**: 36.
- 248 Ambler RP. The structure of beta-lactamases. *Philos Trans R Soc Lond B Biol Sci* 1980; **289**: 321–331.
- 249 Bush K, Jacoby GA. Updated Functional Classification of β -Lactamases. *Antimicrob Agents Chemother* 2010; **54**: 969–976.
- 250 Reddy N, Shungube M, Arvidsson PI, Baijnath S, Kruger HG, Govender T *et al*. A 2018–2019 patent review of metallo beta-lactamase inhibitors. *Expert Opin Ther Pat* 2020; **30**: 541–555.
- 251 Bush K, Bradford PA. Interplay between β -lactamases and new β -lactamase inhibitors. *Nat Rev Microbiol* 2019; **17**: 295–306.
- 252 Bush K, Jacoby GA, Medeiros AA. A functional classification scheme for beta-lactamases and its correlation with molecular structure. *Antimicrob Agents Chemother* 1995; **39**: 1211–1233.
- 253 Meroueh SO, Minasov G, Lee W, Shoichet BK, Mobashery S. Structural Aspects for Evolution of β -Lactamases from Penicillin-Binding Proteins. *J Am Chem Soc* 2003; **125**: 9612–9618.
- 254 Reading C, Cole M. Clavulanic Acid: a Beta-Lactamase-Inhibiting Beta-Lactam from *Streptomyces clavuligerus*. *Antimicrob Agents Chemother* 1977; **11**: 852–857.
- 255 Sutherland R. β -Lactamase inhibitors and reversal of antibiotic resistance. *Trends Pharmacol Sci* 1991; **12**: 227–232.
- 256 Helfand MS, Totir MA, Carey MP, Hujer AM, Bonomo RA, Carey PR. Following the Reactions of Mechanism-Based Inhibitors with β -Lactamase by Raman Crystallography [†]. *Biochemistry* 2003; **42**: 13386–13392.
- 257 Charnas RL, Fisher J, Knowles JR. Chemical studies on the inactivation of *Escherichia coli* RTEM β -lactamase by clavulanic acid. *Biochemistry* 1978; **17**: 2185–2189.
- 258 Fisher J, Charnas RL, Knowles JR. Kinetic studies on the inactivation of *Escherichia coli* RTEM β -lactamase by clavulanic acid. *Biochemistry* 1978; **17**: 2180–2184.
- 259 Ball P, Geddes A, Rolinson G. Amoxycillin Clavulanate: an Assessment after 15 Years of Clinical Application. *J Chemother* 1997; **9**: 167–198.
- 260 Wang DY, Abboud MI, Markoulides MS, Brem J, Schofield CJ. The road to avibactam: the first clinically useful non- β -lactam working somewhat like a β -lactam. *Future Med Chem* 2016; **8**: 1063–1084.
- 261 Zhanel GG, Lawrence CK, Adam H, Schweizer F, Zelenitsky S, Zhanel M *et al*. Imipenem–Relebactam and Meropenem–Vaborbactam: Two Novel Carbapenem- β -Lactamase Inhibitor Combinations. *Drugs* 2018; **78**: 65–98.
- 262 Lomovskaya O, Sun D, Rubio-Aparicio D, Nelson K, Tsivkovski R, Griffith DC *et al*. Vaborbactam: Spectrum of Beta-Lactamase Inhibition and Impact of Resistance Mechanisms on Activity in Enterobacteriaceae. *Antimicrob Agents Chemother* 2017; **61**: e01443-17, e01443-17.
- 263 Tsivkovski R, Lomovskaya O. Biochemical Activity of Vaborbactam. *Antimicrob Agents Chemother* 2019; **64**: e01935-19, /aac/64/2/AAC.01935-19.atom.
- 264 Crass RL, Pai MP. Pharmacokinetics and Pharmacodynamics of β -Lactamase Inhibitors. *Pharmacother J Hum Pharmacol Drug Ther* 2019; **39**: 182–195.
- 265 VanScoy B, Mendes RE, McCauley J, Bhavnani SM, Bulik CC, Okusanya OO *et al*. Pharmacological Basis of β -Lactamase Inhibitor Therapeutics: Tazobactam in Combination with Ceftolozane. *Antimicrob Agents Chemother* 2013; **57**: 5924–5930.
- 266 Jungheim LN, Ternansky RJ. Non- β -lactam mimics of β -lactam antibiotics. In: Page MI (ed). *The Chemistry of β -Lactams*. Springer Netherlands: Dordrecht, 1992, pp 306–324.
- 267 Zervosen A, Sauvage E, Frère J-M, Charlier P, Luxen A. Development of New Drugs for an Old Target — The Penicillin Binding Proteins. *Molecules* 2012; **17**:

- 12478–12505.
- 268 Marchand-Brynaert, J, Ghosez, L. Non β -Lactam Analogs of Penicillins and Cephalosporins. In: *Recent Progress in the Chemical Synthesis of Antibiotics*. 1990, pp 727–794.
 - 269 Phichith D, Bun S, Padiolleau-Lefevre S, Guellier A, Banh S, Galleni M *et al*. Novel peptide inhibiting both TEM-1 β -lactamase and penicillin-binding proteins. *FEBS J* 2010; **277**: 4965–4972.
 - 270 Bicycle Therapeutics. Anti-Infectives. Bicycle Ther. Website. <https://www.bicycletherapeutics.com/beyond-oncology/>. Accessed 22.01.21.
 - 271 Hamrick JC, Docquier J-D, Uehara T, Myers CL, Six DA, Chatwin CL *et al*. VNRX-5133 (Taniborbactam), a Broad-Spectrum Inhibitor of Serine- and Metallo- β -Lactamases, Restores Activity of Cefepime in *Enterobacterales* and *Pseudomonas aeruginosa*. *Antimicrob Agents Chemother* 2019; **64**: e01963-19, /aac/64/3/AAC.01963-19.atom.
 - 272 VenatoRx Pharmaceuticals, Inc. A Phase 3, Randomized, Double-blind, Active Controlled Noninferiority Study Evaluating the Efficacy, Safety, and Tolerability of Cefepime/VNRX-5133 in Adults With Complicated Urinary Tract Infections (cUTI), Including Acute Pyelonephritis. clinicaltrials.gov, 2020 <https://clinicaltrials.gov/ct2/show/NCT03840148>. Accessed 01/02/21.
 - 273 Hecker SJ, Reddy KR, Lomovskaya O, Griffith DC, Rubio-Aparicio D, Nelson K *et al*. Discovery of Cyclic Boronic Acid QPX7728, an Ultrabroad-Spectrum Inhibitor of Serine and Metallo- β -lactamases. *J Med Chem* 2020; **63**: 7491–7507.
 - 274 Asli A, Brouillette E, Krause KM, Nichols WW, Malouin F. Distinctive Binding of Avibactam to Penicillin-Binding Proteins of Gram-Negative and Gram-Positive Bacteria. *Antimicrob Agents Chemother* 2016; **60**: 752–756.
 - 275 Moya B, Barcelo IM, Bhagwat S, Patel M, Bou G, Papp-Wallace KM *et al*. WCK 5107 (Zidebactam) and WCK 5153 Are Novel Inhibitors of PBP2 Showing Potent “ β -Lactam Enhancer” Activity against *Pseudomonas aeruginosa*, Including Multidrug-Resistant Metallo- β -Lactamase-Producing High-Risk Clones. *Antimicrob Agents Chemother* 2017; **61**: e02529-16, e02529-16.
 - 276 Levy N, Bruneau J-M, Le Rouzic E, Bonnard D, Le Strat F, Caravano A *et al*. Structural Basis for *E. coli* Penicillin Binding Protein (PBP) 2 Inhibition, a Platform for Drug Design. *J Med Chem* 2019; **62**: 4742–4754.
 - 277 Rajavel M, Kumar V, Nguyen H, Wyatt J, Marshall SH, Papp-Wallace KM *et al*. Structural Characterization of Diazabicyclooctane β -Lactam “Enhancers” in Complex with Penicillin-Binding Proteins PBP2 and PBP3 of *Pseudomonas aeruginosa*. *mBio* 2021; **12**: e03058-20, /mbio/12/1/mBio.03058-20.atom.
 - 278 Morinaka A, Tsutsumi Y, Yamada M, Suzuki K, Watanabe T, Abe T *et al*. OP0595, a new diazabicyclooctane: mode of action as a serine β -lactamase inhibitor, antibiotic and β -lactam ‘enhancer’. *J Antimicrob Chemother* 2015; **70**: 2779–2786.
 - 279 Livermore DM, Warner M, Mushtaq S, Woodford N. Interactions of OP0595, a Novel Triple-Action Diazabicyclooctane, with β -Lactams against OP0595-Resistant Enterobacteriaceae Mutants. *Antimicrob Agents Chemother* 2016; **60**: 554–560.
 - 280 Durand-Réville TF, Guler S, Comita-Prevoir J, Chen B, Bifulco N, Huynh H *et al*. ETX2514 is a broad-spectrum β -lactamase inhibitor for the treatment of drug-resistant Gram-negative bacteria including *Acinetobacter baumannii*. *Nat Microbiol* 2017; **2**: 17104.
 - 281 Durand-Reville T. ETX0462, A Novel Non- β -lactam PBP Inhibitor, Is Bactericidal Against Gram-Negative Pathogens. 2021.
 - 282 Martin JS, MacKenzie CJ, Fletcher D, Gilbert IH. Characterising covalent warhead reactivity. *Bioorg Med Chem* 2019; **27**: 2066–2074.

- 283 Imming P, Klar B, Dix D. Hydrolytic Stability versus Ring Size in Lactams: Implications for the Development of Lactam Antibiotics and Other Serine Protease Inhibitors [†]. *J Med Chem* 2000; **43**: 4328–4331.
- 284 Frère JM, Kelly JA, Klein D, Ghuysen JM, Claes P, Vanderhaeghe H. Δ 2- and Δ 3-cephalosporins, penicillinate and 6-unsubstituted penems. Intrinsic reactivity and interaction with β -lactamases and d-alanyl-d-alanine-cleaving serine peptidases. *Biochem J* 1982; **203**: 223–234.
- 285 Goldberg JA, Nguyen H, Kumar V, Spencer EJ, Hoyer D, Marshall EK *et al.* A γ -Lactam Siderophore Antibiotic Effective against Multidrug-Resistant Gram-Negative Bacilli. *J Med Chem* 2020; **63**: 5990–6002.
- 286 Allen NE, Hobbs JN, Preston DA, Turner JR, Wu CYE. Antibacterial properties of the bicyclic pyrazolidinones. *J Antibiot (Tokyo)* 1990; **43**: 92–99.
- 287 Baldwin JE, Lynch GP, Pitlik J. Gamma-Lactam analogues of beta-lactam antibiotics. *J Antibiot (Tokyo)* 1991; **44**: 1–24.
- 288 Macheboeuf P, Fischer DS, Brown T, Zervosen A, Luxen A, Joris B *et al.* Structural and mechanistic basis of penicillin-binding protein inhibition by lactivicins. *Nat Chem Biol* 2007; **3**: 565–569.
- 289 Davies GM, Hitchcock PB, Loakes D, Young DW. Synthesis of Reactive γ -Lactams Related to Penicillins and Cephalosporins. *Tetrahedron Lett* 1996; **31**: 5601–5604.
- 290 Zervosen A, Lu W-P, Chen Z, White RE, Demuth TP, Frere J-M. Interactions between Penicillin-Binding Proteins (PBPs) and Two Novel Classes of PBP Inhibitors, Arylalkylidene Rhodanines and Arylalkylidene Iminothiazolidin-4-ones. *ANTIMICROB AGENTS CHEMOTHER* 2004; **48**: 9.
- 291 López-Pérez A, Freischem S, Grimm I, Weiergräber O, Dingley AJ, López-Alberca MP *et al.* Discovery of Pyrrolidine-2,3-diones as Novel Inhibitors of *P. aeruginosa* PBP3. *Antibiotics* 2021; **10**: 529.
- 292 Miguet L, Zervosen A, Gerards T, Pasha FA, Luxen A, Distèche-Nguyen M *et al.* Discovery of New Inhibitors of Resistant *Streptococcus pneumoniae* Penicillin Binding Protein (PBP) 2x by Structure-Based Virtual Screening. *J Med Chem* 2009; **52**: 5926–5936.
- 293 O'Daniel PI, Peng Z, Pi H, Testero SA, Ding D, Spink E *et al.* Discovery of a New Class of Non- β -lactam Inhibitors of Penicillin-Binding Proteins with Gram-Positive Antibacterial Activity. *J Am Chem Soc* 2014; **136**: 3664–3672.
- 294 Bouley R, Ding D, Peng Z, Bastian M, Lastochkin E, Song W *et al.* Structure–Activity Relationship for the 4(3 H)-Quinazolinone Antibacterials. *J Med Chem* 2016; **59**: 5011–5021.
- 295 Bouley R, Kumarasiri M, Peng Z, Otero LH, Song W, Suckow MA *et al.* Discovery of Antibiotic (E)-3-(3-Carboxyphenyl)-2-(4-cyanostyryl)quinazolin-4(3 H)-one. *J Am Chem Soc* 2015; **137**: 1738–1741.
- 296 Janardhanan J, Bouley R, Martínez-Caballero S, Peng Z, Batuecas-Mordillo M, Meisel JE *et al.* The Quinazolinone Allosteric Inhibitor of PBP 2a Synergizes with Piperacillin and Tazobactam against Methicillin-Resistant *Staphylococcus aureus*. *Antimicrob Agents Chemother* 2019; **63**: e02637-18, /aac/63/5/AAC.02637-18.atom.
- 297 Acebrón I, Chang M, Mobashery S, Hermoso JA. The Allosteric Site for the Nascent Cell Wall in Penicillin-Binding Protein 2a: An Achilles' Heel of Methicillin-Resistant *Staphylococcus aureus*. *Curr Med Chem* 2015; **22**: 1678–1686.
- 298 Nicola G, Peddi S, Stefanova M, Nicholas RA, Gutheil WG, Davies C. Crystal Structure of *Escherichia coli* Penicillin-Binding Protein 5 Bound to a Tripeptide Boronic Acid Inhibitor: A Role for Ser-110 in Deacylation [†]. *Biochemistry* 2005; **44**: 8207–8217.
- 299 Pechenov A, Stefanova ME, Nicholas RA, Peddi S, Gutheil WG. Potential

- Transition State Analogue Inhibitors for the Penicillin-Binding Proteins. *Biochemistry* 2003; **42**: 579–588.
- 300 Krajnc A, Lang PA, Panduwawala TD, Brem J, Schofield CJ. Will morphing boron-based inhibitors beat the β -lactamases? *Curr Opin Chem Biol* 2019; **50**: 101–110.
 - 301 Tymiak AA, Culver CA, Malley MF, Gougoutas JZ. Structure of obafluorin: an antibacterial β -lactone from *Pseudomonas fluorescens*. *J Org Chem* 1985; **50**: 5491–5495.
 - 302 Brown NW, Shirley JD, Marshall AP, Carlson EE. Comparison of Bioorthogonal β -Lactone Activity-Based Probes for Selective Labeling of Penicillin-Binding Proteins. *ChemBioChem* 2021; **22**: 193–202.
 - 303 Wells JS, Trejo WH, Principe PA, Sykes RB. Obafluorin, a novel β -lactone produced by *Pseudomonas fluorescens*. Taxonomy, fermentation and biological properties. *J Antibiot (Tokyo)* 1984; **37**: 802–803.
 - 304 Abboud MI, Kosmopoulou M, Krismanich AP, Johnson JW, Hinchliffe P, Brem J *et al*. Cyclobutanone Mimics of Intermediates in Metallo- β -Lactamase Catalysis. *Chem – Eur J* 2018; **24**: 5734–5737.
 - 305 Johnson JW, Gretes M, Goodfellow VJ, Marrone L, Heynen ML, Strynadka NCJ *et al*. Cyclobutanone Analogues of β -Lactams Revisited: Insights into Conformational Requirements for Inhibition of Serine- and Metallo- β -Lactamases. *J Am Chem Soc* 2010; **132**: 2558–2560.
 - 306 Page MI, Tsang WY, Ahmed N. Comparison of the mechanisms of reactions of β -lactams and β -sultams, including their reactions with some serine enzymes. *J Phys Org Chem* 2006; **19**: 446–451.
 - 307 Llinás A, Ahmed N, Cordaro M, Laws AP, Frère J-M, Delmarcelle M *et al*. Inactivation of Bacterial dd-Peptidase by β -Sultams. *Biochemistry* 2005; **44**: 7738–7746.
 - 308 Tsang WY, Ahmed N, Hinchliffe PS, Wood JM, Harding LP, Laws AP *et al*. Different Transition-State Structures for the Reactions of β -Lactams and Analogous β -Sultams with Serine β -Lactamases. *J Am Chem Soc* 2005; **127**: 17556–17564.
 - 309 Pirotte B, Dive G, Delarge J, Masereel B, Dupont L, Thunus L *et al*. Synthèse, étude théorique et évaluation biologique de dérivés du 4-amino-4H-1,2,4-triazole analogues des antibiotiques β -lactamiques. *Eur J Med Chem* 1992; **27**: 193–205.
 - 310 Dzhekieva L, Adediran SA, Herman R, Charlier P, Sauvage E, Pratt RF. Inhibition of DD-Peptidases by a Specific Trifluoroketone: Crystal Structure of a Complex with the *Actinomadura* R39 DD-Peptidase. 2013; : 11.
 - 311 Woon ECY, Zervosen A, Sauvage E, Simmons KJ, Živec M, Inglis SR *et al*. Structure Guided Development of Potent Reversibly Binding Penicillin Binding Protein Inhibitors. *ACS Med Chem Lett* 2011; **2**: 219–223.
 - 312 Silvaggi NR, Kaur K, Adediran SA, Pratt RF, Kelly JA. Toward Better Antibiotics: Crystallographic Studies of a Novel Class of DD-Peptidase/ β -Lactamase Inhibitors [†]. *Biochemistry* 2004; **43**: 7046–7053.
 - 313 Morrison MJ, Li N, Pratt RF. Inverse Acyl Phosph(on)ates: Substrates or Inhibitors of β -Lactam-Recognizing Enzymes? *Bioorganic Chem* 2001; **29**: 271–281.
 - 314 Rahil J, Pratt RF. Phosphonate monoester inhibitors of class A β -lactamases. *Biochem J* 1991; **275**: 793–795.
 - 315 Toney JH, Hammond GG, Leiting B, Pryor KD, Wu JK, Cuca GC *et al*. Soluble Penicillin-Binding Protein 2a: β -Lactam Binding and Inhibition by Non- β -Lactams Using a 96-Well Format. *Anal Biochem* 1998; **255**: 113–119.
 - 316 Turk S, Verlaine O, Gerards T, Živec M, Humljan J, Sosič I *et al*. New Noncovalent Inhibitors of Penicillin-Binding Proteins from Penicillin-Resistant Bacteria. *PLoS ONE* 2011; **6**: e19418.

- 317 Sosič I, Turk S, Sinreih M, Trošt N, Verlaine O, Amoroso A *et al.* Exploration of the chemical space of novel naphthalene-sulfonamide and anthranilic Acid-based inhibitors of penicillin-binding proteins. *Acta Chim Slov* 2012; **59**: 280–388.
- 318 Fedarovich A, Djordjevic KA, Swanson SM, Peterson YK, Nicholas RA, Davies C. High-Throughput Screening for Novel Inhibitors of *Neisseria gonorrhoeae* Penicillin-Binding Protein 2. *PLoS ONE* 2012; **7**: e44918.
- 319 Shilabin AG, Dzhekieva L, Misra P, Jayaram B, Pratt RF. 4-Quinolones as Noncovalent Inhibitors of High Molecular Mass Penicillin-Binding Proteins. *ACS Med Chem Lett* 2012; **3**: 592–595.
- 320 Qian Y, Allegretta G, Janardhanan J, Peng Z, Mahasen KV, Lastochkin E *et al.* Exploration of the Structural Space in 4(3*H*)-Quinazolinone Antibacterials. *J Med Chem* 2020; **63**: 5287–5296.
- 321 Zervosen A, Herman R, Kerff F, Herman A, Bouillez A, Prati F *et al.* Unexpected Tricovalent Binding Mode of Boronic Acids within the Active Site of a Penicillin-Binding Protein. *J Am Chem Soc* 2011; **133**: 10839–10848.
- 322 Contreras-Martel C, Amoroso A, Woon ECY, Zervosen A, Inglis S, Martins A *et al.* Structure-Guided Design of Cell Wall Biosynthesis Inhibitors That Overcome β -Lactam Resistance in *Staphylococcus aureus* (MRSA). *ACS Chem Biol* 2011; **6**: 943–951.
- 323 Zervosen A, Bouillez A, Herman A, Amoroso A, Joris B, Sauvage E *et al.* Synthesis and evaluation of boronic acids as inhibitors of Penicillin Binding Proteins of classes A, B and C. *Bioorg Med Chem* 2012; **20**: 3915–3924.
- 324 Dzhekieva L, Adediran SA, Pratt RF. Interactions of “Bora-Penicilloates” with Serine β -Lactamases and DD-Peptidases. *Biochemistry* 2014; **53**: 6530–6538.
- 325 Dzhekieva L, Kumar I, Pratt RF. Inhibition of Bacterial DD-Peptidases (Penicillin-Binding Proteins) in Membranes and in Vivo by Peptidoglycan-Mimetic Boronic Acids. *Biochemistry* 2012; **51**: 2804–2811.
- 326 Inglis SR, Zervosen A, Woon ECY, Gerards T, Teller N, Fischer DS *et al.* Synthesis and Evaluation of 3-(Dihydroxyboryl)benzoic Acids as β -Carboxypeptidase R39 Inhibitors. *J Med Chem* 2009; **52**: 6097–6106.
- 327 Castanheira M, Rhomberg PR, Flamm RK, Jones RN. Effect of the β -Lactamase Inhibitor Vaborbactam Combined with Meropenem against Serine Carbapenemase-Producing Enterobacteriaceae. *Antimicrob Agents Chemother* 2016; **60**: 5454–5458.
- 328 Hecker SJ, Reddy KR, Totrov M, Hirst GC, Lomovskaya O, Griffith DC *et al.* Discovery of a Cyclic Boronic Acid β -Lactamase Inhibitor (RPX7009) with Utility vs Class A Serine Carbapenemases. *J Med Chem* 2015; **58**: 3682–3692.
- 329 Brem J, Cain R, Cahill S, McDonough MA, Clifton IJ, Jiménez-Castellanos J-C *et al.* Structural basis of metallo- β -lactamase, serine- β -lactamase and penicillin-binding protein inhibition by cyclic boronates. *Nat Commun* 2016; **7**: 12406.
- 330 Burns J, Daigle D, Chu G-H, Jackson RW, Hamrick J, Boyd SA *et al.* PENICILLIN-BINDING PROTEIN INHIBITORS (2018). .
- 331 Burns J, Daigle D, Chu G-H, Hamrick J, Lucas, M, Boyd SA *et al.* PENICILLIN-BINDING PROTEIN INHIBITORS (2018). .
- 332 McKinney DC, Zhou F, Eyermann CJ, Ferguson AD, Prince DB, Breen J *et al.* 4,5-Disubstituted 6-Aryloxy-1,3-dihydrobenzo[*c*][1,2]oxaboroles Are Broad-Spectrum Serine β -Lactamase Inhibitors. *ACS Infect Dis* 2015; **1**: 310–316.
- 333 Newman H, Krajnc A, Bellini D, Eyermann CJ, Boyle GA, Paterson NG *et al.* High-Throughput Crystallography Reveals Boron Containing Inhibitors of a Penicillin Binding Protein with Di- and Tri-covalent Binding Modes. *J Med Chem*; **Accepted**. doi:https://doi.org/10.1021/acs.jmedchem.1c00717.

- 334 Livermore DM. Radiolabelling of penicillin-binding proteins (PBPs) in intact *Pseudomonas aeruginosa* cells: consequences of β -lactamase activity by PBP-5. *J Antimicrob Chemother* 1987; **19**: 733–742.
- 335 Preston DA, Wu CY, Blaszcak LC, Seitz DE, Halligan NG. Biological characterization of a new radioactive labeling reagent for bacterial penicillin-binding proteins. *Antimicrob Agents Chemother* 1990; **34**: 718–721.
- 336 Graves-Woodward K, Pratt RF. Reaction of soluble penicillin-binding protein 2a of methicillin-resistant *Staphylococcus aureus* with β -lactams and acyclic substrates: kinetics in homogeneous solution. *Biochem J* 1998; **332**: 755–761.
- 337 Bebrone C, Moali C, Mahy F, Rival S, Docquier JD, Rossolini GM *et al.* CENTA as a Chromogenic Substrate for Studying β -Lactamases. *Antimicrob Agents Chemother* 2001; **45**: 1868–1871.
- 338 O'Callaghan CH, Morris A, Kirby SM, Shingler AH. Novel Method for Detection of β -Lactamases by Using a Chromogenic Cephalosporin Substrate. *Antimicrob Agents Chemother* 1972; **1**: 283–288.
- 339 Jones RN, Wilson HW, Novick WJ, Barry AL, Thornsberry C. In vitro evaluation of CENTA, a new beta-lactamase-susceptible chromogenic cephalosporin reagent. *J Clin Microbiol* 1982; **15**: 954–958.
- 340 Zhao G, Meier TI, Kahl SD, Gee KR, Blaszcak LC. BOCILLIN FL, a Sensitive and Commercially Available Reagent for Detection of Penicillin-Binding Proteins. *Antimicrob Agents Chemother* 1999; **43**: 1124–1128.
- 341 Bobba S, Ponnaluri VKC, Mukherji M, Gutheil WG. Microtiter Plate-Based Assay for Inhibitors of Penicillin-Binding Protein 2a from Methicillin-Resistant *Staphylococcus aureus*. *Antimicrob Agents Chemother* 2011; **55**: 2783–2787.
- 342 Stefanova M, Bobba S, Gutheil WG. A microtiter plate-based beta-lactam binding assay for inhibitors of high-molecular-mass penicillin-binding proteins. *Anal Biochem* 2010; **396**: 164–166.
- 343 Dargis M, Malouin F. Use of biotinylated beta-lactams and chemiluminescence for study and purification of penicillin-binding proteins in bacteria. *Antimicrob Agents Chemother* 1994; **38**: 973–980.
- 344 Lu W-P, Sun Y, Bauer MD, Paule S, Koenigs PM, Kraft WG. Penicillin-Binding Protein 2a from Methicillin-Resistant *Staphylococcus aureus* : Kinetic Characterization of Its Interactions with β -Lactams Using Electrospray Mass Spectrometry. *Biochemistry* 1999; **38**: 6537–6546.
- 345 Pattnaik P. Surface Plasmon Resonance: Applications in Understanding Receptor–Ligand Interaction. *Appl Biochem Biotechnol* 2005; **126**: 079–092.
- 346 Navratilova I, Hopkins AL. Fragment Screening by Surface Plasmon Resonance. *ACS Med Chem Lett* 2010; **1**: 44–48.
- 347 Huynh K, Partch CL. Analysis of Protein Stability and Ligand Interactions by Thermal Shift Assay. *Curr Protoc Protein Sci* 2015; **79**. doi:10.1002/0471140864.ps2809s79.
- 348 Catherwood AC, Lloyd AJ, Tod JA, Chauhan S, Slade SE, Walkowiak GP *et al.* Substrate and Stereochemical Control of Peptidoglycan Cross-Linking by Transpeptidation by *Escherichia coli* PBP1B. *J Am Chem Soc* 2020; **142**: 5034–5048.
- 349 Perrin F. Polarisation de la lumière de fluorescence. Vie moyenne des molécules dans l'état excité. *J Phys Radium* 1926; **7**: 390–401.
- 350 Owicki JC. Fluorescence Polarization and Anisotropy in High Throughput Screening: Perspectives and Primer. *J Biomol Screen* 2000; **5**: 297–306.
- 351 Roach PL, Baldwin JE, Aplin RT, Robinson CV, Schofield CJ. Peptide mapping of the active site of *Bacillus cereus* β -lactamase I by the use of high pressure liquid chromatography coupled to electrospray ionisation mass spectrometry. *J Chem Soc Chem Commun* 1994; : 849–850.

Chapter 2. Feasibility Studies of a Surface Plasmon Resonance system for PBPs

2.1 Introduction

When attempting to analyse small molecule interactions, it is often desirable to have multiple, independent measurements of the same interaction. Multiple assays to probe PBPs have been designed (see Table 1.2) but in many cases these cannot measure the on- or off-rates of the protein-small molecule interaction. Instead, for this, biophysical methods must be used. A number of these methods exist, each using a different biophysical property of the protein ^{1,2}. Surface plasmon resonance (SPR) and biolayer interferometry both exploit optical phenomenon whilst other methods such as isothermal titration calorimetry measure thermodynamic properties of an interaction. SPR is sensitive, label free and can be used to find the k_{on} and k_{off} of a bimolecular reaction. Whilst these desirable attributes have seen its use increase over recent years ³, its sensitivity demands great care for successful use which can make the method development challenging.

This chapter describes attempts to develop a SPR system for measuring small molecule interactions with PBP3, examining various coupling methods and optimisations of the method required for detecting binding.

Many proteins ^{4,5}, including PBPs and β -lactamases ⁶ have been assayed using SPR. Various methods have been reported to couple a PBP to the chip: through azide “click chemistry” ⁷, binding of a β -lactam ^{8–11}, or moenomycin ^{12,13} on to the chip surface to link the protein to the chip at the transpeptidation (TP) domain or transglycosylation (TG) domain respectively. Much of this work has been carried out by Vollmer and colleagues in order to investigate protein-protein interactions ^{7,8,10,11}. However, due to the much higher molecular mass of proteins, SPR systems investigating protein analytes present very different challenges to those investigating small molecules ^{14,15}. Since PBP3 lacks a TG domain, an accessible TP site for investigating inhibitor binding is required, so coupling via the TP domain is not

feasible. At the commencement of this work, SPR had not been used in the detection of small molecule binding at the PBP transpeptidase site. However in April 2021 a report described SPR for use in the determination of the binding of pyrrolidine-2,3-diones to *P. aeruginosa* PBP3 (PaPBP3)¹⁶, this is compared to this work in section 2.3.6.

Note on terminology

In contrast to other areas of life sciences, SPR literature the term “ligand” refers to the protein bound on to the surface of the chip, whilst “analyte” is used for the molecules flown over the top whose interactions are investigated. For consistency with the literature, this notation will be used throughout this chapter.

2.1.1 Biophysics of SPR

An SPR instrument is able to detect changes in the characteristics of a thin metallic surface by detecting small changes in its refractive index. The detection method is based on physical phenomena that occur when light is incident on the interface with a material (e.g. gold) with a lower refractive index than the refractive index of the material (e.g. glass) it is currently travelling through. At low angles, total internal reflection (TIR) can occur, in which the incident light is reflected, but an additional electronic wave, termed a “evanescent wave field” is generated through the material with the lower refractive index. This wave decays exponentially and typically only penetrates around a quarter of a wavelength of the incident light into the surface. Away from certain resonant wavelengths, no energy from the incident beam is absorbed and the intensity of reflected light equals that of the incident. However, if the interfacing material surface is a metal, at specific combinations of the wavelength of light, the angle of incidence and the refractive index of the interfacing material, resonance with the electrons of the metallic surface (in practice this is a gold surface), leads to absorption of energy by the metallic surface which can be seen as a “dip” in the ratio of incident/reflected light (Figure 2.1). In Biacore systems, only monochromatic light is used, meaning the angle of incidence can be varied to find and observe the dips^{17,18}. The shape and position (as defined by the angle) of the dips are affected by the refractive index of the material (Figure 2.1b).

Due to the thinness of the surface, its refractive index can be changed by binding proteins and even small molecules to the surface. This response is linear with the mass of bound material ^{12,13}. The changes in the position of the minima of the dip following changes in refractive index are converted into “Response Units” (RU) in Biacore machines, which can then be used to quantify binding events.

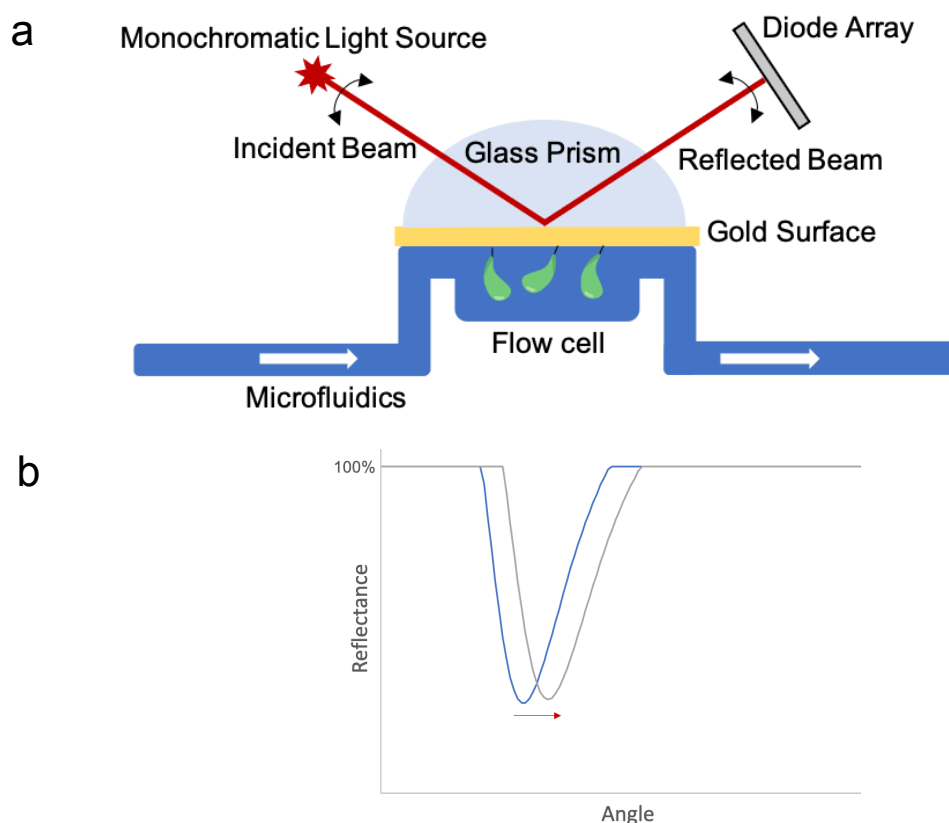


Figure 2.1. The fundamental components of a Biacore SPR instrument. Not to scale. (a) The microfluidics and gold surface are combined on a disposable chip cassette. Once inserted into the machine the gold is placed against the glass prism. Monochromatic light shines onto the gold surface, is reflected with total internal reflectance, and the intensity of the reflected beam is measured by the diode array. The angle of the incident beam can be varied to detect the “dips”. The underside of the gold chip is coated with carboxymethylated dextran to which the ligand is coupled. Analytes can be flown through the microfluidics once the ligand has been bound and the response to their binding measured. (b) Dips recorded by the SPR of the flow cell 1 (blue) and 2 (grey) of the ligand-coupled SA chip (see below). Reflectance, the ratio of the intensity of the reflected and incident beams are plotted against the angle of incidence. The peak minima is converted to the response in response units (RU). The effect of the ligand binding can be seen in the right shift of the curve (as shown by the red arrow), this change corresponds to a 5700 RU change in response. Reflectance is measured by ratio of reflected light to incident light.

2.1.2 Instrumentation

Continually monitoring the surface whilst flowing analytes across it allows measurement of the interactions of the ligand (bound to the metal surface) and the analyte (in solution). An important factor when designing an SPR system is to find an appropriate coupling system for attaching the ligand to the surface. An ideal coupling method is one that gives a stable baseline, with the protein exposed to the flowing buffer at the correct density. For Biacore systems (on which all work in this chapter was carried out)²¹, a variety of coupling methods exist as pre-prepared kits¹⁸ or custom surfaces can be created from blank chips²².

The choice of coupling method depends on: the protein; the aim of the experiment; the ease of regeneration of the system (see below); and size of the analyte being investigated. During the course of this work, five surface coupling methods were investigated.

In any experiment the first step is to attach the protein to the chip surface. The practicalities of this are discussed below but whichever method is used to carry this out, a linear relationship between the mass bound and change in response remains. As such, following immobilisation, the concentration of the protein on the chip can be easily calculated using Equation 2.1^{23,24}. For example, for couplings in which a 10,000 RU of PaPBP3 (MR: ~60,000 Da) is bound to the chip (R_{ligand}) a concentration of ~1.67 mM of protein is bound to the flow cell. The matrix of dextran used on the CM5 chips (used for amide coupling and streptavidin capture) is not a monolayer as depicted in Figure 2.1a but forms a 3D surface.

$$[ligand] (mM) = \frac{R_{ligand} \times 10}{MR_{ligand}} \quad (2.1)$$

Additionally, the theoretical maximal amount of analyte (R_{max}) that can be bound to the chip can be calculated by equation 2.2 using ratio of the molecular masses of the analyte and ligand and the valency of the interaction²⁵. In all cases, a simple 1:1 valency is assumed.

$$R_{max} = \frac{MR_{analyte}}{MR_{ligand}} \times R_{ligand} \times valency \quad (2.2)$$

2.1.3 Coupling and Regeneration

During SPR, the surface can be simplistically described as being in one of the three states shown in Figure 2.2: the uncoupled chip surface (state **1**), the ligand coupled to the chip (state **2**) and the analyte bound to the ligand, which itself is coupled to the chip (state **3**). After analyte binding, the surface must be regenerated in order for a new analyte or different concentration of the same analyte to be applied. As shown in Figure 2.2, this regeneration can go via two routes, either returning to state **1**, a protein-free chip (route **A** in Figure 2.2) or to state **2**, an unbound protein (route **B** in Figure 2.2). Route **B** is perhaps the more common method, but route **A** can be used for effectively irreversible interactions such as those of β -lactams with PBPs. Three methods for route **A** were initially investigated: a streptavidin “CAPture” system and two methods utilising a thiol linkage²¹. Route **B** regeneration was also attempted for an amide-coupled and a streptavidin-coupled chip.

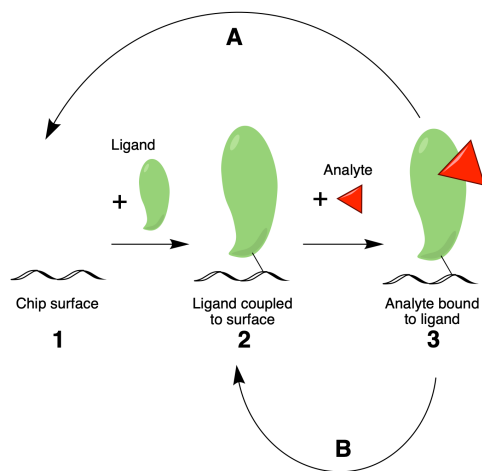


Figure 2.2. Generalised coupling and regeneration methods. A chip with an unmodified surface (**1**) is first coupled to the ligand (**2**) then the analyte is bound (**3**). The chip can be regenerated via route **A**, in which the surface is returned to a ligand-free state, or route **B** in which the analyte is removed from the ligand.

2.2 Methods

2.2.1 Instrument

A Biacore T200 instrument was used for all experiments. Coupling experiments were run using the in-built “Biacore T200 Control Software” (Version 2.0); either as a Manual Run (Thiol coupled experiments) or in-built “Wizard” programs (all others). Analyte binding experiments were performed using the single cycle kinetics or multi cycle kinetics programs of the software. The sample compartment and chip were maintained at 25 °C throughout. The “Desorb” cleaning program was implemented between runs and the “Desorb and Sanitise” program ran every month on the instrument.

Details of the procedures for the coupling regimes are given in section 2.3.

Prior to running the analyte samples 20 “conditioning” start up cycles were used to stabilise the baseline response of the instrument. Solvent correction was run before and after the analyte experiments and the average of the two used to generate calibration curves .

All chips were “S series” chips purchased from Cytiva, handled following manufacturers directions.

2.2.2 Buffers

Running buffers were typically either: 0.01 M N-(2-hydroxyethyl) piperazine N'-(2-ethanesulfonic acid) (Hepes) pH 7.4, 0.15 M NaCl, 3 mM ethylene diamine tetraacetate (EDTA), 5 % (v/v) dimethyl sulfoxide (DMSO), 0.005 % (v/v) Surfactant P20 (for CAPture and thiol coupled experiments); or 10mM sodium phosphate, 2.7 mM KCl, 137 mM NaCl pH 8, 5 % (v/v) DMSO, 0.05 % (v/v) Tween 20 (for amide and streptavidin coupled experiments). Buffers were made up from 10 x stock solutions to 1.05 x solutions then 5 % (v/v) DMSO was added. Buffers were filtered and degassed under vacuum prior to use. Buffers were used within days of their preparation. A separate aliquot of the buffer without 5 % DMSO was kept for preparing the solvent correction curves. Analytes were diluted from high (either > 100 mM in DMSO or dissolved powder) concentration into the running buffer

immediately prior to the beginning of the experiment. Upon changing the buffer system in the instrument in preparation for a run, the “Prime” procedure was run twice.

2.2.3 Reagents

Biotinylated and cysteine mutant PaPBP3 proteins were produced by Dr. Dom Bellini. Briefly, plasmids used previously for the production of PaPBP3 (residues 50 - 579) ²⁶ were modified at the C-terminus (immediately before the STOP codon) by the addition of either a short ‘Avitag’ (GLNDIFEAQKIEWHE) or a single residue of cysteine (no other cysteines are present in the protein). For the biotinylated protein, the plasmid was transformed into *E. coli* BL21 cells as previously ²⁶, with an additional plasmid *pBirAcm* (Avidity) co-transformed into the cells. The manufacturer's protocol (Avidity) was followed for the simultaneous expression of PaPBP3 and BirA as well as the enzymatic reaction to add D-biotin at the Avitag site. Both proteins were purified as previously described ²⁶. MreC (truncated to residues 58-367) was a kind gift from C. Graham.

Reagents were purchased from Sigma or Cytiva.

Solutions of dithiothreitol (DTT), tris(2-carboxyethyl)phosphine (TCEP), N-hydroxysuccinimide (NHS), 1-ethyl-3-(3-dimethylaminopropyl)carbodiimide (EDC) and 2-(2-pyridinyldithio)ethaneamine hydrochloride (PDEA) were prepared directly before use from powder stocks.

Analytes were diluted to their desired concentration from high concentration stocks (either > 100 mM in DMSO or dissolved powder) by serial dilution into the running buffer, keeping DMSO (if present in the stock) constant across all the injections.

2.2.4 Procedure for preparation of activated thiol PaPBP3

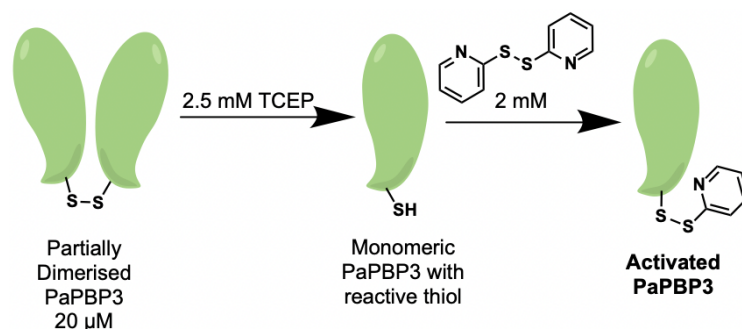


Figure 2.3. Preparation of activated thiol PaPBP3. PaPBP3 with a C-terminal cysteine was partially dimerised (by disulphide bonds between molecules) after purification, presumably due to spontaneous oxidation in air. 2.5 mM TCEP was used to reduce the dimers to monomers, which were then treated with 2 mM 2,2'-Dithiodibispyridine (2,2-DTP) to produce 2-thiopyridine conjugates of PaPBP3, across an asymmetric disulphide bond. Unreacted TCEP and 2,2-DTP were separated from the protein by elution through a gravity-driven PD-10 column.

To prepare activated PaPBP3 for surface thiol coupling, and remove any disulphide-bridged dimers of PaPBP3 (formed by spontaneous oxidation during purification) the following procedure was followed (Figure 2.3). PaPBP3 with a C-terminal cysteine insertion (Cys580, 20 µM, in 10mM 2-amino-2-(hydroxymethyl)propane-1,3-diol (Tris), 500 mM NaCl, pH 8 buffer) was reacted with 2.5 mM TCEP before 2 mM 2,2'-Dithiodibispyridine (2,2-DTP) was added. The solution was then loaded onto a gravity-driven PD10 column (Cytiva, running buffer: 100 mM sodium phosphate, pH 6 buffer) and the protein-containing fractions pooled, to allow separation from the TCEP- and 2,2-DTP-containing fractions. The lack of dimerisation (through Cys580) of the protein was confirmed by gel electrophoresis (without reducing agents in the loading dye). Protein fractions did not react with 5,5-dithio-bis-(2-nitrobenzoic acid) (DTNB), indicating a lack of free thiols. Conjugates similar to this have been shown to have stability in the order of months²⁷, although this conjugation was used within days of preparation.

2.2.5 Reference Surfaces

The microfluidics within the Biacore chips allow for configurations in which the analyte is first flown over a “reference surface” which lacks the protein of interest so

that the non-specific and bulk phase changes caused by the analyte injection can be accounted for. Reference surfaces are used in all analyte binding experiments but varied between the coupling systems used; for the CAPture system streptavidin without biotinylation was used. An injection of the oligo-streptavidin solution only was carried out for this surface. For the thiol-based systems a free cysteine was used, coupled to the chip by NHS/EDC; for the streptavidin system streptavidin without biotinylation was used (no modification); for the amide coupling system ethanolamine was used (or MreC for section 2.3.5.4), coupled to the chip by NHS/EDC. In each case the reference surface was prepared using the same procedures as the active surface, but with the protein injection omitted.

Typically, the reference surface was in flow cell 1 and the “active” (ligand-activated) surface was in flow cell 2. During an analyte binding experiment, the instrument is set to record the response of flow cell 1 and 2 and find the difference between them to give the response signals.

2.2.6 DMSO Calibration Curves

DMSO has a significant effect on SPR, with a 1 % difference in DMSO concentration between the injected sample and the running buffer leading to 1000 RU response. Making up samples to the same exact concentration of DMSO as the running buffer is challenging, and reference subtraction is generally insufficient because the DMSO displaces a volume of water on the chip surface but the extent of this varies depending on the surface modification. It is therefore important to know how the reference and active surfaces respond to a DMSO pulse. For this a DMSO calibration curve is needed. An example is shown in Figure 2.4. A series of known concentrations of DMSO are injected and the response on the active and reference surfaces are recorded. The reference response and the difference between the active and reference are plotted against each other and used to construct a calibration curve. After the sample containing DMSO is injected, a square pulse (correcting for the difference in the response of the active and reference cells to DMSO) is subtracted from the reference-subtracted signal, which corrects for the calculated difference in response of the active and reference cells to DMSO. This correction is carried out automatically by the control software.

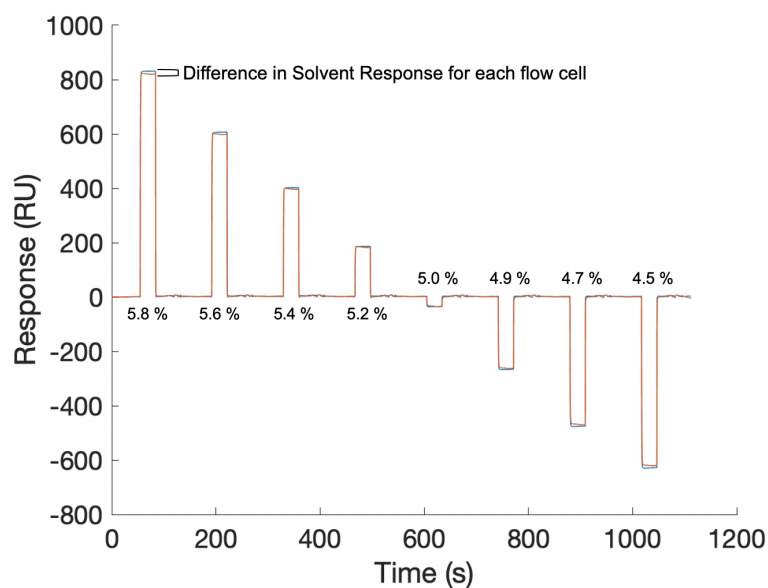


Figure 2.4. A typical Solvent Correction Curve. Eight concentrations of DMSO were flown over both the active (blue) and reference cells (orange) to generate a solvent correction calibration set. Due to the different surfaces, the active and reference flow cells respond differently to DMSO, one such difference is highlighted. Concentrations of DMSO injected are shown on the graph. The buffer contained a nominal 5 % (v/v) DMSO.

2.2.7 Analysis

Curve analysis was performed in the “Biacore T200 Control Software” (Version 2.0). This program can perform reference and solvent corrections. Figures of the traces were produced in Matlab (Version 2020a) using custom scripts. Figures of the coupling models were generated in ChemDraw (Professional version 17.0, PerkinElmer Informatics).

2.3 Results and Discussion

2.3.1 CAPture System

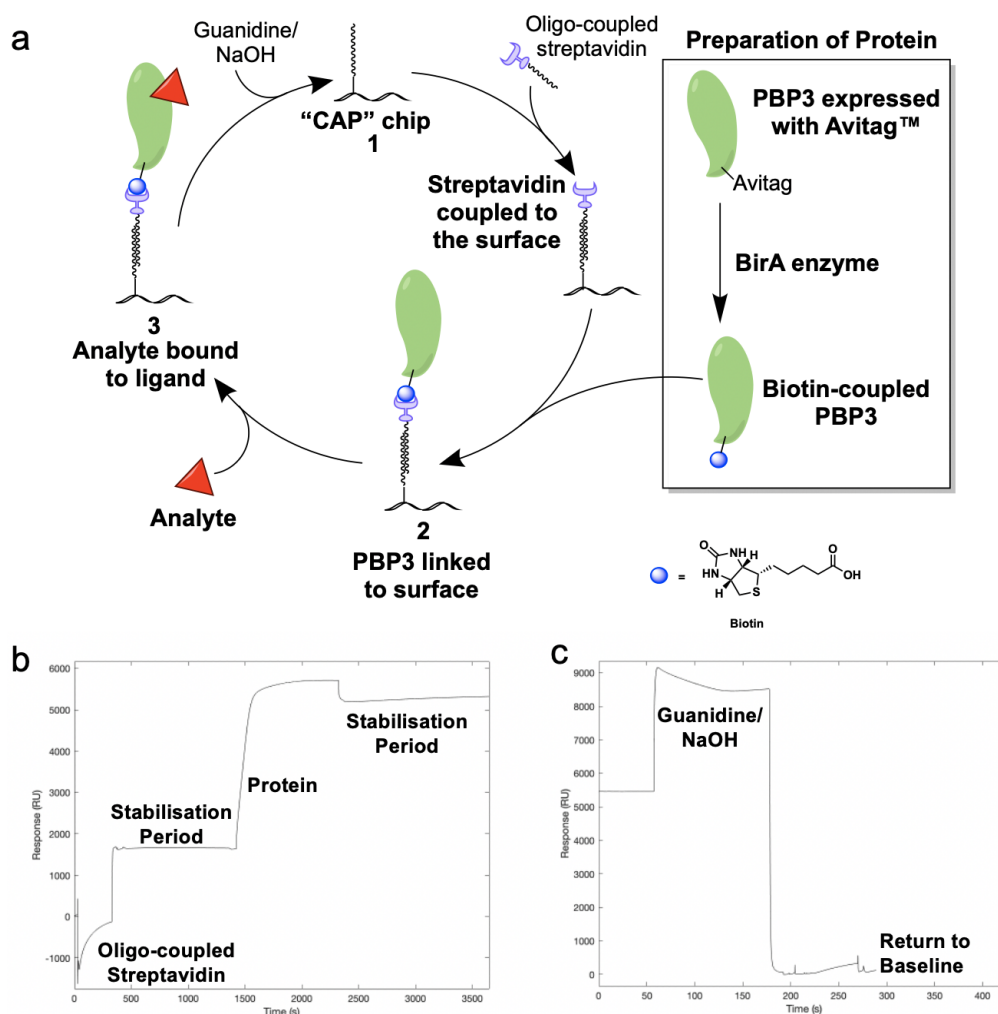


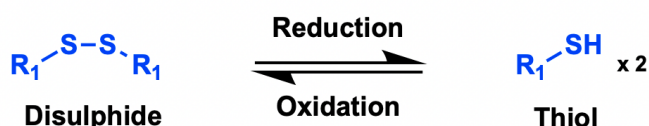
Figure 2.5. Route A regeneration: CAPture coupling system. (a) Scheme for the coupling system. Biotin was added to the PaPBP3 during purification by the addition of the small Avitag (Avidity) sequence to the protein sequence, which is recognised by the enzyme BirA (Avidity) which ligated biotin at a specified point within the binding sequence^{28,29}. The chip (which is supplied with a single stranded oligonucleotide bound to the surface) was prepared by addition of a complementary streptavidin-oligonucleotide conjugate. The oligonucleotides annealed, resulting in a streptavidin-activated surface. When the protein was flown over this surface, the streptavidin bound to the biotin found on the protein with high affinity, coupling the protein to the chip. Once the analyte has bound, the chip can be regenerated by the addition of a solution of guanidine in NaOH to denature the double stranded oligo and return to state 1. Numbers in bold correspond to the three states of the chip shown in Figure 2.2. (b) Response of flow cell 2 to reagents. The chip was activated by flowing over oligonucleotide-coupled streptavidin (proprietary solution, 50 µg/mL, flow rate 2 µL/mL, 5 minute contact time), before the biotin-coupled PBP3 (1.25 mg/mL, flow rate 2 µL/mL, 10 minute contact time) was injected. (c) an injection of guanidine HCl (6 M with 250mM NaOH, flow rate 30 µL/mL, 2 minute contact time) removed both the streptavidin-coupled PaPBP3 and the chip was ready to be used again.

With the CAPture system³⁰, regeneration is possible due to the reversible denaturing and annealing of complementary DNA oligonucleotides, attached to a streptavidin molecule, to capture a biotin-bound protein. Denaturing of the DNA allows the protein to be removed and the surface regenerated (Figure 2.5a). This kit is intended for the use of protein-protein interactions, but there is no fundamental reason why it cannot be used to study protein: small molecule interactions. This method utilises a commercially available kit (Cytiva), in which a chip is supplied with oligos coupled to its surface at predetermined and unchangeable density. Unfortunately, this determines the maximum load of the protein onto the chip, since only one protein molecule can be coupled to each oligo. Consequently, several attempts were made at coupling the protein onto the chip and each time only ~ 4000 RU of protein could be bound, although regeneration was successful and reversible. Additionally, there appeared to be significant amounts of baseline drift which remained even after long equilibrations.

2.3.2 Thiol-based System

The basis of reversibility in thiol-based systems is the reversibility of disulphide reduction/oxidation cycles (Figure 2.6). There are two similar systems.

Disulphide reduction/oxidation reaction



Thiol/disulphide exchange

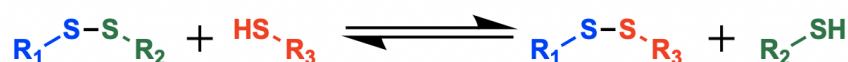


Figure 2.6. Simplified reactions of thiols used for the preparation of the thiol-coupled chip. Disulphide reduction can be driven by reducing agents such as TCEP or DTT. Oxidation can happen spontaneously in air over time and will inactivate any free thiols, preventing them from acting as nucleophiles in the thiol/disulphide exchange reaction. Thiol/disulphide is the reversible exchange of one thiol for another within a disulphide bond. The position of equilibrium between the two states is determined by the relative reactivity and stability of each thiol as well as relative concentrations^{35,36}.

In the first system “ligand-thiol”, the reduced, nucleophilic, sulphur is found on the ligand ^{31,32}, whilst in second “surface-thiol”, the nucleophilic sulphur is on the chip (Figure 2.7 and 2.8) ³²⁻³⁴. The resultant ligand-coupled complex is similar (note the additional carboxyl group in the surface-thiol system (Figure 2.7 and 2.8), but the different methods differ in their re-activation following regeneration.

Using both methods, immobilisation was successful, with 4,552 RU and 7,367 RU binding for the surface and ligand thiol systems respectively. However, in both cases it was not possible to regenerate the chip, with either DTT or TCEP reducing agents at concentrations up to 1 M. Injections of sodium hydroxide (100 mM) did not result in a large reduction in binding, indicating it was not a purely non-covalent attachment (which would not be removed by reducing agents). Long injections (1 hour) with DTT also failed to remove ligand, indicating this is not an issue simply with the rate of reaction.

The lack of ability to remove the PaBPB3 from the chip could therefore be explained several ways: i) incomplete reaction of PDEA or cysteine (depending on the method) and activated chip surface, which would leave free, unreacted NHS-esters to couple covalently to the protein’s free amines (same reaction as used in amide coupling). Long injections with excess of PDEA or cysteine were used to attempt to prevent this issue from occurring, but it is possible these were insufficient. ii) Disulphide bonds may have been inaccessible to the reducing agents, by the protein burying the newly-formed thiol away from the solvent. This is feasible, especially given the electrostatic attraction between the negatively charged surface and positively charged protein at neutral pH. It could potentially be addressed by introducing longer linking molecules, which would act to separate the protein and surface, allowing more access to the disulphide bond. The reversibility of the thiol bond in solution was confirmed by gel electrophoresis in the presence of DTT. Without the expected regeneration it was decided to not pursue this surface further.

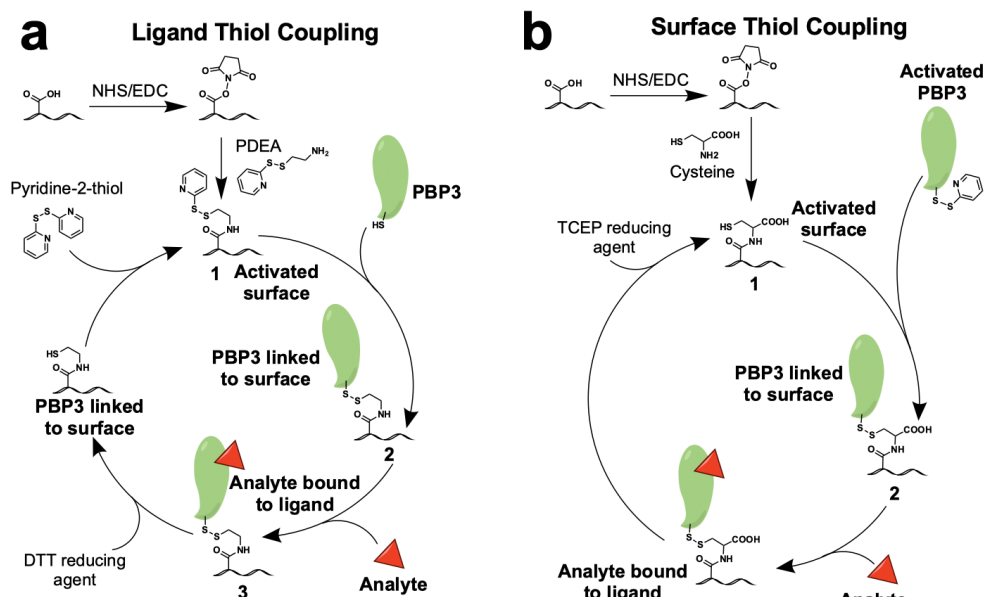


Figure 2.7. Route A regeneration: thiol coupling. (a) Scheme for ligand thiol coupling. A CM5 (Cytiva) chip was used as the starting surface, which is activated by NHS and EDC coupling reagents. PDEA was coupled to the surface by its amine group. Thiol exchange (Figure 2.6) with a free sulphur on the PaPBP3 (introduced by the engineering of a cysteine into the C-terminal of the protein) coupled the protein to the chip. Once the analyte was bound to the surface, Dithiothreitol can be used to reduce the disulphide, regenerating the surface, before another thiol exchange reaction with pyridine-2-thiol re-activates the surface. (b) Scheme for surface thiol coupling. The protein was prepared as described (section 2.2.4) to produce a 2-thiopyridine conjugate of PaPBP3. The chip was prepared using NHS/EDC coupling reagents which were used to couple a molecule of cysteine onto the chip surface. This was then reduced by TCEP to produce a free sulphur which reacted with the protein disulphide to couple the protein onto the chip. After analysis, regeneration can occur by reduction of the disulfide, once again releasing a free-sulphur to react on the next cycle.

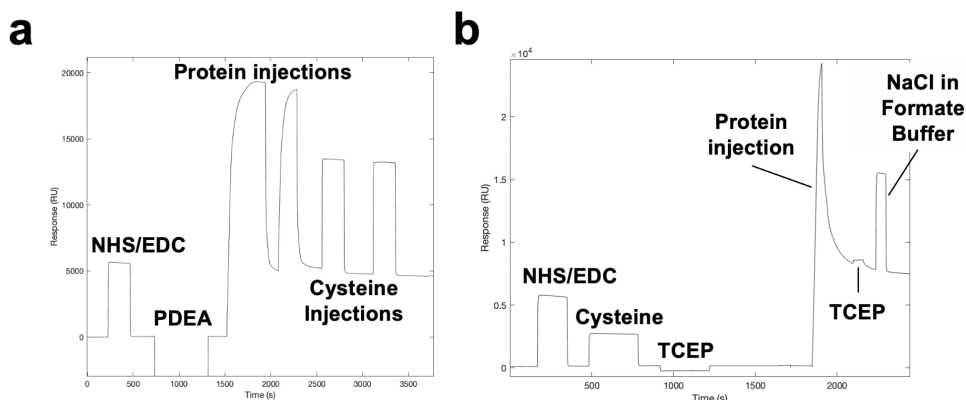


Figure 2.8. Thiol coupling sensorgrams. (a) Response of flow cell 2 to reagents. Flow rate was 5 $\mu\text{l}/\text{min}$ throughout. A mixture of NHS/ EDC (0.1 M and 0.4M respectively in water) was injected onto the surface (4 minute contact time), followed by PDEA (80 mM in Bicine buffer 100 mM, pH 8.3, 8 minute contact time). Two injections of PaBP3 (850 nM in Bicine buffer 100 mM, pH 8.3, contact time: 7 minutes then 3.5 minutes) achieved an immobilisation of 4,552 RU before two injections of cysteine (50 mM in 100mM formate, 1M sodium chloride pH 4.3, contact time of 2 x 4 minutes) were flown over the surface to block remaining free thiols and reduce the baseline drift. Dithiothreitol injections (DTT, 100 mM, contact time: 10 minutes) were used in an attempt to reduce the disulphide, but this was unsuccessful, with only around 180 RU of protein being removed. Higher concentration DTT (1 M, 10 minutes) injections were also ineffective. (b) Response of flow cell 2 to the injection of reagents. A flow rate of 5 $\mu\text{l}/\text{minute}$ was used throughout. Injections of NHS/EDC (0.1 M and 0.4 M, respectively, in water, contact time 3 minutes) then cysteine (50 mM in 100mM formate, 1M sodium chloride pH 4.3, contact time 5 minutes) then TCEP (10 mM in sodium phosphate, pH 6, contact time 5 minutes, to reduce any spontaneously oxidised cysteines and release a free thiol) were flown over the surface. Onto this prepared surface was injected protein (850 nM in sodium phosphate pH 6 buffer, contact time 1 minute) giving an immobilisation of 7,367 RU of protein. However injections of TCEP (10 mM in sodium phosphate buffer 100 mM, pH 6) or NaCl (1 M in a pH 4.5 formate buffer 100 mM) were not able to remove the protein, indicative of an irreversible reaction occurring.

2.3.3 Streptavidin coupling

A second capture system uses the high affinity interactions of biotin (on a biotinylated protein) and streptavidin (pre-bound to the chip surface)³⁷, but unlike the CAPture system, this is irreversible and requires route **B** regeneration (Figure 2.9). The method may be better than the amide coupling system because all proteins are orientated similarly due to the fixed position of the biotin tag and no coupling of important lysines can occur.

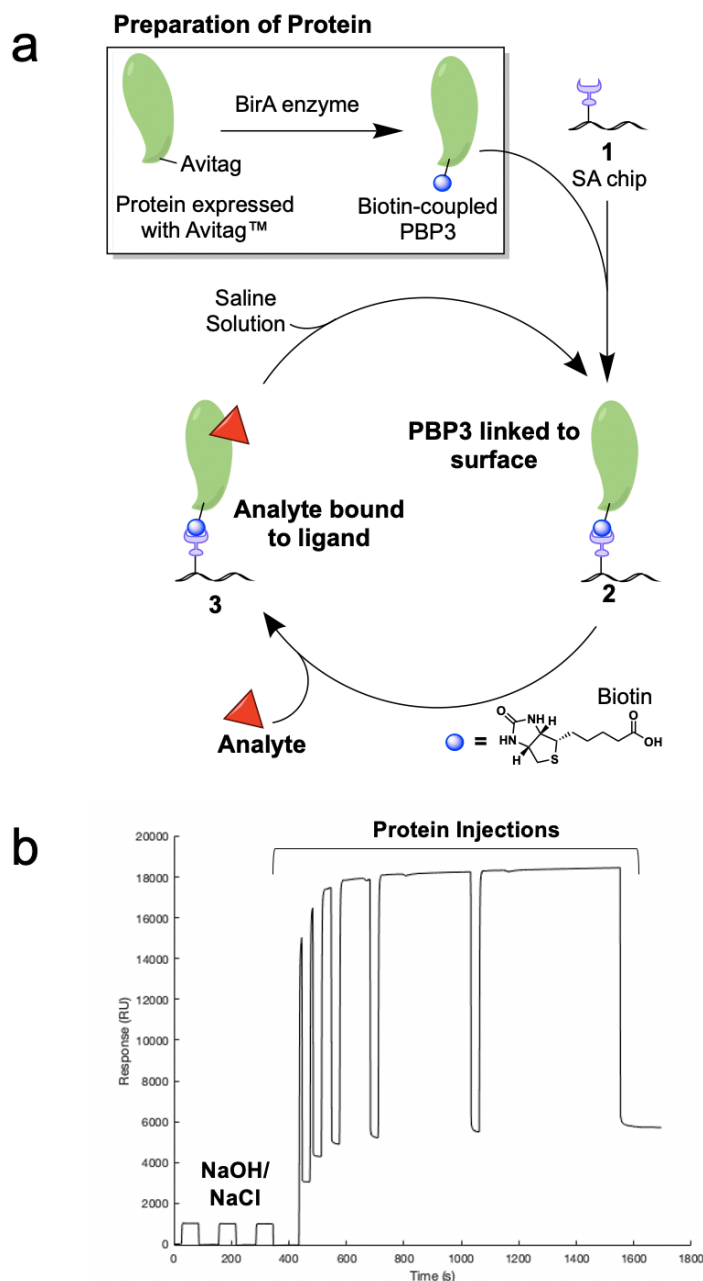


Figure 2.9. Route B regeneration: streptavidin coupling system with biotinylated PaPBP3. (a) Biotinylated PaPBP3 was prepared as with the CAP system, using the BirA/Avitag system (Avidity). The protein was then linked to the chip by the high affinity biotin-streptavidin interaction. As with amide coupling this is an irreversible immobilisation and regeneration is only possible by route **B**. (b) Response in flow cell 2 to reagent injections. The streptavidin on the chip was washed three times (3 x contact time 1 minute, flow rate 5 μ l/min) with a solution of NaOH and NaCl (50 mM and 1 M respectively in water) then the biotinylated PaPBP3 (14 μ M, in sodium phosphate buffer 10 mM, 500 mM NaCl, pH 8, total contact time \sim 17 minutes, flow rate 5 μ l/minute) is flown over the surface until saturation was achieved: 5,700 RU of protein was bound.

2.3.4 Amide Coupling

An amide coupling system can be used to bind the ligand to the chip. This method will couple any solvent exposed amines on the protein to the chip surface. PaPBP3 has 25 lysine side chains as well as the N-terminal amine which may be coupled. These amines form an amide with carboxylic acid groups of the CM5 carboxymethylated dextran (Figure 2.10). The disadvantage of this method is that catalytically important residues (in particular Lys297 and Lys484) may get acylated which will presumably block the active site and lower the effective R_{max} . Additionally the random sampling of coupled lysine residues leads to a range of orientations and conformations of the protein on the chip, which can create an inhomogeneous surface that may interfere with the measurement of kinetics.

In order to optimise the coupling reaction, “pre-concentration experiments” were performed by the instrument “Wizard”. In these experiments protein was injected onto the unmodified CM5 chip surface and the response recorded. If sufficient protein was able to bind non-covalently to the chip surface, a large peak will be recorded during the injection (Figure 2.10b). The weakly bound protein quickly dissociates after the injection (with a NaOH wash to disrupt higher affinity charge-charge interactions) allowing the surface to be activated for covalent interaction. Preliminary experiments found that 1 μ M of PaPBP3 in a low salt, pH 6 sodium phosphate buffer (50 mM NaCl, 10mM sodium phosphate) gave a large pre-concentration response.

2.3.5 Analyte Binding

2.3.5.1 Clinical β -lactams

Initially, the interactions of PaPBP3 with clinical β -lactams (ampicillin and cefotaxime) were investigated. In these cases a technique called single cycle kinetics was used. This method attempts to collect several concentrations of analyte binding data using sequential increases in analyte concentrations. This avoids

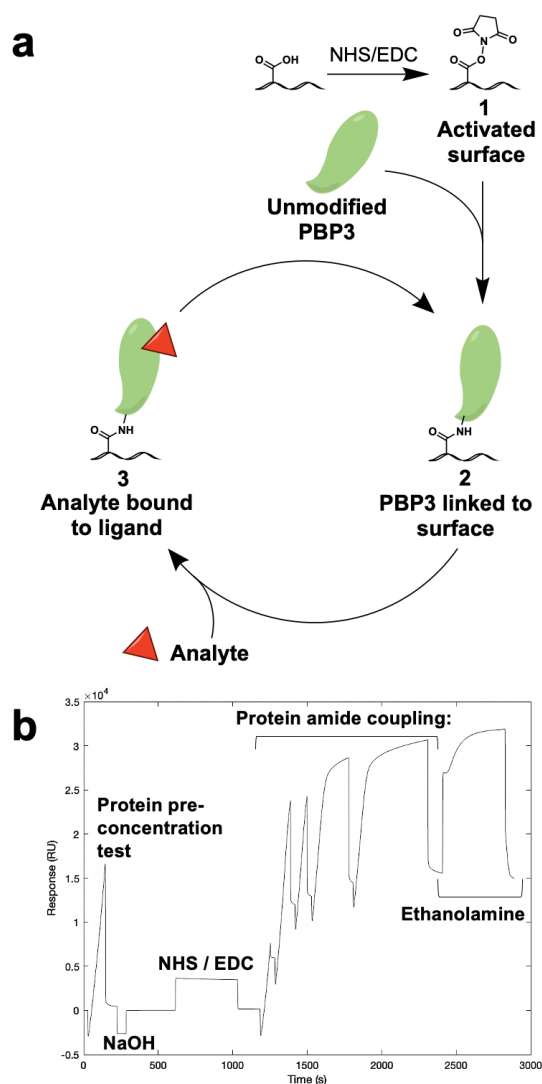


Figure 2.10. Route B regeneration: amide coupling system. (a) Amide coupling links the PaBP3 to the CM5 chip with an amide bond between the carboxyl of the carboxymethylated dextran chip surface and any free amines (lysine side chains and terminal amine) on the protein. This is an irreversible reaction and regeneration can only be achieved via route B. (b) Response of flow cell 2 to coupling reagents. A preconcentration test was initially carried out (see text), achieving around 16,000 RU of protein onto the surface. The majority of this protein was washed off the chip at the end of the injection but any remaining non-specifically bound protein remaining was removed with an injection of NaOH (100 mM in water, contact time 1 minutes, flow rate 30 μ l/min). A mixture of NHS/EDC (0.1 M and 0.4M respectively in water, contact time 7 minutes, flow rate 10 μ l/min) was used to prepare the carboxymethylated dextran surface for covalent coupling to the protein. PaBP3 was then flown over the surface in multiple injections (total contact time ~17 minutes, flow rate 5 μ l/min) achieving a final protein load of 12,086 RU. Ethanolamine (1.0 M, pH 8.5, contact time 7 minutes, flow rate 10 μ l/ml) was then injected to block any unreacted activated surface molecules.

the issue of a single high concentration binding to all the active sites and inactivating the protein, preventing any more data from being collected. For three chip surfaces (CAPture, streptavidin coupling and amide coupling) β -lactam interactions did not generate any specific signal (Figure 2.11). The cause of this is unclear.

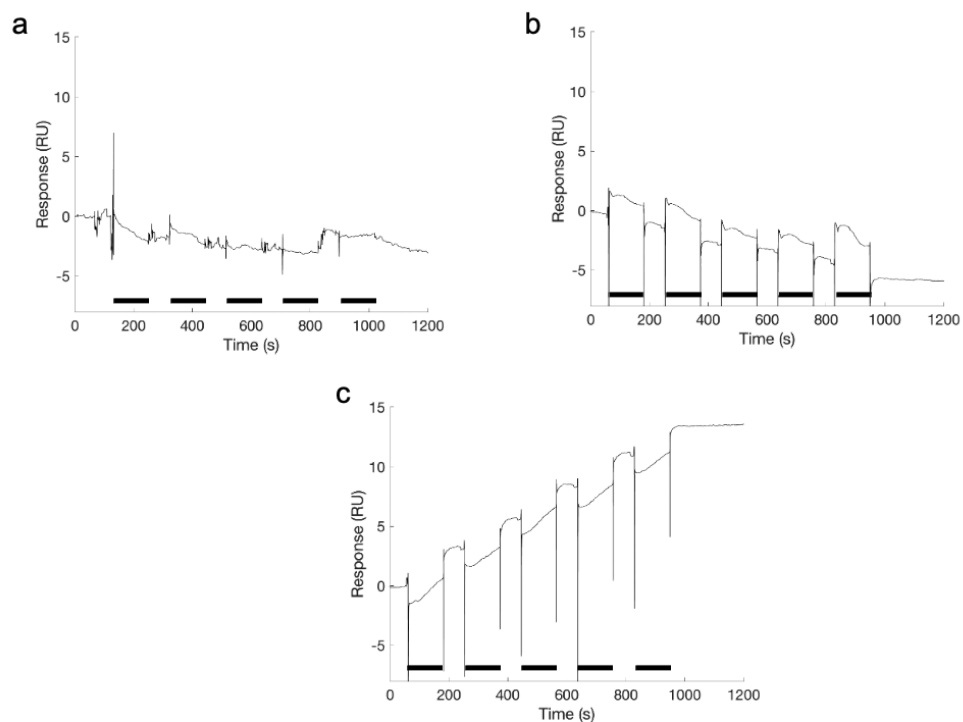


Figure 2.11. β -lactam binding to various chip surfaces (a) Injections of 5 concentrations of cefotaxime (12, 80, 400, 2,000, 10,000 nM) were flown over a PaBPB3 CAPture coupled chip surface using single cycle kinetics. Expected R_{max} of 30 RU. Additionally the baseline following injections was unstable which is undesirable. (b) Injections of 5 concentrations of Ampicillin (8, 16, 32, 64, 128 μ M) were flown over a streptavidin coupled chip surface using single cycle kinetics. Expected R_{max} of 27 RU (c) Injections of 5 concentrations of cefotaxime (33.3, 100, 333, 1000, 3330 nM) were flown over an amide coupled chip surface using single cycle kinetics. Expected R_{max} of 46 RU. Non-specific binding is observed (steep, concentration non-specific increases during injection). In each case the black bars indicate the injection pulse (contact time 120 s, flow rate 30 μ l/min).

2.3.5.2 Nitrocefin

In contrast to clinical β -lactams, nitrocefin could be used to generate positive response curves on an amide coupled surface (Figure 2.12). Nitrocefin has previously been used in an SPR system to investigate β -lactamase behaviour in a custom-made coupled SPR-absorbance system³⁸. A concentration dependent response was observed for nitrocefin, with agreement between repeats. Nitrocefin was anticipated to be a better probe due to its ability to react with PaPBP3 then de-acylate (Chapter 6), which is effectively route **B** regeneration. However, the response could not be fully regenerated with the baseline not returning to zero between injections, even after 1000 s of dissociation or being left overnight. If the value of k_{cat} for PaPBP3 nitrocefin turnover ($\sim 40 \text{ min}^{-1}$: Chapter 6) is assumed to occur under these conditions then it would be expected that the protein would regenerate with a half-life of 1.5 seconds. The lack of regeneration meant that the baseline increased after every injection.

This increase in the baseline did not prohibit further binding of nitrocefin to the protein. For example, due to the sequencing of the injections, half of the injections in Figure 2.12a occur after the 8 μM injection (see legend of Figure 2.12), which by itself lead to ~ 80 RU of response, more than the expected R_{max} (76 RU). Such agreement between repeats as is seen would not be expected if the protein was becoming progressively inhibited. The total change in response over the experiment was much greater than the expected R_{max} , with a total change in response in flow cell 2 of 300 RU. Such a response can be indicative of a large contribution to the signal from non-specific binding (but high affinity binding, hence its irreversibility) of the nitrocefin to the protein.

The irreversible binding was not due to interactions of nitrocefin with the chip. Figure 2.12b shows the individual responses of flow cell 1 and 2 to an injection of 8 μM nitrocefin. The trace shows that whilst there is an interaction of nitrocefin with the chip, this dissociates after the analyte pulse. This means that the gain in response seen in Figure 2.12a is due to binding of nitrocefin to the protein itself (which is only present in flow cell 2).

It is unclear whether the observation of apparent greater-than-stoichiometric binding of nitrocefin to PaPBP3 (discussed in Chapter 6) is relevant here. PaPBP3 does not appear to approach saturation even after a mass equivalent to $\sim 4 \times$ nitrocefin molecules bind (change in baseline/ expected R_{max} : 300/76 Figure 2.12), in contrast to the two binding events anticipated from crystallographic studies. SPR would be a useful tool for the investigation of specific greater-than-stoichiometric binding but unless conditions are identified in which non-specific binding does not occur these studies are not feasible.

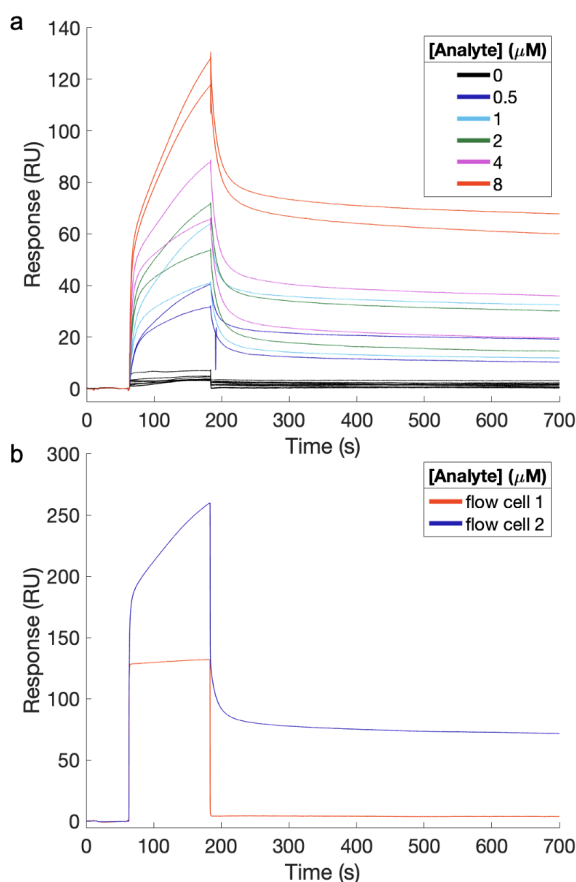


Figure 2.12. Investigation of nitrocefin binding. (a) Reference- and solvent-corrected responses to five concentrations of nitrocefin (0.5-8 μM , see legend) flow over a PaPBP3 amide-coupled CM5 chip. Injections (contact time 120 s, flow rate 30 $\mu\text{l}/\text{min}$, dissociation 1000 s) were run in sequence from the lowest concentration to the highest and then lowest to highest again (giving the two repeats), with a control injection of the running buffer (0 μM nitrocefin) between each experimental injection. Expected R_{max} of 76 RU. Significant increases in the baseline are observed throughout the experiment ($\{\text{reference-subtracted response at the end}\} - \{\text{reference-subtracted response at the beginning}\}$) such that there was an increase in the baseline of almost 300 RU across the entire experiment. In (a) each of the traces is zeroed at the beginning of the experiment to allow easier interpretation. (b) Responses of flow cells 1 (reference) and 2 (active) to the first 8 μM injection.

2.3.5.3 Benzoxaborole

To examine whether the issues of lack of interpretable binding were limited to β -lactams, a benzoxaborole (**13**) analyte was investigated. Biochemical evidence suggests that this binds in a weak reversible manner (K_i of $\sim 80\ \mu\text{M}$) and may be more amenable to SPR. This ligand appears to show PBP-binding activity, however its behaviour is very difficult to interpret, and does not fit into the expected models of ligand:analyte interaction (Figure 2.13).

The rapid increase in the response after the analyte is injected is either indicative of a very rapid on-rate or non-specific interactions. The shape of the curves during injection cycles themselves is not a smooth curve and even at low concentrations does not appear to show any of the curvature expected for bimolecular interactions (see the $8\ \mu\text{M}$ curve, Figure 2.13b). Without this curvature, it is difficult to distinguish specific and non-specific binding (e.g. see the square shape of the non-specific binding curve in Figure 2.12b).

Another issue is that R_{max} (around 100 RU) is not approached, even for high concentrations of analyte (2 mM is 25 times above the biochemically determined equilibrium constant of $80\ \mu\text{M}$). This could perhaps be accounted for by inactive conformations of the ligand, which would reduce the effective R_{max} . However, this is another sign that the system is not behaving as expected, and should be interpreted with caution. Using such high concentrations of analytes typically leads to more non-specific binding.

SPR curves can be simulated with known constants. Figure 2.13b shows an example using values of k_{on} and k_{off} which could give a K_i of $80\ \mu\text{M}$ (although an infinite amount of other combination of these values would also give this dissociation constant). Some similarities can be drawn between Figure 2.13a and b, but it is difficult to be confident in this interaction.

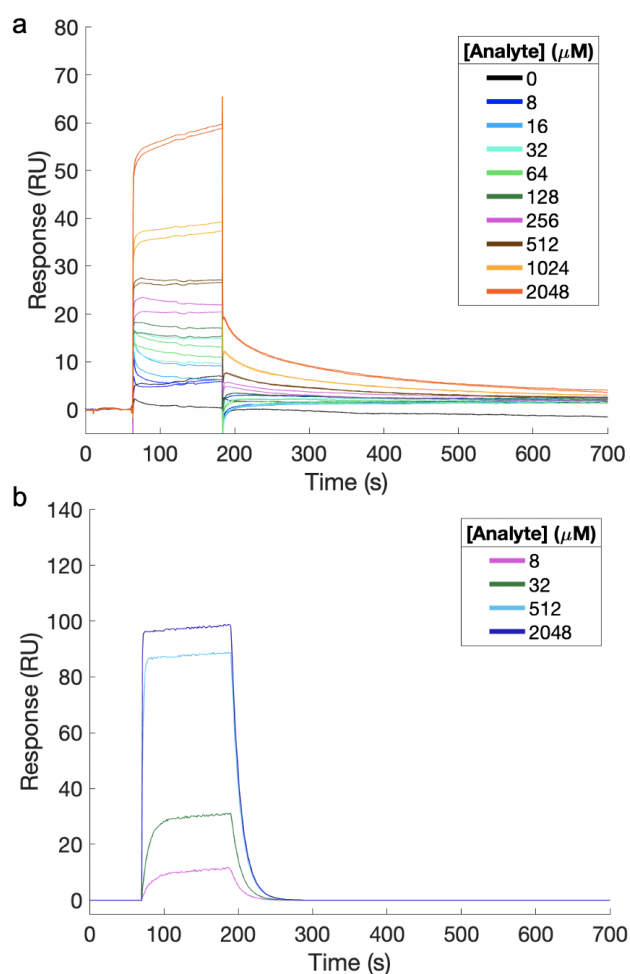


Figure 2.13. Investigation of benzoxaborole binding. (a) Reference- and solvent- corrected responses to nine concentrations (8 μM - 2 mM) of benzoxaborole **13** (Chapter 5) flown over a PaPBP3 amide-coupled CM5 chip. Injections (contact time 120 s, flow rate 30 $\mu\text{l}/\text{min}$, dissociation 1000 s) were run from lowest to highest concentration with repeat injections of a concentration run in pairs. Control injections of the running buffer (0 μM benzoxaborole) were run at the beginning of the experiment. Expected R_{max} of 96 RU. In each of the traces here, the response is zeroed at the beginning of the experiment to allow easier interpretation. (b) Simulated SPR traces using biochemical data (Chapter 5) . Data was generated using the program "SPR-Simulation" (Version 1.3.2.3 Arnoud Marquat, sprpages.nl) using the following settings; k_{on} : $1 \times 10^3 \text{ M}^{-1} \cdot \text{s}$; k_{off} : $8.1 \times 10^{-2} \text{ s}^{-1}$; R_{max} : 100 RU; Noise: 0.4 RU; Drift: 0.02 RU $\cdot \text{s}$; Contact time 120 s. These values of k_{on} and k_{off} give an equilibrium constant ($k_{\text{on}}/k_{\text{off}}$) of 80 μM , approximately the value determined by bocillin competition (Table 5.3).

2.3.5.4 Reasons for Unresponsiveness

For the clinical β -lactams tested, it appears as if no interaction is occurring with the protein at all. This would suggest that the protein is inactive under these conditions. In solution, the protein was demonstrated to be active in the buffers used, however the environment of the coupled chip may cause the protein to behave differently than it does in solution.

The effective concentration of PaBPB3 on the chip surface is in the mM range (see section 2.1). This high concentration may be leading to local aggregation of the protein (the flexible 3D dextran matrix may allow contact between adjacent protein molecules), and its inactivation. However aggregation is typically observable in the response of the chip (Claire Shepherd, Cytiva, personal communication). Alternatively, the protein may be induced into an inactive conformation by protein-protein interactions under these conditions. Steric crowding of the proteins by nearby proteins or the dextran matrix (for CM5 chips used in amide coupling reactions) may be blocking access to the protein active site. The coupling method and surface are known to have a significant effect on the activity of the protein (Claire Shepherd, Cytiva, personal communication).

2.3.5.5 Non-specific Binding and Alternate Reference Surface

For nitrocefin and the benzoxaborole, there appears to be a large amount of non-specific (irreversible and non-stoichiometric) binding to the protein. This obscures any specific interaction that may be occurring between ligand and analyte and makes the results difficult to interpret. The non-specific binding appears to be mainly with the protein and not the chip surface itself, and occurs despite the presence of the Tween 20 detergent (0.05 % (v/v)). Similar non-specific binding appears to occur for another PaBPB3 system ¹⁶ (section 2.3.6).

An alternative, protein-coated reference surface can be used to account for this difference in the degree of analyte binding to the active surface and the simple, ethanolamine reference surface. A surface was loaded with MreC (a bacterial cell wall protein not known to bind β -lactams ³⁹) using amide coupling as shown for PaBPB3 (Figure 2.10), to a response level of 3500 RU and then the analyte was

flowed over and the sensorgrams for the PaPBP3-containing active cell was corrected with the response of the same analyte over the MreC reference cell.

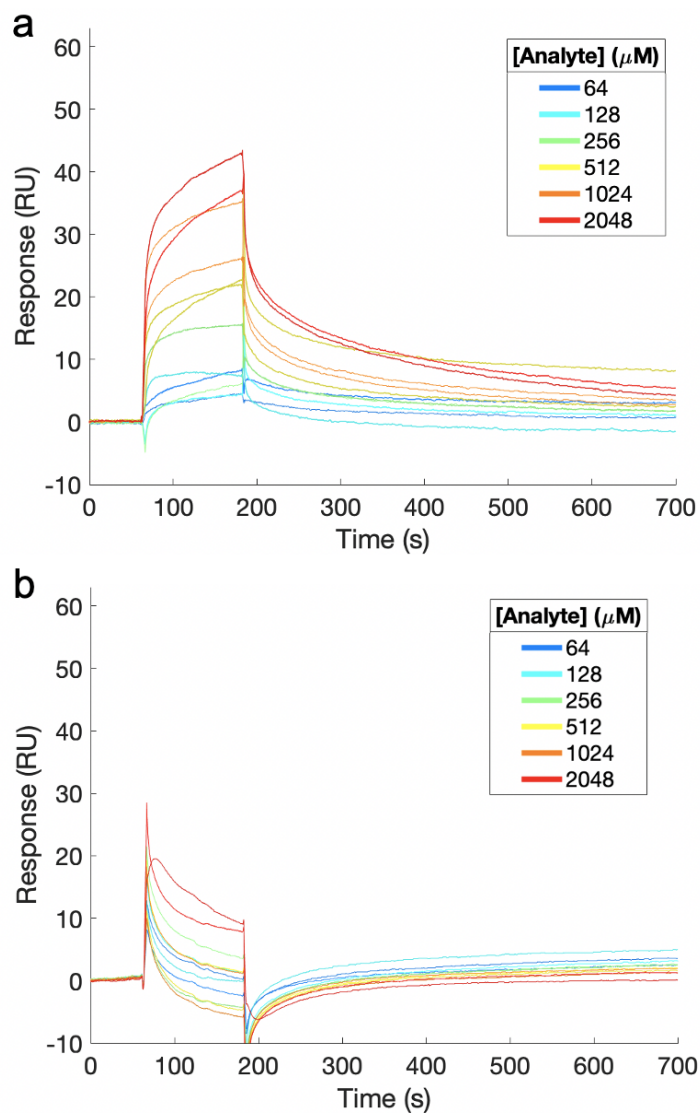


Figure 2.14. Binding of benzoxaborole 13 corrected with an MreC reference. (a) Active cell - coupled to PaPBP3 corrected with the response on an MreC-coupled reference cell. (b) Response on the MreC cell to **13**. Colours correspond to the concentration of **13**. Injections (contact time 120 s, flow rate 30 $\mu\text{l}/\text{min}$, dissociation 1000 s) were run from lowest to highest concentration with repeat injections of a concentration run in pairs. Expected R_{max} of 96 RU. In each of the traces here, the response is zeroed at the beginning of the experiment to allow easier interpretation.

Compared to Figure 2.13a, the addition of the MreC reference leads to an improvement in the corrected signal by reducing the degree of non-specific binding.

However, challenges remain: there are significant differences between the two repeats of the concentrations (although these are generally not as pronounced in the dissociation phase). Even at ~ 2 mM of **13** there is not saturated binding of analyte (it is still increasing towards the end of the pulse and far from the R_{max} of 96 RU, contrast to the simulated Figure 2.13b), which would be expected if the value of the K_i found by the fluorescence anisotropy assay is correct (~ 74 μ M - Chapter 5). Additionally, the signal from the reference cell (Figure 2.14b) is not the square wave expected for a simple fast associating and dissociating non-specific analyte-ligand interaction (For example that seen at flow cell 1 during the interaction of nitrocefin with ethanolamine in Figure 2.12b). Under these circumstances, subtracting this reference signal from the active may lead to the introduction of further errors. Using another protein to coat the reference surface may avoid this challenge.

2.3.5.6 Buffer Screen

One factor relevant to non-specific binding is the buffer used. This was briefly investigated using an inactivated protein, Five different buffers were investigated for their effect on the non-specific binding of ampicillin, with the trace of the active and reference and difference between the two shown. Omission of the salt from the buffer leads to a small amount of non-specific binding of the ampicillin to the protein, which is only slowly washed off. This is likely due to the high pI of PaPBP3 (pI 8.8 as estimated from the sequence by protPARAM⁴⁰) which may indicate that the protein has a significant positive charge at neutral pH. Non-specific binding can be suppressed by raising the salt concentration ((Figure 2.15c) or raising the pH (Figure 2.15d,e) which makes the protein less charged and the interactions less strong. However, the protein may be less stable at these conditions and the interactions less physiological.

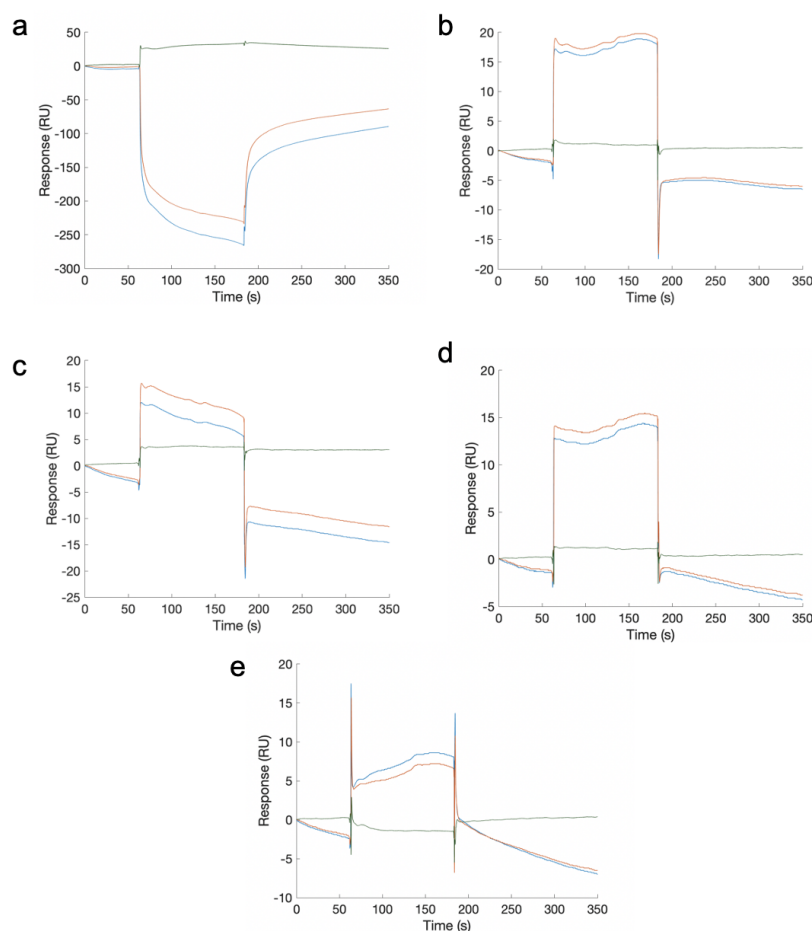


Figure 2.15. Buffer Screening. In each case ampicillin was injected over a streptavidin coupled chip equilibrated in the following buffers: (a) No NaCl, 10mM Tris pH7, 0.05 % (v/v) Tween 20, 5 % (v/v) DMSO (b) 10mM Tris pH7, 150mM NaCl, 0.05 % (v/v) Tween 20, 5 % (v/v) DMSO (c) 500 mM NaCl, 10mM Tris pH7, 0.05 % (v/v) Tween 20, 5 % (v/v) DMSO (d) 10mM Tris pH8, 0.15M NaCl, 0.05 % (v/v) Tween 20, 5 % (v/v) DMSO (e) 10mM 2,2'-(propane-1,3-diyl)bis[2-(hydroxymethyl)propane-1,3-diol] (Bis-tris propane), pH 9, 0.15 M NaCl, 0.05 % Tween 20, 5 % (v/v) DMSO. Injection is ampicillin (20 μ M, contact time 120 s, flow rate 30 s). The response of the active (blue) and reference (orange) as well as the active-reference subtraction (green) is shown. No specific binding is expected as the protein was previously treated by the addition of an excess of ampicillin, which should block the active site. Before each injection the “prime” procedure was performed and the chip exposed to 20 startup cycles in the new buffer.

2.3.6 Comparisons with López-Pérez *et al.* (2021)

During the write-up of this thesis, López-Pérez *et al.* (2021)¹⁶ reported an SPR system for the detection of the binding of pyrrolidine-2,3-diones (Table 1.1) to PaBP3. The SPR system they report uses amide coupling with a similar buffer

system to ours (although the salt and buffer concentrations were much lower: (13 mM NaCl, 257 μ M KCl, 171 μ M KH_2PO_4 , 950 μ M Na_2HPO_4 , 0.05% Tween-20 and 5% DMSO)) and the pH was lower: pH 7.4 vs pH 8. They also use a Biacore T200 and a CM5 chip, on which they achieved comparable coupling levels (12,086 RU vs 11, 820 RU, for this work and López-Pérez et al. (2021) respectively), with an ethanolamine reference surface. K_d values determined for 4 out of 5 of their compounds were on the same order of magnitude as the IC_{50} s determined by S2d and bocillin FL fluorescent polarisation, but one showed significantly weaker binding as determined by SPR compared to the other assays. This validates their SPR method to some degree, but they did not include an external control (e.g. a β -lactam) to compare the results to, likely as a result of similar challenges to those described in section 2.3.5. Sensorgrams have a similar shape to those shown in e.g. Figure 2.13, which they ascribe to very fast association and dissociation rates. At least some of this response appears to be due to non-specific binding because at least for one compound low concentrations of inhibitor do not approach zero response (the authors didn't comment on this). Additionally they use harsh conditions for regeneration (50 % DMSO for 30 s, whereas the chip CM5 tolerance for DMSO only 10 % for 1 minute ⁴¹) which may be required to remove irreversible binding of the compound (although this is not referenced). This regeneration method was not tested in our system. This report appears to partially corroborate our findings that non-specific binding is a problem for amide coupled PBP3 SPR systems, but demonstrates it can be used to determine K_d values that correlate to competition assays.

2.4 Future Work

It is possible that other coupling methods or conditions could be found in which the protein is active. Both the thiol-coupled and biotin coupled proteins were modified at the C-terminus, so N-terminal modification could be investigated. After the conclusion of this work, a team at AstraZeneca published a paper describing three methods of creating a stable but reversible SPR system ⁴². These include the use of "switchavidin": a mutant of streptavidin with biotin affinity that can be modified by changing the pH ⁴². Investigation of these methods for a PBP3-based SPR system may give better responses than the reversible systems tried here (sections 2.3.1 and 2.3.2).

The buffer screen provided initial evidence that the buffer conditions can affect the response of the chip (both non-specific and specific interactions). Further screening for activity under various conditions (including different detergents) may be fruitful. A PBP3 from a different species could also be tested as the issues here may be unique to PaPBP3.

2.5 Conclusions

An SPR system for PBP3 would be highly beneficial to the study of novel inhibitors or even the interactions of the natural substrate at the PBP transpeptidation site. This work was initiated to provide in-solution biophysical evidence of the interactions of boronates with PBPs (Chapter 5). A direct observation (i.e. no biochemical competition) technique would be very useful in the study of target mechanisms of resistance in PBPs (Chapter 4). The results of feasibility studies for the design of a PaPBP3 SPR system, were insufficient to justify continuation of this work. A reliable response could not be obtained using any of the analytes tested. An ideal system should corroborate biochemical data and demonstrate specific, readily dissociating (route **B**) binding.

This work was made more challenging by a lack of convenient, reversible, high affinity, positive controls for the ligand-analyte interaction. Initial attempts to validate the system using β -lactams in a route **A** regenerating system by two methods (CAPture oligonucleotide denaturation (2.3.1) and thiol reduction (2.3.2)) were unsuccessful. Using β -lactams (including nitrocefin) as controls in a non-regenerating or route **B** regenerating system did not provide necessary validation. Work with a benzoxaborole (**13**) was partially successful but demonstrated large amounts of non-specific interaction, which obscured the specific signal. The relatively weak affinities of the benzoxaboroles ($\sim 80 \mu\text{M}$) makes them a poor ligand for validation of the system. Recent reports demonstrate that SPR can be a useful tool in the context of PBPs ¹⁶, and further optimisation of the system may find more applications.

2.6 References

- (1) Kairys, V.; Baranauskiene, L.; Kazlauskiene, M.; Matulis, D.; Kazlauskas, E. Binding Affinity in Drug Design: Experimental and Computational Techniques. *Expert Opin. Drug Discov.* **2019**, *14* (8), 755–768. <https://doi.org/10.1080/17460441.2019.1623202>.
- (2) Sandoval, P. J.; Santiago, J. In Vitro Analytical Approaches to Study Plant Ligand-Receptor Interactions. *Plant Physiol.* **2020**, *182* (4), 1697–1712. <https://doi.org/10.1104/pp.19.01396>.
- (3) Schasfoort, R. B. M. Chapter 1. Introduction to Surface Plasmon Resonance. In *Handbook of Surface Plasmon Resonance*; Schasfoort, R. B. M., Ed.; Royal Society of Chemistry: Cambridge, 2017; pp 1–26. <https://doi.org/10.1039/9781788010283-00001>.
- (4) Pattnaik, P. Surface Plasmon Resonance: Applications in Understanding Receptor–Ligand Interaction. *Appl. Biochem. Biotechnol.* **2005**, *126* (2), 079–092. <https://doi.org/10.1385/ABAB:126:2:079>.
- (5) Navratilova, I.; Hopkins, A. L. Fragment Screening by Surface Plasmon Resonance. *ACS Med. Chem. Lett.* **2010**, *1* (1), 44–48. <https://doi.org/10.1021/ml900002k>.
- (6) Lund, B. A.; Christopeit, T.; Guttormsen, Y.; Bayer, A.; Leiros, H.-K. S. Screening and Design of Inhibitor Scaffolds for the Antibiotic Resistance Oxacillinase-48 (OXA-48) through Surface Plasmon Resonance Screening. *J. Med. Chem.* **2016**, *59* (11), 5542–5554. <https://doi.org/10.1021/acs.jmedchem.6b00660>.
- (7) van't Veer, I. L.; Leloup, N. O. L.; Egan, A. J. F.; Janssen, B. J. C.; Martin, N. I.; Vollmer, W.; Breukink, E. Site-Specific Immobilization of the Peptidoglycan Synthase PBP1B on a Surface Plasmon Resonance Chip Surface. *ChemBioChem* **2016**, *17* (23), 2250–2256. <https://doi.org/10.1002/cbic.201600461>.
- (8) Bertsche, U.; Breukink, E.; Kast, T.; Vollmer, W. In Vitro Murein (Peptidoglycan) Synthesis by Dimers of the Bifunctional Transglycosylase-Transpeptidase PBP1B from *Escherichia coli*. *J. Biol. Chem.* **2005**, *280* (45), 38096–38101. <https://doi.org/10.1074/jbc.M508646200>.
- (9) Terrak, M.; Ghosh, T. K.; van Heijenoort, J.; Van Beeumen, J.; Lampilas, M.; Aszodi, J.; Ayala, J. A.; Ghuysen, J.-M.; Nguyen-Disteche, M. The Catalytic, Glycosyl Transferase and Acyl Transferase Modules of the Cell Wall Peptidoglycan-Polymerizing Penicillin-Binding Protein 1b of *Escherichia coli*. *Mol. Microbiol.* **1999**, *34* (2), 350–364. <https://doi.org/10.1046/j.1365-2958.1999.01612.x>.
- (10) Vollmer, W.; Rechenberg, M. von; Höltje, J.-V. Demonstration of Molecular Interactions between the Murein Polymerase PBP1B, the Lytic Transglycosylase MltA, and the Scaffolding Protein MipA of *Escherichia coli*. *J. Biol. Chem.* **1999**, *274* (10), 6726–6734. <https://doi.org/10.1074/jbc.274.10.6726>.
- (11) Gray, A. N.; Egan, A. J.; van't Veer, I. L.; Verheul, J.; Colavin, A.; Koumoutsis,

- A.; Biboy, J.; Altelaar, A. F. M.; Damen, M. J.; Huang, K. C.; Simorre, J.-P.; Breukink, E.; den Blaauwen, T.; Typas, A.; Gross, C. A.; Vollmer, W. Coordination of Peptidoglycan Synthesis and Outer Membrane Constriction during *Escherichia coli* Cell Division. *eLife* **2015**, *4*, e07118. <https://doi.org/10.7554/eLife.07118>.
- (12) Bury, D. Development and applications of an SPR biosensor assay for moenomycins and other glycosyltransferase inhibitors. UNIVERSITY OF WUPPERTAL, Wuppertal, Germany, 2015.
 - (13) Bury, D.; Dahmane, I.; Derouaux, A.; Dumbre, S.; Herdewijn, P.; Matagne, A.; Breukink, E.; Mueller-Seitz, E.; Petz, M.; Terrak, M. Positive Cooperativity between Acceptor and Donor Sites of the Peptidoglycan Glycosyltransferase. *Biochem. Pharmacol.* **2015**, *93* (2), 141–150. <https://doi.org/10.1016/j.bcp.2014.11.003>.
 - (14) Myszka, null. Kinetic Analysis of Macromolecular Interactions Using Surface Plasmon Resonance Biosensors. *Curr. Opin. Biotechnol.* **1997**, *8* (1), 50–57. [https://doi.org/10.1016/s0958-1669\(97\)80157-7](https://doi.org/10.1016/s0958-1669(97)80157-7).
 - (15) Myszka, D. G. Improving Biosensor Analysis. *J. Mol. Recognit. JMR* **1999**, *12* (5), 279–284. [https://doi.org/10.1002/\(SICI\)1099-1352\(199909/10\)12:5<279::AID-JMR473>3.0.CO;2-3](https://doi.org/10.1002/(SICI)1099-1352(199909/10)12:5<279::AID-JMR473>3.0.CO;2-3).
 - (16) López-Pérez, A.; Freischem, S.; Grimm, I.; Weiergräber, O.; Dingley, A. J.; López-Alberca, M. P.; Waldmann, H.; Vollmer, W.; Kumar, K.; Vuong, C. Discovery of Pyrrolidine-2,3-Diones as Novel Inhibitors of *P. aeruginosa* PBP3. *Antibiotics* **2021**, *10* (5), 529. <https://doi.org/10.3390/antibiotics10050529>.
 - (17) Van Der Merwe, P. A. Surface Plasmon Resonance. *Protein-Ligand Interact. Hydrodyn. Calorim.* **2001**, *1*, 137–170.
 - (18) Sensor Surface Handbook. Biacore.
 - (19) Stenberg, E.; Persson, B.; Roos, H.; Urbaniczky, C. Quantitative Determination of Surface Concentration of Protein with Surface Plasmon Resonance Using Radiolabeled Proteins. *J. Colloid Interface Sci.* **1991**, *143* (2), 513–526. [https://doi.org/10.1016/0021-9797\(91\)90284-F](https://doi.org/10.1016/0021-9797(91)90284-F).
 - (20) De Feijter, J. A.; Benjamins, J.; Veer, F. A. Ellipsometry as a Tool to Study the Adsorption Behavior of Synthetic and Biopolymers at the Air-Water Interface. *Biopolymers* **1978**, *17* (7), 1759–1772. <https://doi.org/10.1002/bip.1978.360170711>.
 - (21) Jason-Moller, L.; Murphy, M.; Bruno, J. Overview of Biacore Systems and Their Applications. *Curr. Protoc. Protein Sci.* **2006**, *45* (1). <https://doi.org/10.1002/0471140864.ps1913s45>.
 - (22) Gedig, E. T. Chapter 6. Surface Chemistry in SPR Technology. In *Handbook of Surface Plasmon Resonance*; Schasfoort, R. B. M., Ed.; Royal Society of Chemistry: Cambridge, 2017; pp 171–254. <https://doi.org/10.1039/9781788010283-00171>.
 - (23) Müller, K. M.; Arndt, K. M.; Plückthun, A. Model and Simulation of Multivalent Binding to Fixed Ligands. *Anal. Biochem.* **1998**, *261* (2), 149–158. <https://doi.org/10.1006/abio.1998.2725>.
 - (24) Marquart, A. Immobilization strategy <https://www.sprpages.nl/immobilization/immobilization-strategy>. Accessed 09/09/20
 - (25) Biacore. Biacore Assay Handbook. Biacore.
 - (26) Bellini, D.; Koekemoer, L.; Newman, H.; Dowson, C. G. Novel and Improved

- Crystal Structures of *H. influenzae*, *E. coli* and *P. aeruginosa* Penicillin-Binding Protein 3 (PBP3) and *N. gonorrhoeae* PBP2: Toward a Better Understanding of β -Lactam Target-Mediated Resistance. *J. Mol. Biol.* **2019**, *431* (18), 3501–3519. <https://doi.org/10.1016/j.jmb.2019.07.010>.
- (27) Carlsson, J.; Drevin, H.; Axén, R. Protein Thiolation and Reversible Protein-Protein Conjugation. N-Succinimidyl 3-(2-Pyridyldithio)Propionate, a New Heterobifunctional Reagent. *Biochem. J.* **1978**, *173* (3), 723–737. <https://doi.org/10.1042/bj1730723>.
- (28) Boucher, L. E.; Bosch, J. Development of a Multifunctional Tool for Drug Screening against Plasmodial Protein-Protein Interactions via Surface Plasmon Resonance: MULTIFUNCTIONAL TOOL FOR DRUG SCREENING VIA SPR. *J. Mol. Recognit.* **2013**, *26* (10), 496–500. <https://doi.org/10.1002/jmr.2292>.
- (29) Beckett, D.; Kovaleva, E.; Schatz, P. J. A Minimal Peptide Substrate in Biotin Holoenzyme Synthetase-Catalyzed Biotinylation. *Protein Sci. Publ. Protein Soc.* **1999**, *8* (4), 921–929. <https://doi.org/10.1110/ps.8.4.921>.
- (30) Biotin Capture Kit: Label-Free Interactions Analysis Manual. Cytiva.
- (31) Tsai, W.-C.; Pai, P.-J. R. Surface Plasmon Resonance-Based Immunosensor with Oriented Immobilized Antibody Fragments on a Mixed Self-Assembled Monolayer for the Determination of Staphylococcal Enterotoxin B. *Microchim. Acta* **2009**, *166* (1–2), 115–122. <https://doi.org/10.1007/s00604-009-0171-1>.
- (32) Marquart, A. SPR Pages: Thiol Immobilisation <https://www.sprpages.nl/immobilization/immobilization-procedures/thiol>. Accessed 17/08/20.
- (33) Löfås, S.; Johnsson, B.; Edström, Å.; Hansson, A.; Lindquist, G.; Hillgren, R.-M. M.; Stigh, L. Methods for Site Controlled Coupling to Carboxymethyl-dextran Surfaces in Surface Plasmon Resonance Sensors. *Biosens. Bioelectron.* **1995**, *10* (9–10), 813–822. [https://doi.org/10.1016/0956-5663\(95\)99220-F](https://doi.org/10.1016/0956-5663(95)99220-F).
- (34) Schlecht, U.; Nomura, Y.; Bachmann, T.; Karube, I. Reversible Surface Thiol Immobilization of Carboxyl Group Containing Haptens to a BIAcore Biosensor Chip Enabling Repeated Usage of a Single Sensor Surface. *Bioconjug. Chem.* **2002**, *13* (2), 188–193. <https://doi.org/10.1021/bc0100399>.
- (35) Singh, R.; Whitesides, G. M. Thiol-Disulfide Interchange. In *The Chemistry of Sulfur-Containing Functional Groups*; Patai, S., Ed.; J. Wiley and Sons, Ltd.: London, 1993; Vol. Supplement S, pp 633–658.
- (36) Hermanson, G. T. The Reactions of Bioconjugation. In *Bioconjugate Techniques*; Elsevier, 2013; pp 229–258. <https://doi.org/10.1016/B978-0-12-382239-0.00003-0>.
- (37) O'Shannessy, D. J.; Brigham-Burke, M.; Peck, K. Immobilization Chemistries Suitable for Use in the BIAcore Surface Plasmon Resonance Detector. *Anal. Biochem.* **1992**, *205* (1), 132–136. [https://doi.org/10.1016/0003-2697\(92\)90589-Y](https://doi.org/10.1016/0003-2697(92)90589-Y).
- (38) Xu, F.; Zhen, G.; Yu, F.; Kuennemann, E.; Textor, M.; Knoll, W. Combined Affinity and Catalytic Biosensor: In Situ Enzymatic Activity Monitoring of Surface-Bound Enzymes. *J. Am. Chem. Soc.* **2005**, *127* (38), 13084–13085. <https://doi.org/10.1021/ja050818q>.
- (39) van den Ent, F.; Leaver, M.; Bendezu, F.; Errington, J.; de Boer, P.; Löwe, J. Dimeric Structure of the Cell Shape Protein MreC and Its Functional Implications. *Mol. Microbiol.* **2006**, *62* (6), 1631–1642. <https://doi.org/10.1111/j.1365-2958.2006.05485.x>.

- (40) Gasteiger, E.; Hoogland, C.; Gattiker, A.; Duvaud, S.; Wilkins, M. R.; Appel, R. D.; Bairoch, A. Protein Identification and Analysis Tools on the ExPASy Server. In *The Proteomics Protocols Handbook*; Walker, J. M., Ed.; Humana Press: Totowa, NJ, 2005; pp 571–607.
<https://doi.org/10.1385/1-59259-890-0:571>.
- (41) Cytiva. Series S Sensor Chip CM5: Instructions for Use. Cytiva.
- (42) Gunnarsson, A.; Stubbs, C. J.; Rawlins, P. B.; Taylor-Newman, E.; Lee, W.; Geschwindner, S.; Hytönen, V.; Holdgate, G.; Jha, R.; Dahl, G. Regenerable Biosensors for Small-Molecule Kinetic Characterization Using SPR. *SLAS Discov. Adv. Sci. Drug Discov.* **2021**, 26 (5), 730–739.
<https://doi.org/10.1177/2472555220975358>.

Chapter 3. Design and Optimisation of a High-Throughput Antimicrobial Screening Platform

3.1 Introduction

One of the potential avenues to fill the presently empty antibiotic pipeline is the use of whole cell screening (Chapter 1). The smaller companies now responsible for the majority of antibiotic development ¹ are typically less likely to have significant biological testing capacity in house and instead outsource this work to specialist “contract research organisations”, such as Warwick Antimicrobial Screening Facility ².

Warwick Antimicrobial Screening Facility provides an array of microbiological services to academic and industrial clients for early stage drug development run by an experienced, UK NEQAS accredited team. Most work is done manually following Clinical & Laboratory Standards Institute (CLSI) protocols ³, which is possible for fewer than 50 compounds, but becomes increasingly expensive and time consuming for larger libraries. In order for larger libraries to be screened, development of automated methods was required.

In developing higher throughput low volume antimicrobial screens, requiring significantly less compound than traditional MIC methodology, we hope to facilitate the early stage development of novel antibiotics. The CO-ADD platform at the University of Queensland, Australia is driven by similar principles and even offers free screening in the hope of “emptying the drawers” and finding antimicrobial hits in compound libraries that otherwise would never have been screened against bacteria ⁴.

We therefore aimed to create a highly automated assay (to minimise costs) with quick results turnaround and low sample volume. By minimising sample consumption, antimicrobial activity data can be included in an early stage in the discovery cycle, placing whole cell activity data at the centre of discovery efforts. Additionally, by miniaturising the assay consumable costs are lowered and throughput is increased

because more wells can be run on each plate. To create this platform it was necessary to optimise the bacterial growth rates within the system, create methods for liquid handling as well as develop and validate data processing pipelines to determine the minimum inhibitory concentration (MIC) of a given compound with minimal human intervention.

3.2 Methods

3.2.1 Antimicrobial Assays

The assay was run in 80 µl volume in 384-well black-walled, clear bottom plates (Greiner Bio-One) at 37 °C and the plates were prepared and analysed in a Tecan Freedom EVO liquid handling robot with an 8 channel “LiHa” liquid handling arm, a 96 multichannel arm “MCA 96”, a robotic manipulator arm “RoMa”, a cooling plate, an incubator and a plate reader (Tecan Infinite M200Pro) ⁵.

Source plates, separately containing inoculating media and antibiotic stocks were placed on carriers on the deck of the robot at the start of the run.

When testing organisms other than *E. coli* ΔTolC, a different plate reader (Tecan Spark 10M) in a biosafety level 2 laboratory was used.

3.2.2 Inocula

Bacteria were recovered from glycerol stocks (kept at -80 °C), and spread onto a petri dish containing lysogeny (LB) agar (except for *N. gonorrhoeae*, which was grown on chocolate agar in a 5 % (v/v) CO₂-enriched environment) then allowed to grow overnight at 37 °C. This dish was kept at 4 °C for up to 1 week. The inoculum was prepared by diluting bacteria collected from the dish by a cotton wool swab into phosphate buffered saline (137 mM NaCl, 2.7 mM KCl, 10 mM phosphate buffer pH 7.4) to a concentration of 1.5 x 10⁸ CFU/ml, as determined by comparison with a 0.5 McFarland standard. This stock was then diluted into 2 x cation-adjusted Mueller-Hinton broth 2 (caMHB, Merck) to a concentration of 9.2 x 10⁶ CFU/ml and pipetted into 2 ml 96-well blocks (Brand). All but three wells of the block contained inoculum whilst the remaining wells contained 2 x caMHB for the negative control. This was prepared

immediately before the initiation of the experiment within the robot. Whilst in the liquid handling robot, the inoculum was placed on a cooled carrier to maintain its temperature at 4°C.

3.2.3 Antibiotics Stocks

Antibiotic stocks were prepared at 4 x the desired final concentration (e.g. 512 µg/ml for a highest final concentration of 128 µg/ml) and manually pipetted into 96 well plates (Falcon). The bottom row of the 96 well plate is reserved for controls: 2 containing only water for injection into the positive and negative controls and 2 wells for known antibiotic controls (also at 4 x the desired final concentration) (Figure 3.1).

Protocols for running the liquid handling system were written and operated by Dr. Sarah Bennett. Briefly, all the wells of a 384 well 'destination' plate were filled with 40 µl of sterile milliQ water using the MCA and 40 µl of each compound was pipetted using the LiHa, from the source plate into separate wells in the "destination" plate. The wells were mixed using aspirate and dispense commands, followed by a 40µl transfer into a new well containing 40 µl of water, thereby initiating a serial dilution that continued across the plate. At the last dilution step, 40 µl of diluted compound was removed and discarded. Once the inhibitor was plated out, 40 µl of inoculum was added to each well using the MCA. The RoMa then fitted a clear lid (Greiner microplate lid sterile) to the plate and transferred the plate to a plate reader (Tecan Infinite M200Pro). The plate was incubated at 37 °C, and OD₆₀₀ measurements were taken at 600 nm every 10 minutes for 4-8 hours

3.2.4 Gonococcal (GC) media

For the GC media brain-heart infusion broth (Merck) was prepared, then supplemented with 5 % (v/v) horse blood (E & O Laboratories) and autoclaved. After cooling, the supernatant was poured off and filtered through a 0.22 µm sterile filter (Merck) before use.

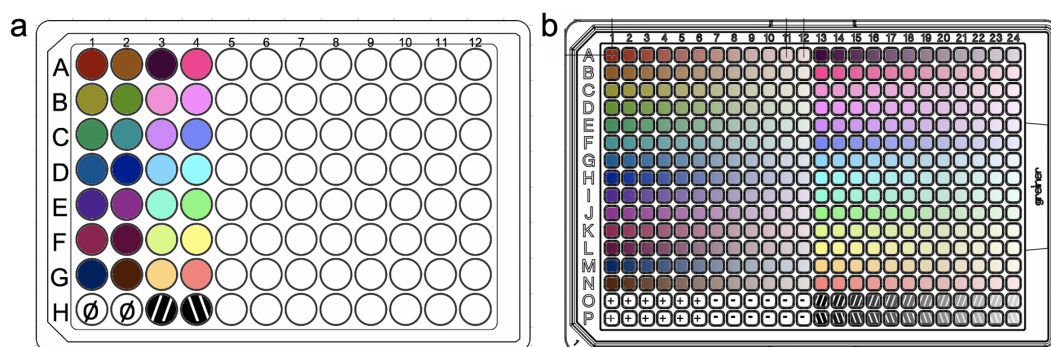


Figure 3.1. Antibiotic source and destination plates. A 96-well plate (a) is used as the antibiotic source plate. 28 wells on the source plate are used to fill 1 384-well destination plate (b) when 12 concentrations of antibiotic are tested. Maps (see text) can be used to change the conformation. Each colour indicates a different antibiotic, whilst the lightness indicates the concentration. Note how wells from alternating columns on the source plate interlace as rows on the destination plate. Each source plate can be used to fill 3 destination plates. The negative (-) and positive (+) controls wells receive water (\emptyset). Hashed wells indicate the control antibiotics.

3.3 Results and Discussion

3.3.1 Optimisation of Growth Rates

In order to increase throughput of the assay and minimise the amount of incubator space required, the microbroth serial dilution method of measuring growth inhibition, which is typically undertaken in 96 well plates with 100 μ l total volume³ was miniaturised into a 384-well, 80 μ l format. Additionally, by moving from a typical endpoint of 18-24 hours³ to an endpoint of less than 8 hours we are able to increase throughput of automated runs. However, we needed to ensure growth was sufficient in this period to differentiate between cells affected and unaffected by the treatment.

Investigation of the literature shows various methods for monitoring growth implemented in phenotypic screens have been used previously. : i) visual inspection for turbidity, as used in low throughput screens⁶, ii) commercial luminescence detection kits^{7,8}, iii) fluorescent staining^{9,10}, iv) strains mutated to induce bioluminescence¹¹ or fluorescence¹², v) resazurin to detect changes in the redox environment¹³, vi) changes

in turbidity detected by measurements at 600 nm^{14–16}.

Whilst staining, fluorescent and luminescent methods may increase sensitivity as these methods amplify the signal, they also risk possible chances for compound interference in the read out and false discovery. Additionally genetic modifications to cells cannot be carried out on clinical strains. Therefore, we opted to use turbidity as the read out for this assay.

A validated mutant of *Escherichia coli* with a knock out of the transmembrane efflux pump *TolC* gene (*E. coli* Δ TolC) was selected for use during the development phase of this work as it is a biosafety level 1 organism and it is a useful tool for screening since it reduces the permeability barrier (see thesis Introduction), making hit discovery more likely¹⁷.

Figure 3.2 shows the growth curves produced when inoculating wells with different initial concentrations of *E. coli* Δ TolC cells in 80 μ l of media in a 384 well plate. These growth curves were used to select an appropriate time point for measuring the endpoint in subsequent runs as well as a dilution of bacterial cells for the inoculum. As expected, end point change in optical density correlates with concentration of inoculum due to the binary growth of bacteria (Figure 3.2b). Using this data, an inoculum concentration of 4.6×10^6 CFU/ml was chosen as this gives good balance between sufficient change in optical density to detect growth within a short time frame (Figure 3.2b), and with relatively low variance between repeats (Figure 3.2c). After 240 minutes bacteria are in the middle of the growth phase.

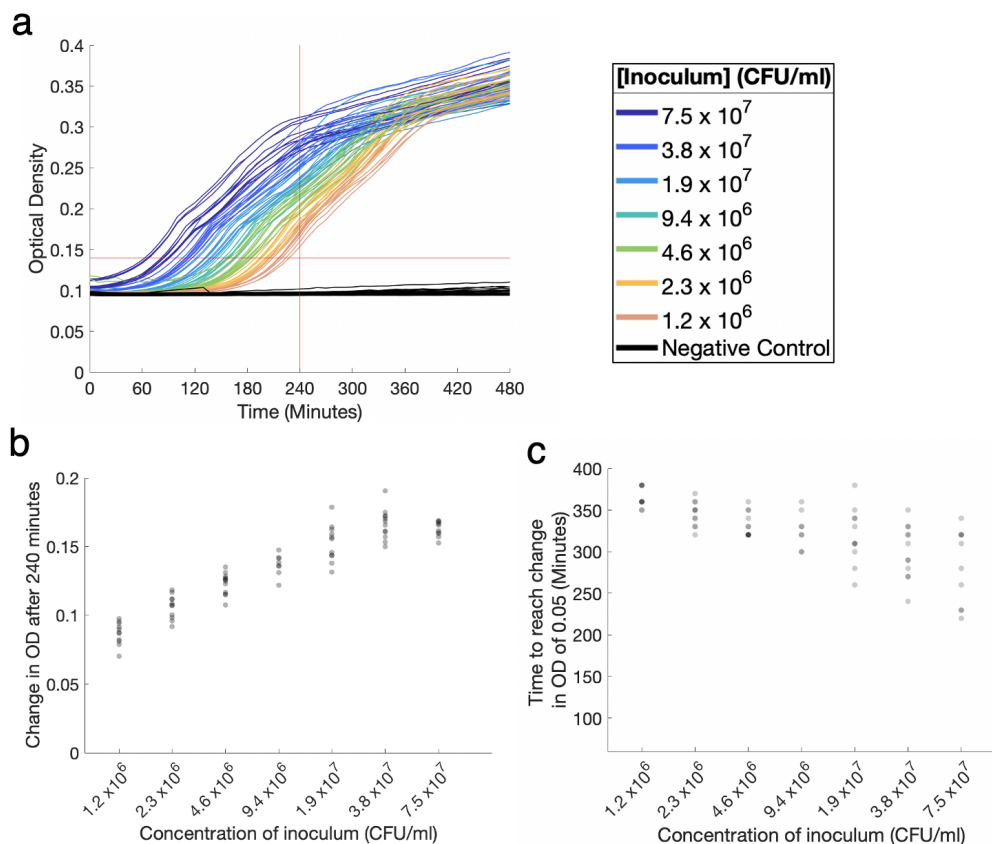


Figure 3.2. Optimisation of Growth Conditions. (a) Overlay of growth curves of *E. coli* ΔTolC over 8 hours. Colours indicate the concentration of cells in the inoculum (see key), the negative control (black) has no inoculation. The red lines show the threshold for a change in optical density (OD₆₀₀) of 0.05 (horizontal) and 240 minutes (vertical). The intersections of these lines and the growth curves are shown in (b) and (c) respectively. (b) For each concentration of inoculum, time for the *E. coli* growth curve to have a change in OD₆₀₀ of 0.05 is shown, darker markers show more data points at that position. (c) Similarly, the change in OD₆₀₀ after 240 minutes is shown for each concentration of *E. coli* inoculum. In (b) and (c) the x axis is a log₂ scale.

Comparison of the turbidity of a suspension of bacterial cells to a 0.5 McFarland standard is used to estimate the concentration of bacteria. Due to the potential sensitivity of the method to errors caused by variations in estimations of turbidity when making up the inoculum, replicates with the same starting concentration of inocula were used to confirm the reproducibility of the growth curves. Eight different inocula (“replicates”) with bacteria at a concentration of 4.6×10^6 CFU/ml, as determined by comparison with a McFarland standard 8 different times, were used to initiate grow in

48 wells each. The data show that starting concentration is responsible for a small amount of variation between “replicates”, but that variation within each “replicate” is consistent (Figure 3.3). When running screens, all wells were inoculated with bacteria made up as a single inoculum, which will eliminate variation between “replicates” but variation within “replicates” is likely to have similar distribution. Variation between runs can be standardised by comparison of the positive controls.

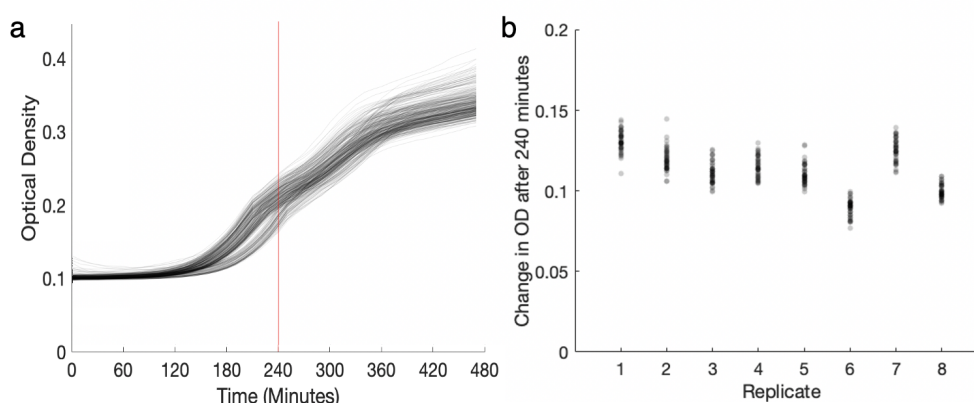


Figure 3.3. Variation due to starting inoculant. (a) Overlay of growth curves of *E. coli* Δ TolC over 8 hours, darker grey indicates more data at that position. The red line is set at 240 minutes. (b) The change in turbidity for each curve in (a) is plotted against the “replicate”, where each replicate was made up by diluting bacterial cells to a concentration estimated to be equal to 4.6×10^6 CFU/ml, as determined by comparison with a McFarland standard.

3.3.2 Z-factor

The Z-factor is a parameter which can be used to assess the quality of an assay¹⁸. It is a measure of the signal to noise ratio of an assay, taking into account the standard deviation and means of the positive and negative controls of the assay. It is defined as in equation 3.1:

$$Z = 1 - \frac{3\sigma_p + 3\sigma_n}{|\mu_p - \mu_n|} \quad (3.1)$$

where σ is the standard deviation and μ is the mean of the positive (μ_p) and negative (μ_n) controls.

The Z-factor was found to be 0.75 for this assay (*E. coli* Δ TolC growth in 4 hours with automated liquid handling), which is defined as “an excellent assay” by Zhang et al.¹⁸, in terms of its ability to distinguish between growth and no growth.

3.3.3 Robotic Liquid Handling

These initial investigations showed that bacteria tolerated the low volume well and grew reproducibly. We then developed automated methods to measure and determine MICs. We envisaged two example use cases for the platform: a prototypical 12 concentration MIC with two-fold concentration steps, and a miniturised MIC test in which only four concentrations of compound were investigated, which allows for increased throughput. Protocols for both these methods were developed.

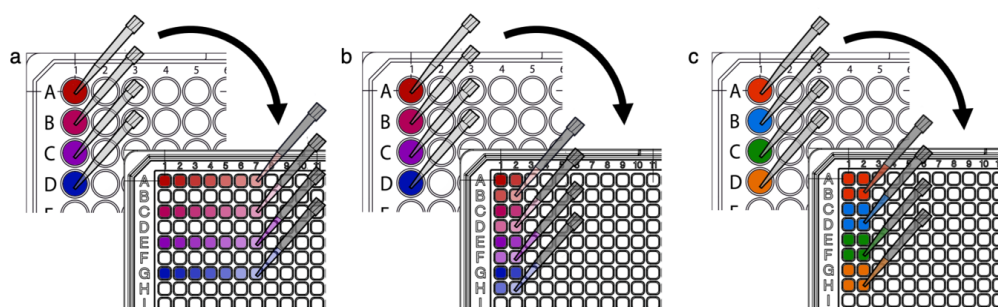


Figure 3.4. Liquid handling methods to transfer solutions between 96 well and 384 well plates and generate concentration series. (a) Linear two-fold serial dilution across the plate. (b) Two-fold serial dilution for four concentrations in square grids. In both (a) and (b) lightness of the colour indicates increasing dilution. Two-fold dilution is achieved by mixture of equal volumes (40 μ l) of compound-containing solution and water (c) Inoculating the wells with a constant concentration of bacterial cells. The operation shown in (a) can only be achieved by the 8 channel “LiHa” arm, whilst the operation shown in (b) and (c) can be carried out by the MCA 96 arm.

The protocol takes two “source” plates: one loaded with bacterial inoculum and one with test compounds at a single concentration (Figure 3.1). Four controls are included on every “destination” plate: negative, which has no inocula, positive which has no

inhibitor, and two antibiotics of known MIC to ensure consistency of dilution.

The contents of these plates are then distributed to the “destination” plates by the robotic liquid handling system before the assay can begin. The Tecan Freedom EVO liquid handling robot has 2 liquid handling heads: a 8 channel “LiHa” and a 96 multichannel arm “MCA 96”, and a robotic manipulator arm “RoMa”.

The robot can mimic a hand-held 8-well multichannel pipette and quickly dilute a compound across the long axis of a plate, as shown in Figure 3.4a. Alternatively, when test only 4 compound concentrations, the MCA 96 arm can be used to dilute the compounds in a 2 x 2 grid (Figure 3.4b). Due to the high multiplicity of the arm, this is very rapid. Following dilution of the compounds, the wells are inoculated with bacteria using the MCA 96 (Figure 3.4c), initiating the experiment.

The RoMa arm transfers the completed plates to a 37 °C incubator, and then moves the plate between the incubators and the plate reader at the reading intervals. The data is then outputted ready for processing.

3.3.4 DMSO

High-throughput compound libraries are often solvated in DMSO, so determining the sensitivity of the assay to DMSO is important to ensure any effect observed is not due to DMSO. The sensitivity of *E. coli* Δ TolC to DMSO is shown in Figure 3.5. The results show total inhibition above 10 % but significant inhibition is not seen for concentrations below 2 % DMSO. A 2 % limit on DMSO concentration when diluting compounds was used in all subsequent work.

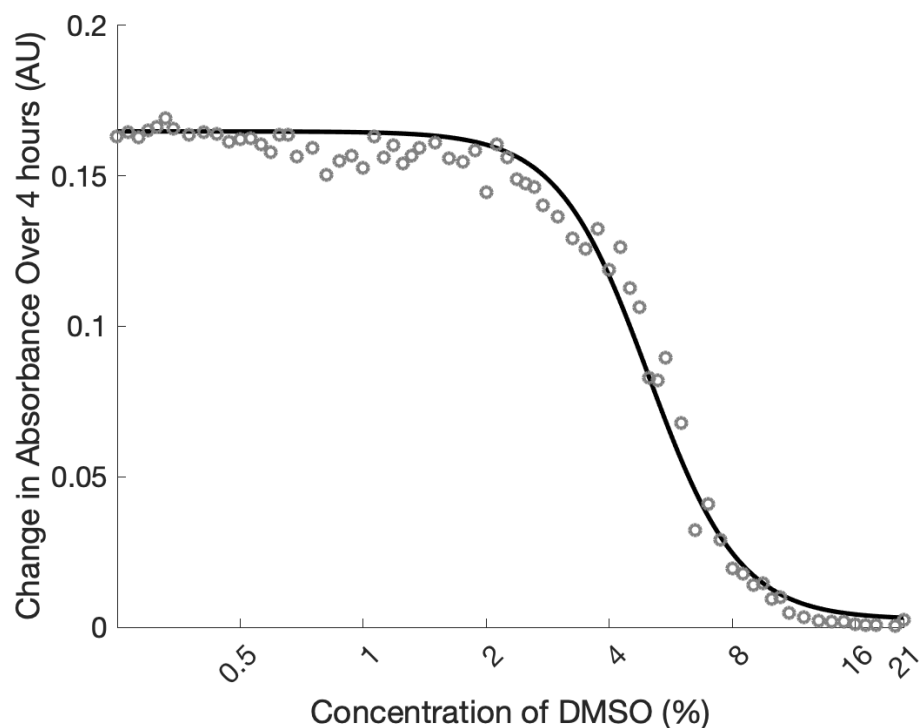


Figure 3.5. Sensitivity of *E. coli* Δ TolC to DMSO. DMSO concentrations between 21 % and 0.25 % were tested on their ability to prevent growth of *E. coli* Δ TolC, measured by the change in optical density after 4 hours.

3.3.5 Data Processing

3.3.5.1 Workflow

Figure 3.6 shows the workflow used to process the data. It requires three inputs (shown as triangular boxes): the growth data (taken from a microplate reader); the names of the compounds and the “Maps”. Maps are directory files used to describe the layout of the destination plate (equivalent to the matching of colours in Figure 3.1. They increase the flexibility of the system since these can be easily changed to meet the desired number of concentrations of compounds to be tested, different arrangements of compounds on the destination plate and the types of controls used.

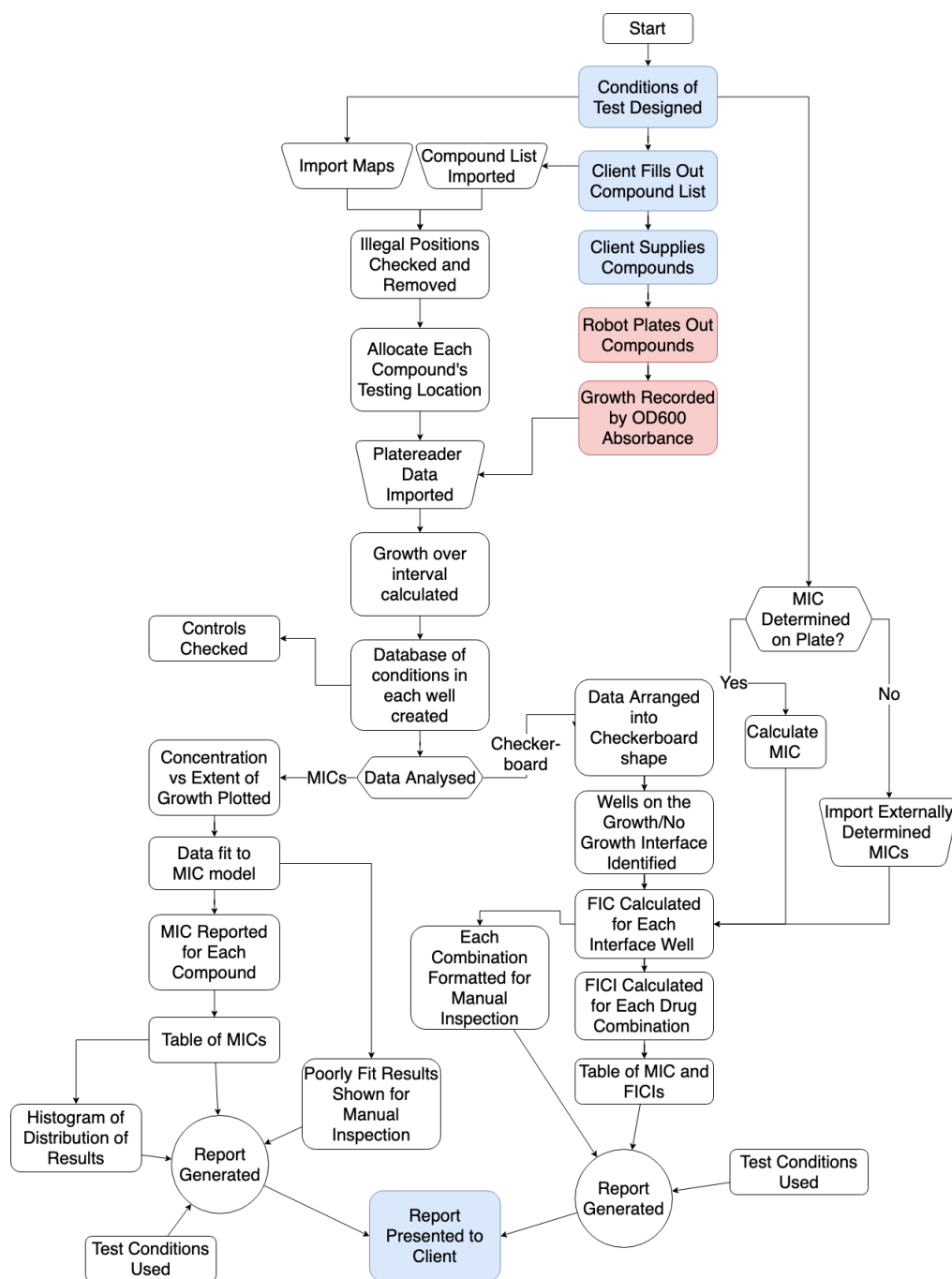


Figure 3.6. Overview of the workflows used to prepare a report of a set of MICs. Each box represents a process (typically run by an individual script) required to process the inputted data into the final report. Operations in white are those carried out by the code, in blue are client-facing operations, in red are experimental procedures. FIC(I): fractional inhibitory concentration (index).

One of the complications of the data processing is that the source plates are 96-well plates, whilst the destination plates are 384-well. 96-well plates are used due to their higher capacity and easier handling (pipettes and the robotic arms have tips spaced at these dimensions). The solution is the use of Maps, which correlate the positions in the two plates and allow the growth data to be stored in a database alongside information on the compound concentration and name so that this can correctly be outputted together in the report.

A series of Matlab scripts then prepares the data into a format in which the MIC can be determined. Essential scripts are those that reformat the data; calculate the growth over 4 hours; fit models to the data; and generate reports.

3.3.5.2 Determining the MIC

When determining an MIC using manual methods, the MIC is defined as the last well in which no turbidity can be detected by eye following incubation of the test compound. This is possible because over 16-24 hours an antimicrobial compound will typically prevent visible growth at its MIC, creating a clearly defined “cliff” of efficacy. Preliminary experiments with different inhibitors using short (4 hours) growth times revealed a number of possible shapes of the dose-response curves (Figure 3.7). Some inhibitors, such as polymyxin B (Figure 3.7a), produce a clear “cliff” in response at a critical threshold of activity, but others, such as tetracycline (Figure 3.7b) have log-linear responses because weak growth is still possible. Models to fit the curves to find a value for the MIC were investigated.

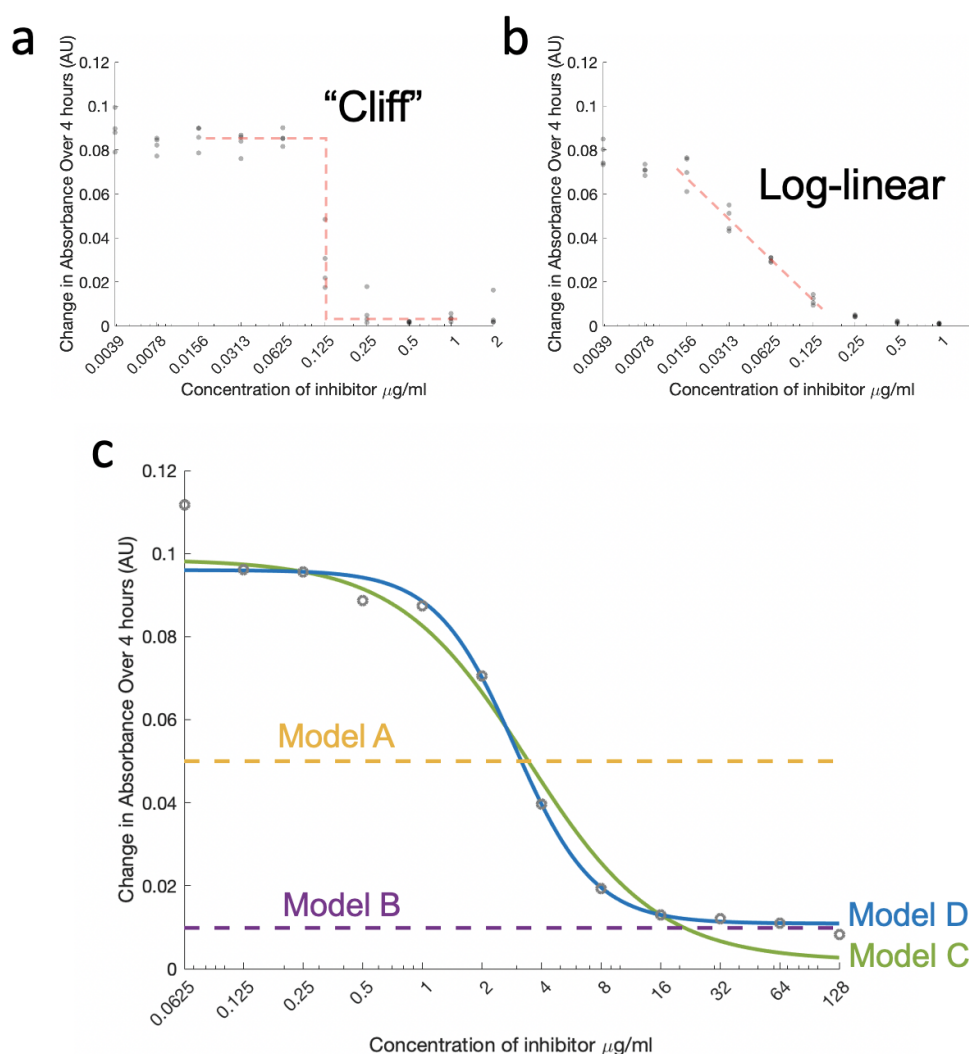


Figure 3.7. Dose responses of *E. coli* Δ TolC to different compounds. (a) Polymyxin B (b) Tetracycline (c) a novel compound (undisclosed). Each example shows a different slope of the curve. (c) is fitted with 4 models, **Models A-D** in **Table 3.1**: **Model A** (orange dashed line) the threshold for change in absorbance of 50 % of the positive control; **Model B** (purple dashed line) the threshold for change in absorbance of 10 % of the positive control; **Model C** (green solid line) and **Model D** (blue solid line). The MICs determined using each model for this compound are shown in Table 3.1. Grey circles show the change in absorbance over 4 hours for each concentration of compound. In (a) and (b) each circle indicates a repeat, darker circles indicating multiple (2-4) data points overlapping. This compound was determined to have an MIC of 16 μ g/ml by methods following CLSI standards.

Four methods were tested for their ability to accurately determine a compound's MIC from the dose-response curves (Figure 3.7c and Table 3.1). Models **A** and **B** determine

the MIC using a fixed threshold (*Threshold*) in optical density relative to the average of the positive and negative controls for that screen (equation 3.2). For **A** the threshold is 50 % ($k = 0.5$), for **B** the threshold is 10 % ($k = 0.1$). The MIC is simply found as the first concentration of inhibitor that gives a change in optical density of less than *Threshold*.

$$Threshold = k \times (positive\ control - negative\ control) + negat \quad (3.2)$$

Models **C** and **D** use a 4-term sigmoidal curves to fit the data (equation 3.3) ²⁰, using the “fitype” curve fitting function in Matlab ²⁴.

$$y = bottom + \frac{top - bottom}{1 + \left(\frac{x}{EC_{50}} \right)^{slope}} \quad (3.3)$$

Where y is the response and x is the \log_2 of the concentration of the inhibitor. **C** constrains the *top* and *bottom* terms of equation 3.3 to the change in $OD_{600\text{ nm}}$ of the positive and negative controls of the experiment, whilst **D** allows these terms to be dynamically fitted but constrains the *slope* term to >2 , which prevents the data being fit to too shallow a curve, which was shown to lead to very poor fits during evaluative fitting.

The EC_{90} , defined as the effective concentration at which 90 % of the growth is inhibited, is then found (equation 3.4). For **C**, the 10 % threshold (*Thres10*) is defined using equation 3.2 with $k = 0.1$. *Thres10* is substituted into equation 3.4 to find a value for EC_{90} . This can be graphically visualised as the intersect of the green line (**C**) and the purple dashed line (**B**) in Figure 3.7c.

For **D**, after fitting the data with the sigmoid from equation 3.3, *Thres10* is simply defined relative to the *top* and *bottom* terms found by the fit (equation 3.5) and then the EC_{90} found using equation 3.4.

In both cases, after finding the EC_{90} , the MIC is reported as the lowest concentration tested which was greater than the EC_{90} .

$$EC_{90} = EC_{50} \times \sqrt[\text{slope}]{\frac{\text{top} - \text{bottom}}{\text{Thres10} - \text{bottom}}} - 1 \quad (3.4)$$

$$\text{Thres10} = k \times (\text{top} - \text{bottom}) + \text{bottom} \quad (3.5)$$

When analysing the results of high-throughput screens, ensuring the correct fitting of the data for every compound is important. The R^2 (coefficient of determination) term is determined by the Matlab *fit* function and describes the goodness of fit of the curve to the data, where 1 is a perfect fit. This value can be used to flag data sets in which the curve fits the data very poorly, so they can be manually inspected. Compounds in which all concentrations are far above or below the MIC do not show sigmoidal curves, but can be instead compared to the positive and negative controls and the MIC reported as greater than the highest concentration tested or less than the lowest concentration tested.

	Model	Constraints	Fitting curve in Figure 3.7c		Results from the test set
			EC_{90} ($\mu\text{g/ml}$)	MIC Reported ($\mu\text{g/ml}$)	Results within 4 fold of standardized result (%) ^a
A	Threshold (50%)	N/A	N/A	4	73.2
B	Threshold (10%)	N/A	N/A	128	79.8
C	Sigmoid equation 3.3	<i>top</i> and <i>bottom</i> : see text	19.5	32	85.7
D	Sigmoid equation 3.3	<i>slope</i> > 2	8.5	16	76.8

Table 3.1. Details of the models investigated for determining the MIC in the automated pipeline N/A: not applicable. ^aThe percentage of results indicated by each model to be within 4 fold of the result from a standardised test is listed. This is used as a measure of accuracy of the model on a novel data set. See Figure 3.8.

These models were used to determine the MIC for unseen inhibition data of novel compounds. 51 novel compounds (provided by a collaborator), along with 5 known

antibiotics (amikacin, ticarcillin, minocycline, rifampin, clarithromycin) were tested in triplicate and each of the 168 runs was analysed individually (Figure 3.8) and compared with the results determined by a standardised, low throughput method (following CLSI protocols ²). As expected, the model **A** overestimates compound potency relative to the standardised data set (Figure 3.8a). The reason for this can easily be understood from Figure 3.7c as concentrations which give weak inhibition are designated as the MIC. It is likely this method would be more accurate for compounds which generate very steep inhibition curves (large *slope* term), of the type observed with polymyxin B (Figure 3.7a). A comparison of the histograms of the **B** and **C** demonstrates the benefit of using a sigmoidal fit to find EC_{90} rather than using only a simple threshold. Whilst the distributions of Figure 3.8b and Figure 3.8c are generally similar, **B** produces a left handed tail which is absent from **C**. As illustrated in Figure 3.7c, this occurs when points lie close to, but do not cross the 10% threshold, leading to the model underestimating the compounds efficacy. Finally **D**, gives results broadly similar to **C** but has many outliers, these occur due to poor fitting of the data, leading to a major misinterpretation of the result.

One case where model **D** is particularly useful is to fit curves well for compounds such as aztreonam. Aztreonam is not biocidal, even at concentrations many fold above the MIC, due to its specific inhibition of PBP3, which prevents division but allows cellular elongation ^{19–21}. This means that even at high concentrations of inhibitors there is a non-zero change in absorbance over the course of the experiment. The novel compound in Figure 3.7c is displaying this kind of behaviour, as demonstrated by the deviation between the green (**C**) and blue (**D**) at concentrations greater than 16 µg/ml. Allowing variation in *bottom* helps fit the data more accurately in this case.

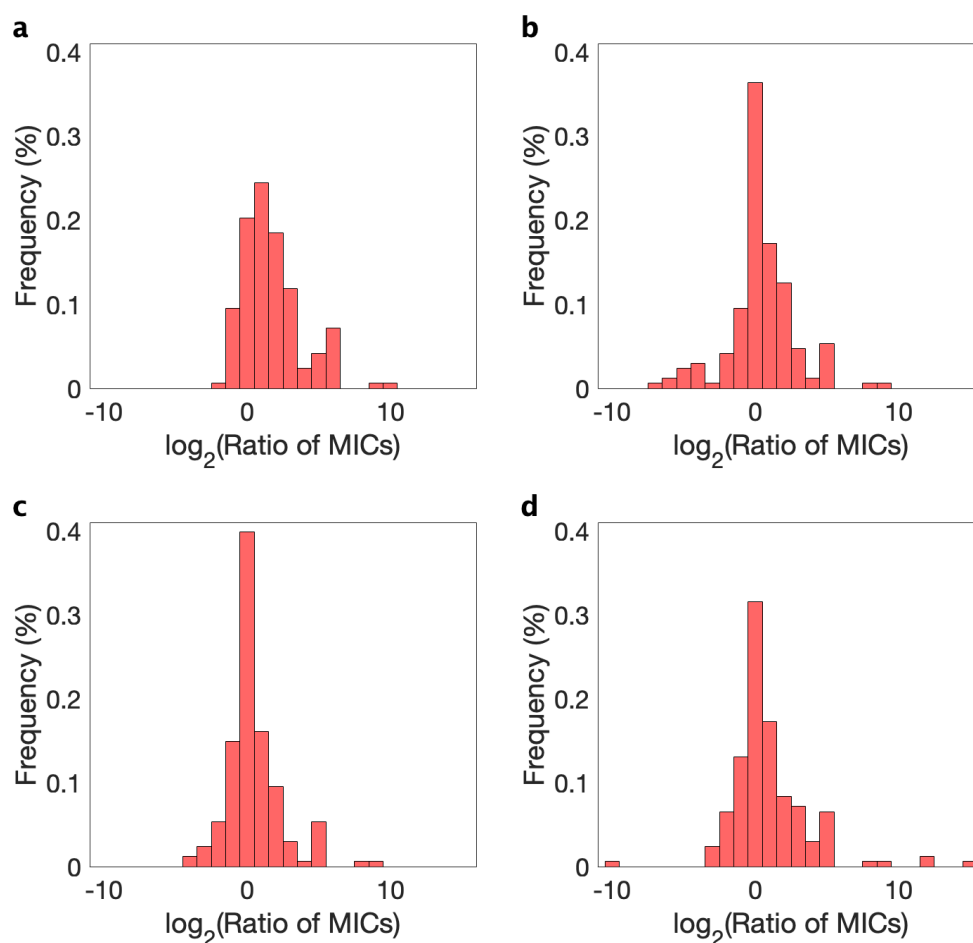


Figure 3.8. Results generated by each model (A-D) when analysing MICs of novel compounds. Models: (a) **A**; (b) **B**; (c) **C**; (d) **D**. The automated method was used to generate inhibition curves for 56 compounds in triplicate. The MICs calculated by each model for each individual replicate were compared to the MIC for that compound determined by standardised methods, expressed as a ratio ("Ratio of MICs"). This ratio is logged (base 2) and plotted against the frequency that result was observed by that model. 0 on the x-axis indicates the model generated the same result as the standardised test, negative values indicate that result from the standardised method was lower (more effective inhibition) than the result generated by the model, with the opposite being true for positive results. Any results which were recorded as less than the lowest value tested were treated as being 8-fold lower than the lowest concentration tested, similarly for when no inhibition was observed (treated as 8-fold higher. This is likely to be overly conservative.

In the early stages of a screening program, a result needs to be rapidly returned to give an indication of the potential of a novel compound. The exact measure of the MIC may

not be important in the early stages. For this purpose scripts were also written into the pipeline which allow just four concentrations to be tested for each compound. This allows a more than three-fold increase in the throughput as dilution of the type shown in Figure 3.4b can be used which gives a further improvement in throughput. Concentrations can be chosen to give a categorical description; e.g. a compound with an MIC of 64 $\mu\text{g/ml}$ or greater may be categorised as ineffective, whilst one with an MIC of 8 $\mu\text{g/ml}$ may be worth follow-up.

3.3.6 Screening Boronates

The liquid handling platform was used to screen a small library (49 compounds) of boron-containing compounds (those in Chapter 5 as well as a small collection of phenylboronic acids) against *E. coli* ΔTolC (Figure 3.9). Few active compound hits were identified, with the exception of tavorole, an antifungal agent^{22,23}, which was found to have an MIC of 2 $\mu\text{g/ml}$.

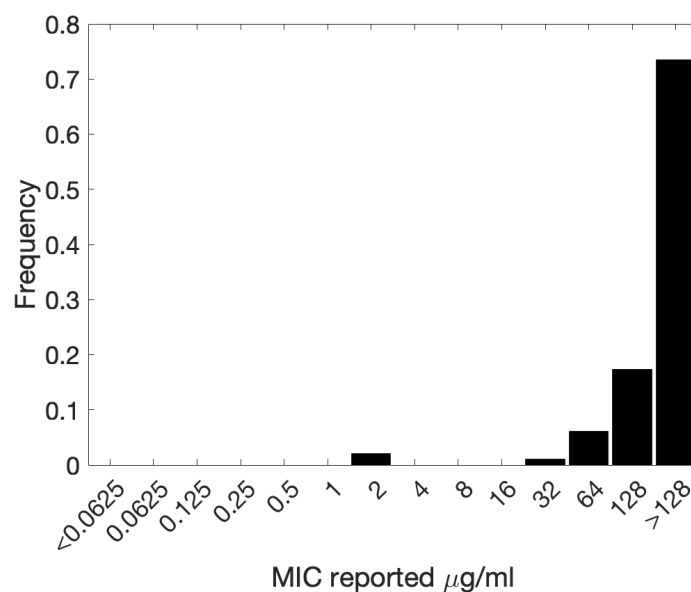


Figure 3.9. Histogram of MICs of boron-containing compounds screened. 49 boron-containing compounds were screened in duplicate and their MIC determined by model C.

3.3.7 Synergy Studies

We have additionally developed methods to investigate compound synergy using the automated platform. Synergy occurs between two antimicrobial compounds when their activity together is greater than the sum of their parts ²⁶. Due to the number of possible combinations of compounds, even from a small library, these studies are very labour-intensive when done by hand, making them an excellent candidate for automation. Protocols were established for the liquid handling system which allows both compounds to be diluted separately, before they are combined to a 2D gradient of concentration. Each compound is diluted two-fold in perpendicular directions and then 20 µl of each is added to the plate before inoculation. Protocols were designed to allow either 4 x 4 well grids (i.e. 4 concentrations of each of the inhibitors) or 11 x 7 well grids. As shown in Figure 3.6, the data processing pipeline is similar, but also includes the optional addition of calculations of the fractional inhibitory concentration index (FICI) ²⁷ (equation 3.6), a measure of the size of the synergistic effect of a combination. This is found after the determination of MIC of each of the two compounds (*i* and *j*).

Examples of the 4 x 4 well “checkboards”: grids of two concentrations of inhibitors - are shown in Figure 3.10. Beneficial interaction of the β-lactamase inhibitor clavulanic acid and β-lactams is well characterised for β-lactamase-expressing strains and this combination is used in the clinic ^{24–26}. In this case it is not possible to calculate the FICI because clavulanic acid does not have antimicrobial effect alone (no MIC_i term for equation 3.6).

$$FICI = FIC_i + FIC_j = \frac{[i]}{MIC_i} + \frac{[j]}{MIC_j} \quad (3.6)$$

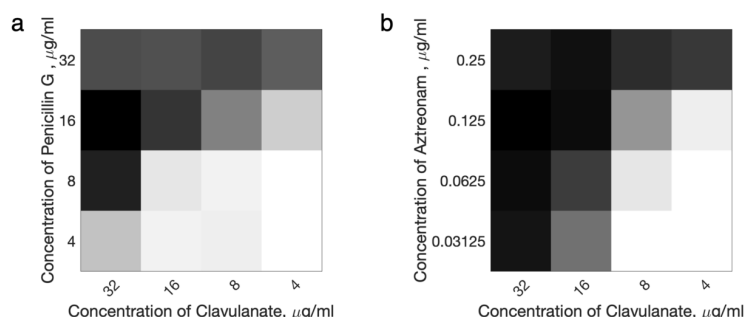


Figure 3.10. Synergy Studies. 4 x 4 “checkerboards” showing interactions between clavulanic acid and a β -lactam when inhibiting the growth of β -lactamase (CTX-M-15) expressing *E. coli* strain NCTC 13353. (a) Penicillin G (b) Aztreonam. Note that the MIC of aztreonam is much lower than penicillin G so the concentrations tested are also lowered. Shading in each cell is greyscale with black indicating lack of growth and white indicating the same amount of growth as the positive control.

3.3.8 Growth of Other Organisms

With the protocols established for a basic dose response curve against *E. coli* ΔTolC , we aimed to expand the capabilities of the platform. Screening compounds against *E. coli* ΔTolC mutant is informative for certain projects, but novel compounds need to be effective against clinically relevant, priority organisms²⁵. The growth of these needed to be validated in the low volume, high throughput format (Figure 3.11). Currently the liquid handling robot is not in a Biological Safety Level 2 environment, so inoculation must be carried out manually in the appropriate environment. Additionally, *P. aeruginosa*, *K. pneumoniae*, *A. baumannii* and *N. gonorrhoeae* required higher initial concentrations of inoculum to ensure growth in the timescale, and in some cases different media. *N. gonorrhoeae* grew poorly and can often fail to grow all together, and may require further optimisation of conditions for this to be sufficiently robust for high throughput screening (Figure 3.11). One interesting observation from the growth curves of *Salmonella typhimurium* (Figure 3.11b), *Enterobacter cloacae* (Figure 3.11c) and to a lesser extent *E. coli* ΔTolC (Figure 3.3a) is the ‘jagged’ appearance of the growth curves in the exponential phase, compared to the smooth exponential growth of e.g. *E. coli* NCTC 25922 (Figure 3.11a). This is termed “diauxic growth”, and can be caused by sequential substrate utilisation with the different substrates allowing for different growth rates^{27,28}.

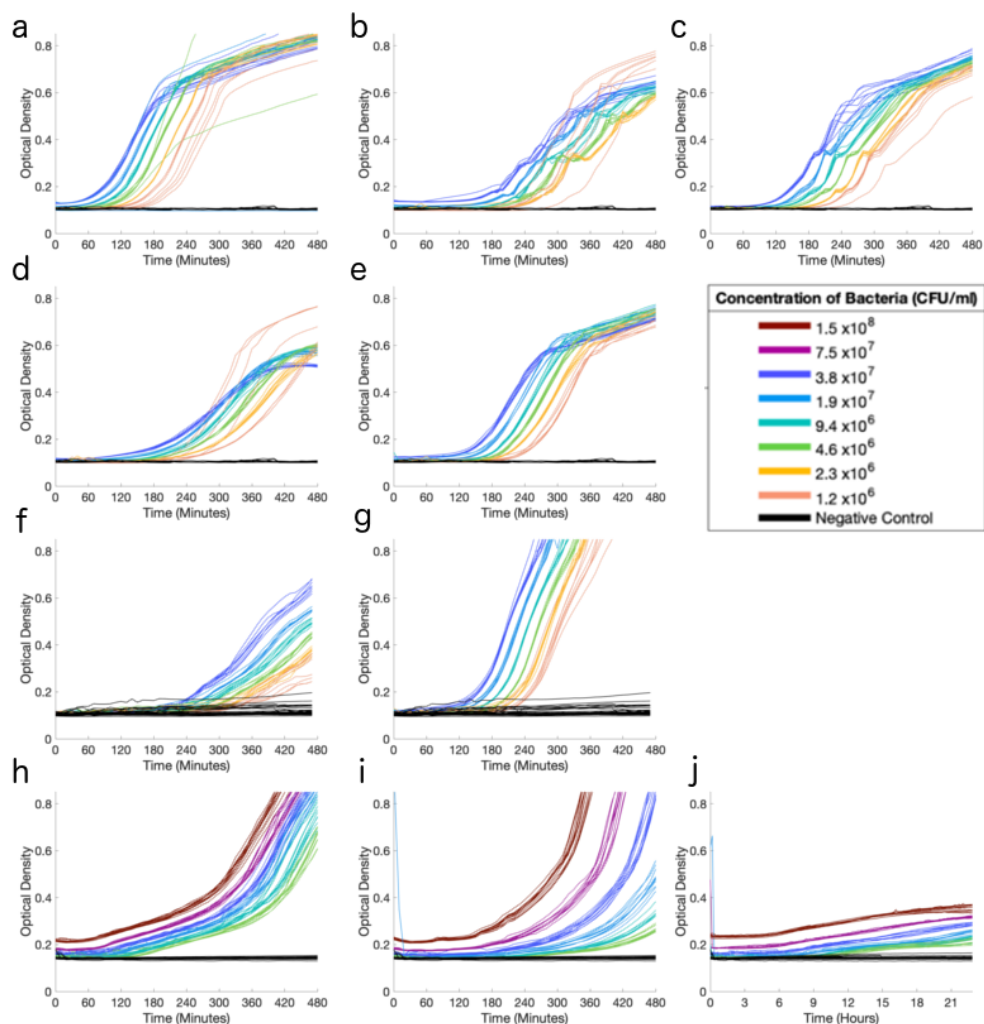


Figure 3.11. Growth curves of clinically relevant species. Growth curves for 10 species of bacteria are shown: (a) *E. coli* NCTC 25922, (b) *S. typhimurium* ATCC 19585, (c) *E. cloacae* NCTC 13405, (d) *Enterococcus faecalis* ATCC 47077, (e) *Staphylococcus aureus* ATCC 29213, (f) *P. aeruginosa* PAO1, (g) *K. pneumoniae* ATCC 700603, (h) *A. baumannii* NCTC 19606, (i) *P. aeruginosa* NCTC 13437 (j) *N. gonorrhoeae* ATCC 49226. Different growth media is required for the different species: (a-e) calcium adjusted Mueller Hinton broth, (f & g) Brain heart infusion (h-j) specialised GC media (section 3.2.4). For *A. baumannii* NCTC 19606, *P. aeruginosa* NCTC 13437 and *N. gonorrhoeae* (h-j) a 5% CO₂ -enhanced environment (generated using the plate reader) was used to further stimulate growth as well as the use of GC media (despite the name this media also stimulates the growth of other bacteria). The concentration of inoculating bacteria is indicated by colour, as shown in the key. Note that the time scale for (j) is in hours, due to the slow growth of *N. gonorrhoeae*.

3.3.9 Case Studies

Several academic groups have also developed automated and semi-automated screens for antimicrobial discovery, as well as the screening of large chemical libraries. Their screens have had different objectives, including drug repurposing, “unconventional” screening and discovery of synergistic partnerships, and investigation of cellular permeability. Examples of recent large scale screening attempts by academic groups are given below, demonstrating the potential uses of this platform.

3.3.9.1 Repurposing Screens

One accessible source of chemical matter is the commercially available libraries of known and approved compounds ^{29–32}, which can be used to search for new uses for old drugs, termed “repurposing” ³³. The advantage of repurposing is its significantly lower cost since the expensive safety stages of the drug discovery process have already been carried out, allowing a quick and cheap route to the clinic for a repurposed compound ³⁴, compared with the estimated \$1.7 billion cost of a novel compound ³⁵.

An extensive screen by the American National Institutes of Health screened 5,170 known compounds in an attempt to find inhibitors of *K. pneumoniae*. This screen found only 25 hits (0.5%) and follow-up work showing that the maximum concentration possible in the blood for these compounds was too low for them to be effective as antimicrobials ¹⁴. Disappointingly, other recent repurposing attempts ^{6,7,9} have similarly often only identified compounds with known antimicrobial activity (whether that be antimalarial, antiviral or antifungal). Potential reasons for the low hit discovery rate are discussed in the thesis Introduction.

3.3.9.2 Synergy Screens

Automated screening can also be used to search for novel synergistic partners of known antibiotics, in order to bypass mechanisms of resistance ^{36–38} or unlock cryptic activity. Eric Brown, Gerard Wright and colleagues at McMaster Canada have implemented a semi-automatic platform in a series of “unconventional” screens ^{15,16,39,40}, which aim to leverage observations such as the increased sensitivity of *E. coli* to vancomycin when cold stressed to find novel inhibitors of outer membrane proteins and

the ability of loperamide (Imodium) to potentiate the antimicrobial potency of tetracyclines against multi-drug resistant *P. aeruginosa*³⁹. These screens can also help identify targets which have yet to be challenged by antibiotics¹⁶. For example, observations of the β -lactam-potentiating activity of tunicamycin in methicillin-resistant *Staphylococcus aureus*⁴¹ has lead to several attempts to find more drug-like inhibitors of the target of the highly cytotoxic tunicamycin, the wall teichoic acid synthesis machinery^{15,42–44}. The identification of compounds such as tarocins⁴³ and the anti-platelet drug ticlopidine¹⁵ which lack antimicrobial activity but bypass resistance to β -lactams demonstrates the importance of synergy studies in combating antibiotic resistance.

Synergistic studies can also be used to find drug combinations that lower the clinical dose required and avoid the effects of resistance to a single therapy. Sun *et al.* used their high throughput “HIGA” platform to screen large numbers of combinations of 2 or 3 known antibiotics to find cocktails that could be given to patients with multiple drug resistance infections where single therapy is failing¹⁴. Without automation screening the many potential combinations would be prohibitive.

3.4 Conclusion

We have developed and validated a series of methods that can allow antimicrobial screening data to be obtained quickly and cheaply, with little compound usage. The accuracy of results is within the tolerance needed for a first round screen, as successful candidates are likely to be repeated via standardised methodologies. This platform will be used for projects within our group as well as being offered as a commercial service to small and medium drug discovery companies via Warwick Antimicrobial Facility.

3.5 References

- 1 Dheman N, Mahoney N, Cox EM, Farley JJ, Amini T, Lanthier ML. An Analysis of Antibacterial Drug Development Trends in the United States, 1980–2019. *Clin Infect Dis* 2020; : ciaa859.
- 2 Warwick Antimicrobial Screening Facility - University of Warwick. https://warwick.ac.uk/fac/cross_fac/amrscreening/. Accessed 12/03/21.

- 3 National Committee for Clinical Laboratory Standards Methods for Dilution Antimicrobial Susceptibility Tests for Bacteria That Grow Aerobically—11th Edition: Approved Standard M07-A11. Clinical and Laboratory Standards Institute (CLSI), Wayne, PA, USA, 2018.
- 4 Blaskovich MAT, Zuegg J, Elliott AG, Cooper MA. Helping Chemists Discover New Antibiotics. *ACS Infect Dis* 2015; **1**: 285–287.
- 5 Robotics – WISB. <https://www.wisb-uow.co.uk/robotics/>. Accessed 12/03/21.
- 6 Chopra S, Torres-Ortiz M, Hokama L, Madrid P, Tanga M, Mortelmans K *et al*. Repurposing FDA-approved drugs to combat drug-resistant *Acinetobacter baumannii*. *J Antimicrob Chemother* 2010; **65**: 2598–2601.
- 7 Jacobs AC, DiDone L, Jobson J, Sofia MK, Krysan D, Dunman PM. Adenylate Kinase Release as a High-Throughput-Screening-Compatible Reporter of Bacterial Lysis for Identification of Antibacterial Agents. *Antimicrob Agents Chemother* 2012; **57**: 26–36.
- 8 Pothineni V, Wagh D, Babar MM, Inayathullah M, Solow-Cordero D, Kim K-M *et al*. Identification of new drug candidates against *Borrelia burgdorferi* using high-throughput screening. *Drug Des Devel Ther* 2016; : 1307.
- 9 Feng J, Shi W, Zhang S, Zhang Y. Identification of new compounds with high activity against stationary phase *Borrelia burgdorferi* from the NCI compound collection. *Emerg Microbes Infect* 2015; **4**: 1–15.
- 10 Feng J, Yee R, Zhang S, Tian L, Shi W, Zhang W-H *et al*. A Rapid Growth-Independent Antibiotic Resistance Detection Test by SYBR Green/Propidium Iodide Viability Assay. *Front Med* 2018; **5**. doi:10.3389/fmed.2018.00127.
- 11 Imperi F, Massai F, Facchini M, Frangipani E, Visaggio D, Leoni L *et al*. Repurposing the antimycotic drug flucytosine for suppression of *Pseudomonas aeruginosa* pathogenicity. *Proc Natl Acad Sci* 2013; **110**: 7458–7463.
- 12 Molin MD, Selchow P, Schäfle D, Tschumi A, Ryckmans T, Laage-Witt S *et al*. Identification of novel scaffolds targeting *Mycobacterium tuberculosis*. *J Mol Med* 2019; **97**: 1601–1613.
- 13 Driessche FV den, Brackman G, Swimberghe R, Rigole P, Coenye T. Screening a repurposing library for potentiators of antibiotics against *Staphylococcus aureus* biofilms. *Int J Antimicrob Agents* 2017; **49**: 315–320.
- 14 Sun W, Weingarten RA, Xu M, Southall N, Dai S, Shinn P *et al*. Rapid antimicrobial susceptibility test for identification of new therapeutics and drug combinations against multidrug-resistant bacteria. *Emerg Microbes Infect* 2016; **5**: 1–11.
- 15 Farha MA, Leung A, Sewell EW, D'Elia MA, Allison SE, Ejim L *et al*. Inhibition of WTA Synthesis Blocks the Cooperative Action of PBPs and Sensitizes MRSA to β -Lactams. *ACS Chem Biol* 2012; **8**: 226–233.
- 16 Stokes JM, MacNair CR, Ilyas B, French S, Côté J-P, Bouwman C *et al*. Pentamidine sensitizes Gram-negative pathogens to antibiotics and overcomes acquired colistin resistance. *Nat Microbiol* 2017; **2**. doi:10.1038/nmicrobiol.2017.28.
- 17 Yep A, McQuade T, Kirchhoff P, Larsen M, Mobley HLT. Inhibitors of TonB Function Identified by a High-Throughput Screen for Inhibitors of Iron Acquisition in Uropathogenic *Escherichia coli* CFT073. *mBio* 2014; **5**. doi:10.1128/mbio.01089-13.
- 18 Zhang J-H, Chung TDY, Oldenburg KR. A Simple Statistical Parameter for Use in Evaluation and Validation of High Throughput Screening Assays. *J Biomol Screen* 1999; **4**: 67–73.
- 19 Brogden RN, Heel RC. Aztreonam: A Review of its Antibacterial Activity, Pharmacokinetic Properties and Therapeutic Use. *Drugs* 1986; **31**: 96–130.
- 20 Spratt BG. Distinct penicillin binding proteins involved in the division, elongation,

- and shape of *Escherichia coli* K12. *Proc Natl Acad Sci U S A* 1975; **72**: 2999–3003.
- 21 Kocaoglu O, Carlson EE. Profiling of β -Lactam Selectivity for Penicillin-Binding Proteins in *Escherichia coli* Strain DC2. *Antimicrob Agents Chemother* 2015; **59**: 2785–2790.
 - 22 Elewski BE, Aly R, Baldwin SL, González Soto RF, Rich P, Weisfeld M *et al*. Efficacy and safety of tavaborole topical solution, 5%, a novel boron-based antifungal agent, for the treatment of toenail onychomycosis: Results from 2 randomized phase-III studies. *J Am Acad Dermatol* 2015; **73**: 62–69.
 - 23 Sharma N, Sharma D. An upcoming drug for onychomycosis: Tavaborole. *J Pharmacol Pharmacother* 2015; **6**: 236.
 - 24 Ball P, Geddes A, Rolinson G. Amoxycillin Clavulanate: an Assessment after 15 Years of Clinical Application. *J Chemother* 1997; **9**: 167–198.
 - 25 Reading C, Cole M. Clavulanic Acid: a Beta-Lactamase-Inhibiting Beta-Lactam from *Streptomyces clavuligerus*. *Antimicrob Agents Chemother* 1977; **11**: 852–857.
 - 26 Bush K, Bradford PA. β -Lactams and β -Lactamase Inhibitors: An Overview. *Cold Spring Harb Perspect Med* 2016; **6**: a025247.
 - 27 Monod J. The Growth of Bacterial Cultures. *Annu Rev Microbiol* 1949; **3**: 371–394.
 - 28 Kremling A, Geiselmann J, Ropers D, de Jong H. Understanding carbon catabolite repression in *Escherichia coli* using quantitative models. *Trends Microbiol* 2015; **23**: 99–109.
 - 29 LOPAC1280 – Library of Pharmacologically Active Compounds. <https://www.sigmaaldrich.com/life-science/cell-biology/bioactive-small-molecules/lopac1280-navigator.html>. Accessed 10/03/21.
 - 30 Prestwick Library Profile. <http://www.prestwickchemical.com/pdf/2018-pcl-a-valuable-tool.pdf>. Accessed 10/03/21.
 - 31 Corsello SM, Bittker JA, Liu Z, Gould J, McCarren P, Hirschman JE *et al*. The Drug Repurposing Hub: a next-generation drug library and information resource. *Nat Med* 2017; **23**: 405–408.
 - 32 Microsource Pharmakon Library. <http://www.msdiscovery.com/pharmakon.html>. Accessed 10/03/21.
 - 33 Farha MA, Brown ED. Drug repurposing for antimicrobial discovery. *Nat Microbiol* 2019; **4**: 565–577.
 - 34 Pushpakom S, Iorio F, Eyers PA, Escott KJ, Hopper S, Wells A *et al*. Drug repurposing: progress challenges and recommendations. *Nat Rev Drug Discov* 2018; **18**: 41–58.
 - 35 Rex J, Krause K. All-In Cost Of A New Antibiotic From Discovery To 10 Years On Market. 2021. <https://amr.solutions/2021/01/09/all-in-cost-of-a-new-antibiotic-from-discovery-to-10-years-on-market/>. Accessed 19/01/21.
 - 36 Hind CK, Dowson CG, Sutton JM, Jackson T, Clifford M, Garner RC *et al*. Evaluation of a Library of FDA-Approved Drugs for Their Ability To Potentiate Antibiotics against Multidrug-Resistant Gram-Negative Pathogens. *Antimicrob Agents Chemother* 2019; **63**. doi:10.1128/aac.00769-19.
 - 37 El-Halfawy OM, Czarny TL, Flannagan RS, Day J, Bozelli JC, Kuiack RC *et al*. Discovery of an antivirulence compound that reverses β -lactam resistance in MRSA. *Nat Chem Biol* 2019; **16**: 143–149.
 - 38 Poole K, Gilmour C, Farha MA, Mullen E, Lau CH-F, Brown ED. Potentiation of Aminoglycoside Activity in *Pseudomonas aeruginosa* by Targeting the AmgRS Envelope Stress-Responsive Two-Component System. *Antimicrob Agents Chemother* 2016; **60**: 3509–3518.

- 39 Ejim L, Farha MA, Falconer SB, Wildenhain J, Coombes BK, Tyers M *et al.* Combinations of antibiotics and nonantibiotic drugs enhance antimicrobial efficacy. *Nat Chem Biol* 2011; **7**: 348–350.
- 40 Farha MA, Brown ED. Unconventional screening approaches for antibiotic discovery: Unconventional approaches for antibiotic discovery. *Ann N Y Acad Sci* 2015; **1354**: 54–66.
- 41 Campbell J, Singh AK, Maria JPS, Kim Y, Brown S, Swoboda JG *et al.* Synthetic Lethal Compound Combinations Reveal a Fundamental Connection between Wall Teichoic Acid and Peptidoglycan Biosyntheses in *Staphylococcus aureus*. *ACS Chem Biol* 2010; **6**: 106–116.
- 42 Swoboda JG, Meredith TC, Campbell J, Brown S, Suzuki T, Bollenbach T *et al.* Discovery of a Small Molecule that Blocks Wall Teichoic Acid Biosynthesis in *Staphylococcus aureus*. *ACS Chem Biol* 2009; **4**: 875–883.
- 43 Lee SH, Wang H, Labroli M, Koseoglu S, Zuck P, Mayhood T *et al.* TarO-specific inhibitors of wall teichoic acid biosynthesis restore β -lactam efficacy against methicillin-resistant staphylococci. *Sci Transl Med* 2016; **8**: 329ra32–329ra32.
- 44 Wang H, Gill CJ, Lee SH, Mann P, Zuck P, Meredith TC *et al.* Discovery of Wall Teichoic Acid Inhibitors as Potential Anti-MRSA β -Lactam Combination Agents. *Chem Biol* 2013; **20**: 272–284.

Chapter 4. Target-Mediated Resistance in PBP3: Role of Loop Flexibility

Chapter 4.S (p170-173) contains additional crystal views and data referred to in this chapter

4.1 Introduction

In response to treatment with antibiotics, bacteria have developed a number of mechanisms of resistance (Chapter 1) ¹. Target mediated resistance occurs when mutations are introduced into a protein which affects drug-protein interactions, and protects the bacterium from the drug's effects. Mutations could introduce resistance to β -lactams through a number of mechanisms: (i) reduction of the pre-acyl affinity of the β -lactam for the active site, (ii) reduction of the acylation rate (covalent bond formation or (iii) increase of the de-acylation rate, leading to faster clearance of the drug from the protein ². Change in the protein sequence at just a few specific points is sufficient to induce resistance via one of these mechanisms ²⁻⁷.

4.1.1 Mapping the Locations of Mutations

We first undertook a literature search for clinically relevant mutations that occur within class B PBPs of gram-negative species and mapped them onto new and improved high-resolution crystal structures ⁶ (Table 4.1 and Figure 4.1). There is extensive literature on the presence of point mutations causing β -lactam-resistance in *H. influenzae* PBP3 (HiPBP3, mutations prefixed by ^{Hi}) ^{3,8-19} and in *N. gonorrhoeae* PBP2 (NgPBP2, mutations prefixed by ^{Ng}) ^{2,4,5,20-25}, whereas only a few mutations have been reported in *P. aeruginosa* PBP3 (PaPBP, mutations prefixed by ^{Pa}) ^{26,27} or *E. coli* PBP3 (EcPBP, mutations prefixed by ^{Ec}) ²⁸⁻³⁰ (Table 4.1). By plotting the mutations onto crystal structures (Figure 4.1), it was clear that they cluster primarily in loops adjacent to the active site cleft of class B PBPs (Figure 1.4 for an overview of the protein). Loops are defined as stretches of residues between secondary structure elements, but they are increasingly understood to have important roles within proteins beyond simple connectivity ³¹. The four loops

identified by mutation clustering were the $\beta 2$ region (comprising of a series of loops between the short β strands $\beta 2a-d$), the $\alpha 10$ – $\beta 3$ loop, the $\beta 3$ – $\beta 4$ loop and the $\beta 5$ – $\alpha 11$ loop (Table 4.1).

	PaPBP3	HiPBP3	NgPBP2	EcPBP3
$\beta 2$ region	–	^{Hi} Ser357Asn	^{Ng} Asp346a insertion	^{Ec} (T/R)IPY, ^{Ec} YRI(N/K) insertions (around Tyr334)
$\alpha 10$ – $\beta 3$	–	^{Hi} Arg501Leu, ^{Hi} Ala502Val, ^{Hi} Val511Ala	–	–
$\beta 3$ – $\beta 4$	^{Pa} Arg504Cys/His	^{Hi} Arg517His, ^{Hi} Asn526Lys	^{Ng} Phe504Leu, ^{Ng} Ala510Val, ^{Ng} Asn512Tyr, ^{Ng} Ala516Gly	–
$\beta 5$ – $\alpha 11$	^{Pa} Pro527Ser/Thr, ^{Pa} Gly531Asp/Glu	^{Hi} Gly555Glu, ^{Hi} Tyr557His	^{Ng} Gly542Ser, ^{Ng} Gly545Ser, ^{Ng} Pro551Ser/Leu	–

Table 4.1. Mutants observed in the class B PBPs of three species of gram-negative pathogens cluster in various regions. Modified from Bellini et al. ⁶.

4.1.2 $\beta 2$ region

Simple comparisons of the crystal structures of wild type and mutant proteins can give an initial indication of the role of a particular mutation. To see if the presence of the ^{Ng}Asp346a on the $\beta 2$ region had an effect on its conformation, we crystallised and solved a novel structure (NgTP2^{HR-6140}, PDB: 6HZJ) ⁶ of an NgPBP2 mutant with 5 clinical mutations (Pro551Ser + Phe504Leu + Ala510Val+ Ala516Gly + the insertion Asp346a) from *N. gonorrhoeae* strain FA6140 ²¹. The conformation of the $\beta 2$ region changes significantly compared to a lower resolution structure of the same protein (NgTP2^{t3-6140}, PDB: 4U3T) ²⁰ or the wild type protein (PDB: 3EQU) ⁴.

Insertions of 4 residues into this loop have been repeatedly reported in carbapenem-expressing *E. coli* strains ^{28–30}. The exact sequence inserted varies between strains but the effect is likely to be a rearrangement of the $\beta 2$ loop. In both EcPBP3 and NgPBP2 as this loop sits above the active site cleft, these changes may restrict active site accessibility.

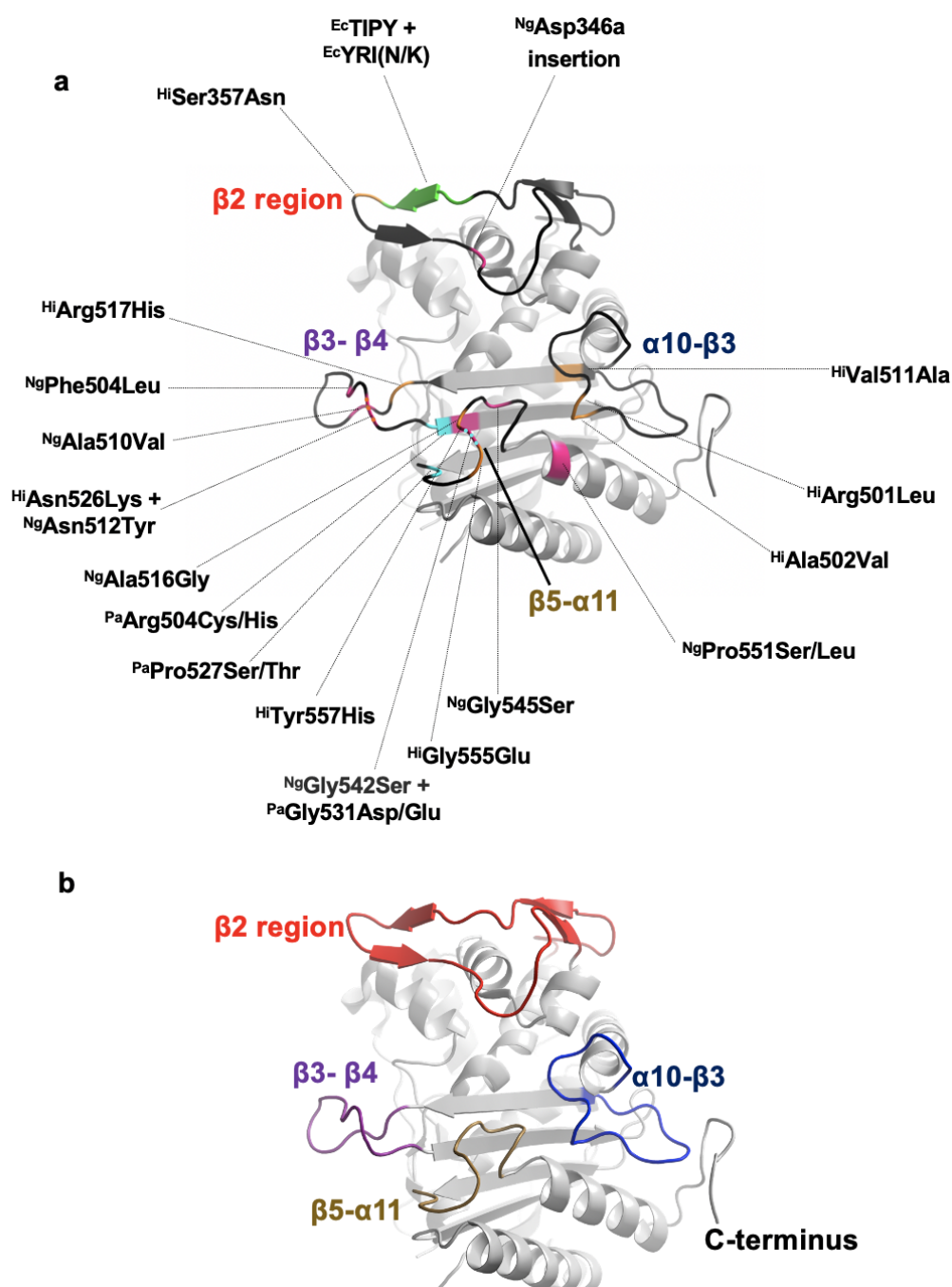


Figure 4.1. Plotting locations of clinical mutants on the class B transpeptidase domain. (a) Locations of the mutations listed in Table 4.1, plotted onto a NgPBP2 crystal structure (PDB: 6HZJ⁶). Mutations are coloured by the originating class B PBP: PaPBP (cyan), HiPBP3 (orange), NgPBP2 (pink) and EcPBP3 (green). Labelled loops are highlighted in black. (b) Locations of mutations appear to cluster within 4 loops: the $\beta 2$ region (in NgPBP2: residues 324-353), the $\alpha 10 - \beta 3$ loop (in NgPBP2: residues 477-494), the $\beta 3 - \beta 4$ loop (in NgPBP2: residues 501-513) and the $\beta 5 - \alpha 11$ (in NgPBP2: residues 537-548).

4.1.3 β 3- β 4 loop

The β 3- β 4 loop is a flexible region where clinical mutations can arise. In the four available PaPBP3 wild type apo structures (PDB: 3OC2³², 3PBN³³, 6HR4 and 6HZR⁶) this loop is unresolved, likely due to conformational flexibility. The binding of piperacillin (PDB: 6R3X⁶) or cefoperazone (PDB: 5DF8³⁴) appears to constrain the loop and allow it to be fully resolved.

Comparison of the *apo* and ceftriaxone reacted forms of wildtype NgPBP2 found that the β 3- β 4 loop was closer to the active site serine in the reacted form. A twisting of the β 3 strand accompanied this change³⁵. Recent crystallographic evidence in a mutant NgPBP2 suggests that the effect of mutations in the β 3- β 4 region may be to prevent the contraction of the β 3- β 4 loop upon ceftriaxone binding², as the *apo* and ceftriaxone reacted forms of a clinical mutant of this protein had little structural variation.

A structure of PaPBP3 with the ^{Pa}Arg504Cys mutation appeared to have no structural differences with the wild type, when *apo* or piperacillin-reacted⁶. The β 3- β 4 loop is the site of two frequently observed mutations (93 % in one study³⁶) in HiPBP3: ^{Hi}Arg517His and ^{Hi}Asn526Lys^{6,36}. These mutations provide little resistance by themselves but precede the development of further, high resistance, mutations in *H. influenzae*⁶.

4.1.4 β 5- α 11 loop

The β 5- α 11 loop was observed in β -lactam reacted PaPBP3 structures to transition from an outward “open” conformation (PDB: 3PBN³³ and 6HZR⁶) to an inward “closed” conformation upon binding of compounds such as piperacillin (PDB: 6R3X⁶) or aztreonam (PDB: 3PBS³³) (Figure 4.S2). In the closed conformation residues ^{Pa}Tyr503, ^{Pa}Tyr532 and ^{Pa}Phe533 form a “hydrophobic wall” against a hydrophobic section of a reacted compound³³. Mutations that occur in this region (Table 4.1) are primarily to proline or glycine residues which are likely to change the flexibility and mobility of this loop and its ability to do this movement. In NgPBP2, the role of the ^{Ng}Gly545Ser mutation (located at the N-terminal end of the α 11 helix) has been

suggested to play a more direct role, as Ser545 was observed to form a hydrogen bond to Thr500 on the $\beta 3$ strand, resulting in a conformational shift in the position of the ceftriaxone carboxylate group ².

4.1.5 $\alpha 10$ - $\beta 3$ loop

There has been little crystallographic evidence of the flexibility of the $\alpha 10$ - $\beta 3$ loop, but recent boronate-bound PaPBP3 structures show conformational plasticity here (see below).

From the locations of the mutations and the crystallographic conformational flexibility already seen in some of these regions, we hypothesised that these loops have a more important role in PBP3 biology than previously understood ⁶. Mutations responsible for β -lactam resistance may cause their effect by changing the flexibility of the loops and this is what causes changes in the dynamic behaviour of the protein. This chapter investigates loop flexibility using published crystallographic data as well as insight from novel PBP3:boronate complexes and then discusses methods beyond crystallography that could be used to further understand the dynamics of loops in PBP3s.

4.2 Methods

4.2.1 Ensemble refinement

In order to generate the ensemble models of PBPs, Ensemble refinement (ER) was run using Phenix (Version 1.18.2) ^{37–39}. Published structures (PDB: 6HZR and 6HZJ ⁶) were used for the input. To optimise the ensemble refinement, different values of the TLS (translation/libration/screw) parameter can be used. This parameter allows for flexibility of subsections of the model ³⁹. Refinement was run with TLS input values of 0.8, 0.9 and 1.0 and for both proteins it was found that 0.8 gave the lowest R factors. The ER led to a smaller R_{work} value for the PaPBP3 and NgPBP2 models and a decreased R_{free} value for the PaPBP3 model, but essentially unchanged R_{free} value for the NgPBP2 model, compared to the deposited structure (Table 4.2). Resultant structures containing all of the conformational models (85 and 50 for the PaPBP3 and NgPBP2 models respectively) were exported and analysed by

MDAnalysis^{40,41} and PyMOL (Open-Source PyMOL Molecular Graphics System, Schrodinger, LLC. Version 3.8.2).

4.2.2 RMSDs

The difference in the positions of main chain atoms (C, CA, N and O, following PDB notation) of a given residue was found for each of the conformational models generated by ER, compared to the deposited structure. The value for each residue was found by taking the mean across all the conformational models. The difference was assessed by determination of the root-mean-square deviation (RMSD). RMSD was found using the *MDAnalysis.analysis.rms* module^{42,43} of MDAnalysis, using custom scripts.

When determining the per-residue RMSD between two structures (e.g. Figure 4.S1), a similar procedure was used, but with only two input structures. Regions in which sections of the model were missing in one of the structures were omitted from analysis.

4.2.3 B factors

Refined B factors were extracted from the published model files by custom scripts in MDAnalysis. The mean of the B-factors of each main chain atom (C, CA, N, O, following PDB notation) of each residue was determined for each model or subunit.

4.2.4 PDBFlex

The PDBFlex server⁴⁴ was used to examine the conformations of PaBPB3 structures in the “4kqrA cluster” which consisted of 38 structures (in the 16th May 2020 PDB release). These correspond to structures with PDB codes: 3OC2, 3OCL, 3OCN, 3PBN, 3PBO, 3PBQ, 3PBR, 3PBS, 3PBT, 4FSF, 4KQO*, 4KQQ*, 4KQR, 4L0L, 4OOL, 4OOM, 4WEJ, 4WEK, 4WEL, 5DF7*, 5DF8*, 5DF9, 6HR4, 6HR6, 6HR9, 6HZR, 6I1E, 6R3X, 6R40, 6R42, 6UN1, 6UN3, 6VJE and 6VOT, all of which have > 99 % sequence similarity. Structures marked with an asterisk have both A and B subunits, which were considered separately. Only 5 of these are apo structures (PDB codes 3OC2, 6HR4, 3PBN, 6HZR, 6R40), with the rest being bound to a ligand. The average local root mean squared deviation of the Ca carbon (RMSD) was exported and plotted against the residue number in Matlab.

Boron-containing crystal structures were crystallised as described in section 5.2 and reference ⁴⁵.

4.3 Results and Discussion

4.3.1 Assessing Backbone Flexibility with Crystallography

Crystallographic data can be further exploited to gain insight into the role of loops in PBPs. We used three methods to assess loop flexibility: ensemble refinement (ER), refined structure B factors, and the PDBFlex server.

In high resolution data maps, it may be possible to fit a region of electron density with more than one model, which can be used to understand the flexibility of that region. The Phenix.Ensemble refinement program uses molecular dynamics simulations to generate alternative models of the protein conformation and then refines them into the available electron density ^{38,39}. Structures of PaPBP3 (PDB code 6HZR ⁶) and NgTP2^{HR-6140} (PDB code 6HZJ ⁶) were refined with ER in Phenix.Ensemble and the resultant models were compared to the published structure (Figure 4.2a and d). ER led to unchanged or improved R values (Table 4.2), indicating that the ER models fit well to the crystallographic data.

	PaPBP3		NgPBP2	
	Published Value (6HZR)	ER	Published Value (6HZJ)	ER
Resolution (Å)	1.19		1.43	
R _{free}	0.226	0.204	0.301	0.302
R _{work}	0.207	0.174	0.278	0.255

Table 4.2. R values of different refinement methods. Comparison of R values between published values and ER values.

The B-factor is a measure of the change in intensity of the X-ray scattering of an atom due to its dynamic and static disorder, which is determined for each atom during refinement cycles ⁴⁶. B-factors can be used to describe the intrinsic flexibility of a crystallographic model ⁴⁷.

Finally it is possible to exploit the large number of structural datasets available for PaPBP3 using the "PDBFlex" server ⁴⁴, to see flexibility of the protein across different crystal preparations and with different ligands. This server clusters and aligns protein structures with high sequence similarity (> 95 % identity) and assesses regions of structural similarity. There are 38 PaPBP3 structures in their cluster (none of the structures described in the Chapter 5 of this thesis were included in the dataset) but there are only 5 in the cluster of NgPBP2, which is insufficient for representative work.

The amount of conformational flexibility observed using the Phenix.Ensemble method correlates well with the crystallographic B-factor of a residue (Figure 4.2a and d). The 3D structures of the ensemble models show the positions that are possible: the positional variations are not random but are constrained to specific movements, within specific sections of the loop (Figure 4.2b and d). The results from the PDBFlex server cluster generally agree with the results from the single structure in Figure 4.2a, but are typically less noisy. The flexibility of the β 3- β 4 loop appears to have been underestimated by the server because it is not present in many of the structures analysed.

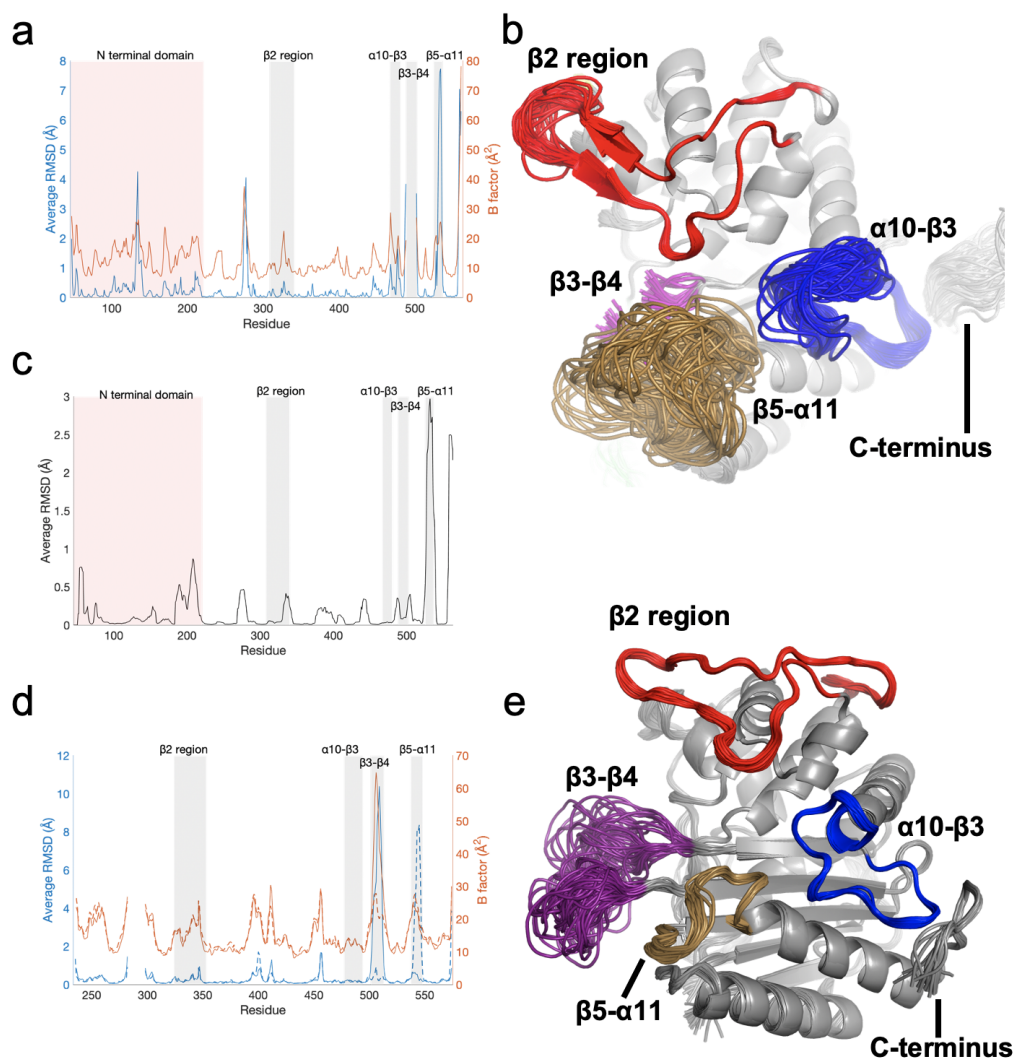


Figure 4.2. Investigation of loop movements of PaPBP3 and NgPBP2. (a) Results of ensemble refinement (ER) by Phenix. Ensemble of PaPBP3 (PDB code 6HZR⁶). Root-mean-square deviations (RMSD) of each residue of *P. aeruginosa* PBP3 following ER. The RMSD of each of the 64 models generated by Phenix. Ensemble are compared to their position in the published crystal structure and then averaged and plotted for each residue (blue, left axis). The refined B-factor of each atom in the published crystal structure is shown (orange, right axis). Loop regions are highlighted in grey and labelled, the N-terminal domain (up to residue 221) is highlighted with a red box. Residues 489-501 are not resolved in the crystal structure and are missing from the analysis. (b) Overlays of the models generated by ER of PaPBP3 (PDB code 6HZR⁶). The protein is represented in cartoon and certain loops are coloured and labelled. The greatest loop positional variation is seen for the β 5- α 11 and α 10- β 3 loops. The β 3- β 4 loop is too flexible to be resolved in the crystal model. (c) The PDBFlex server generated a per-residue RMSD using a cluster of 38 models of PaPBP3. These are plotted similarly to (a). The dual peaks in the β 3- β 4 loop is likely due to the frequent absence of residues in this region from refined structures. (d) Results of ER of the transpeptidase domain of NgTP2^{HR-6140} (PDB code 6HZJ⁶). As in (a), the RMSD of each of the 50 models generated by ER are compared to their position in the same subunit in the

published crystal structure and then averaged and plotted for each residue (blue, left axis). The refined B-factor of each atom in the published crystal structure is shown (orange, right axis). Two subunits (A and B) are found in the asymmetric unit, each with slightly different conformations. A is shown by a solid line and B with a dashed line. (e) Overlays of the models generated by ER of subunit A of NgTP2^{HR-6140} (PDB code 6HZJ⁶). The protein is represented in cartoon and certain loops are coloured and labelled.

By all three analysis methods, flexible loops appear as sharp spikes compared to the overall relatively static protein (see protein median values in Table 4.S1). In the PaPBP3 transpeptidase domain, the flexibility of the β 2 region, the β 3- β 4 loop and particularly the β 5- α 11 is clear. The α 10- β 3 region has a high RMSD in the single high resolution crystal structure (Figure 4.2a) but this is not consistent across the PaPBP3 crystals (Figure 4.2c). In NgPBP2, the subunits within the asymmetric unit each have differently flexible loops. In subunit A the β 3- β 4 loop has a high degree of flexibility, whilst the β 5- α 11 loops are static. The opposite is true in subunit B. The α 10- β 3 loop has no more flexibility than an average section of the mainchain (Figure 4.2d).

Three other flexible regions are highlighted by three flexibility analysis techniques (Figure 4.2a, c and d). These regions located within the following loops on the “back” face of the transpeptidase domain: β 1b- α 2 (residues 266-293), in the nominal α 8 region (residues 374-398), α 9- α 10 (residues 427-450) (Figure 4.3). Mutations were not consistently identified in these regions.

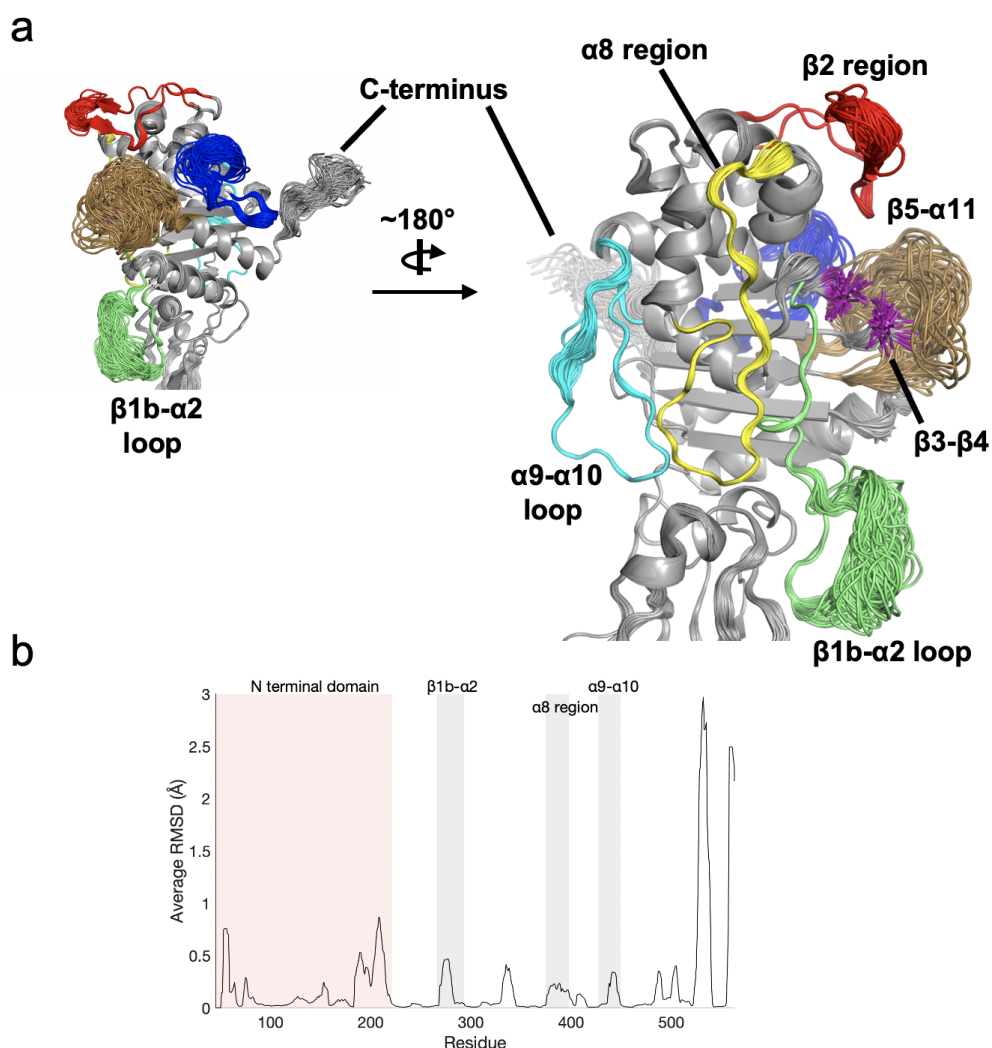


Figure 4.3. Loops on the “back” face of PaBP3. Models generated by ER of PaBP3, as in Figure 4.2b. Analysis (Figure 4.2 in the main text), shows flexibility occurring in an additional 3 loops to those discussed in detail in the text: the $\beta 1b$ - $\alpha 2$ loop (green, residues 266-293), in the nominal ⁴⁸ $\alpha 8$ region (yellow, residues 374-398), the $\alpha 9$ - $\alpha 10$ loop (cyan, residues 427-450). The $\alpha 8$ helix is not fully resolved in the PaBP3 crystal structure. These regions have little significant secondary structure, but still only show flexibility in limited sections of the loops. All three loops are on the “back” face of the protein relative to the active site. (b) Replot of the graph shown in Figure 4.2c (generated by the PDBFlex server), highlighting the peaks in the RMSD curve due to the flexibility of the 3 loops.

The core secondary structure provided by the $\alpha + \beta$ fold of the transpeptidase domain (shared across the penicilloyl-serine transferase superfamily, Chapter 1) gives overall rigidity to the protein. Its secondary structure inflexibility is shown by the very low RMSDs of the main chain atoms (Figure 4.2). For example, residues

294-305 of PaPBP3 (helix $\alpha 2$) for which all residues have an average RMSD of less than 0.1 Å, as assessed by ER and PDBflex (Figure 4.2a and c). Consequently, the catalytic residues: (e.g. in PaPBP3 Ser294, Ser349, Lys297 and Lys484) all exhibit low flexibility (Table 4.S1) as these residues are all located with the core structural elements. It has been suggested that rigidity of the active site residues allows for the fast catalysis of β -lactamases⁴⁹. Rigidity of these residues may ensure they stay optimally spaced to allow for rapid activity once the substrate binds^{50,51}. The possible movements of the loops are constrained by the rigidity of the adjacent secondary structure elements.

These results build a picture in which certain privileged regions (with some consistency between species) are flexible, but much of the protein is highly constrained. It has previously been observed that the global motions (slowest dynamics of a protein) are defined by the protein fold⁵² and that the movement of individual loops are determined by the global motions of the protein^{53,54}. Like the secondary structure, loop dynamics may be a “structure-encoded” property of the penicilloyl-serine transferase superfamily fold.

4.3.2 Novel Ligands Generate Novel Conformations

Chapter 5 describes the interactions of PBPs with boronates. While investigating the crystal structures of boronates bound to PaPBP3, it was observed that the $\beta 5$ - $\alpha 11$ and $\alpha 10$ - $\beta 3$ loops adopt novel conformations compared to previously published β -lactam reacted or *apo* structures. Whilst the protein used was wildtype, its response to novel ligands may indicate cryptic behaviours of the protein, which may be contributing to the resistance mechanism.

4.3.2.1 Conformations of the $\beta 5$ - $\alpha 11$ Loop

In the majority of the PaPBP3:boronate structures investigated in Chapter 5, the density of residues in the $\beta 5$ - $\alpha 11$ loop was too poor to allow a model to be fit, likely due to the flexibility of the region. However, structures with **1**, **2** and **14** all display unique conformations of the loop (Figure 4.4). Whilst the density of the side chains is not complete in all models, they provide some insight into the flexibility of the region. Density for each of the structures is shown in Figure 4.4b-d. The conformation adopted by **1** is particularly unique, with the loop folding closer to the $\beta 3$ strand than it is observed in any other structure (Figure 4.4a and b).

These structures provide further evidence of the flexibility of the $\beta 5$ - $\alpha 11$ loop and also indicate that its conformation is dependent on the nature of the ligand binding at the active site, despite the fact that these ligands make few direct interactions with residues of the loop (**1** and **14** with Gly534 and Gly535 and **2** with only Gly534).

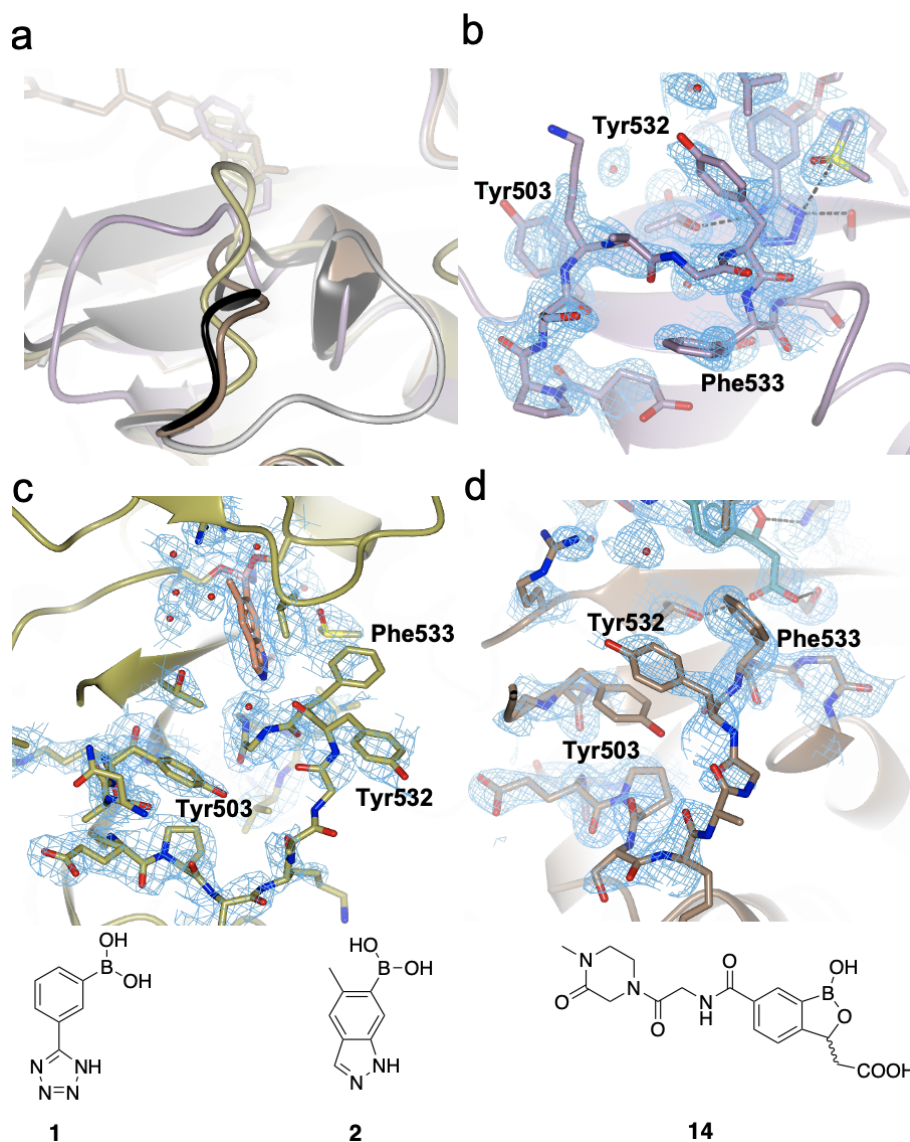


Figure 4.4. Boronate binding can affect the conformation of the $\beta 5$ - $\alpha 11$ loop in PaBP3. (a) Conformations of the $\beta 5$ - $\alpha 11$ loop in PaBP3 structures with **1** (lilac), **2** (yellow), **14** (brown), and reacted piperacillin (black, molecule of reacted piperacillin itself not shown, PDB code: 6R3X⁶) bound, as well as the apo structure (white, PDB code: 6HZR⁶). Electron density for the loop with: (b) **1**, (c) **2** and (d) **14** bound. The PaBP3:**14** complex (d) and the piperacillin reacted PaBP3 have similar main chain conformations, however residues Tyr503, Tyr532 and Phe333 have a different arrangement of their π -stack. Electron densities were contoured at 1 σ and produced using the comit function in the CCP4 suite⁵⁵.

4.3.2.2 Conformations of the α 10- β 3 Loop

The α 10- β 3 loop has not been observed to exist in many conformations in previously published structures of PaPBP3 (i.e Figure 4.2c shows a low RMSD for this region). However, compounds **2** and **13** both change the conformation of the α 10- β 3 loop.

The structure of PaPBP3:**13** shows two alternate conformations of four residues (476-480), each with comparable occupancy (48 % and 52 %) (Figure 4.5). Movement of this portion of the loop is within the bounds set by the ER (Figure 4.2a and b), but other PaPBP3 structures (e.g. piperacillin reacted (6R3X), *apo* (6HZR⁶) nor any of the other structures with boronate described in this thesis) do not have sufficient density to so clearly define the two alternate conformations.

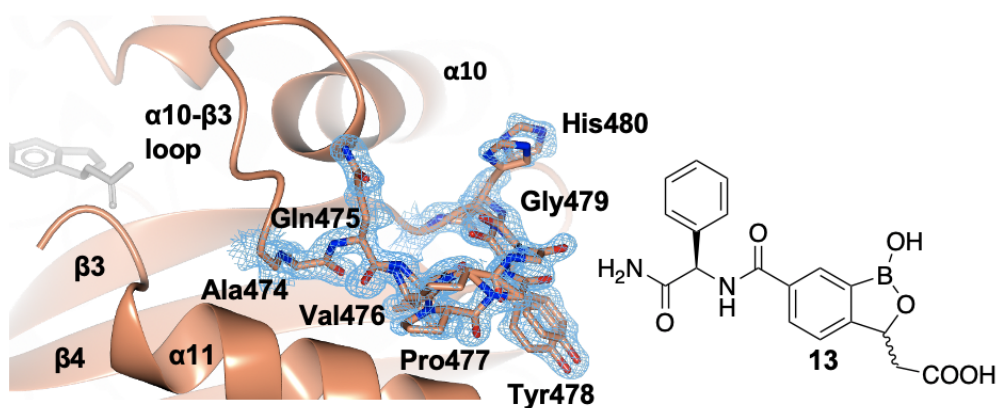


Figure 4.5. The crystal structure of PaPBP3:13** shows two alternate conformations of the α 10- β 3 loop.** Omit map density (blue mesh) for residues 474-480 is shown. Electron densities were contoured at 1 σ and produced using the comit function in the CCP4 suite⁵⁵.

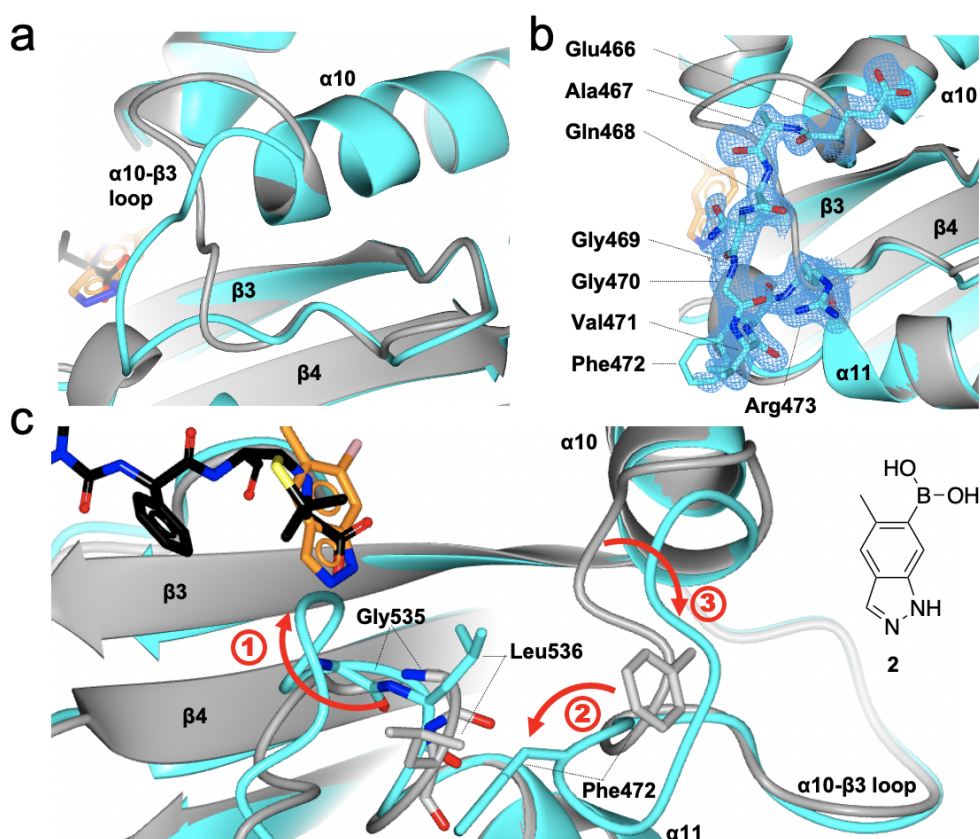


Figure 4.6. Boronate binding can affect the conformation of the $\alpha10$ - $\beta3$ loop in PaBPB3. (a) Comparison of the $\alpha10$ - $\beta3$ loop position in the crystal structure of PaBPB3:2 (cyan and orange) and in a piperacillin reacted structure (PDB: 6R3X⁶, black and grey). The loop is significantly displaced between residues 466 and 473, compared to the piperacillin reacted structure, which is itself much like the *apo* structure (PDB: 6HZR⁶, Figure 4.S2). (b) Omit map density (blue mesh) for residues 466-473 of the PaBPB3:2 structure. The density of all the residues is well defined. Electron densities were contoured at 1 σ and produced using the comit function in the CCP4 suite⁵⁵. (c) Proposed mechanism for the transmittance of changes at the active site to changes in the $\alpha10$ - $\beta3$ loop. (1) the binding of the imidazole group at the 'acid binding pocket' (hydrogen bonding to Ser485 and Gly534) leads to a rearrangement of the $\beta5$ - $\alpha11$ loop and the $\alpha11$ helix. (2) The sidechain of Phe472 moves towards the $\alpha11$ helix, with a resultant change in the position of the $\alpha10$ - $\beta3$ loop (3).

The change in conformation observed with the PaBPB3:2 is more significant (Figure 4.6) and to my knowledge entirely novel. The loop extends out from the protein and away from the preceding $\alpha10$ helix which aligns well to the piperacillin reacted structure (PDB: 6R3X⁶), as does the loop beyond residue Ala474. The cause of the change in conformation is unclear, as no new hydrogen bond interactions, (e.g. with the $\alpha11$ helix) are formed. The effect is not caused by the

tri-covalent bonding of the protein (see Chapter 5), as the binding of **1** (also tri-covalent) does not elicit this change in PaPBP3. It could be linked to the novel conformation of the $\beta 5$ - $\alpha 11$ loop that is observed in the structure of PaPBP3:**2** (Figure 4.4a and c). One explanation could be that the binding of the pyrazole group of **2** causes the change in the conformation of the $\beta 5$ - $\alpha 11$ loop, and tightens the first twist of the $\alpha 11$ helix, leading to a displacement of residues Gly535 and Leu536 ((**1**), Figure 4.4c). The displacement allows Phe472 to shift towards the active site (**2**) with the accompanying shift in the $\alpha 10$ - $\beta 3$ loop (**3**) (Figure 4.4c). In this way changes at the active site are transmitted to a change at the $\alpha 10$ - $\beta 3$ loop. Separately, in both TEM-1⁵⁶ and SHV-1⁵⁷ β -lactamases, the region between the $\alpha 10$ - $\beta 3$ loop and helix $\alpha 11$ has been shown to be a “cryptic” binding site for weak allosteric inhibitors (Figure 4.S3). Demonstration of the conformational flexibility of this region raises the possibility of allosteric inhibition of PBP3, something which is previously unreported.

4.3.2.3 Networks of Coupled Promoting Motions

The above examples suggest the presence of an indirect link between the binding of a specific ligand at the active site and the conformation of peripheral loops. This same link could be used to transfer the effect of mutations on the peripheral loops to changes in the active site. In bacterial dihydrofolate reductase (DHFR, the target of trimethoprim), it has been suggested that resistance mutations can affect the rate of catalysis through “networks of coupled promoting motions”^{58,59}. These networks consist of interacting chains of amino acids which transmit information through the protein by their concerted motions^{58,59}. Studies show that point mutations up to 20 Å away can influence the rate of catalysis as much as 200 fold^{58,60} by this proposed mechanism. These networks are suggested to be a common feature of protein families, which may explain the conservation of locations of mutations across class B PBPs from different gram-negative species (Table 4.1). As has been previously observed with PBP3⁶, the clinical mutations of a protein target do not necessarily lead to a change in the protein crystal structure^{60,61}. Instead, mutations can elicit a change in the protein dynamics, which affects the ligand processing^{60,61}.

4.4 Future Work: Beyond

Cryo-Crystallography

Methods that do not rely on crystallographic evidence are required to assess protein dynamics. An over-reliance on crystallographic data may lead to overinterpretation of conformations that are actually the consequence of crystallographic artifacts such as crystal packing and are not biologically relevant. Crystal structures of the NgTP2^{HR-6140} and NgTP2^{I3-6140} are illustrative (Figure 4.S1): the crystal structures prepared by different researchers have significant deviations in conformations of local regions, which are difficult to account for ^{6,20}.

The change in dynamic behaviour of the protein (assessed with some of the tools below) could be correlated with the β -lactam-binding activity of the protein (using some of the methods listed in Table 1.2), for each of the mutations of interest. In this way, the changes in protein dynamics could be used to explain the mechanism of resistance, and perhaps even the contributions of each of the three pathways (i-iii, described above).

4.4.1 Room Temperature Crystallography

Protein crystallography is typically conducted at around 100 K, which helps reduce the effect of radiation damage that samples experience when exposed to the high energy beams of a synchrotron ⁶². However, this rapid freezing is thought to further bias the crystals into conformations which may not exist under physiological conditions ^{63,64}. When X-ray diffraction patterns are instead collected at room temperature, studies have shown that different side chain conformations can be adopted and that additional backbone conformations become possible ⁶³, presumably making the protein more similar to the physiological solution state. Due to the complex energy networks within the protein, *a priori* prediction of the effects of warming on protein structure is challenging ⁶³. Methods to study proteins at room temperature (including techniques which circumvent the issue of increased radiation damage) are being constantly improved, such as the VMXi beamline (being commissioned at Diamond Light Source) ⁶⁵ and X-ray free electron lasers ⁶⁶.

4.4.2 Tryptic Digestion

A simple method to observe flexibility is to use limited tryptic digestion of a protein, which was used to validate the effects of mutations in NgPBP2⁵ and PBP2x from *S. pneumoniae*⁶⁷. Decreased flexibility of the β 2 loop region (caused by the introduction of mutations that provide resistance to β -lactams) was used to explain the lack of tryptic digestion within this section of the protein, compared to the wild type. When more rigid, the protein does not allow the trypsin to access the site of proteolysis. This technique is quick and highly site specific, but provides a very qualitative insight into the changes occurring.

4.4.3 NMR

Nuclear magnetic resonance (NMR), can show the interactions and dynamics of amino acids within proteins in solution at physiological temperature with atomic resolution⁶⁸ and is well suited for the task of analysing protein dynamics. NMR tools are available which can study protein dynamics on timescales of ps-ns or μ s-s⁶⁹. Whilst solving a full protein model by NMR is challenging, NMR can be used in a more limited context to understand individual movements. After tagging mutated cysteines with fluorine-based probes the Schofield group and others from the University of Oxford were able to study the loop dynamics of metallo- β -lactamases using ¹⁹F NMR^{70,71}. The ¹⁹F signal is highly sensitive to local changes in the environment, with movements of the loops the probes are placed on and binding of ligands to the active site leading to a change in signal. Two loops can even be tagged simultaneously and their varying interactions with different ligands observed⁷¹. One limitation of this is that it requires the addition of a cysteine residue to the loop which itself may act as a resistance determining mutation.

4.4.4 Molecular dynamics

Molecular dynamics, where the internal structure of a protein is mechanically modelled as a series of masses and springs can be used to simulate the movements of proteins⁷². The method analyses the protein as a series of very small (~femtosecond), discrete timesteps, so long simulations can be computationally expensive (typically up to a few nanoseconds of simulation is possible). However

the global dynamics of the protein (large scale movements) such as loop movements, allostery and substrate binding occur on the timescale of microseconds to milliseconds^{73–75}. This means that feasible simulations may be too short to appreciate loop dynamics. This type of analysis has been applied to penicilloyl-serine transferase superfamily proteins and revealed their dynamics^{49,76–79}.

A recent work using MD to understand the loop dynamics of class A β -lactamases (TEM-1 and KPC-2) shows the loops of these β -lactamases have important roles in β -lactamases, as we propose for PBPs⁷⁹. Simulations at equilibrium on the enzymes showed greatest fluctuations for the equivalent regions to the (PBP3) α 10- β 3 (referred to as the 'hinge' and α 11 in TEM-11), the β 3- β 4 loop (β 7- β 8 in TEM-1) and the β 5- α 11 loop (β 9- α 12 in TEM-1), similar to the conclusions I have drawn from the crystal structures of class B PBPs (section 4.3.1).

The authors also investigated the effect of removing a TEM-1 allosteric inhibitor (Figure 4.S3), which sits between the TEM-1 equivalent of the α 10- β 3 loop and the α 11 helix. Simulations of non-equilibrium protein dynamics for the 5 ns following removal of the allosteric ligand showed 'signal propagation' that led to changes in the equivalent region to β 2 region, \sim 33 Å from the allosteric site. One of the signal propagation pathways proposed was via the equivalent to the α 11- β 5 loop. As in PBPs, clinical mutants map onto the regions proposed for the signal propagation route⁷⁹. This example parallels our hypothesis that the active site loops of PBPs have important roles for β -lactam binding and that clinical mutants modify this.

Combinations of molecular dynamics and NMR can be a powerful tool for studying protein dynamics. In TEM-1 β -lactamase, NMR analysis of rigidity (measured over a short $<$ ps timescale) and molecular dynamics simulations (which model movements occurring over a ps-low ns timescale) showed that loop regions are more flexible than NMR analysis alone predicts⁴⁹. The authors develop a model in which there is high rigidity over short time scales to increase the rate of catalysis, coupled with conformational changes happening over a μ s-ms timescale, which has been supported by further NMR in chimeric β -lactamases⁸⁰.

4.5 Conclusions

Our study on the locations of point mutations that cause target-mediated resistance in PBP3 as well as observations from crystal structures lead us to hypothesise certain loops may play a more important role in PBP3 structural dynamics than previously understood ⁶. Analysis with ensemble refinement and comparisons across many structures of PaPBP3 indicates flexibility within these same regions, but tools beyond crystallography are needed to better characterise their movements. Work in DHFR on correlations between mutations and flexibility provide a useful precedent for how work on PBPs may be conducted ^{58,81,82}.

Use of unligated proteins will only provide limited information, and a more complete picture of target mediated resistance requires a better understanding of the exact nature of protein:drug interactions. Currently, only crystal structures of the *apo* and covalently reacted PBP3s (as well as a few examples of hydrolysed β -lactam structures in the active site ^{34,83}) are available. Work with cephalosporins bound to mutant and wild-type NgPBP2 is helping to explain the effects of some mutations ^{2,35}. We have demonstrated that novel ligands such as boronates can influence the conformations of the loop regions. Further crystal structures with novel ligands may be beneficial in this effort. Perhaps the most important ligand to crystallise is the natural substrate, for which there remains no crystal structures in a class B PBP. Any successful mutation to a PBP must reduce β -lactam binding, but allow natural substrate processing to proceed at sufficient rates to allow growth. Studies are required to assess how this is possible.

It is interesting to consider the impact of introduction of new, non- β -lactam PBP inhibitors (Table 1.1). For example, if inhibitors are found which lack β -lactamase susceptibility (e.g. boronates: Chapter 5) will this lead to a bias in the evolved mechanism of resistance towards target-mediated resistance?

Better knowledge of PBP3 target mediated resistance may allow for its emergence to be predicted and for ligands to be developed in which resistance by this mechanism is minimised.

4.6 References

- (1) King, D. T.; Sobhanifar, S.; Strynadka, N. C. J. The Mechanisms of Resistance to β -Lactam Antibiotics. In *Handbook of Antimicrobial Resistance*; Berghuis, A., Matlashewski, G., Wainberg, M. A., Sheppard, D., Eds.; Springer New York: New York, NY, 2017; pp 177–201. https://doi.org/10.1007/978-1-4939-0694-9_10.
- (2) Singh, A.; Turner, J. M.; Tomberg, J.; Fedarovich, A.; Unemo, M.; Nicholas, R. A.; Davies, C. Mutations in Penicillin-Binding Protein 2 from Cephalosporin-Resistant *Neisseria gonorrhoeae* Hinder Ceftriaxone Acylation by Restricting Protein Dynamics. *J. Biol. Chem.* **2020**, 295 (21), 7529–7543. <https://doi.org/10.1074/jbc.RA120.012617>.
- (3) Tomberg, J.; Unemo, M.; Davies, C.; Nicholas, R. A. Molecular and Structural Analysis of Mosaic Variants of Penicillin-Binding Protein 2 Conferring Decreased Susceptibility to Expanded-Spectrum Cephalosporins in *Neisseria gonorrhoeae*: Role of Epistatic Mutations. *Biochemistry* **2010**, 49 (37), 8062–8070. <https://doi.org/10.1021/bi101167x>.
- (4) Powell, A. J.; Tomberg, J.; Deacon, A. M.; Nicholas, R. A.; Davies, C. Crystal Structures of Penicillin-Binding Protein 2 from Penicillin-Susceptible and -Resistant Strains of *Neisseria gonorrhoeae* Reveal an Unexpectedly Subtle Mechanism for Antibiotic Resistance. *Journal of Biological Chemistry*, 2009, 284, 1202–1212.
- (5) Tomberg, J.; Temple, B.; Fedarovich, A.; Davies, C.; Nicholas, R. A. A Highly Conserved Interaction Involving the Middle Residue of the SXN Active-Site Motif Is Crucial for Function of Class B Penicillin-Binding Proteins: Mutational and Computational Analysis of PBP 2 from *N. gonorrhoeae*, 2012. <https://doi.org/10.1021/bi2017987>.
- (6) Bellini, D.; Koekemoer, L.; Newman, H.; Dowson, C. G. Novel and Improved Crystal Structures of *H. influenzae*, *E. coli* and *P. aeruginosa* Penicillin-Binding Protein 3 (PBP3) and *N. gonorrhoeae* PBP2: Toward a Better Understanding of β -Lactam Target-Mediated Resistance. *J. Mol. Biol.* **2019**, 431 (18), 3501–3519. <https://doi.org/10.1016/j.jmb.2019.07.010>.
- (7) Tomberg, J.; Unemo, M.; Ohnishi, M.; Davies, C.; Nicholas, R. A. Identification of Amino Acids Conferring High-Level Resistance to Expanded-Spectrum Cephalosporins in the *PenA* Gene from *Neisseria gonorrhoeae* Strain H041. *Antimicrob. Agents Chemother.* **2013**, 57 (7), 3029–3036. <https://doi.org/10.1128/AAC.00093-13>.
- (8) Ubukata, K.; Shibasaki, Y.; Yamamoto, K.; Chiba, N.; Hasegawa, K.; Takeuchi, Y.; Sunakawa, K.; Inoue, M.; Konno, M. Association of Amino Acid Substitutions in Penicillin-Binding Protein 3 with β -Lactam Resistance in β -Lactamase-Negative Ampicillin-Resistant *Haemophilus influenzae*. *Antimicrob Agents Chemother*, 2001, 45, 1693–1699. <https://doi.org/10.1128/aac.45.6.1693-1699.2001>.
- (9) Dabernat, H.; Delmas, C.; Seguy, M.; Pelissier, R.; Faucon, G.; Bennamani, S.; Pasquier, C. Diversity of β -Lactam Resistance-Confering Amino Acid Substitutions in Penicillin-Binding Protein 3 of *Haemophilus influenzae*. *Antimicrob Agents Chemother*, 2002, 46, 2208–2218.
- (10) Skaare, D.; Anthonisen, I. L.; Kahlmeter, G.; Matuschek, E.; Natås, O. B.; Steinbakk, M.; Sundsfjord, A.; Kristiansen, B. E. Emergence of Clonally

Related Multidrug Resistant *Haemophilus influenzae* with Penicillin-Binding Protein 3-Mediated Resistance to Extended-Spectrum Cephalosporins, Norway, 2006 to 2013, 2014.

<https://doi.org/doi:10.2807/1560-7917.ES2014.19.49.20986>.

- (11) Osaki, Y.; Sanbongi, Y.; Ishikawa, M.; Kataoka, H.; Suzuki, T.; Maeda, K.; Ida, T. Genetic Approach To Study the Relationship between Penicillin-Binding Protein 3 Mutations and *Haemophilus influenzae* β -Lactam Resistance by Using Site-Directed Mutagenesis and Gene Recombinants. *Antimicrobial Agents and Chemotherapy*, 2005, 49, 2834.
- (12) Sanbongi, Y.; Suzuki, T.; Osaki, Y.; Senju, N.; Ida, T.; Ubukata, K. Molecular Evolution of Beta-Lactam-Resistant *Haemophilus influenzae*: 9-Year Surveillance of Penicillin-Binding Protein 3 Mutations in Isolates from Japan. *Antimicrob Agents Chemother*, 2006, 50, 2487–2492. <https://doi.org/10.1128/AAC.01316-05>.
- (13) Skaare, D.; Lia, A.; Hannisdal, A.; Tveten, Y.; Matuschek, E.; Kahlmeter, G.; Kristiansen, B. E. *Haemophilus influenzae* with Non-Beta-Lactamase-Mediated Beta-Lactam Resistance: Easy To Find but Hard To Categorize. *J Clin Microbiol*, 2015, 53, 3589–3595. <https://doi.org/10.1128/jcm.01630-15>.
- (14) Straker, K.; Wootton, M.; Simm, A. M.; Bennett, P. M.; MacGowan, A. P.; Walsh, T. R. Cefuroxime Resistance in Non-Beta-Lactamase *Haemophilus influenzae* Is Linked to Mutations in FtsI. *J Antimicrob Chemother*, 2003, 51, 523–530.
- (15) García-Cobos, S.; Campos, J.; Lázaro, E.; Román, F.; Cercenado, E.; García-Rey, C.; Pérez-Vázquez, M.; Oteo, J.; Abajo, F. de. Ampicillin-Resistant Non- β -Lactamase-Producing *Haemophilus influenzae* in Spain: Recent Emergence of Clonal Isolates with Increased Resistance to Cefotaxime and Cefixime, 2007. <https://doi.org/10.1128/AAC.00354-07>.
- (16) Fluit, A. C.; Florijn, A.; Verhoef, J.; Milatovic, D. Susceptibility of European Beta-Lactamase-Positive and -Negative *Haemophilus influenzae* Isolates from the Periods 1997/1998 and 2002/2003. *J Antimicrob Chemother*, 2005, 56, 133–138. <https://doi.org/10.1093/jac/dki167>.
- (17) Kishii, K.; Chiba, N.; Morozumi, M.; Hamano-Hasegawa, K.; Ubukata, K.; Kurokawa, I.; Masaki, J. Diverse Mutations in the FtsI Gene in Ampicillin-Resistant *Haemophilus influenzae* Isolates from Pediatric Patients with Acute Otitis Media. *Journal of Infection and Chemotherapy*, 2010, 16, 87–93. <https://doi.org/10.1007/s10156-009-0011-6>.
- (18) Barbosa, A. R.; Giufrè, M.; Cerquetti, M.; Bajanca-Lavado, M. P. Polymorphism in FtsI Gene and β -Lactam Susceptibility in Portuguese *Haemophilus influenzae* Strains: Clonal Dissemination of β -Lactamase-Positive Isolates with Decreased Susceptibility to Amoxicillin/Clavulanic Acid. *J Antimicrob Chemother*, 2011, 66, 788–796. <https://doi.org/10.1093/jac/dkq533>.
- (19) Del Barrio-Tofiño, E.; López-Causapé, C.; Cabot, G.; Rivera, A.; Benito, N.; Segura, C.; Montero, M. M.; Sorlí, L.; Tubau, F.; Gómez-Zorrilla, S.; Tormo, N.; Durá-Navarro, R.; Viedma, E.; Resino-Foz, E.; Fernández-Martínez, M.; González-Rico, C.; Alejo-Cancho, I.; Martínez, J. A.; Labayru-Echverría, C.; Dueñas, C.; Ayestarán, I.; Zamorano, L.; Martínez-Martínez, L.; Horcajada, J. P.; Oliver, A. Genomics and Susceptibility Profiles of Extensively Drug-Resistant *Pseudomonas aeruginosa* Isolates from Spain. *Antimicrob Agents Chemother*, 2017, 61. <https://doi.org/10.1128/AAC.01589-17>.

- (20) Fedarovich, A.; Cook, E.; Tomberg, J.; Nicholas, R. A.; Davies, C. Structural Effect of the Asp345a Insertion in Penicillin-Binding Protein 2 from Penicillin-Resistant Strains of *Neisseria gonorrhoeae*. *Biochemistry* **2014**, *53* (48), 7596–7603. <https://doi.org/10.1021/bi5011317>.
- (21) Faruki, H.; Sparling, P. F. Genetics of Resistance in a Non-Beta-Lactamase-Producing Gonococcus with Relatively High-Level Penicillin Resistance. *Antimicrob. Agents Chemother.* **1986**, *30* (6), 856–860. <https://doi.org/10.1128/AAC.30.6.856>.
- (22) Tomberg, J.; Fedarovich, A.; Vincent, L. R.; Jerse, A. E.; Unemo, M.; Davies, C.; Nicholas, R. A. Alanine 501 Mutations in Penicillin-Binding Protein 2 from *Neisseria gonorrhoeae*: Structure, Mechanism, and Effects on Cephalosporin Resistance and Biological Fitness. *Biochemistry* **2017**, *56* (8), 1140–1150. <https://doi.org/10.1021/acs.biochem.6b01030>.
- (23) Whiley, D. M.; Limnios, E. A.; Ray, S.; Sloots, T. P.; Tapsall, J. W. Diversity of PenA Alterations and Subtypes in *Neisseria gonorrhoeae* Strains from Sydney, Australia, That Are Less Susceptible to Ceftriaxone[▼]. *Antimicrob Agents Chemother*, 2007, *51*, 3111–3116. <https://doi.org/10.1128/aac.00306-07>.
- (24) Whiley, D. M.; Goire, N.; Lambert, S. B.; Ray, S.; Limnios, E. A.; Nissen, M. D.; Sloots, T. P.; Tapsall, J. W. Reduced Susceptibility to Ceftriaxone in *Neisseria gonorrhoeae* Is Associated with Mutations G542S, P551S and P551L in the Gonococcal Penicillin-Binding Protein 2. *J Antimicrob Chemother*, 2010, *65*, 1615–1618. <https://doi.org/10.1093/jac/dkq187>.
- (25) Nabu, S.; Nantasenamat, C.; Owasirikul, W.; Lawung, R.; Isarankura-Na-Ayudhya, C.; Lapins, M.; Wikberg, J. E. S.; Prachayasittikul, V. Proteochemometric Model for Predicting the Inhibition of Penicillin-Binding Proteins. *Journal of Computer-Aided Molecular Design*, 2015, *29*, 127–141. <https://doi.org/10.1007/s10822-014-9809-0>.
- (26) Clark, S. T.; Sinha, U.; Zhang, Y.; Wang, P. W.; Donaldson, S. L.; Coburn, B.; Waters, V. J.; Yau, Y. C. W.; Tullis, D. E.; Guttman, D. S.; Hwang, D. M. Penicillin-Binding Protein 3 Is a Common Adaptive Target among *Pseudomonas aeruginosa* Isolates from Adult Cystic Fibrosis Patients Treated with β -Lactams. *Int. J. Antimicrob. Agents* **2019**, *53* (5), 620–628. <https://doi.org/10.1016/j.ijantimicag.2019.01.009>.
- (27) Diaz Caballero, J.; Clark, S. T.; Coburn, B.; Zhang, Y.; Wang, P. W.; Donaldson, S. L.; Tullis, D. E.; Yau, Y. C. W.; Waters, V. J.; Hwang, D. M.; Guttman, D. S. Selective Sweeps and Parallel Pathoadaptation Drive *Pseudomonas aeruginosa* Evolution in the Cystic Fibrosis Lung. *mBio* **2015**, *6* (5), e00981-15. <https://doi.org/10.1128/mBio.00981-15>.
- (28) Alm, R. A.; Johnstone, M. R.; Lahiri, S. D. Characterization of *Escherichia coli* NDM Isolates with Decreased Susceptibility to Aztreonam/Avibactam: Role of a Novel Insertion in PBP3. *J. Antimicrob. Chemother.* **2015**, *70* (5), 1420–1428. <https://doi.org/10.1093/jac/dku568>.
- (29) Zhang, Y.; Kashikar, A.; Brown, C. A.; Denys, G.; Bush, K. Unusual *Escherichia coli* PBP 3 Insertion Sequence Identified from a Collection of Carbapenem-Resistant Enterobacteriaceae Tested. *Antimicrob Agents Chemother*, 2017, *61*. <https://doi.org/10.1128/AAC.00389-17>.
- (30) Patiño-Navarrete, R.; Rosinski-Chupin, I.; Cabanel, N.; Gauthier, L.; Takissian, J.; Madec, J.-Y.; Hamze, M.; Bonnin, R. A.; Naas, T.; Glaser, P. Stepwise Evolution and Convergent Recombination Underlie the Global Dissemination of Carbapenemase-Producing *Escherichia coli*. *Genome Med.*

- 2020**, 12 (1), 10. <https://doi.org/10.1186/s13073-019-0699-6>.
- (31) Papaleo, E.; Saladino, G.; Lambrugh, M.; Lindorff-Larsen, K.; Gervasio, F. L.; Nussinov, R. The Role of Protein Loops and Linkers in Conformational Dynamics and Allostery. *Chem. Rev.* **2016**, 116 (11), 6391–6423. <https://doi.org/10.1021/acs.chemrev.5b00623>.
 - (32) Sainsbury, S.; Bird, L.; Rao, V.; Shepherd, S. M.; Stuart, D. I.; Hunter, W. N.; Owens, R. J.; Ren, J. Crystal Structures of Penicillin-Binding Protein 3 from *Pseudomonas aeruginosa*: Comparison of Native and Antibiotic-Bound Forms. *J. Mol. Biol.* **2011**, 405 (1), 173–184. <https://doi.org/10.1016/j.jmb.2010.10.024>.
 - (33) Han, S.; Zaniewski, R. P.; Marr, E. S.; Lacey, B. M.; Tomaras, A. P.; Evdokimov, A.; Miller, J. R.; Shanmugasundaram, V. Structural Basis for Effectiveness of Siderophore-Conjugated Monocarbams against Clinically Relevant Strains of *Pseudomonas aeruginosa*. *Proc. Natl. Acad. Sci.* **2010**, 107 (51), 22002–22007. <https://doi.org/10.1073/pnas.1013092107>.
 - (34) Ren, J.; Nettleship, J. E.; Males, A.; Stuart, D. I.; Owens, R. J. Crystal Structures of Penicillin-Binding Protein 3 in Complexes with Azlocillin and Cefoperazone in Both Acylated and Deacylated Forms. *FEBS Lett.* **2016**, 590 (2), 288–297. <https://doi.org/10.1002/1873-3468.12054>.
 - (35) Singh, A.; Tomberg, J.; Nicholas, R. A.; Davies, C. Recognition of the β -Lactam Carboxylate Triggers Acylation of *Neisseria gonorrhoeae* Penicillin-Binding Protein 2. *J. Biol. Chem.* **2019**, 294 (38), 14020–14032. <https://doi.org/10.1074/jbc.RA119.009942>.
 - (36) Garcia-Cobos, S.; Arroyo, M.; Campos, J.; Perez-Vazquez, M.; Aracil, B.; Cercenado, E.; Orden, B.; Lara, N.; Oteo, J. Novel Mechanisms of Resistance to Beta-Lactam Antibiotics in *Haemophilus parainfluenzae*: Beta-Lactamase-Negative Ampicillin Resistance and Inhibitor-Resistant TEM Beta-Lactamases. *J. Antimicrob. Chemother.* **2013**, 68, 1054–1059. <https://doi.org/10.1093/jac/dks525>.
 - (37) Liebschner, D.; Afonine, P. V.; Baker, M. L.; Bunkóczi, G.; Chen, V. B.; Croll, T. I.; Hintze, B.; Hung, L.-W.; Jain, S.; McCoy, A. J.; Moriarty, N. W.; Oeffner, R. D.; Poon, B. K.; Prisant, M. G.; Read, R. J.; Richardson, J. S.; Richardson, D. C.; Sammito, M. D.; Sobolev, O. V.; Stockwell, D. H.; Terwilliger, T. C.; Urzhumtsev, A. G.; Videau, L. L.; Williams, C. J.; Adams, P. D. Macromolecular Structure Determination Using X-Rays, Neutrons and Electrons: Recent Developments in *Phenix*. *Acta Crystallogr. Sect. Struct. Biol.* **2019**, 75 (10), 861–877. <https://doi.org/10.1107/S2059798319011471>.
 - (38) Forneris, F.; Burnley, B. T.; Gros, P. Ensemble Refinement Shows Conformational Flexibility in Crystal Structures of Human Complement Factor D. *Acta Crystallogr. D Biol. Crystallogr.* **2014**, 70 (Pt 3), 733–743. <https://doi.org/10.1107/S1399004713032549>.
 - (39) Burnley, B. T.; Afonine, P. V.; Adams, P. D.; Gros, P. Modelling Dynamics in Protein Crystal Structures by Ensemble Refinement. *eLife* **2012**, 1, e00311. <https://doi.org/10.7554/eLife.00311>.
 - (40) Michaud-Agrawal, N.; Denning, E. J.; Woolf, T. B.; Beckstein, O. MDAnalysis: A Toolkit for the Analysis of Molecular Dynamics Simulations. *J. Comput. Chem.* **2011**, 32 (10), 2319–2327. <https://doi.org/10.1002/jcc.21787>.
 - (41) Gowers, R.; Linke, M.; Barnoud, J.; Reddy, T.; Melo, M.; Seyler, S.; Domański, J.; Dotson, D.; Buchoux, S.; Kenney, I.; Beckstein, O. MDAnalysis: A Python Package for the Rapid Analysis of Molecular Dynamics Simulations; Austin, Texas, 2016; pp 98–105.

- <https://doi.org/10.25080/Majora-629e541a-00e>.
- (42) Theobald, D. L. Rapid Calculation of RMSDs Using a Quaternion-Based Characteristic Polynomial. *Acta Crystallogr. A* **2005**, *61* (4), 478–480. <https://doi.org/10.1107/S0108767305015266>.
 - (43) Liu, P.; Agrafiotis, D. K.; Theobald, D. L. Fast Determination of the Optimal Rotational Matrix for Macromolecular Superpositions. *J. Comput. Chem.* **2010**, *31* (7), 1561–1563. <https://doi.org/10.1002/jcc.21439>.
 - (44) Hrabe, T.; Li, Z.; Sedova, M.; Rotkiewicz, P.; Jaroszewski, L.; Godzik, A. PDBFlex: Exploring Flexibility in Protein Structures. *Nucleic Acids Res.* **2016**, *44* (D1), D423–D428. <https://doi.org/10.1093/nar/gkv1316>.
 - (45) Newman, H.; Krajnc, A.; Bellini, D.; Eyermann, C. J.; Boyle, G. A.; Paterson, N. G.; McAuley, K.; Lesniak, R.; Gangar, M.; von Delft, F.; Brem, J.; Chibale, K.; Schofield, C. J.; Dowson, C. G. High-Throughput Crystallography Reveals Boron Containing Inhibitors of a Penicillin Binding Protein with Di- and Tri-Covalent Binding Modes. *J. Med. Chem.* *Accepted*.
 - (46) Blow, D. M. *Outline of Crystallography for Biologists*; Oxford University Press: Oxford ; New York, 2002.
 - (47) Sun, Z.; Liu, Q.; Qu, G.; Feng, Y.; Reetz, M. T. Utility of B-Factors in Protein Science: Interpreting Rigidity, Flexibility, and Internal Motion and Engineering Thermostability. *Chem. Rev.* **2019**, *119* (3), 1626–1665. <https://doi.org/10.1021/acs.chemrev.8b00290>.
 - (48) Pares, S.; Mouz, N.; Pétillet, Y.; Hakenbeck, R.; Dideberg, O. X-Ray Structure of *Streptococcus pneumoniae* PBP2x, a Primary Penicillin Target Enzyme. *Nat. Struct. Biol.* **1996**, *3* (3), 284–289. <https://doi.org/10.1038/nsb0396-284>.
 - (49) Fisette, O.; Morin, S.; Savard, P.-Y.; Lagüe, P.; Gagné, S. M. TEM-1 Backbone Dynamics—Insights from Combined Molecular Dynamics and Nuclear Magnetic Resonance. *Biophys. J.* **2010**, *98* (4), 637–645. <https://doi.org/10.1016/j.bpj.2009.08.061>.
 - (50) Richard, J. P. Protein Flexibility and Stiffness Enable Efficient Enzymatic Catalysis. *J. Am. Chem. Soc.* **2019**, *141* (8), 3320–3331. <https://doi.org/10.1021/jacs.8b10836>.
 - (51) Kamal, Md. Z.; Mohammad, T. A. S.; Krishnamoorthy, G.; Rao, N. M. Role of Active Site Rigidity in Activity: MD Simulation and Fluorescence Study on a Lipase Mutant. *PLoS ONE* **2012**, *7* (4), e35188. <https://doi.org/10.1371/journal.pone.0035188>.
 - (52) Bahar, I.; Lezon, T. R.; Yang, L.-W.; Eyal, E. Global Dynamics of Proteins: Bridging Between Structure and Function. *Annu. Rev. Biophys.* **2010**, *39* (1), 23–42. <https://doi.org/10.1146/annurev.biophys.093008.131258>.
 - (53) Kurkcuoglu, Z.; Bakan, A.; Kocaman, D.; Bahar, I.; Doruker, P. Coupling between Catalytic Loop Motions and Enzyme Global Dynamics. *PLOS Comput. Biol.* **2012**, *8* (9), e1002705. <https://doi.org/10.1371/journal.pcbi.1002705>.
 - (54) Vuillon, L.; Lesieur, C. From Local to Global Changes in Proteins: A Network View. *Curr. Opin. Struct. Biol.* **2015**, *31*, 1–8. <https://doi.org/10.1016/j.sbi.2015.02.015>.
 - (55) Winn, M. D.; Ballard, C. C.; Cowtan, K. D.; Dodson, E. J.; Emsley, P.; Evans, P. R.; Keegan, R. M.; Krissinel, E. B.; Leslie, A. G. W.; McCoy, A.; McNicholas, S. J.; Murshudov, G. N.; Pannu, N. S.; Potterton, E. A.; Powell, H. R.; Read, R. J.; Vagin, A.; Wilson, K. S. Overview of the CCP 4 Suite and Current Developments. *Acta Crystallogr. D Biol. Crystallogr.* **2011**, *67* (4), 235–242. <https://doi.org/10.1107/S0907444910045749>.

- (56) Horn, J. R.; Shoichet, B. K. Allosteric Inhibition Through Core Disruption. *J. Mol. Biol.* **2004**, *336* (5), 1283–1291. <https://doi.org/10.1016/j.jmb.2003.12.068>.
- (57) Kuzin, A. P.; Nukaga, M.; Nukaga, Y.; Hujer, A. M.; Bonomo, R. A.; Knox, J. R. Structure of the SHV-1 β -Lactamase. *Biochemistry* **1999**, *38* (18), 5720–5727. <https://doi.org/10.1021/bi990136d>.
- (58) Benkovic, S. J. A Perspective on Enzyme Catalysis. *Science* **2003**, *301* (5637), 1196–1202. <https://doi.org/10.1126/science.1085515>.
- (59) Agarwal, P. K.; Billeter, S. R.; Rajagopalan, P. T. R.; Benkovic, S. J.; Hammes-Schiffer, S. Network of Coupled Promoting Motions in Enzyme Catalysis. *Proc. Natl. Acad. Sci.* **2002**, *99* (5), 2794–2799. <https://doi.org/10.1073/pnas.052005999>.
- (60) Bhabha, G.; Lee, J.; Ekiert, D. C.; Gam, J.; Wilson, I. A.; Dyson, H. J.; Benkovic, S. J.; Wright, P. E. A Dynamic Knockout Reveals That Conformational Fluctuations Influence the Chemical Step of Enzyme Catalysis. *Science* **2011**, *332* (6026), 234–238. <https://doi.org/10.1126/science.1198542>.
- (61) Gagné, D.; French, R. L.; Narayanan, C.; Simonović, M.; Agarwal, P. K.; Doucet, N. Perturbation of the Conformational Dynamics of an Active-Site Loop Alters Enzyme Activity. *Structure* **2015**, *23* (12), 2256–2266. <https://doi.org/10.1016/j.str.2015.10.011>.
- (62) Nave, C.; Garman, E. F. Towards an Understanding of Radiation Damage in Cryocooled Macromolecular Crystals. *J. Synchrotron Radiat.* **2005**, *12* (3), 257–260. <https://doi.org/10.1107/S0909049505007132>.
- (63) Keedy, D. A.; van den Bedem, H.; Sivak, D. A.; Petsko, G. A.; Ringe, D.; Wilson, M. A.; Fraser, J. S. Crystal Cryocooling Distorts Conformational Heterogeneity in a Model Michaelis Complex of DHFR. *Struct. Lond. Engl.* **1993** **2014**, *22* (6), 899–910. <https://doi.org/10.1016/j.str.2014.04.016>.
- (64) Weik, M.; Colletier, J.-P. Temperature-Dependent Macromolecular X-Ray Crystallography. *Acta Crystallogr. D Biol. Crystallogr.* **2010**, *66* (4), 437–446. <https://doi.org/10.1107/S0907444910002702>.
- (65) VMXi - - Diamond Light Source <https://www.diamond.ac.uk/Instruments/Mx/VMXi.html>. Accessed 15/05/20.
- (66) Tenboer, J.; Basu, S.; Zatsepin, N.; Pande, K.; Milathianaki, D.; Frank, M.; Hunter, M.; Boutet, S.; Williams, G. J.; Koglin, J. E.; Oberthuer, D.; Heymann, M.; Kupitz, C.; Conrad, C.; Coe, J.; Roy-Chowdhury, S.; Weierstall, U.; James, D.; Wang, D.; Grant, T.; Barty, A.; Yefanov, O.; Scales, J.; Gati, C.; Seuring, C.; Srajer, V.; Henning, R.; Schwander, P.; Fromme, R.; Ourmazd, A.; Moffat, K.; Van Thor, J. J.; Spence, J. C. H.; Fromme, P.; Chapman, H. N.; Schmidt, M. Time-Resolved Serial Crystallography Captures High-Resolution Intermediates of Photoactive Yellow Protein. *Science* **2014**, *346* (6214), 1242–1246. <https://doi.org/10.1126/science.1259357>.
- (67) Carapito, R.; Chesnel, L.; Vernet, T.; Zapun, A. Pneumococcal β -Lactam Resistance Due to a Conformational Change in Penicillin-Binding Protein 2x. *J. Biol. Chem.* **2006**, *281* (3), 1771–1777. <https://doi.org/10.1074/jbc.M511506200>.
- (68) Sapienza, P. J.; Lee, A. L. Using NMR to Study Fast Dynamics in Proteins: Methods and Applications. *Curr. Opin. Pharmacol.* **2010**, *10* (6), 723–730. <https://doi.org/10.1016/j.coph.2010.09.006>.
- (69) Chao, F.-A.; Byrd, R. A. Protein Dynamics Revealed by NMR Relaxation Methods. *Emerg. Top. Life Sci.* **2018**, *2* (1), 93–105.

<https://doi.org/10.1042/ETLS20170139>.

- (70) Rydzik, A. M.; Brem, J.; van Berkel, S. S.; Pfeffer, I.; Makena, A.; Claridge, T. D. W.; Schofield, C. J. Monitoring Conformational Changes in the NDM-1 Metallo- β -Lactamase by ^{19}F NMR Spectroscopy. *Angew. Chem. Int. Ed.* **2014**, *53* (12), 3129–3133. <https://doi.org/10.1002/anie.201310866>.
- (71) Abboud, M. I.; Hinchliffe, P.; Brem, J.; Macsics, R.; Pfeffer, I.; Makena, A.; Umland, K.-D.; Rydzik, A. M.; Li, G.-B.; Spencer, J.; Claridge, T. D. W.; Schofield, C. J. ^{19}F -NMR Reveals the Role of Mobile Loops in Product and Inhibitor Binding by the São Paulo Metallo- β -Lactamase. *Angew. Chem. Int. Ed.* **2017**, *56* (14), 3862–3866. <https://doi.org/10.1002/anie.201612185>.
- (72) Karplus, M.; McCammon, J. A. Molecular Dynamics Simulations of Biomolecules. *Nat. Struct. Biol.* **2002**, *9* (9), 646–652. <https://doi.org/10.1038/nsb0902-646>.
- (73) Boehr, D. D.; Dyson, H. J.; Wright, P. E. An NMR Perspective on Enzyme Dynamics. *Chem. Rev.* **2006**, *106* (8), 3055–3079. <https://doi.org/10.1021/cr050312q>.
- (74) Feher, V. A.; Cavanagh, J. Millisecond-Timescale Motions Contribute to the Function of the Bacterial Response Regulator Protein Spo0F. *Nature* **1999**, *400* (6741), 289–293. <https://doi.org/10.1038/22357>.
- (75) Henzler-Wildman, K. A.; Lei, M.; Thai, V.; Kerns, S. J.; Karplus, M.; Kern, D. A Hierarchy of Timescales in Protein Dynamics Is Linked to Enzyme Catalysis. *Nature* **2007**, *450* (7171), 913–916. <https://doi.org/10.1038/nature06407>.
- (76) Ge, Y.; Wu, J.; Xia, Y.; Yang, M.; Xiao, J.; Yu, J. Molecular Dynamics Simulation of the Complex PBP-2x with Drug Cefuroxime to Explore the Drug Resistance Mechanism of *Streptococcus suis* R61. *PLOS ONE* **2012**, *7* (4), e35941. <https://doi.org/10.1371/journal.pone.0035941>.
- (77) Wang, F.; Zhou, H.; Wang, X.; Tao, P. Dynamical Behavior of β -Lactamases and Penicillin- Binding Proteins in Different Functional States and Its Potential Role in Evolution. *Entropy* **2019**, *21* (11), 1130. <https://doi.org/10.3390/e21111130>.
- (78) Gobeil, S. M. C.; Ebert, M. C. C. J. C.; Park, J.; Gagné, D.; Doucet, N.; Berghuis, A. M.; Pleiss, J.; Pelletier, J. N. The Structural Dynamics of Engineered β -Lactamases Vary Broadly on Three Timescales yet Sustain Native Function. *Sci. Rep.* **2019**, *9* (1), 6656. <https://doi.org/10.1038/s41598-019-42866-8>.
- (79) Galdadas, I.; Qu, S.; Oliveira, A. S. F.; Olehnovics, E.; Mack, A. R.; Mojica, M. F.; Agarwal, P. K.; Tooke, C. L.; Gervasio, F. L.; Spencer, J.; Bonomo, R. A.; Mulholland, A. J.; Haider, S. Allosteric Communication in Class A β -Lactamases Occurs via Cooperative Coupling of Loop Dynamics. *eLife* **2021**, *10*, e66567. <https://doi.org/10.7554/eLife.66567>.
- (80) Clouthier, C. M.; Morin, S.; Gobeil, S. M. C.; Doucet, N.; Blanchet, J.; Nguyen, E.; Gagné, S. M.; Pelletier, J. N. Chimeric β -Lactamases: Global Conservation of Parental Function and Fast Time-Scale Dynamics with Increased Slow Motions. *PLOS ONE* **2012**, *7* (12), e52283. <https://doi.org/10.1371/journal.pone.0052283>.
- (81) Watney, J. B.; Agarwal, P. K.; Hammes-Schiffer, S. Effect of Mutation on Enzyme Motion in Dihydrofolate Reductase. *J. Am. Chem. Soc.* **2003**, *125* (13), 3745–3750. <https://doi.org/10.1021/ja028487u>.
- (82) Goldstein, M.; Goodey, N. M. Distal Regions Regulate Dihydrofolate Reductase-Ligand Interactions. In *Allostery*; Di Paola, L., Giuliani, A., Eds.; Methods in Molecular Biology; Springer US: New York, NY, 2021; Vol. 2253,

- pp 185–219. https://doi.org/10.1007/978-1-0716-1154-8_12.
- (83) van Berkel, S. S.; Nettleship, J. E.; Leung, I. K. H.; Brem, J.; Choi, H.; Stuart, D. I.; Claridge, T. D. W.; McDonough, M. A.; Owens, R. J.; Ren, J.; Schofield, C. J. Binding of (5 S)-Penicilloic Acid to Penicillin Binding Protein 3. *ACS Chem. Biol.* **2013**, *8* (10), 2112–2116. <https://doi.org/10.1021/cb400200h>.

Chapter 4.S. Supplementary Information for Chapter 4

4.S1 Additional Crystallographic Views and Data

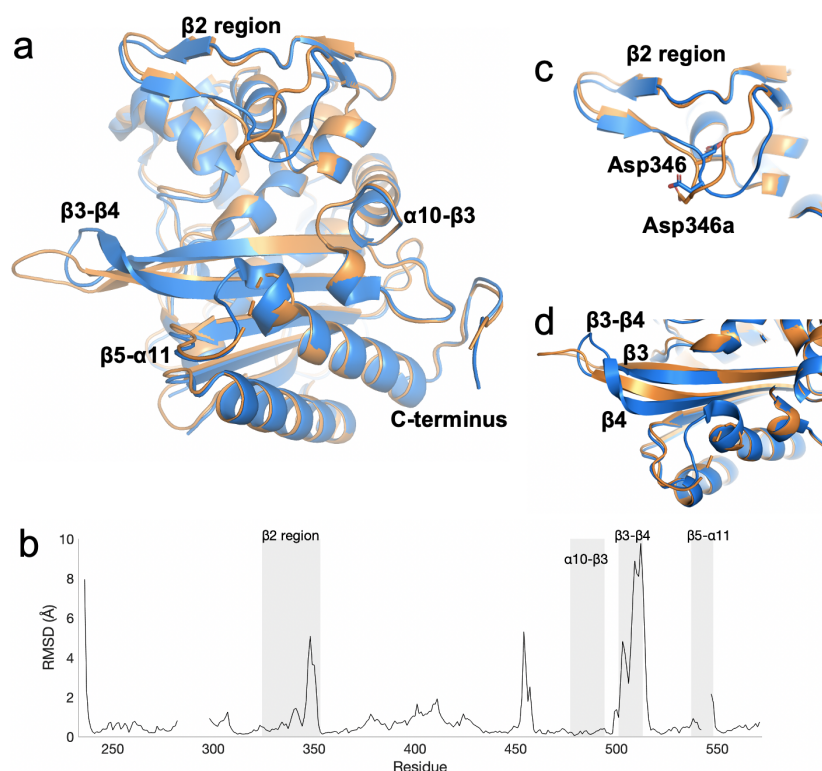


Figure 4.S1. Comparisons between two structures of the transpeptidase domain of NgPBP2 from strain FA6140. The two structures NgTP2^{HR-6140} and NgTP2^{I3-6140} (PDB: 6HZJ ¹ (blue) and 4U3T ² (orange)) are of the same protein but have different resolutions (1.4 vs 2.2 Å respectively) and different crystallisation conditions. All data here are comparisons of subunit A in both structures. (b) Root-mean-square deviation (RMSD) between the backbone atoms of each residue of the two structures. Large deviations between the structures are observed in the later part of the $\beta 2$ region (c) and at the $\beta 3$ - $\beta 4$ loop (d), as well as in the $\alpha 9$ - $\alpha 10$ loop (residues 451-461) on the “rear” of the protein (Figure 4.3). Part of the $\beta 4$ - $\alpha 11$ loop was not fully resolved in NgTP2^{I3-6140} subunit A so these four residues (residues 542-545) were omitted from the analysis. (c) The $\beta 2$ region, with residues Asp346 and Asp346a (sometimes denoted as Asp345a and Asp346 respectively ²) shown in stick representation. The latter part of the region (residues 345-354) has the greatest conformational deviation. (d) The $\beta 3$ - $\beta 4$ loops of the proteins adopt different conformations.

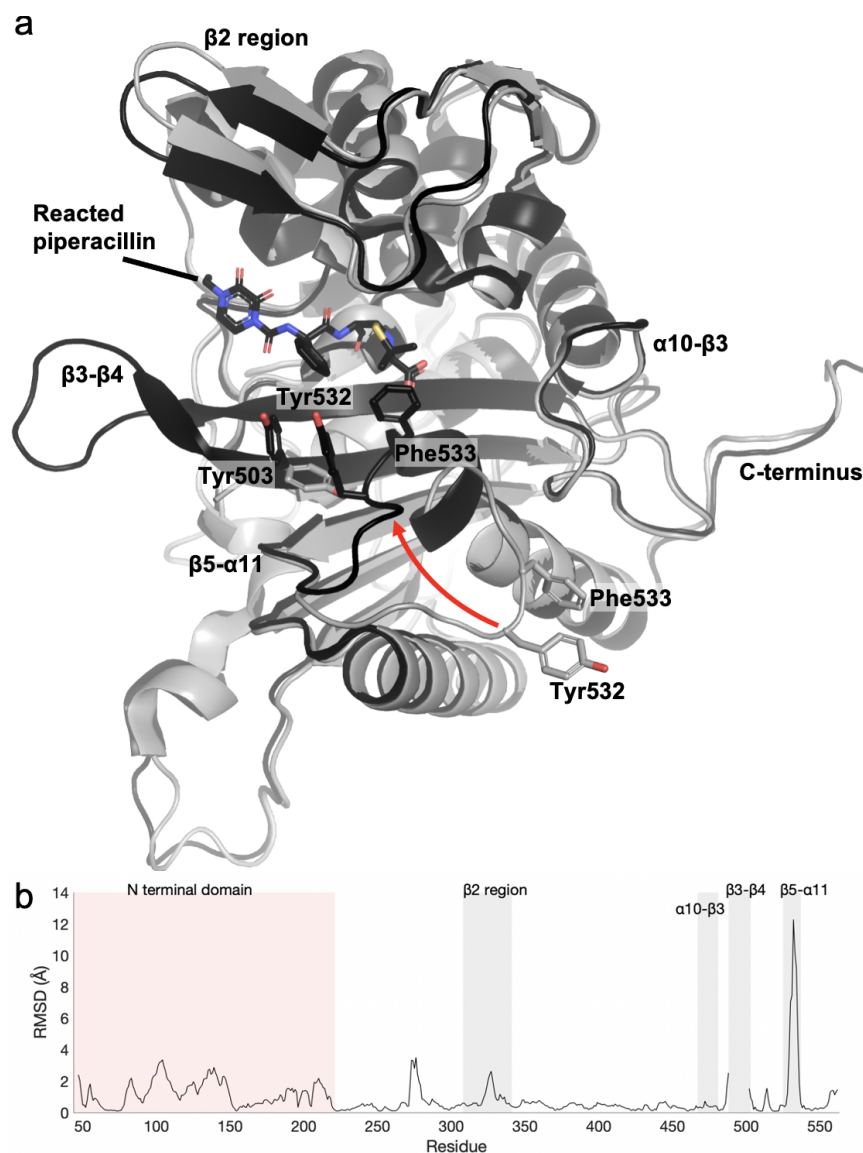


Figure 4.S2. Comparison of *apo* and piperacillin reacted PaBPB3 crystal structures. *Apo* PaBPB3 (PDB: 6HZR¹, white) and piperacillin reacted PaBPB3 (PDB: 6R3X¹, black) show different conformations, particularly at the $\beta 5$ - $\alpha 11$ (residues 488-503) and $\beta 3$ - $\beta 4$ (residues 525-537) loops. The $\beta 5$ - $\alpha 11$ loop transitions from the open conformation in the *apo* model to the closed formation in the piperacillin reacted model (indicated by a red arrow). Residues Tyr503, Tyr532 and Phe533 are shown in sticks and labelled. They form a hydrophobic wall against the phenyl group of reacted piperacillin in the closed conformation. The $\beta 3$ - $\beta 4$ loop is unresolved in the *apo* structure, but resolved in the piperacillin reacted model, which may indicate a decrease in conformational flexibility upon β -lactam binding. (b) The RMSD between the two structures, plotted for each residue. The N terminal domain is highlighted in pink and the 4 loop regions are labelled. The $\beta 5$ - $\alpha 11$ loop is the region of greatest difference between the two structures.

Residue ^a	B factor in PaPBP3 (Å ²) ^b	RMSD in PaPBP3 by ER (Å) ^b	RMSD in PaPBP3 <i>PDBflex</i> (Å) ^c	B factor in NgPBP2 subunit A (Å ²) ^d	B factor in NgPBP2 subunit B by ER (Å ²) ^d	RMSD in NgPBP2 subunit A by ER (Å) ^d	RMSD in NgPBP2 subunit B by ER (Å) ^d
SXXK	6.75	0.0380	0.0288	11.99	11.37	0.1221	0.0969
SXX K	6.82	0.0396	0.0156	10.05	9.99	0.0931	0.0767
SXN	8.62	0.0591	0.0162	10.07	11.17	0.0999	0.1127
K(S/T)G	8.26	0.0833	0.1442	10.53	11.43	0.1216	0.1343
Median Value ^e	10.86	0.0985	0.04	13.31	13.85	0.1717	0.1788

Table 4.S1. Local flexibility of active site residues. Values are means of the value for the residue given in bold and the adjacent 2 residues either side of the residue in bold.^a For PaPBP3 the residues are (top to bottom): Ser294 (**SXXK**), Lys297 (SXX**K**), Ser349 (**SXN**) and Lys 484 (**KSG**), for NgPBP2 they are: Ser310 (**SXXK**), Lys310 (SXX**K**), Ser362 (**SXN**), Lys 497 (**KTG**). ^b see Figure 4.1a ^c see Figure 4.1c ^d see Figure 4.1d. ^eMedian value for the structure/subunit.

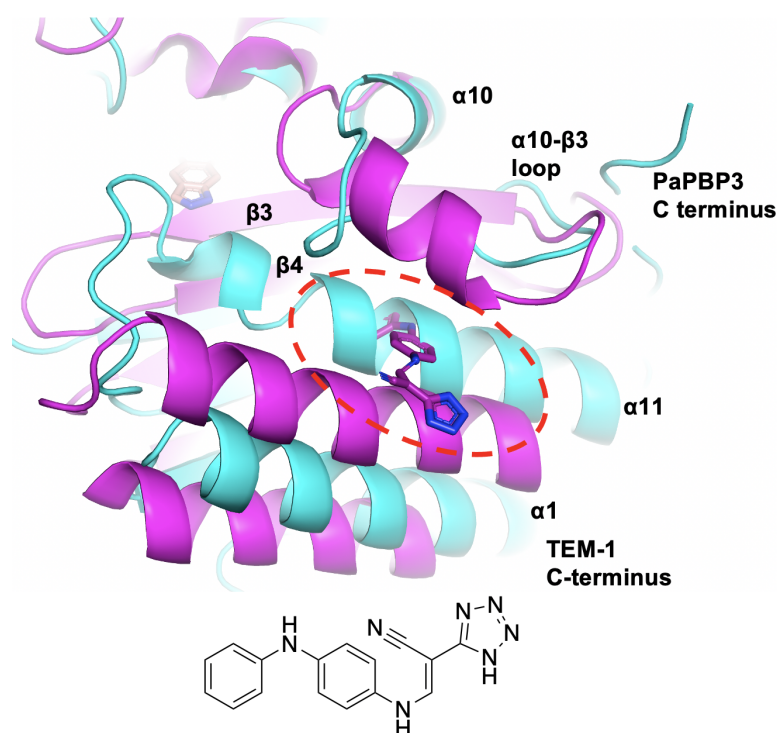


Figure 4.S3. TEM-1 was found to have a cryptic allosteric site between the $\alpha 11$ helix and the $\alpha 10$ - $\beta 3$ loop. The crystal structure of TEM-1 bound to the tetrazole-containing compound shown (pink, PDB: 1PZP³), reveals two binding sites for the compound. One of these is between the $\alpha 10$ - $\beta 3$ loop and the $\alpha 11$ helix. TEM-1 and PBP3 are both members of the penicilloyl-serine transferase superfamily and share the same structural fold, the structure of TEM-1 is compared to the crystal structure of PaPBP3:2 (cyan), with the secondary structure of PaPBP3 labelled. The cryptic allosteric binding site of the tetrazole-containing compound is shown by the red dashed line. If the $\alpha 10$ - $\beta 3$ loop is sufficiently flexible, it may be possible to find similar allosteric inhibitors of PBP3.

4.S2 References

- (1) Bellini, D.; Koekemoer, L.; Newman, H.; Dowson, C. G. Novel and Improved Crystal Structures of *H. influenzae*, *E. coli* and *P. aeruginosa* Penicillin-Binding Protein 3 (PBP3) and *N. gonorrhoeae* PBP2: Toward a Better Understanding of β -Lactam Target-Mediated Resistance. *J. Mol. Biol.* **2019**, *431* (18), 3501–3519. <https://doi.org/10.1016/j.jmb.2019.07.010>.
- (2) Fedarovich, A.; Cook, E.; Tomberg, J.; Nicholas, R. A.; Davies, C. Structural Effect of the Asp345a Insertion in Penicillin-Binding Protein 2 from Penicillin-Resistant Strains of *Neisseria gonorrhoeae*. *Biochemistry* **2014**, *53* (48), 7596–7603. <https://doi.org/10.1021/bi5011317>.
- (3) Horn, J. R.; Shoichet, B. K. Allosteric Inhibition Through Core Disruption. *J. Mol. Biol.* **2004**, *336* (5), 1283–1291. <https://doi.org/10.1016/j.jmb.2003.12.068>.

Chapter 5. Boron-based Inhibitors of PBP3: Benzoxaboroles with Novel Binding Modes

Chapter 5.S (p219-234) contains additional information referred to in this chapter

5.1 Introduction

Currently, the most effective way to combat AMR is to discover compounds with novel modes of action or with novel chemistry for old targets. Previous attempts to target PBPs with novel chemistry are summarised in Section 1.4.5. One of the groups of compounds described therein (Table 1.1) are the boronates.

In the early 2000's, the first boron-containing compound, bortezomib, was approved for use against multiple myeloma ^{1,2} (Table 5.1A), affirming observations since the 1970's that boronates could be used to bind and inhibit serine (and threonine) proteases ^{3,4}. Vaborbactam (approved)⁵⁻⁷ and bicyclic boronate taniborbactam (in clinical trials) ⁸⁻¹⁰ demonstrate that boronates can be clinically useful against penicilloyl serine transferase family proteins (both of these examples are β -lactamase inhibitors). However there are no compounds in academic literature which can act with the same high affinity against high molecular mass HMM PBPs, although other investigations have been reported ¹¹⁻²². Boronate PBP inhibitors would be insensitive to β -lactamase hydrolysis which is a highly desirable property.

Boronates inhibit serine- (and metallo-) β -lactamases by mimicking the transition states in penicillin catalysis ^{11,23}, which themselves are analogous to the transition states passed through during the natural substrate turnover of PBPs (Figure 5.1). On the catalytic pathway of both β -lactam hydrolysis and transpeptidation, the central carbonyl carbon transitions (twice) from sp^2 to sp^3 then back to sp^2 hybridisation (Figure 5.1). Boron can similarly transition between a neutral sp^2 hybridisation state and an anionic sp^3 hybridisation state, and it is this 'morphing' property in particular that makes it successful at inhibiting β -lactamases ²³.

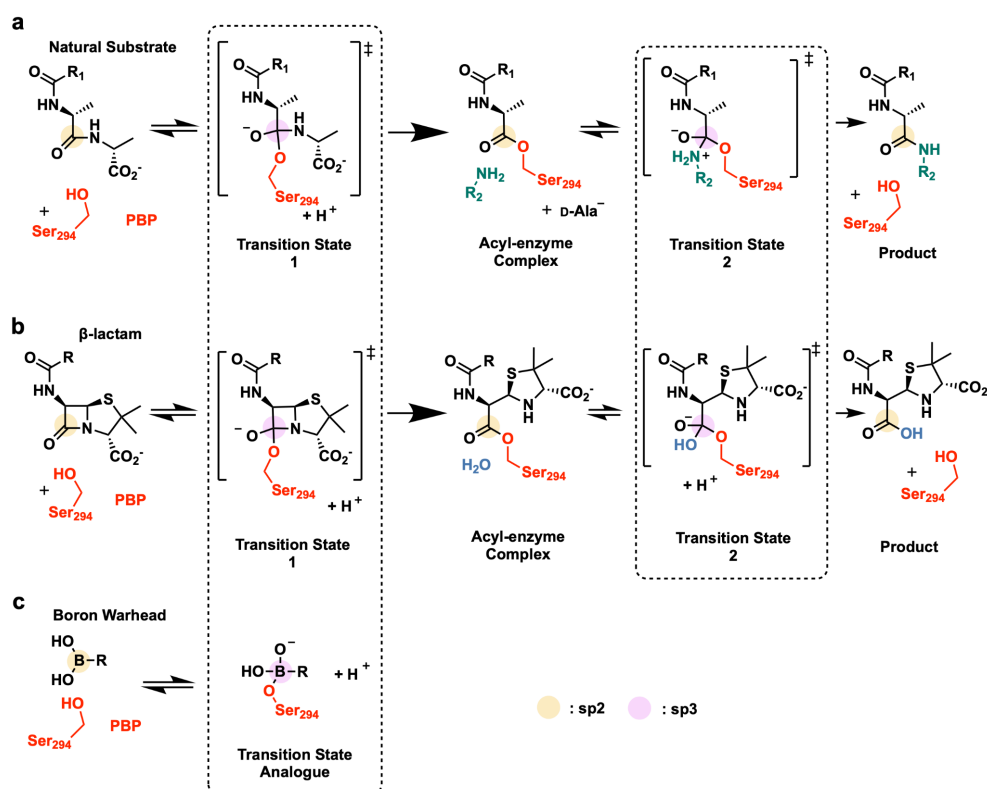


Figure 5.1. Boron mimicry of transition states on the transpeptidation and penicillin catalysis pathways of PBPs. General mechanism of (a) transpeptidation by class B PBPs and (b) the reaction of a β -Lactam with a PBP, exemplified with penicillin. This reaction is described in Figure 1.2. (c) Boron transitions between sp^2 and sp^3 hybridisation states and is able to mimic the tetrahedral transition states and inhibit the PBP. Hybridisation states of the central carbonyl carbon (or boron) of each species is shown with a coloured circle; yellow: sp^2 , pink: sp^3 .

Crystal structures of boronates with various proteins (including PBPs and β -lactamases) have shown the boron atom can form high valency complexes: with the hydroxyls of the ribose sugars of the 3'-adenosine monophosphoryl moiety of tRNA (Table 5.1B), with the active site residues of R39 DD-peptidase (Table 5.1C) and with nucleophilic serine and histidine residues in trypsin (Table 5.1D and E).

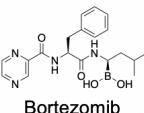
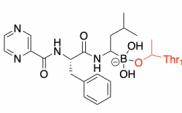
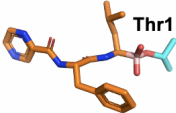
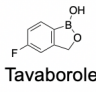
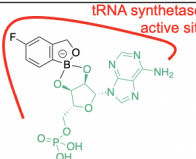
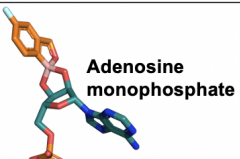
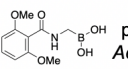
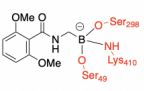
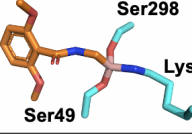
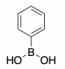
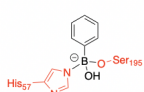
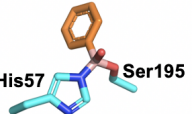
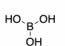
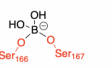
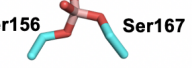
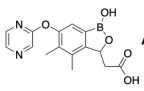
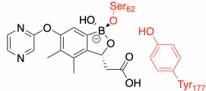

Ligand	Protein	Binding Mode	Ligand Interaction	Crystal Structure	Reference
 Bortezomib	Yeast 20S proteasome	Mono-covalent		 Thr1	A
 Tavaborole	Leucyl-tRNA synthetase from <i>Thermus thermophilus</i>	Di-covalent to vicinal hydroxyls of the 3' adenosine phosphoryl moiety of tRNA	 tRNA synthetase active site	 Adenosine monophosphate	B
	R39 – DD peptidase from <i>Actinomadura sp.</i>	Tri-covalent (mono-covalent also observed)		 Ser298 Lys410 Ser49	C
	Porcine pancreatic trypsin	Di-covalent		 His57 Ser195	D
	Porcine pancreatic trypsin	Di-covalent		 Ser156 Ser167	E
	AmpC from <i>P. aeruginosa</i>	Mono-covalent		 Ser62 Tyr177	F

Table 5.1. Crystallography shows boronates can form a number of interesting and high valency complexes. (A) The first approved boron-containing drug was bortezomib, a peptido-mimetic proteasome inhibitor. It reacts with a nucleophilic threonine to reversibly inhibit the proteasome of cancer cells^{11,23}. This example is from a yeast homolog of the human proteasome (PDB: 2F16)²⁴. (B) Tavaborole (a benzoxaborole) is an approved topical antifungal agent²⁵. It engages the vicinal hydroxyls of the ribose moiety of the 3' adenosine of tRNA^{Leu} within the leucyl-tRNA synthetase editing site (PDB: 2VOG²⁶). (C) The first reported example of tri-covalent binding of a boronate¹⁶. This alkyl boronate can engage 3 residues of the active site of R39 (a LMM PBP) of *Actinomadura sp.* The residues shown are from the **SXXK**, **SXN** and **K(S/T)G** conserved motifs, like the examples shown in this chapter (PDB: 3ZVT)¹⁶. (D) and (E) examples of boronates reacting with trypsin²⁷. Trypsin crystal structures indicate fragments can bind at multiple sites within the protein (some sites have a lower occupancy) (PDB: 2A32 and 2A31, respectively)²⁷. A di-covalent His/Ser complex was also observed with a boronate in a chymotrypsin crystal structure²⁸. In (D) only one of the two refined alternate conformations of benzene boronic acid is shown. In the other conformation, the positions of the phenyl and hydroxyl groups are switched. (F) The benzoxaborole warhead has previously been studied for its use as a β -lactamase inhibitor. In AmpC, the residue equivalent to Ser349 of PaBPB3 is replaced by a tyrosine (Tyr177). Perhaps as a result, di-covalency is not observed, and the catalytic serine (Ser62, equivalent to Ser294) attacks the benzoxaborole from the other face compared to the direction of attack in PaBPB3 (Figure 5.S1).

The chemistry of boronates makes them particularly able to engage nucleophilic serines, with selectivity over cysteine nucleophiles ²⁹. An NMR study of the reactivity of cysteine and serine residues in solution found that the benzoxaborole pharmacophore was the most reactive warhead tested towards serine, but had low reactivity against cysteine ²⁹.

The high valency reversible covalent attachment, serine selectivity and “morphing” properties of boron are all highly desirable for a warhead designed to engage PBPs. As antimicrobials, boronates (against other targets) have precedent in gram-negative bacteria ^{30,31}, gram-positive bacteria ^{32,33} and *Mycobacterium tuberculosis* ³⁴.

A previous attempt by our group to use the XChem fragment screening capabilities available at Diamond (section 1.3.3) to screen PaPBP3 with a library of 1,300 diverse fragments returned only one hit (Table 1.1), which is a far lower hit rate than anticipated for this technique ³⁵. The fact that the sole hit covalently bonded to the protein seemed remarkable so we decided to re-screen the protein with a library of known serine-enzyme covalent warheads, further enriched with boron-containing compounds.

5.2 Methods

5.2.1 Proteins and Crystallography

Proteins were expressed, purified and crystallised by D. Bellini, who was also responsible for collecting the crystallographic data. Protocols as previously published³⁶ were followed, further details are described in ³⁷.

All collected crystallographic data were processed using the automated pipeline at Diamond Light Source with data reduction by XDS (Version Nov. 11, 2017) and data scaling by AIMLESS (Version 0.6.3). Processing was carried out by either autoPROC or STARANISO ³⁸. STARANISO was used when there was significant anisotropy of the data, (all PaPBP3 complexes except PaPBP3:**8** and PaPBP3:**16**). PaPBP3:**8** and PaPBP3:**16**, were isotropic and processed with autoPROC.³⁹ Structures were phased with molecular replacement by *Phaser_MR* ⁴⁰ using a high

resolution structure of PaPBP3 (PDB: 6HZR³⁶) as the search model. Manual building and ligand fitting were performed with COOT.⁴¹ Refinement was carried primarily using REFMAC5⁴² within the CCP4 suite⁴³ as well as in phenix.refine.⁴⁴ Ligand constraints were generated by the grade webserver⁴⁵. Structures were validated with MolProbity.⁴⁶ Figures of structures were prepared using PyMOL (The PyMOL Molecular Graphics System, Schrödinger, LLC) or CCP4mg.⁴⁷ Composite OMIT maps that are shown they were calculated by 'comit' in the ccp4 suite.⁴³

The structures are published in the PDB under the following IDs; PaPBP3 in complex with: **1**, 7ATM; **2**, 7ATO; **3**, 7ATW; **4**, 7ATX; **8**, 7AU0; **13**, 7AU1; **14**, 7AU8; **15**, 7AU9; **16**, 7AUB; **Vaborbactam**, 7AUH. Note that there are fewer compounds in the published paper for these entries³⁷, so the compound numbers in the PDB entries do not correlate to those in this thesis.

Docking protocols (performed by J. Eyermann) are given in 5.S4.

5.2.2 BOCILLIN FL Assays

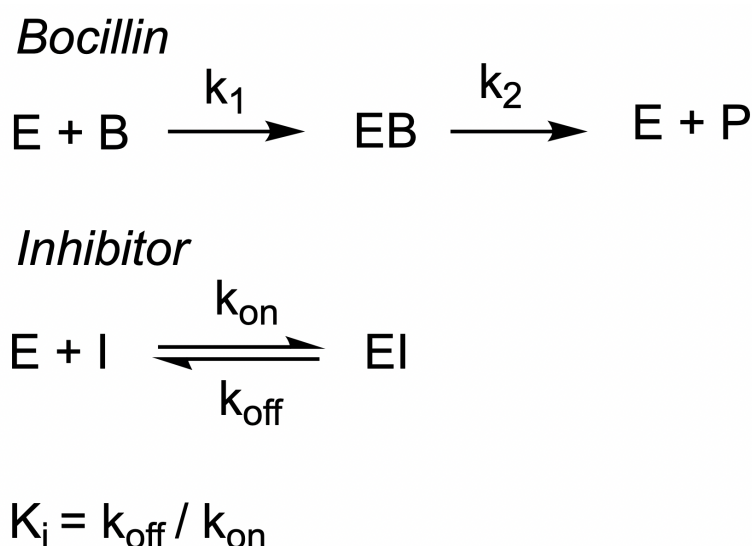
Unless otherwise stated, assays were run in triplicate, using 60 nM purified protein, 30 nM BOCILLIN FL in pH 7, 100 mM sodium phosphate buffer, with 0.01 % Triton X-100 to reduce promiscuous ligand binding¹². Assays were in a volume of 50 μ L, in black, flat bottom, 384 well microplates (Greiner Bio-One) at 30 °C. The change in fluorescence anisotropy (r) was measured using a ClarioStar plate reader (BMG Labtech) with polarised filters at excitation: 482 ± 16 nm, emission: 530 ± 4 nm and calculated using MARS software v3.32 (BMG Labtech) using the equation:

$$r = \frac{I_{\text{parallel}} - I_{\text{perpendicular}}}{I_{\text{parallel}} + 2 \cdot I_{\text{perpendicular}}}$$

where I_{parallel} and $I_{\text{perpendicular}}$ are the fluorescence intensity parallel and perpendicular to the excitation plane respectively (Section 1.4.6 and Figure 1.5).

Residual activities were found by pre-incubating the test compound and protein with 1024 μ M test compound for 1 hour at 30 °C, before the reaction was initiated by the addition of BOCILLIN FL. The change in fluorescence anisotropy after 30 minutes was compared to the uninhibited control to determine the residual activity.

In order to calculate K_i , the compound and BOCILLIN FL were mixed and the reaction was initiated by the addition of the PBP. Also included in the experiment were progress curves of nine concentrations of PBP (40–110 nM). Progress curves were analysed with Global Kintek Explorer 8.0 (KinTek, USA), as described^{48,49}. Reported errors represent the standard error of the fit of the data to the model, produced by the software. The reaction between the PBP and BOCILLIN FL (Scheme 5.1) is simplified to a one-step model, with rate constant k_1 ⁴⁸. However, unlike the previous studies, we found it was necessary to include a term (k_2) to account for the de-acylation of BOCILLIN FL from the PBP, which releases a hydrolysed product (P) (Scheme 5.1). The fluorescence intensity was constant throughout the reaction. Inhibitor binding was modelled as a reversible reaction to form the enzyme-inhibitor complex (EI) (Scheme 5.1). K_i was calculated as the ratio of the off-rate k_{off} to the on-rate k_{on} (Scheme 5.1).



Scheme 5.1. The model used to determine K_i in Kintek Global Explorer.⁵⁰

Terms E , B , EB , P , I and EI represent the PBP, BOCILLIN FL, enzyme-BOCILLIN FL complex, hydrolysed BOCILLIN FL, the inhibitor and the enzyme-inhibitor complex, respectively. k_1 models the acylation rate of BOCILLIN FL and k_2 the de-acylation rate of BOCILLIN FL⁴⁸. The enzyme-inhibitor interactions are modelled by the inhibitor k_{off} and k_{on} rates, with the K_i the ratio of these values.

5.2.3 S2d Assay

To confirm compound activity in an analogous assay, residual activities of substrate analogue **S2d** turnover by PaPBP3^{13,51–53} were determined in the presence of the compounds. Assays were conducted in 50 μ L in a 384 well, clear bottom, black walled microplate (Greiner Bio-One). PaPBP3 (400 nM) was incubated with 2 mM of

each compound for one hour at 30 °C in 100 mM sodium phosphate, pH 7, supplemented with 0.01 % (v/v) Triton X-100 (total volume 25 µL). A solution of 5,5'-dithiobis-(2-nitrobenzoic acid) (DTNB) and **S2d** (total volume 25 µL), diluted in the same buffer (to give a final concentration in the assay of 1 mM for both reagents) was added to each well to initiate the reaction (final volume 50 µL). The final concentration of protein was 200 nM and the final inhibitor concentration was 1 mM. The reaction was followed by a ClarioStar plate reader (BMG Labtech) measuring the change in absorbance at 412 nm at 30 °C. The assay was conducted in the absence of an inhibitor (positive control) as well as with an excess of aztreonam (1 mM) which completely inhibits PaPBP3. Treatment with aztreonam was therefore used to find the rate of spontaneous **S2d** hydrolysis in the buffer. The initial rate of **S2d** turnover was calculated using Prism 9 (Prism 9 for macOS, GraphPad Software LLC) and the standard error calculated from three replicates. The **S2d** turnover rate was corrected for non-enzymatic hydrolysis then expressed as a ratio of the positive control:

$$\text{Residual Activity (\%)} = 100 \times \frac{[\text{Initial rate in the presence of inhibitor}] - [\text{non-enzymatic rate}]}{[\text{Initial rate of positive control}] - [\text{non-enzymatic rate}]}$$

5.2.4 Nitrocefin Assay

Nitrocefin^{54,55} turnover by PaPBP3^{11,56} was used to determine the effect of a two-fold dilution on the $pI_{C_{50}}$ of **13**. Assays were performed in clear bottom 384 well plates (Greiner Bio-One). Assays at an initial volume of 40 µL, contained 50 mM bisTris propane, pH 8.5, containing 1 % (v/v) Triton X-100 and 20 mM MgCl₂ and 150 µM Nitrocefin (Abcam). Assays were initiated by the addition of 238 nM PaPBP3, and the absorbance at 482 nm was monitored for 120 s at 30 °C using a ClarioStar plate reader (BMG Labtech). At this point, an additional 40 µL of buffer was then added (final volume: 80 µL), and the plate was shaken (40 s at 500 rpm), following which additional readings were taken. Rates of these linear curves (corrected for background nitrocefin turnover) were calculated using the in-built data analysis package of the plate-reader (MARS; BMG Labtech) and compared to the untreated control to determine relative rates. Relative rates were then plotted against the inhibitor concentration. $pI_{C_{50}}$ was determined using Prism 9 (Prism 9 for macOS, GraphPad Software LLC).

5.2.5 Antimicrobial Assays

Minimum inhibitory concentration (MIC)s of compounds were determined against CLSI reference strains of the following Gram negative organisms: *E. coli* (NCTC 25922), *P. aeruginosa* (PAO1 and a permeabilised strain which was a kind gift from Zgurskaya and colleagues),⁵⁷ *H. influenzae* (ATCC 49766), *A. baumannii* (ATCC 19606) and *N. gonorrhoeae* (ATCC 49226) by the broth microdilution method using a control antibiotic. CLSI procedures were strictly adhered to throughout, with the exception of total volume, which was reduced to minimise compound consumption. The *E. coli* and *P. aeruginosa* strains were tested in a 10 μ L final volume in cation-adjusted Mueller Hinton broth on the lids of inverted 96 well Costar microplates (Corning, USA) and incubated at 37 °C for 18 hours in a humidor (~98% humidity) to reduce evaporation. *H. influenzae*, *A. baumannii* and *N. gonorrhoeae* were tested in 50 μ L of cation-adjusted Mueller Hinton broth supplemented with 5% lysed blood in 96-well Costar microplates (Corning, USA) and incubated at 37 °C for 18 hours in ~5% CO₂. Growth was determined by visual inspection of the plate after the incubation period. Data with the *E. coli* Δ TolC strain was collected as part of the automated screen of boronates, carried out by the high throughput screening platform (Chapter 3).

Synergy studies were conducted using the checkerboard titration method⁵⁸ with *E. coli* and *P. aeruginosa* in a total volume of 10 μ L cation adjusted Mueller Hinton broth, piperacillin at concentrations in the range of 32 to 0.25 μ g/mL and benzoxaborole concentrations varied between 64 and 1 μ g/mL, diluted in perpendicular directions across the plate. Growth was determined by visual inspection of the plate after 18 hours at 37 °C at 95 % humidity.

5.2.6 Chemoinformatics

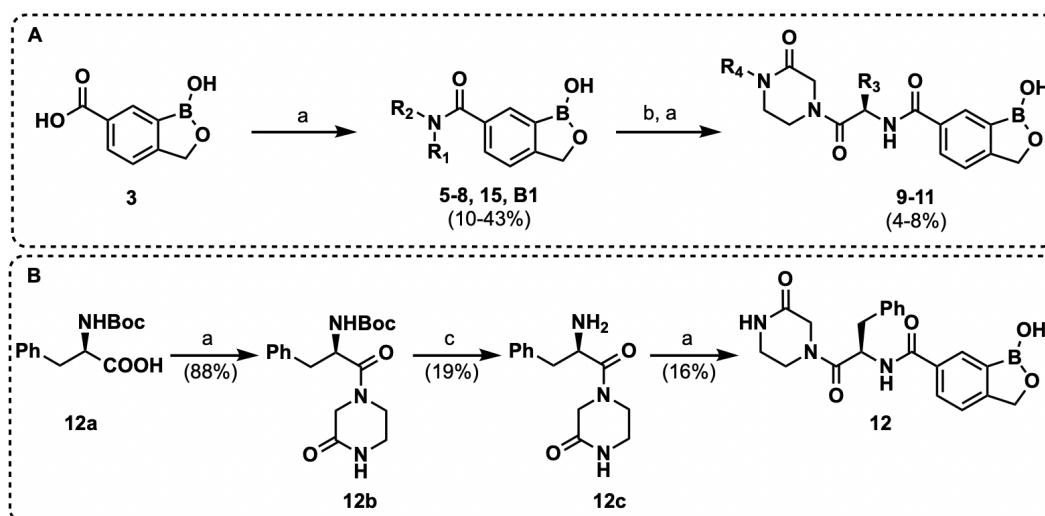
Data pipelining software KNIME v3.5.3⁵⁹ was used to triage fragments of the “Serine Focused Covalent Fragments” compound set from Enamine. The compound set was manually assessed and then grouped by warheads of interest (using SMILES of the functional groups shown in Table 5.2). The desired number of compounds from each group was chosen and then the most diverse subset of fragments from each of the warhead groups was purchased for screening. Diversity was selected for using the “Diversity Picker” module by RDKit, which implements the MaxMin algorithm^{60,61}. Further compounds were added manually after the

selection. The molecular properties shown in Figure 5.2 were calculated using the “Molecular Properties” core KNIME module and the XlogP module from CDK^{59,62}. A complete list of the fragments screened is given in Table 5.S1.

5.2.7 Synthetic Chemistry

All commercial reagents were from Sigma-Aldrich, Fisher Scientific, Combi-Blocks, Enamine, or Fluorochem and were used without further purification. **1** and **3** were from Combi-Blocks, Inc., **2** and **4** were from Enamine. These were used without further purification in the X-ray fragment screen; **13** and **14** were purchased from Wuxi Aptec; **16** was a gift from Mukesh Gangar (H3D, University of Cape Town); vaborbactam was purchased from MedChemExpress; 2-((Benzoyl-D-alanyl)thio)acetic acid (**S2d**) was a gift from Robert Lesniak (University of Oxford).

Solvents were used as received. Flash column chromatography was performed using a Teledyne ISCO flash purification system using a Silicycle SiliaSep™ C18 cartridge. Purity of all final derivatives (except **7**: 88 %) for biological testing was confirmed to be > 95 % (section 5.S5) as determined using an Agilent UPLC–MS : Agilent Technologies 6150 quadrupole mass spectrometer with positive mode electrospray ionisation, coupled with an Agilent Technologies 1290 Infinity II series UPLC system Agilent 1290 series UPLC at two wavelengths 254 and 280 nm. The following conditions were employed: Chromatography was performed using a 50 mm x 2.1 mm Kinetex 1.7 µm particle size Evo C18 100A, LC column 50 mm × 2.1 mm, in solvent A of (0.1 % (v/v) formic acid in water), and solvent B of (0.1 % (v/v) formic acid in acetonitrile). The structures of the final products were confirmed by NMR and mass spectrometric analysis. ¹H and ¹³C nuclear magnetic resonance (NMR) spectra were collected on a Varian Mercury 300 MHz spectrometer or a Bruker AVIII 600 MHz spectrometer. Deuterated solvents were used as supplied. Residual solvent peaks were used to reference chemical shifts (δ) which are reported in parts per million downfield from the residual solvent peak as an internal standard. Peak multiplicity is expressed as s (singlet), d (doublet), t (triplet), q (quartet), m (multiplet), br (broad), or a combination of these. Coupling constants (J) are reported in hertz (Hz) to the nearest 0.5 Hz. High-resolution mass spectra were recorded using a Bruker MicroTOF instrument with an electrospray ionisation source and Time of Flight (TOF) analyser. The parent ion is quoted with the indicated ion: [M - H]⁻ or [M + Na]⁺.



Scheme 5.2. Synthesis of benzoxaborole derivatives (A) 5-11 and 15, (B) 12. Reagents and conditions: (a) 1,1'-carbonyldiimidazole (CDI), *N,N*-dimethylformamide (DMF), 40 °C, 4 – 16 hours; (b) LiOH·H₂O, 1,4-dioxane:H₂O (3:1), 40 °C, 60 min; (c) HCl (4 M solution in 1,4-dioxane), CH₂Cl₂, rt, 16 hours; Note that low isolation yields for substituted benzoxaboroles (e.g. 9-11) in part reflect significant losses during purification on silica gel and provide scope for further optimisation. For B1, R₁ = H and R₂ = CH(R₃)CO₂Me. The complete structures of 5 - 8, 15 and 9 - 11 are shown in Table 5.3. Dppf: 1,1'-bis (diphenylphosphino)ferrocene; Boc, tert-butoxycarbonyl. Thank you to Alen Krajnc for assistance with this figure.

5.2.7.1 General Protocol 1: amide coupling

To a solution of the appropriate carboxylic acid (1 equiv.) in *N,N*-dimethylformamide (2 mL) was added 1,1'-carbonyldiimidazole (2 equiv.). The reaction was stirred for 5 minutes at room temperature; the appropriate amine (1, 1.2 or 1.5 equiv.) was then added, and the reaction was stirred 4–16 hours at 40 °C. The solvent was removed *in vacuo*, and the crude product was purified using a Teledyne ISCO CombiFlash chromatography system eluting a C18 column with a reverse phase solvent gradient of MeOH in 0.1 % (v/v) CH₃CO₂H in water. The product-containing fractions were then combined, and the organic solvent was removed *in vacuo*. When amide coupling yielded a target intermediate compound (e.g. methyl esters of general structure **B1**, Scheme 5.2) it was used in the next step without further purification, else lyophilisation was used to afford the desired products as solids (i.e. for **5 - 11**, and **15**).

1-Hydroxy-*N*-[2-(methylamino)-2-oxo-ethyl]-3*H*-2,1-benzoxaborole-6-carboxamide (**5**)

General Protocol 1 was followed using the following quantities of reagents: **3** (100

mg, 0.56 mmol, 1 equiv.); dimethylformamide (2 mL); 1,1'-carbonyldiimidazole (182 mg, 1.12 mmol, 2 equiv.); 2-amino-*N*-methylacetamide. HCl (104 mg, 0.84 mmol, 1.5 equiv.). Product: crystalline solid (47 mg, 32 %). Purity: >96 % (by HPLC). **¹H NMR** (600 MHz, DMSO-*d*₆) δ 9.55 (br s, 1H, OH), 8.71 (t, *J* = 6.0 Hz, 1H, NH), 8.18 (s, 1H, Ar-*H*), 7.93 (dd, *J* = 8.0, 2.0 Hz, 1H, Ar-*H*), 7.85 (q, *J* = 5.0 Hz, 1H, NHCH₃), 7.49 (d, *J* = 8.0 Hz, 1H, Ar-*H*), 5.02 (s, 2H, -CH₂OB), 3.85 (CH₂, obscured by solvent peak), 2.59 (d, *J* = 5.0 Hz, 3H, CH₃); **¹³C NMR** (151 MHz, DMSO-*d*₆) δ 170.3, 167.8, 157.6, 133.2, 130.3, 130.1, 121.9, 70.4, 43.1, 26.1; **LCMS** (ESI⁺, *m/z*) calculated for C₁₁H₁₃N₂O₄¹⁰B, [M+H]⁺: 249, found 249; **HRMS** (ESI-TOF, *m/z*) [M - H]⁻: 247.0896, found 247.0895.

***N*-[(1*R*)-2-Amino-1-benzyl-2-oxo-ethyl]-1-hydroxy-3*H*-2,1-benzoxaborole-6-carboxamide (6)**

General Protocol 1 was followed using the following quantities of reagents: **3** (100 mg, 0.56 mmol, 1 equiv.); dimethylformamide (2 mL); 1,1'-carbonyldiimidazole (182 mg, 1.12 mmol, 2 equiv.); (*R*)-2-amino-3-phenylpropanamide HCl (169mg, 0.84 mmol, 1.5 equiv.). Product: crystalline solid (80 mg, 43 %). Purity: >98 % (by HPLC). **¹H NMR** (600 MHz, DMSO-*d*₆) δ 9.31 (br s, 1H, OH), 8.45 (d, *J* = 8.5 Hz, 1H, NH), 8.18 – 8.15 (m, 1H, Ar-*H*), 7.89 (dd, *J* = 8.0, 2.0 Hz, 1H, Ar-*H*), 7.59 – 7.52 (m, 1H, Ar-*H*), 7.46 (d, *J* = 8.0 Hz, 1H, Ar-*H*), 7.33 – 7.30 (m, 2H, NH₂), 7.24 (t, *J* = 7.5 Hz, 2H, Ar-*H*), 7.20 – 7.13 (m, 1H, Ar-*H*), 7.12 – 7.08 (m, 1H, Ar-*H*), 5.02 (s, 2H, -CH₂OB), 4.66 (ddd, *J* = 10.5, 8.5, 4.0 Hz, 1H, -CHNH), 3.12 (dd, *J* = 14.0, 4.0 Hz, 1H, -CH₂Ph), 2.99 (dd, *J* = 14.0, 4.0 Hz, 1H, -CH₂Ph); **¹³C NMR** (151 MHz, DMSO) δ 173.8, 166.9, 157.3, 139.0, 133.5, 130.3, 130.2, 129.6, 128.5, 126.7, 121.6, 70.4, 55.2, 37.7; **LCMS** (ESI⁺, *m/z*) calculated for C₁₇H₁₇N₂O₄¹⁰B, [M+H]⁺: 325, found 325; **HRMS** (ESI-TOF, *m/z*) [M + Na]⁺: 347.1174, found 347.1176.

***N*-[(1*R*)-2-Amino-2-oxo-1-phenyl-ethyl]-1- hydroxy-3*H*-2,1-benzoxaborole-6-carboxamide (7)**

General Protocol 1 was followed using the following quantities of reagents: **3** (100 mg, 0.56 mmol, 1 equiv.); dimethylformamide (2 mL); 1,1'-carbonyldiimidazole (182 mg, 1.12 mmol, 2 equiv.); (*R*)-2-amino-2-phenylacetamide (127 mg, 0.84 mmol, 1.5

equiv.). Product: crystalline solid (74 mg, 37 %). Purity: 88 % (by HPLC). **¹H NMR** (600 MHz, DMSO-*d*₆) δ 9.32 (br s, 1H, OH), 9.20 (d, *J* = 7.0 Hz, 1H, NH), 8.26 (t, *J* = 1.0 Hz, 1H, Ar-*H*), 7.99 (dd, *J* = 8.0, 2.0 Hz, 1H, Ar-*H*), 7.52 – 7.45 (m, 3H, Ar-*H*), 7.43 – 7.31 (m, 3H, Ar-*H*), 5.68 (d, *J* = 7.0 Hz, 1H, -CHNH), 5.04 (s, 2H, -CH₂OB), 3.66 (s, 3H, -OCH₃); **¹³C NMR** (151 MHz, DMSO-*d*₆) δ 172.2, 166.7, 157.5, 139.3, 133.3, 130.5, 130.4, 128.8, 128.0, 127.9, 121.8, 70.4, 57.3; **LCMS** (ESI⁺, *m/z*) calculated for C₁₆H₁₅N₂O₄¹⁰B, [M+H]⁺: 311, found 311.

Methyl (2*R*)-2-[(1-hydroxy-3*H*-2,1-benzoxaborole-6-carbonyl)amino]-2-phenyl-acetate (8)

General Protocol 1 was followed using the following quantities of reagents: **3** (100 mg, 0.56 mmol, 1 equiv.); dimethylformamide (2 mL); 1,1'-carbonyldiimidazole (182 mg, 1.12 mmol, 2 equiv.); methyl (2*R*)-2-amino-2-phenyl-acetate (139 mg, 0.84 mmol, 1.5 equiv.). Product: crystalline solid (38 mg, 20 %). Purity: >96 % (by HPLC). **¹H NMR** (600 MHz, DMSO-*d*₆) δ 9.32 (br s, 1H, OH), 9.20 (d, *J* = 7.0 Hz, 1H, NH), 8.26 (t, *J* = 1.0 Hz, 1H, Ar-*H*), 7.99 (dd, *J* = 8.0, 2.0 Hz, 1H, Ar-*H*), 7.52 – 7.45 (m, 3H, Ar-*H*), 7.43 – 7.31 (m, 3H, Ar-*H*), 5.68 (d, *J* = 7.0 Hz, 1H, -NHCH), 5.04 (s, 2H, -CH₂OB), 3.66 (s, 3H, -OCH₃); **¹³C NMR** (151 MHz, DMSO-*d*₆) δ 171.6, 167.4, 157.7, 137.6, 136.7, 133.0, 130.7, 129.3, 128.7, 127.6, 70.4, 57.4, 52.8; **LCMS** (ESI⁺, *m/z*) calculated for C₁₇H₁₆N₂O₅¹⁰B, [M+H]⁺: 326, found 326; **HRMS** (ESI-TOF, *m/z*) [M + Na]⁺: 348.1014, found 348.1016.

***N,N*-Dibenzyl-1-hydroxy-3*H*-2,1-benzoxaborole-6-carboxamide (15)**

General Protocol 1 was followed using the following reagents: **3** (100 mg, 0.56 mmol, 1 equiv.); dimethylformamide (2 mL); 1,1'-carbonyldiimidazole (182 mg, 1.12 mmol, 2 equiv.); dibenzylamine (133 mg, 0.67 mmol, 1.2 equiv.). Product: Crystalline solid (20 mg, 10 %). Purity: >99 % (by HPLC). **¹H NMR** (300 MHz, DMSO-*d*₆) δ 9.26 (br s, 1H, OH), 7.85 (s, 1H, Ar-*H*), 7.61 – 7.52 (m, 1H, Ar-*H*), 7.47 (d, *J* = 8.0 Hz, 1H, Ar-*H*), 7.44 – 7.08 (m, 10H, Ar-*H*), 5.02 (s, 2H, -CH₂OB), 4.75 – 4.24 (m, 4H, 2 x -CH₂Ph). **¹³C NMR** (151 MHz, DMSO-*d*₆) δ 171.6, 167.4, 157.7, 136.7, 133.0, 130.7, 130.6, 129.3, 129.0, 128.7, 121.7, 70.4, 57.4, 52.7; **LCMS** (ESI⁺, *m/z*) calculated for C₂₂H₂₀N₂O₃¹⁰B, [M+H]⁺: 358 found 358; **HRMS** (ESI-TOF, *m/z*) [M + Na]⁺: 380.1429, found 380.1429.

5.2.7.2 General Protocol 2: Synthesis of **9**, **10** and **11** (Scheme 5.2A)

Step (i): *General Protocol 1* was followed to afford an appropriate methyl ester intermediates, **B1**, which were then directly subjected to saponification. Step (ii): To a solution of **B1** (1 equiv.) in 1,4-dioxane/water (3:1; 10 mL) was added lithium hydroxide monohydrate (either 4 or 6 equiv.) in one-portion. The reaction mixture was then stirred for 1 hour at 40 °C, before the volatiles were removed *in vacuo*. The residue thus obtained was then lyophilised to afford corresponding free carboxylic acids (confirmed by LC-MS analysis) as solids. Step (iii): Crude carboxylic acids were immediately coupled with selected piperazin-2-one derivatives using conditions outlined in *General Protocol 1*, giving target benzoxaboroles as solids.

1-Hydroxy-N-[2-oxo-2-(3-oxo-piperazin-1-yl)ethyl]-3H-2,1-benzoxaborole-6-carboxamide (9)

General Protocol 2 was followed with the following quantities of reagents: Step (i): **3** (250 mg, 1.40 mmol, 1 equiv.); dimethylformamide (2 mL); 1,1'-carbonyldiimidazole (455 mg, 2.8 mmol, 2 equiv.) methyl glycinate HCl (133 mg, 0.67 mmol, 1.2 equiv.); step (ii): methyl 2-[(1-hydroxy-3H-2,1-benzoxaborole-6-carbonyl)amino]acetate (**B1**, 349 mg, 1.40 mmol, 1 equiv.); 1,4-dioxane/water (2.5 ml water, 7.5 ml dioxane); lithium hydroxide (134 mg, 5.61 mmol, 4 equiv.); step (iii): 2-[(1-hydroxy-3H-2,1-benzoxaborole-6-carbonyl)amino]acetic acid (50 mg, 0.21 mmol, 1 equiv.); N,N-dimethylformamide (2 mL); 1,1'-carbonyldiimidazole (69 mg, 0.69 mmol, 2 equiv.); piperazin-2-one (32 mg, 0.32 mmol, 1.5 equiv.). Product: crystalline solid (14 mg). Purity: >97 % (by HPLC). ¹H NMR (600 MHz, DMSO-*d*₆) δ 9.37 (br s, 1H, OH), 8.63 – 8.56 (m, 1H, NH), 8.33 – 8.20 (m, 1H, Ar-H), 7.96 (dd, *J* = 8.0, 2.0 Hz, 1H, Ar-H), 7.51 (d, *J* = 8.0 Hz, 1H, Ar-H), 5.05 (s, 2H, -CH₂OB), 4.21 – 4.10 (m, 3H, CH₂), 3.96 (s, 1H, CH₂), 3.72 – 3.61 (m, 2H, CH₂), 3.32 – 3.18 (m, 2H, CH₂); ¹³C NMR (151 MHz, DMSO-*d*₆) δ 172.1, 155.5, 135.4, 129.2, 129.2, 129.2, 129.1, 129.1, 127.9, 127.6, 127.5, 122.1, 70.4, 52.1; LCMS (ESI⁺, *m/z*) calculated for C₁₄H₁₆N₃O₅¹⁰B, [M+H]⁺: 318, found 318; (ESI-TOF, *m/z*) [M + Na]⁺: 340.1076, found 340.1076.

(R)-1-Hydroxy-N-(1-(4-methyl-3-oxo-piperazin-1-yl)-1-oxo-3-phenylpropan-2-yl)-1,3-dihydrobenzo[c][1,2]oxaborole-6-carboxamide (10)

General Protocol 2 was followed using the following quantities of reagents: step (i): **3** (100 mg, 0.56 mmol, 1 equiv.); dimethylformamide (2 mL); 1,1'-carbonyldiimidazole (182 mg, 1.12 mmol, 2 equiv.); methyl D-phenylalaninate hydrochloride (121 mg, 0.56 mmol, 1 equiv.); step (ii): methyl(1-hydroxy-1,3-dihydrobenzo[c][1,2]oxaborole-6-carbonyl)-D-phenylalanine (**B1**, 187 mg, 0.55 mmol, 1 equiv.); 1,4-dioxane/water (2.5 ml water, 7.5 ml dioxane); lithium hydroxide (79.23 mg, 3.31 mmol, 6 equiv.); step (iii): (1-hydroxy-1,3-dihydrobenzo[c][1,2]oxaborole-6-carbonyl)-D-phenylalanine (30 mg, 0.09 mmol, 1 equiv.); *N,N*-dimethylformamide (2 mL); 1,1'-carbonyldiimidazole (30 mg, 0.18 mmol, 2 equiv.); 1-methylpiperazin-2-one (16 mg, 0.14 mmol, 1.5 equiv.). Product: crystalline solid (16 mg). Purity: >97% (by HPLC). **¹H NMR** (300 MHz, DMSO-*d*₆) δ 8.85 (br s, 1H, OH), 8.24-8.16 (m, 1H, NH), 7.98 – 7.86 (m, 1H, Ar-*H*), 7.48 (d, *J* = 8.0 Hz, 1H, Ar-*H*), 7.36 – 7.14 (m, 6H, Ar-*H*), 5.20-4.95 (m, 2H, -CH₂OB), 4.20 – 3.93 (m, 2H), 3.34 – 2.96 (m, 5H), 2.80 (s, 3H); **LCMS** (ESI⁺, *m/z*) calculated for C₂₂H₂₄N₃O₅¹⁰B, [M+H]⁺: 422, found 422.

1-Hydroxy-*N*-[2-(4-methyl-3-oxo-piperazin-1-yl)-2-oxo-ethyl]-3*H*-2,1-benzoxaborole-6- carboxamide (11)

General Protocol 2 was followed with the following quantities of reagents: step (i): **3** (250 mg, 1.40 mmol, 1 equiv.); dimethylformamide (2 mL); 1,1'-carbonyldiimidazole (455 mg, 2.8 mmol, 2 equiv.) methyl glycinate HCl (133 mg, 0.67 mmol, 1.2 equiv.); step (ii): methyl 2-[(1-hydroxy-3*H*-2,1-benzoxaborole-6-carbonyl)amino]acetate (**B1**, 349 mg, 1.40 mmol, 1 equiv.); 1,4-dioxane/water (2.5 ml water, 7.5 ml dioxane); lithium hydroxide (134 mg, 5.61 mmol, 4 equiv.); step (iii): 2-[(1-hydroxy-3*H*-2,1-benzoxaborole-6- carbonyl)amino]acetic acid (47 mg, 0.2 mmol, 1 equiv.); *N,N*-dimethylformamide (2 mL); 1,1'-carbonyldiimidazole (65 mg, 0.4 mmol, 2 equiv.); 1-methylpiperazin-2-one (34 mg, 0.30 mmol, 1.5 equiv.). Product: crystalline solid (17 mg). Purity: >96 % (by HPLC). **¹H NMR** (300 MHz, DMSO-*d*₆) δ 8.58 (br s, 1H, OH), 8.26 (s, 1H, Ar-*H*), 7.97 (d, *J* = 6.0 Hz, 1H, Ar-*H*), 7.51 (d, *J* = 8.0 Hz, 1H, Ar-*H*), 5.05 (s, 2H, CH₂), 4.24 – 4.07 (m, 3H, -CH₂OB and CH₂), 4.05-3.94 (m, 2H, CH₂), 3.48-3.30 (m, 2H, CH₂), 2.89 (s, 3H, -NCH₃); **¹³C NMR** (151 MHz, DMSO-*d*₆) δ 167.6, 167.3, 165.2, 157.5, 133.4, 130.2, 130.0, 121.8, 70.3, 48.0, 47.5, 46.2, 41.2, 33.9; **LCMS** (ESI⁺, *m/z*) calculated for C₁₅H₁₈N₃O₅¹⁰B, [M+H]⁺: 332, found 332;

5.2.7.3 Synthesis of 12 (Scheme 5.2A)

Step (i): To a solution of (**12a**) (tert-butoxycarbonyl)-D-phenylalanine) (300 mg, 1.13 mmol) in *N,N*-dimethylformamide (3 mL) was added 1,1-carbonyldiimidazole (367 mg, 2.26 mmol); the reaction was stirred for 5 minutes at room temperature. To the reaction mixture was then added piperazin-2-one (170 mg, 1.70 mmol) and the resultant solution was stirred for 4 hours at 40 °C. Ethyl acetate (10 mL) and water (10 mL) were added. The layers were separated. The aqueous layer was extracted with ethyl acetate (3 × 20 mL). Combined organic layers were dried (MgSO₄), filtered, and concentrated *in vacuo* to afford **12b** as a yellow oil (350 mg, 88 %), which was used in the next step without further purification.

Step (ii): To a stirred solution of (**12b**) (350 mg, 1.01 mmol, 1 equiv.) in CH₂Cl₂ (10 mL) was added HCl (4M in 1,4-dioxane, 0.76 mL, 3.02 mmol, 3 equiv.) at room temperature under nitrogen. The reaction mixture was stirred overnight to afford an insoluble precipitate. The precipitate, **12c**, was washed three times with CH₂Cl₂, then filtered, dried in air and used in the next step without further purification (54 mg, 19 %).

Step (iii): General Protocol 1 was followed using the following quantities of reagents: **3** (54 mg, 0.3 mmol, 1 equiv.); *N,N*-dimethylformamide (3 mL); 1,1-carbonyldiimidazole (98 mg, 0.600 mmol, 2 equiv.); **12c** (103 mg, 0.360 mmol, 1.2 equiv.). Product (**12**): white powder (20 mg, 16 %). Purity: >99 % (by HPLC). ¹H NMR (300 MHz, methanol-*d*₄) δ 8.31 (br s, 1H, OH), 8.14 (dd, *J* = 8.0, 2.0 Hz, 2H, Ar-*H*), 7.93 (d, *J* = 8.0 Hz, 1H, Ar-*H*), 7.56 – 7.45 (m, 2H, Ar-*H*), 7.36 – 7.22 (m, 3H, Ar-*H*), 5.15 (m, 5H, 2 × CH₂ and CH), 4.33 – 3.96 (m, 2H, CH₂), 3.88 – 3.40 (m, 3H, CH₂), 3.28 – 3.06 (m, 3H, CH₂); ¹³C NMR (151 MHz, DMSO-*d*₆) δ 170.5, 167.3, 167.3, 157.8, 137.7, 132.1, 131.9, 130.3, 129.6, 128.7, 127.1, 122.5, 70.4, 51.5, 46.1, 42.3, 40.4, 37.5; LCMS (ESI⁺, *m/z*) calculated for C₂₁H₂₂N₃O₅¹⁰B, [M+H]⁺: 408, found 408; HRMS (ESI-TOF, *m/z*), [M + Na]⁺: 430.1543, found 430.1546.

5.3 Results

5.3.1 X-ray Fragment Screen

A small compound library was assembled to be screened against PaPBP3 on the XChem platform. The library (261 compounds in total) was selected to include a small number of known electrophilic warheads (nitriles, epoxides, sulphonyl fluorides and esters), but was especially enriched with boron-containing compounds (Table 5.2). Most of the compounds were selected from Enamine's "Serine focused Covalent Fragments" library⁶³. Within each of the chemotype groups, selections from the catalogue were made to make the most chemically diverse set possible. The library generally conformed to the rule of 3 of fragment libraries⁶⁴ (after Lipinski's rule of 5⁶⁵) (Figure 5.2), although this may not be as relevant to covalent fragment libraries, which may be more dependent on the chemistry of the warhead.

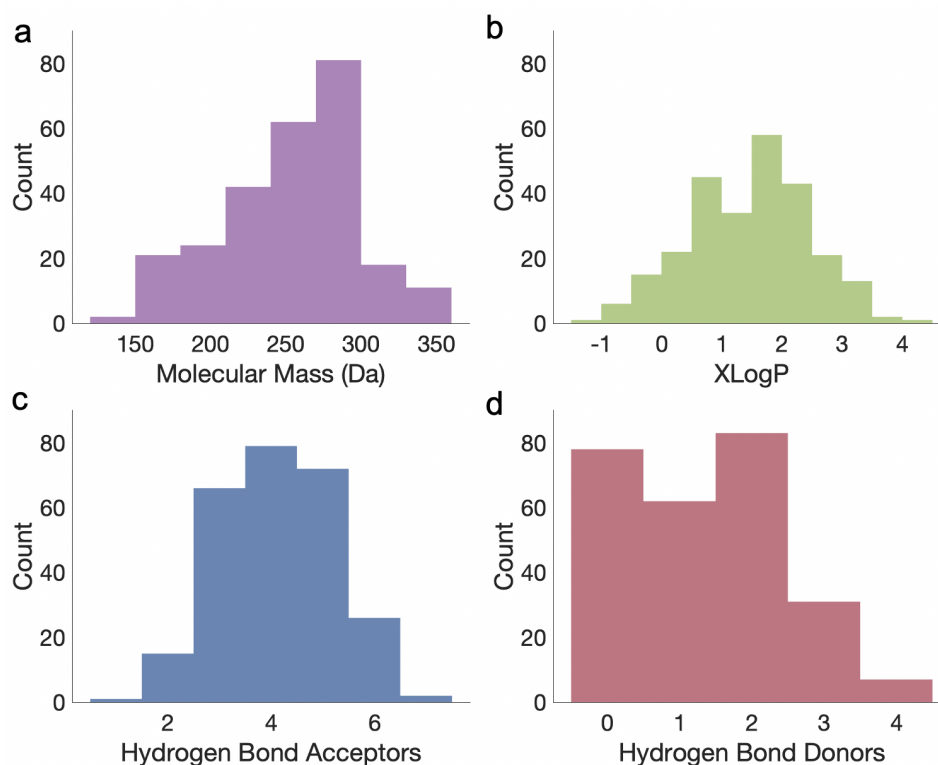


Figure 5.2. Properties of the fragments screened. The fragments screened mostly conformed to the 'rule of 3'⁶⁴, such that the molecular mass was <300 Da (a), the calculated log of partition coefficient (XlogP)⁶² (b) and hydrogen bond donors (d) are <3. The number of hydrogen bond acceptors (predicted that <3 is best) (c) is the least compliant, but has a median of 4 hydrogen bond acceptors.

Boron-containing compounds are known to exhibit pH-dependent behaviour⁶⁶, so the library was screened against PaPBP3 once with the crystals at pH 6 and once with the crystals at pH 8.


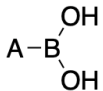
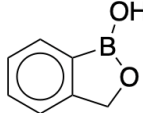
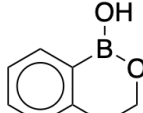
Chemotype		Number of compounds incorporating chemotype ^a	Hits found by XChem
$R-C\equiv N$	Nitrile	5	0
	Epoxide	4	0
$R-S(=O)_2-F$	Sulphonyl fluoride	4	0
	Boronic acid ^b A = aromatic C	80	26
	A = aliphatic C	7	1
	Benzoxaborole	18	7
	6,6-bicyclic boronate	16	0
$R-C(=O)OC$	Ester	92	0

Table 5.2. Electrophilic fragments screened against PaPBP3. ^a Some compounds incorporate multiple chemotypes. ^b Boronic acids bonded to aliphatic or aromatic carbons are distinguished. The boronic acid chemotype is explicitly defined as two free hydroxyls, such that benzoxaboroles or 6,6-bicyclic boronates are not a subset of this group. A complete list of fragments screened is given in Table 5.S1.

In total, 34 ‘hits’ were identified by the screen, although not all had complete density for the ligand. All hits were from the boronic acid (26 hits, all tri-covalent) or benzoxaborole (7 hits, all di-covalent) chemotypes, and all showed covalent bonding to the protein through the boron atom. The correlation of the valency of the binding and the chemotype was striking. Tri-covalent boronate binding has been

described in LMM PBPs¹⁶, and di-covalency has been previously reported for other boronate compounds^{27,28} (Table 5.1), but this is the first time di-covalency has been reported for benzoxaboroles and the first time multi-covalent interactions have been observed in HMM PBPs.

5.3.2 Fragment Hit Examples

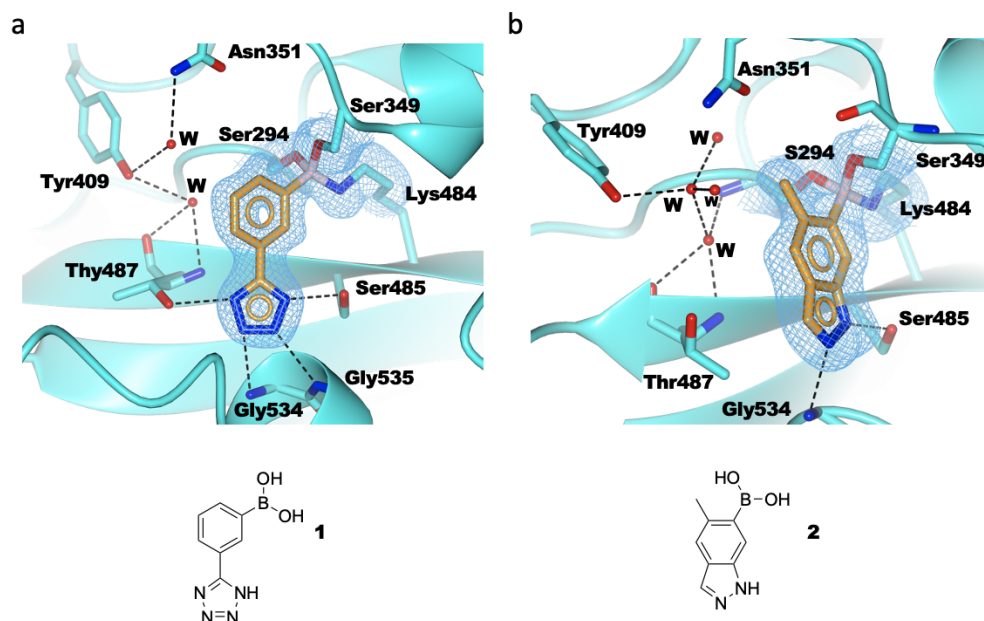


Figure 5.3. Tri-covalency is observed in the reaction between boronic acids 1 and 2 and PaPBP3 by crystallography. Boron atoms in (a) **1** and (b) **2** are ligated by Ser294, Ser349, and Lys484. Residues neighbouring the ligand are as shown in sticks and are labelled, hydrogen bonds are represented by black dashed lines. A network of hydrogen bonded waters (**W**) is also shown. Composite omit maps (contoured at 1σ) are shown as light blue mesh around the ligand and covalently bonded residues. A DMSO molecule is also found in the active site of both structures, but omitted for clarity.

A selection of the fragment hits which were representative of the binding modes were investigated in more detail. Boronic acids **1** and **2** react with PaPBP3 such that the boron becomes sp^3 hybridised and tri-covalently bonded to Ser294 (the 'active site' or 'catalytic' serine in the **SXXK** motif), Ser349 (in the **SXN** motif), and Lys484 (in the **KSG** motif), forming a tri-covalent complex Figure 5.3. The aromatic groups of **1** and **2** occupy similar, but not identical, regions of the active site. Ser294 is displaced to the right by rotation of its side chain bonds, compared to its position when reacting with β -lactams. This allows a water to occupy the

'oxyanion hole' which the β -lactam-derived carbonyl often occupies. The tetrazole group of **1** makes four hydrogen bonds to PaPBP3: two to the backbone nitrogens of Gly534 and Gly535; two to the flanking residues Thr487 and Ser485. Residues Thr487 and Ser485 are typically engaged by the C-3 penicillin carboxylate (or equivalent group) found on all β -lactams.

Hydrogen bonds are also formed with the backbone nitrogens of Gly535 and the Ser485 by the imidazole group of **2**. These structures therefore provide support for future design of PBP3 inhibitors incorporating either weakly acidic non-carboxylates or neutral groups⁶⁷ that interact with the 'acid binding pocket' of PBP3 (Figure 5.S2).

A similar binding mode is reported for a boronate bound to R39 D,D-peptidase from *Actinomadura* sp. (PDB: 3ZVT¹⁶). In particular, the boron atoms and bonded side chains are similarly positioned and superimpose well, regardless of the enzyme and the different boron-bonded functional group, i.e. alkyl (Zervosen *et al.*¹⁶) versus phenyl (this work) (Figure 5.S2d).

In contrast to boronic acids, benzoxaborole fragments bind to PaPBP3 with a di-covalent binding mode (Figure 5.4). The boron engages both Ser349 and Ser294 and the benzoxaborole also hydrogen bonds through the 'endocyclic' 2-position oxygen (atom numbering shown in Figure 5.5) to Lys484. As with the phenyl boronic acids, a water is found in the oxyanion hole. Both **3** and **4** form hydrogen bonds to the sidechain NH₂ group of Asn351, and both PaPBP3:**3** and PaPBP3:**4** complexes show hydrogen bonding between Tyr409 and the backbone carbonyl of Thr487 (Figure 5.4).

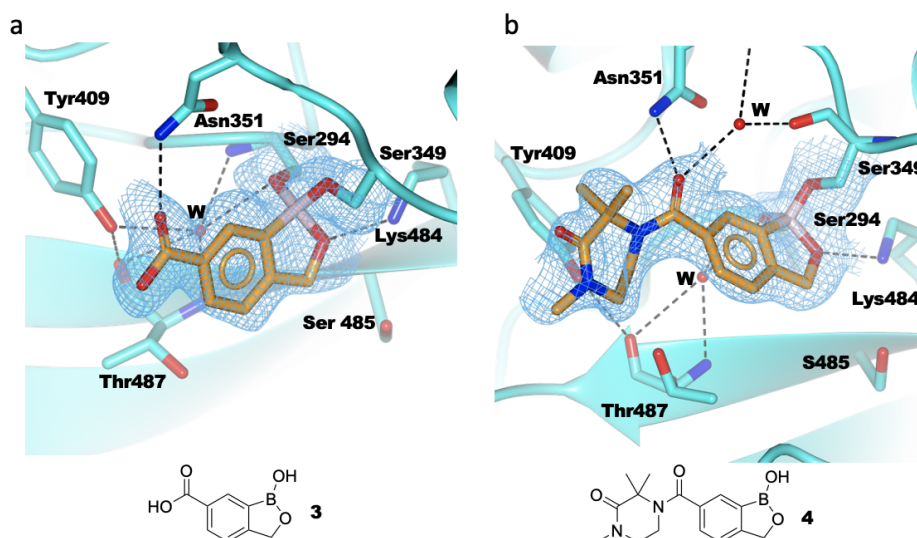


Figure 5.4. Benzoxaborole fragments form di-covalent complexes with PaPBP3. Crystal structures of (a) PaPBP3:**3** and (b) PaPBP3:**4** complexes. The boron atom of both molecules reacts with the side chains of Ser294 and Ser349. Hydrogen bonds (black dashed lines) are formed with Lys484 and Asn351. A water (w) occupies the oxyanion hole. Composite omit maps (light blue mesh, maps contoured at 1 σ) are shown for the ligand and the bonded serine sidechains.

5.3.3 Hit Expansion: Design and Synthesis

The novel binding mode of benzoxaboroles was investigated by the generation of a small number of chemical derivatives in an attempt to improve their affinities. The derivatives were designed using computational docking starting from fragments **3** and **4** as well as the complexes of PaPBP3 with β -lactams^{36,68}. It was hoped compounds would interface with the protein at the regions engaged by reacted piperacillin (Figure 1.4e, Figure 5.5.). From examination of the PaPBP3:**3** complex it was hypothesised that substitution of the benzoxaborole at the 6-position would allow side chain conformations which aligned closely to the reacted piperacillin R1 (C-6) side chain (Figure 5.5).

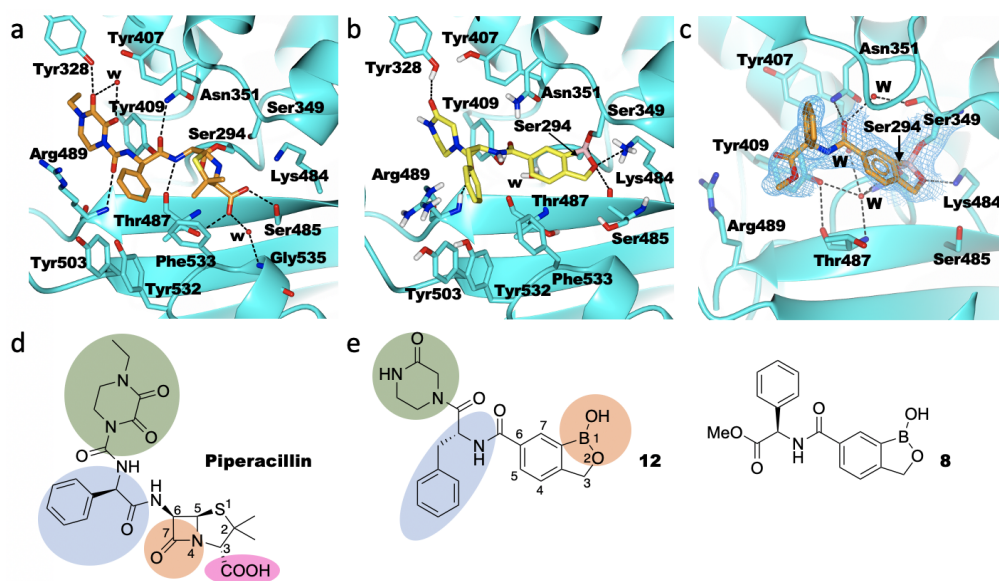


Figure 5.5. Binding modes of reacted piperacillin and benzoxaboroles 12 (predicted) and 8 (observed) complexed with PaBP3. (a) Reacted piperacillin (PDB: 6R3X³⁶) engages multiple regions of PaBP3 (Figure 1.4e), as observed by crystallography. (b) Predicted binding mode of **12** determined by docking, showing the regions of PaBP3 which it was hoped would be engaged by parts of the sidechain, in analogy with piperacillin. (c) Crystallographically observed binding modes of **8** in complex with PaBP3. Hydrogen bonds (black dashed lines) are shown. A composite omit map (light blue mesh, map contoured at 1σ) is shown for **8** and the bonded serine sidechains. Functional groups of piperacillin (d) and **12** (e): Serine binding region (orange), C-3 carboxylate (pink), group 1 (blue) and group 2 (green). Atom numbering on the penicillin and benzoxaborole cores is given.

Initial derivatives (**5-8**) were produced by coupling C-terminally protected amino acids (glycine, D-phenylglycine and D-phenylalanine) to the C-6 carboxyl group of **3**, with additional derivatives (**9-12**) incorporating a ketopiperazine group at the C-terminal end of the first amino acid. **15** was synthesised with a C-6 dibenzylamine group in order to investigate the binding of a non-amino acid benzoxaborole. All reactions were carried out by amide coupling with 1,1'-carbonyldiimidazole (CDI). Purification was challenging, and several other compounds which had been designed could not be purified after synthesis, a known challenge for benzoxaboroles⁶⁹.

Initial crystal structures (as exemplified by **8**) of benzoxaboroles **5-12**, showed that whilst all derivatives bound in the same di-covalent binding mode, the benzoxaborole side chains were angled incorrectly for engagement with the active site as proposed.

The C-3 carboxylate is ubiquitous in β -lactams, so derivatives incorporating this group were investigated (**13**, **14** and **16** were synthesised by WuxiAppTec and collaborators). The incorporation of a second acidic group requires a more complex synthetic route involving ring closure of the benzoxaborole 5 membered ring. The presence of the acid group did not affect the position of the benzoxaborole ring within the active site of the protein and **3**, **4**, **8**, and **13** - **16** all showed di-covalent binding. **16**, which is derivatised at the 5-position, offers new avenues for further synthesis. Side chains originating from this point may be better positioned to form piperacillin-like interactions with the protein (Figure 5.6d). Similarly the non-amino acid **15** also exploits a region of the protein that is not occupied by the amino acid derivatives e.g. **3**, **4**, **8**, **13** or **14** (Figure 5.6c).

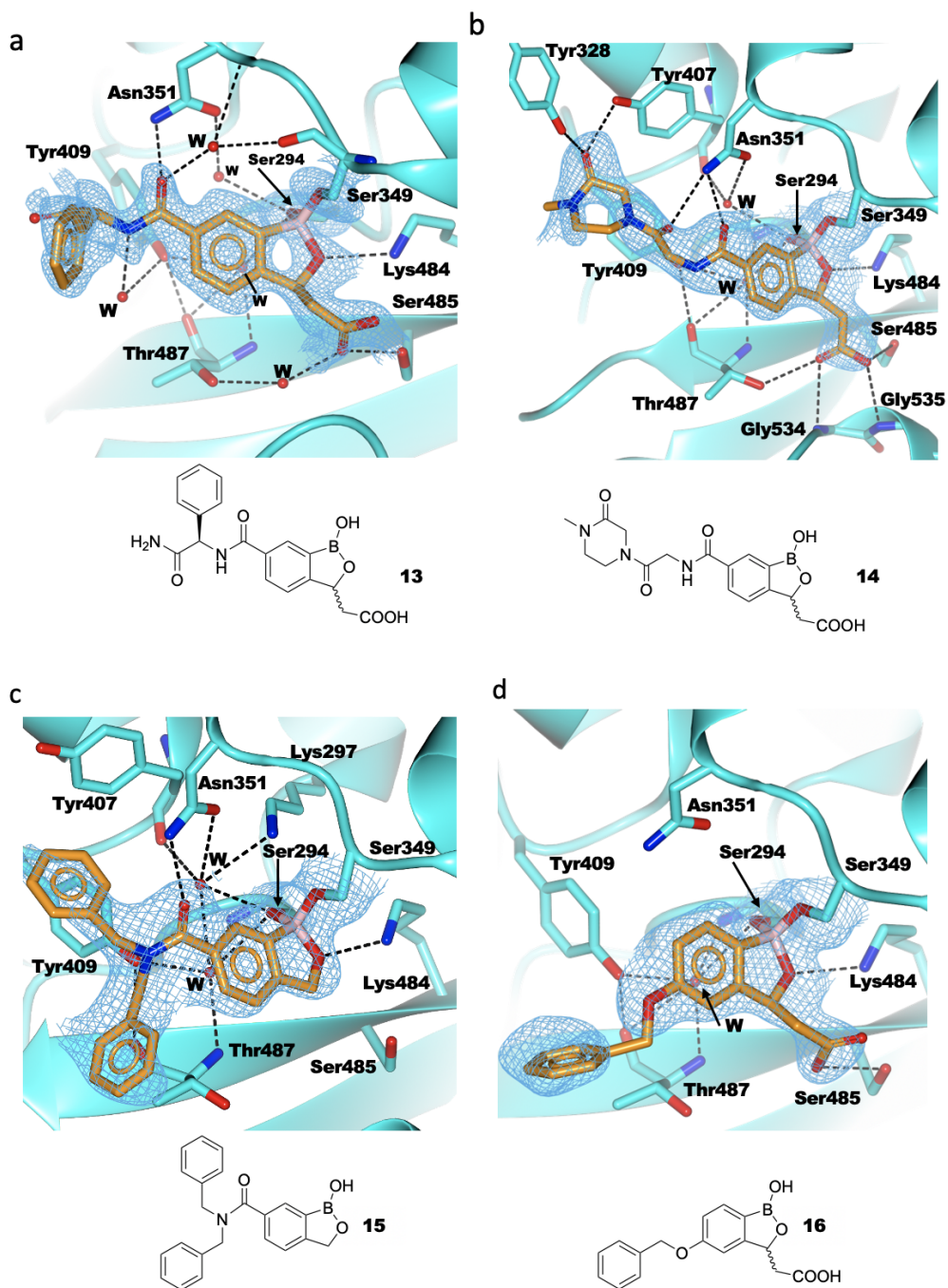


Figure 5.6. PaBPB3 complex with C-3 acid group containing benzoxaboroles (13, 14 and 16) and 15. Crystal structures of (a) the PaBPB3:13 complex; (b) the PaBPB3:14 complex; (c) the PaBPB3:15 complex; (d) the PaBPB3:16 complex. There are two alternative conformations of Tyr409 in the PaBPB3:13 complex but only one is shown in (a). Both conformations are shown in Figure 6.S1b. Relevant hydrogen bonds (dashed black lines) are shown. Composite omit maps (light blue mesh, maps contoured at 1σ) are shown for the ligand and the bonded serine sidechains.

5.3.4 Vaborbactam

Vaborbactam, a boron-based serine β -lactamase inhibitor^{5–7} lacking antimicrobial activity, was also investigated alongside the benzoxaboroles to allow the behaviour of these different scaffolds to be compared. The PaPBP3:vaborbactam complex shows that vaborbactam reacts with Ser294 mono-covalently (Figure 5.7).

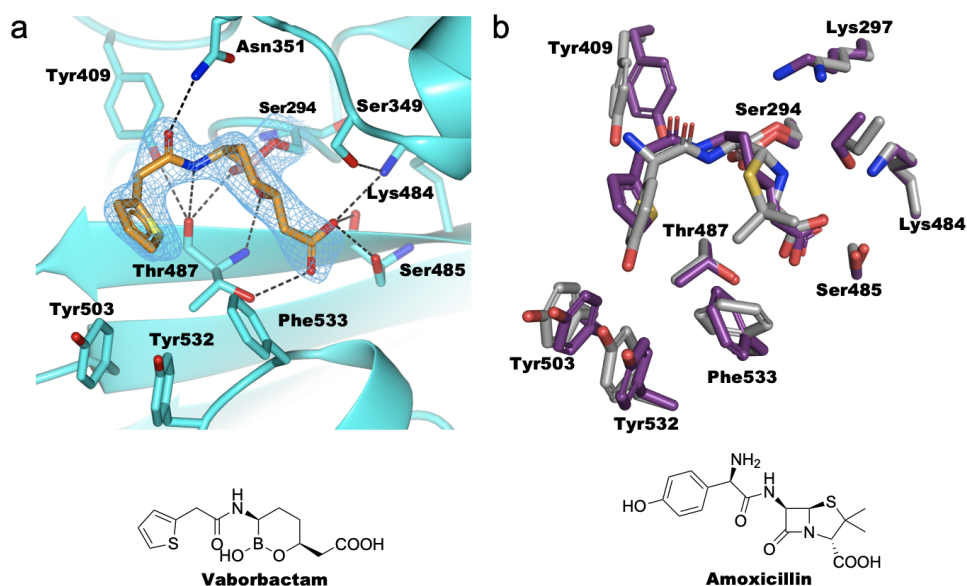


Figure 5.7. The PaPBP3:vaborbactam complex as observed by crystallography. (a) Vaborbactam bonds covalently to Ser294 and engages the active site with a number of hydrogen bonds (black dashed lines). Composite omit maps (light blue mesh, maps contoured at 1σ) are shown for vaborbactam and the bonded serine sidechain. (b) Overlay of vaborbactam (purple) and amoxicillin (PDB code: 6I1E, grey)³⁶ binding PaPBP3. Residues neighbouring the ligand are shown in the same colour as the ligand and are labelled. The overlay shows considerable alignment of both residue side chains and reacted ligand conformations.

Comparison of the PaPBP3:vaborbactam complex with the structure of amoxicillin reacted PaPBP3 shows they superimpose well, particularly at the the C-3 carboxylate, the nucleophilic serine and the R1 side chain of amoxicillin (Figure 5.7b). Hydrogen bonds are formed between vaborbactam and residues Asn351, Tyr409, Thr487, Ser485, and the hydrophobic wall (residues Tyr503, Tyr532 and Phe533, Figure 1.4e) forms around the thiophene group.

5.3.5 Inhibition Assays

The ability of **1-16**, as well as vaborbactam, to engage PaPBP3 in solution was assessed by competition with BOCILLIN FL in a fluorescence anisotropy (FA) assay⁴⁸ and an assay of PBP-mediated thioester **S2d** hydrolysis^{13,51–53} (Table 5.3, Figure 5.8). The results obtained by both assays were consistent with each other, but most compounds exhibit little inhibition even at the high concentration tested (1 mM). Dissociation constants (K_i) were determined for **13**, **14**, **16**, and vaborbactam, which had the lowest residual activities in both assays (Figure 5.8a-d). The most potent was found to be **13** (which is a racemate) with a K_i of $73.9 \pm 0.8 \mu\text{M}$ (Table 5.3). Vaborbactam showed only weak affinity, despite its crystallographic homology with amoxicillin and apparently successful engagement with the protein. Overall binding is weak, which is consistent with other reports of μM affinities for boronates binding to HMM PBPs^{12–14,21,22}.

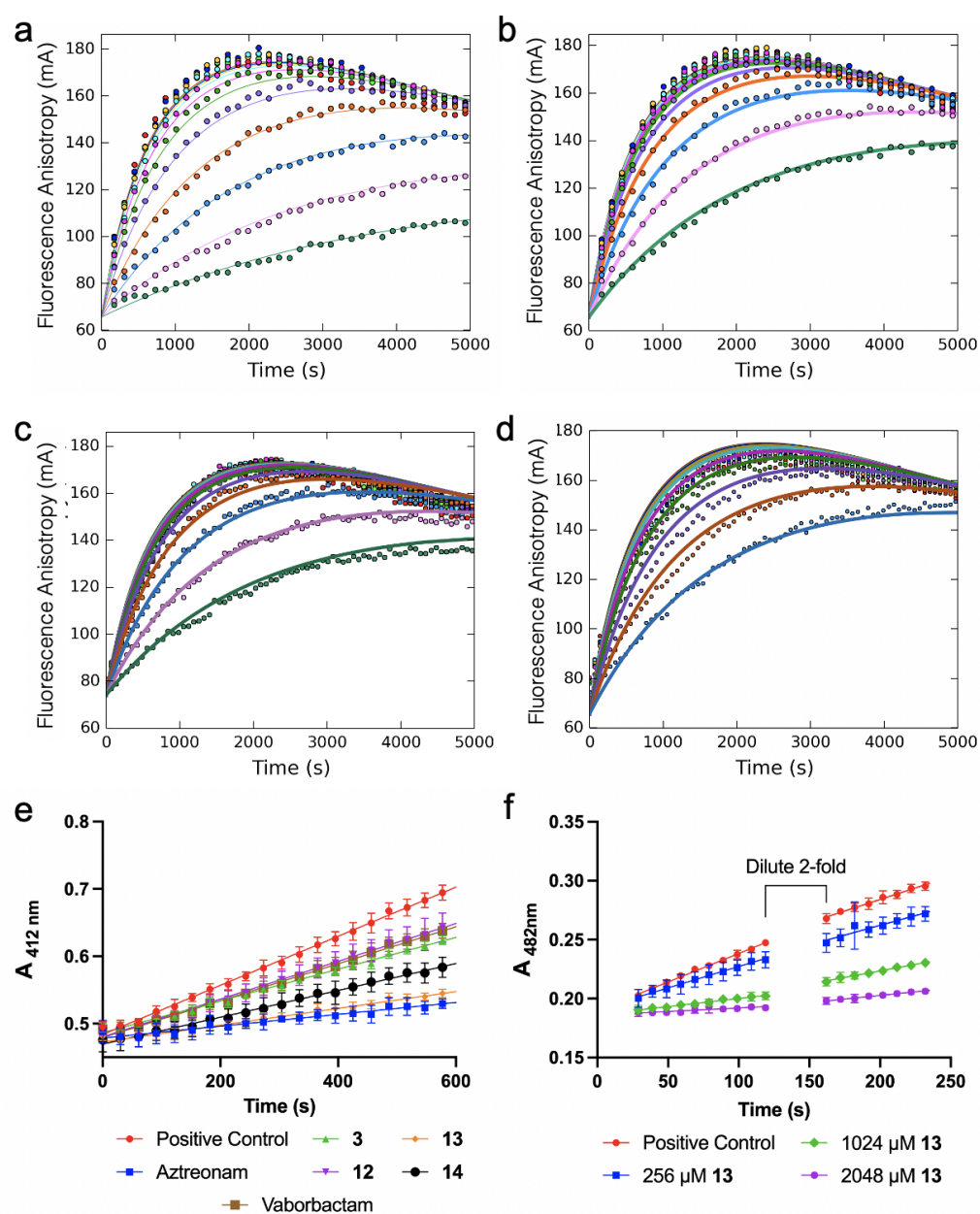


Figure 5.8. Progress curves of boronate inhibition of PaBP3. (a-d) BOCILLIN FL fluorescence anisotropy competition curves are shown for (a) **13**, (b) **14**, (c) **16** and (d) vaborbactam reacting with PaBP3. Kintek Global explorer was used to fit the fluorescence anisotropy progress curves in the presence of increasing concentrations of each inhibitor to the model in Scheme 5.1. (e) Progress curves for determining residual activities by PaBP3-mediated **S2d** turnover, following the absorbance of DTNB at 412 nm. (f) Progress curves of the inhibition of PaBP3-mediated nitrocefin turnover by compound **13** to investigate reversibility. The rates were determined before and after the assay volume was doubled (at the indicated point), then used to create the $pI_{C_{50}}$ curve shown in Figure 5.9.

		Residual Activity by BOCILLIN FL FA (%)	Residual Activity by S2d Turnover (%)	K_i (μ M)
1		82 \pm 4	ND	ND
2		ND	ND	ND
3		75 \pm 1	57.8 \pm 0.6	ND
4		ND	ND	ND
5		>90	>90	ND
6		>90	>90	ND
7		>90	>90	ND
8 ^b		>90	>90	ND
9		>90	ND	ND
10		>90	ND	ND
11		>90	ND	ND
12		84 \pm 1	80.9 \pm 1.3	ND
13		16 \pm 6	19.6 \pm 0.4	73.9 \pm 0.8
14		42 \pm 6	47.5 \pm 0.6	172.0 \pm 3.0
15 ^b		87 \pm 3	ND	ND
16		20 \pm 5	ND	78.1 \pm 0.9
Vaborbactam		54 \pm 5	75.8 \pm 0.7	201.0 \pm 2.3

Table 5.3. Activity profiles of 1-16 and vaborbactam against PaPBP3.

Residual activities were determined in the presence of 1 mM inhibitor and expressed as a percentage of the activity of the untreated control. Errors are standard errors ($n = 3$) from independent measurements. K_i determined using global fitting in Kintek Global Explorer, errors are standard errors generated by fitting^{48,50}. ^aResidual activity measured at 100 μ M due to insolubility at 1 mM. ND, not determined.

13 was assessed for its ability to bind class B PBPs from *E. coli*, *A. baumannii*, *H. influenzae*, and *N. gonorrhoeae* (Table 5.4) by competition with BOCILLIN FL. The apparent differences in the ability of **13** to bind each PBP indicates a degree of selectivity of the compound, given the similarity between these proteins (Figure 1.3).

Protein Tested	Residual Activity by BOCILLIN FL FA (%)
PBP3 from <i>P. aeruginosa</i>	16 ± 6
PBP3 from <i>H. influenzae</i>	32 ± 3
PBP3 from <i>A. baumannii</i>	73 ± 3
PBP3 from <i>E. coli</i>	>90
PBP2 from <i>N. gonorrhoeae</i>	>90

Table 5.4. Inhibition of various class B PBPs by 13. Residual activities were determined in the presence of 1 mM **13** and expressed as a percentage of the activity of the untreated control. Errors are standard errors (n = 3) from independent measurements. *N. gonorrhoeae* PBP2 was a transpeptidase domain only construct.

The interaction of **13** with PaPBP3 was further confirmed in assays with nitrocefin (Table 1.2), which allowed a $pI_{C_{50}}$ to be found (Figure 5.9). The reversibility of the binding of **13** could also be assessed by this method: determining the half maximal inhibitory concentration $pI_{C_{50}}$ before and after a two-fold dilution of the assay solution showed a doubling of the $pI_{C_{50}}$. Which indicates the reaction was rapidly reversible (equilibrium established in <30 s). Irreversibly binding ceftazidime does not exhibit a change in $pI_{C_{50}}$ following the dilution of the assay. Similarly, pre-incubating **13** with PaPBP3 for 0, 30 or 60 minutes prior to initiation of the BOCILLIN FL assay appeared to have no significant effect on level of inhibition and the BOCILLIN FL fluorescence anisotropy progress curves can be fit well using a simple reversible, one step binding model (Scheme 5.1).

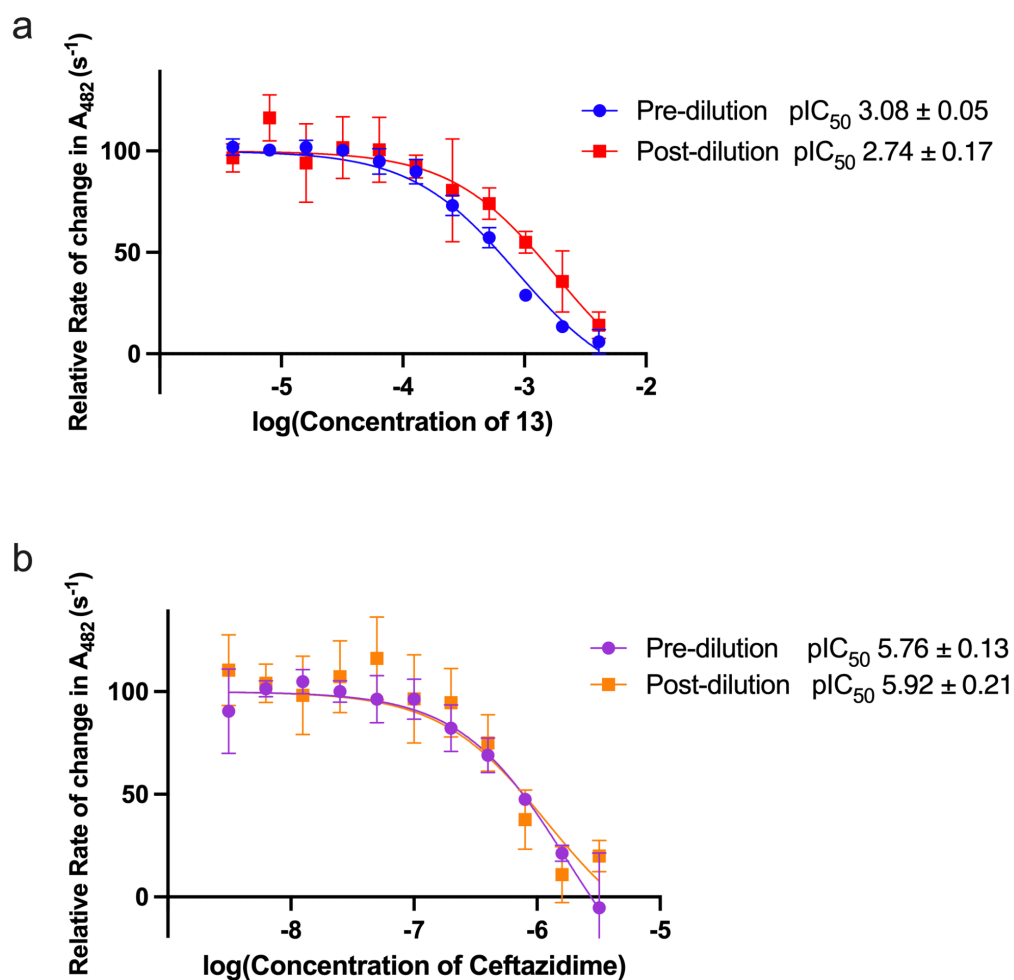


Figure 5.9. The effect of 2-fold dilution on the PaBPB3 pIC_{50} of 13 and ceftazidime. The rate of nitrocefin turnover (measured at 482 nm) by PaBPB3 in the presence and absence of inhibitors was determined before and after a 2-fold dilution of the assay and the rates compared to the uninhibited control. Errors shown for each point are standard deviations from three repeats, errors on pIC_{50} values are standard errors of the mean as determined by Prism 9 (Prism 9 for macOS, Graphpad Software, LLC).

5.3.6 Microbiology

Several compounds were screened against wild type *E. coli*, *P. aeruginosa*, *H. influenzae*, *A. baumannii* and *N. gonorrhoeae* strains. All were ineffective (MICs \geq 64 $\mu\text{g/ml}$) (Table 5.5). Screening against *E. coli* ΔTolC (Chapter 3.3.6) or a *P. aeruginosa* strain engineered to remove the outer membrane permeability barrier by the introduction of a large pore⁷⁰ did not show any antimicrobial activity (Table 5.5), indicating the lack of activity was not due to permeability issues. Synergy with piperacillin (which can be used to identify weak PBP inhibition) was not observed in non- β -lactamase-expressing *E. coli* and *P. aeruginosa*.

A separate screen of a library of phenyl boronic acids was conducted by the robotic screening platform (Chapter 3), which included all of the compounds in this study (except vaborbactam). This screen (against *E. coli* ΔTolC) did not identify any hits amongst the compounds in this chapter (Table 5.5).

	<i>P. aeruginosa</i> PAO1	<i>E. coli</i> NCTC25922	<i>P. aeruginosa</i> Permeabilized ^a	<i>N. gonorrhoeae</i> ATCC 49226	<i>A. baumannii</i> ATCC 19606	<i>H. influenzae</i> ATCC 49766	<i>P. aeruginosa</i> PAO1: piperacillin synergy	<i>E. coli</i> NCTC 25922: piperacillin synergy
8	>64 $\mu\text{g/mL}$	>64 $\mu\text{g/mL}$	>64 $\mu\text{g/mL}$	NT	NT	NT	NT	NT
13	>64 $\mu\text{g/mL}$	>64 $\mu\text{g/mL}$	>64 $\mu\text{g/mL}$	>64 $\mu\text{g/mL}$	>64 $\mu\text{g/mL}$	>64 $\mu\text{g/mL}$	No Effect	No Effect
14	>64 $\mu\text{g/mL}$	>64 $\mu\text{g/mL}$	>64 $\mu\text{g/mL}$	NT	NT	NT	NT	NT
15	>64 $\mu\text{g/mL}$	>64 $\mu\text{g/mL}$	>64 $\mu\text{g/mL}$	NT	NT	NT	NT	NT

Table 5.5. Minimum inhibitory concentrations of selected compounds for a panel of gram-negative bacteria. ^aPermeabilised strains with the introduction of a FhuA pore and knockout of export pumps⁷⁰.

5.4 Discussion

5.4.1 Boron Binding Modes

Complexes of boronates with PaPBP3 reveal three distinct binding modes: (i) mono-covalent (reaction with Ser294; Figure 5.10a), (ii) di-covalent (reaction with Ser294 and Ser349; Figure 5.10b), and (iii) tri-covalent (reaction with Ser294, Ser349 and Lys484; Figure 5.10c). The binding mode correlates with the nature of the boron compound: monocyclic vaborbactam bind mono-covalently, benzoxaboroles (**3-16**) bind di-covalently, and phenyl boronates (**1** and **2**) bind tri-covalently. Tri-covalent¹⁶ and mono-covalent^{11,14–16,18,19} interactions of boron compounds with PBPs are known, but to my knowledge there are no reports on the di-covalent bonding of benzoxaborole compounds to PBPs. Crystallographic data was collected at pH 6 and pH 8 but the binding mode doesn't appear to relate to the crystallisation conditions, only to the warhead (Table 5.S3).

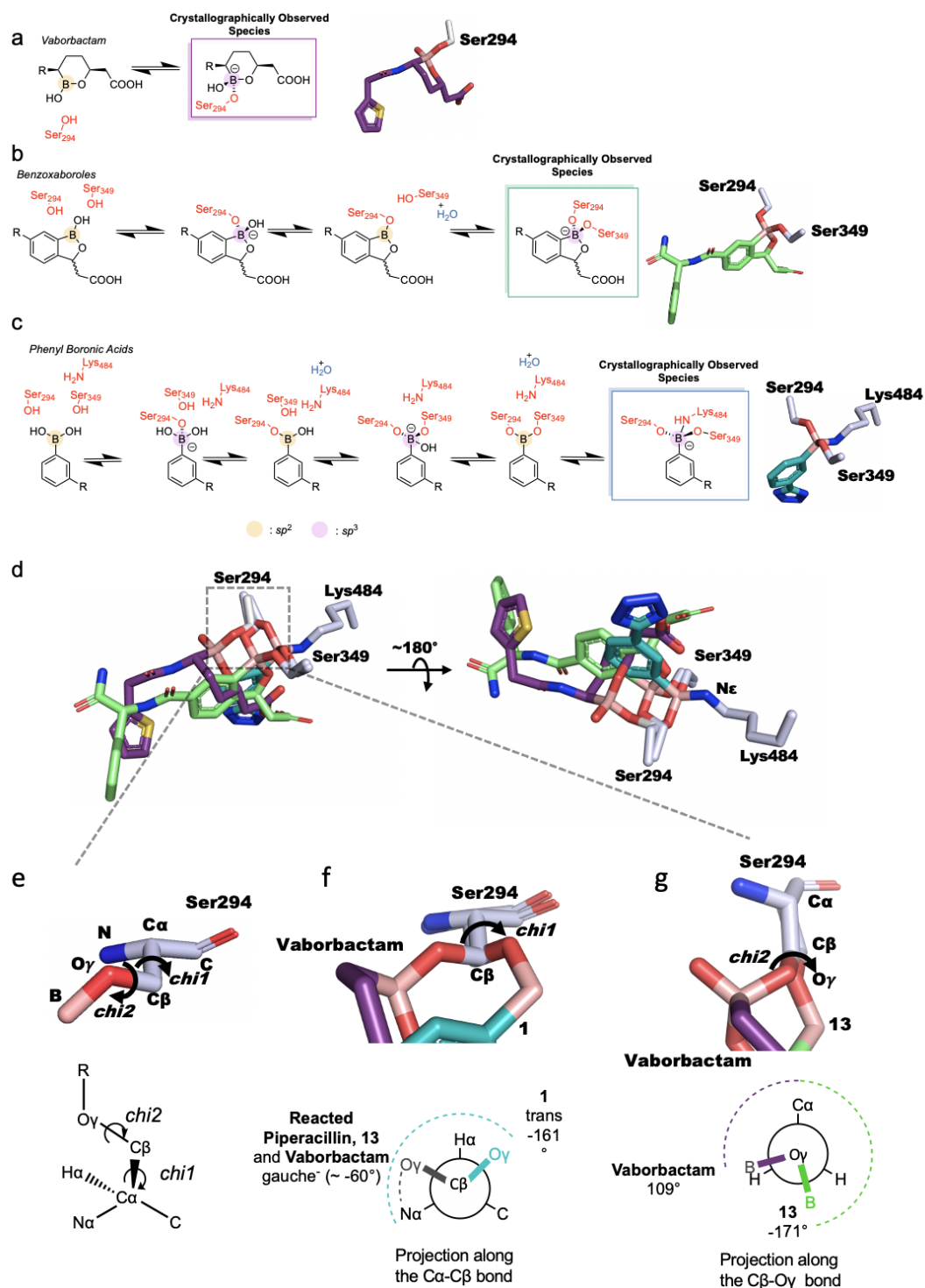


Figure 5.10. Three distinct binding modes of complexes of PBPs with boron-containing compounds. (a-c) Outline mechanisms for the formation of the different complexes. (a) Vaborbactam reacts mono-covalently with Ser294 of PaPBP3. (b) Benzoxaboroles (**3-16**) bind di-covalently to Ser294 and Ser349 of PaPBP3. (c) Phenyl boronic acids (**1** and **2**) bind tri-covalently to Ser294, Ser349 and Lys484 of PaPBP3, similarly to alkyl boronic acids reacting with R39 DD-peptidase

from *Actinomadura* sp.¹⁶. Boron must transition between sp^2 and sp^3 hybridisation states (highlighted in yellow and pink, respectively, Figure 5.1) to exchange hydroxyls for the nucleophilic side chain. The order in which nucleophilic side chains covalently react with the boron is unknown; (d) Two views of the overlay of crystallographically observed states of different boronates binding to PaPBP3, the lysine N ϵ is labelled. (e-g) The position of the boron atom within the active site relates to rotations of the *chi1* and *chi2* angles of the Ser294 sidechain from PaPBP3 (e). Ser349 (which binds to the boron of **13** and **1**) and Lys484 (which binds to the boron of **1**) are not shown. (e) Atom and angle labels of serine. (f) Newman projection aligned along the C α -C β bond of Ser294 of PaPBP3 and crystal structures of vaborbactam and **1**. Like a β -lactam reacted structure, the mono-covalently bonded vaborbactam structure has a Ser294 *chi1* angle gauche to the serine backbone amine, whilst the tri-covalent (**1**) complex with PaPBP3 has a *chi1* angle trans to the serine backbone amine. The di-covalently reacted PaPBP3:**13** also has a gauche *chi1* angle (Figure 5.S3), but unlike the mono-covalent structures, it has a Ser294 *chi2* angle of -171° . A complete set of structural views and Newman projections are shown in Figure 5.S3.

Structures of **3**, **4**, **8**, **10**, **13**, **14**, **15**, and **16** with PaPBP3 show a consistent positioning of the benzoxaborole relative to the active site, irrespective of C-6, C-5 or C-3 functionalisation (Figure 5.11). This is likely caused by the constraint of having both serines reacted to the boron.

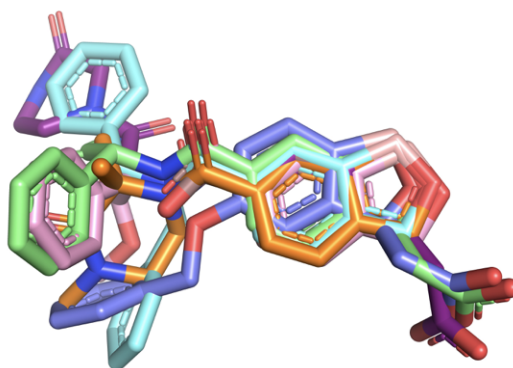


Figure 5.11. Overlay of various benzoxaborole conformations observed in complex with PaPBP3. Crystal structures of PaPBP3 with benzoxaborole compounds **3** (brown), **4** (orange), **8** (pink), **13** (green), **14** (purple), **15** (cyan), **16** (blue), reveal that they bind in a conserved mode. The protein structure is hidden for clarity. All compounds bind di-covalently: the tetrahedral boron is reacted with the hydroxyl groups of residues Ser294 and Ser349 (not shown for clarity) of the active site.

Analysis of the bond angles of the nucleophilic residues (Ser294, Ser349 and Lys484) shows how each of the different binding modes affects the protein (Figure 5.10 and Figure 5.S3). In each of the binding modes, the side chains of

Ser349 and Lys484 are not displaced significantly, with the O γ of Ser349 and the N ϵ of Lys484 moving <1 Ångström relative to their position in the piperacillin reacted structure PaBPB3 (PDB: 6R3X)³⁶. In contrast, Ser294 has a number of rotations of the first and second bonds of the side chain (described by dihedral angles *chi1* and *chi2*, Figure 5.10e). The PaBPB3 structures of mono-covalently reacted β -lactams (e.g. piperacillin) and vaborbactam, as well as di-covalently reacted benzoxaboroles (**3**, **4**, **8**, **10**, **13**, **14**, **15**, and **16**) all have a Ser294 *chi1* that is gauche⁻ ($\sim -60^\circ$) to the serine amine (as defined in reference⁷¹), whilst the tri-covalently reacted structure PaBPB3:1 has a trans *chi1* angle (Figure 5.10f and Figure 5.S3). The Ser294 *chi2* angle of the di-covalently reacted structures however is almost orthogonal to the *chi2* of the mono-covalently reacted structures (-171° vs 109° , relative to the C α), which displaces the boron to the right (as depicted in Figure 5.10d, left hand side image).

The previous report of a boronate engaging a PBP in a tri-covalent binding mode suggested that binding to the catalytic Ser49 (equivalent to Ser294) occurs first, with the other nucleophilic substitutions happening subsequently¹⁶. Our data cannot be used to determine an order of reactions. Tri-covalent substitution of benzoxaboroles with a reaction by Lys484 is prevented by the strength of the endocyclic B¹-O² bond of the benzoxaborole 5-membered ring^{72,73}.

As depicted in Figure 5.10, Lys484 must be neutrally charged to act as a nucleophile and form the observed tri-covalent complex. If a lysine is buried and in a hydrophobic region of the active site, it is possible for its pK_a to become more acidic and low pK_a lysines have been described in the literature^{74–78}. The equivalent neutral lysine has previously been proposed to act as a general base in the β -lactam de-acylation of PBP5¹⁸, although generally the lysine equivalent to Lys297 is proposed as the general base in the PBP active site^{79–81}.

The initial data presented here indicates that binding equilibrium is achieved at least within minutes. Previous reports have suggested that boron binds with a fast, weak reversible mode, which agrees with this data²⁰. The time resolution of the dilution method used is not good enough to observe behaviour on the seconds timescale, but work on the tri-covalent PBP:boron complex has suggested that the interaction is a rapid equilibrium association followed by a slower phase in which the covalent reaction occurs and the mono-covalent complex forms¹⁶. Following this, it was suggested the tri-covalent complex forms in rapid equilibrium with the

mono-covalent complex (Figure 5.10c) ¹⁶. As shown in Figure 5.1, boronates are thought to act as analogues of the PBP tetrahedral transition state ^{17–19}. The relevance of the multi-covalent complexes to this mimicry is unclear, and the evidence here is not enough to conclusively determine whether the multi-covalency affects the potency; it may only be a crystallographic artefact.

5.4.2 Structural Views

The benzoxaboroles were designed to engage the hydrogen bond network which piperacillin exploits when reacting with PaPBP3 (Figure 5.5), but the constrained benzoxaborole ring (Figure 5.11) prevented the formation of important active site hydrogen bonds. In particular, the hydrogen bond to Thr487 (which is formed by the C-6 amide of β -lactams (Figure 5.S4)) was not made. The conformation of the β 3 β -strand is thought to be associated with formation of the hydrophobic wall formation (Figure 1.4) ⁶⁸, perhaps by interactions of the inhibitor with Thr487 and Arg489. The β 3 strand of the PaPBP3:**13** has a similar conformation to the β 3 strand in the meropenem reacted PaPBP3 structure (Figure 5.12a). Additionally, in these structures Tyr409 forms a hydrogen-bond to the backbone carbonyl of Thr487. In contrast, when amoxicillin, aztreonam, ceftazidime and piperacillin react with PaPBP3, the inhibitors form a hydrogen-bond to the backbone carbonyl of Thr487 (Figure 5.S4). The constrained benzoxaborole core positions the C-6 amide 'above' the C-6 amide of reacted piperacillin and the larger distance prevents the benzoxaborole amide from interacting with Thr487 ((Figure 5.12b and c). A C-5 amide may be better positioned to engage this residue. A hydrogen bond is made by the C-6 amide to Asn351 (e.g. Figure 5.4b), but a C-5 amide may be unable to form this interaction. Interaction with Asn351 may be important as it is found in many β -lactams (e.g. piperacillin, Figure 5.5a).

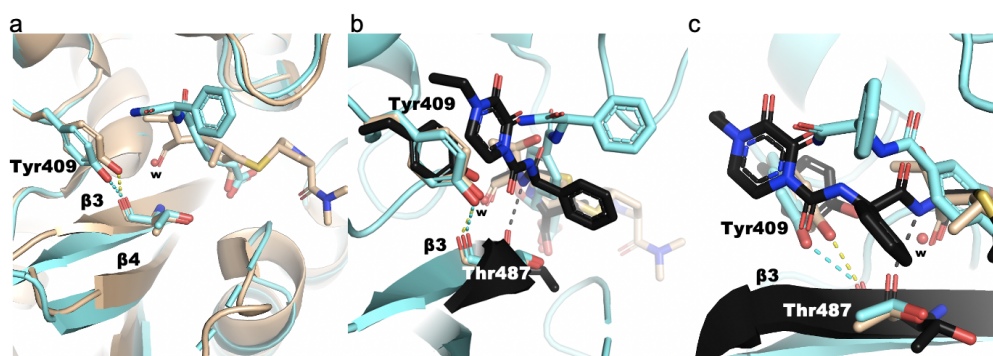


Figure 5.12. Comparisons between PaBP3 reacted with meropenem and **13 reveal similar conformations for the $\beta 3$ strand, unlike that of the piperacillin reacted crystal structure.** (a) Active site of the PaBP3:meropenem complex (beige, PDB code: 3PBR⁶⁸) compared to the PaBP3:**13** complex (cyan). (b and c) Two views of the $\beta 3$ strand conformation of the PaBP3:**13** complex (cyan) compared to the meropenem (beige) and piperacillin (black, PDB code: 6R3X)³⁶ reacted structures. Tyr409 and its hydrogen bond (dashed line) to the backbone amine of Thr487 is shown. A hydrogen bond between Thr487 and the reacted piperacillin amine is shown. The protein structure shown is the PaBP3:**13** complex, but the $\beta 3$ strand of the piperacillin reacted structure is overlaid. The conformation of the $\beta 3$ strand in the PaBP3:**13** or meropenem complexes is unlike the PaBP3 $\beta 3$ strand conformation seen when reacted with other β -lactams (piperacillin, ceftazidime, amoxicillin, aztreonam): Figure 5.S4.

The $\beta 3$ strand and $\beta 5$ - $\alpha 11$ loops of the PaBP3:**14** complex have conformations analogous to those of the piperacillin reacted PaBP3 structure (Figure 5.13). **14** has a ketopiperazine substituent (designed to mimic the diketopiperazine of piperacillin), but lacks a phenyl group analogous to that of the D-Phe of piperacillin. Like the diketopiperazine of piperacillin, the ketopiperazine of **14** forms hydrogen bonds with the O η oxygens of Tyr328 and Tyr407 (Figure 5.13), it is unclear whether there is link between the hydrogen bonds and the $\beta 3$ strand conformation.

One clear conclusion from comparing the compound structures and their affinity is that the presence of a C-3 acid group is important. The affinities of **14** ($K_i = 172.0 \pm 3.0 \mu\text{M}$) and **11** (residual activity by BOCILLIN FL FA > 90 %) or **13** ($K_i = 73.9 \pm 0.8 \mu\text{M}$) and **7** (RA > 90 %) nicely demonstrate the effect of a C-3 acid group (Table 5.3). This is consistent with the conservation of the C-3 (or equivalent) carboxylate group in β -lactams as well as studies which show that the addition of a C-3 acid group to benzoxaboroles leads to up to 100 fold increases in β -lactamase binding affinity⁸².

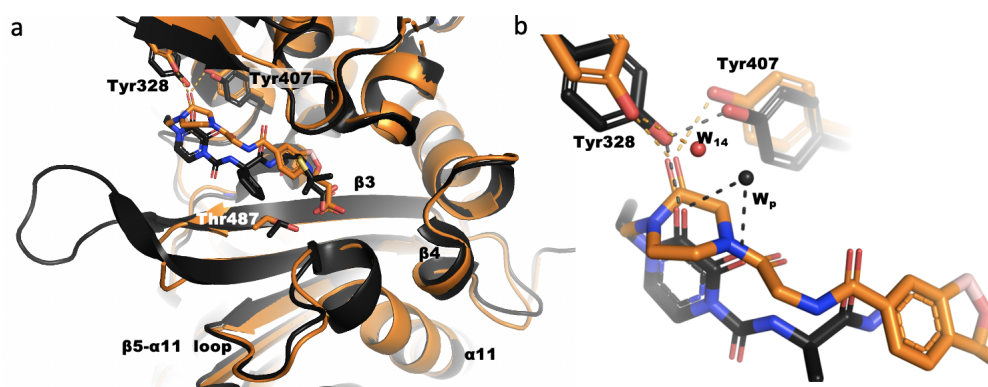


Figure 5.13. Comparisons between crystal structures of PaBPB3 reacted with piperacillin (black, PDB code: 6R3X³⁶) and 14 (orange). (a) The protein backbone conformation is similar in both structures, particularly the $\beta 3$ strand and the $\beta 5$ - $\alpha 11$ loop. The $\beta 3$ - $\beta 4$ loop is incomplete in the PaBPB3:14 complex, likely due to flexibility of this region (Chapter 4). (b) The hydrogen bonding network (dashed lines) around the ketopiperazine group of 14 and the diketopiperazine of piperacillin with Tyr328 and Tyr407. Waters from the PaBPB3:14 complex (W_{14}) and the piperacillin reacted structure (W_p), are shown.

The $\beta 5$ - $\alpha 11$ loop is a flexible region that undergoes induced fit upon β -lactam binding and forms a “hydrophobic wall” (Chapter 4). Several of the benzoxaboroles (**10**, **12**, **13**, **15** and **16**) were designed such that their phenyl groups might engage the hydrophobic wall. In all cases this was unsuccessful and the wall was not formed (Figure 5.14). The structures of the PaBPB3:15 and PaBPB3:16 show a phenyl is situated in the same region of the active site as the phenyl rings of reacted piperacillin, but with a different orientation of the ring. The phenyl of **13** sits at a distance from the expected position of the hydrophobic wall. It is possible that designing compounds that better exploit this part of the protein would improve their affinity, although it is not essential to inhibition of the protein as inhibitors such as meropenem do not lead to wall formation (PDB: 3PBR)⁶⁸.

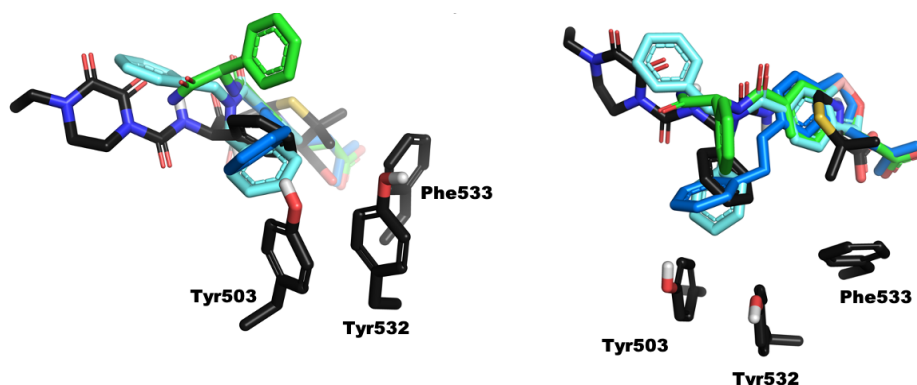


Figure 5.14. Phenyl groups of the benzoxaboroles were designed to engage the hydrophobic wall, but do not do so. Two views of the crystallographically observed conformations of PaPBP3 in complex with **13** (green), **15** (cyan) and **16** (blue), compared to reacted piperacillin and residues of the hydrophobic wall (Tyr503, Tyr532 and Phe533) from the piperacillin reacted PaPBP3 structure (black, PDB code: 6R3X)³⁶.

2 induces a novel conformation of both the PaPBP3 α 10- β 3 and β 5- α 11 loops and ligands **1** and **14** also modify the β 5- α 11. These changes can be used to understand the conformational flexibility of the protein; this is discussed further in Chapter 4.

5.5 Future Work and Conclusions

The benzoxaborole compounds investigated were not very potent in activity but this study demonstrated their potential as a new class of PBP inhibitors. Future studies investigating benzoxaboroles will be able to benefit from the structural data presented here, in particular the observation that the benzoxaborole warhead binds to the protein in a highly constrained and consistent manner (Figure 5.11), a conformation which appears to be relatively insensitive to modification at three different positions of the benzoxaborole (C-3, C-5 and C-6). This fact, and some of the insights gained from the crystal structures (section 5.3.7) could be used to generate further iterations of the compound series, with the aim of improving affinity. Derivatisation of the C-4, and C-7 positions, and further exploration of the C-5 positions⁸² may be interesting and lead to improved potency.

High affinity HMM PBP boron-based inhibitors have yet to be discovered^{11–14}, with only a single example in the academic literature of a PBP-targeting,

boron-containing compound having antimicrobial activity¹⁴. The most potent (and with antimicrobial activity) are 6,6-bicyclic boronates (a taniborbactam-like scaffold, Table 1.1) in the patent literature^{21,22}. The efficacy of boronates against the structurally related β -lactamases offers hope for the discovery of more effective boronic PBP inhibitors, but an explanation for the much weaker affinities of reported boronates against PBPs is not yet forthcoming²³.

The lack of antimicrobial activity is disappointing. This can be explained to some degree by the compounds' relatively low on-target affinity, perhaps coupled to poor cellular accumulation (although the 'permeabilised' *E. coli* and *P. aeruginosa* strains showed no increase in activity). An alternative hypothesis posits that the mode of binding is important for inhibition of PBP cellular functioning and the apparent rapid equilibrium binding of these boronates is not sufficient to prevent the binding of the polymeric PBP3 substrate. In this scenario, the natural substrate is fed continuously into the PBP3 activity site at a high effective local concentration, easily displacing any bound boronate. In contrast, the effective irreversible inhibition with a β -lactam entirely prevents natural substrate binding and transpeptidation. It may be possible to use novel natural substrate assays⁸³ to test the ability of boronates to prevent transpeptidation and create new benzoxaborole derivatives which do this more effectively, thereby improving their antimicrobial activity.

The three binding modes of boronates engaging with HMM PBPs have not previously been reported, but the binding modes have precedence in other proteins^{16,27}. More work is needed to understand the significance of these observations for inhibitor design and their importance for potency. It might be expected that the multivalent reaction increases the potency, but it is not possible to make this conclusion from the data. A better understanding of the time-dependence of the reaction may be beneficial. Mass spectrometry or NMR (particularly ¹¹B NMR²⁷) studies would perhaps be the best approach for this as these techniques are able to probe the hybridisation state of the boron; mass spectrometry would be able to identify the mass change associated with the loss and gain of water in the transition to multivalency (e.g. Figure 5.10b). A working SPR system (Chapter 2) would provide an insight into the kinetics of the reaction but is unlikely to give the same level of detail about the state of the boron atom. Kinetic studies employing a S349A mutant of PaPBP3 (Chapter 6) could be used to study the binding of benzoxaboroles under conditions in which only a single serine is available in the active site.

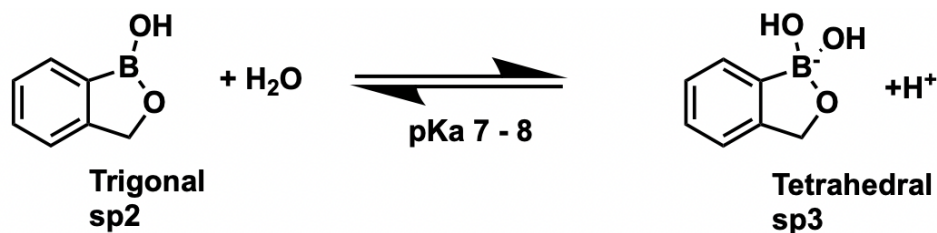


Figure 5.15. The hybridisation state transition of benzoxaboroles. Transition between sp^2 and sp^3 in benzoxaboroles following nucleophilic attack by water. pK_a is typically 7-8 but can be modified by ring substituents ⁸⁴.

The pK_a of a boronate is a measure of its ability to transition between the sp^2 and sp^3 states (Figure 5.15). It has been shown that substitutions on the benzoxaborole can modify the boronate pK_a by changing the stability of the anionic (sp^3) species ^{84,85}, which in turn can affect a compound's covalent ⁸⁵ and non-covalent interactions ⁸⁶. Given the likely importance of the covalent interaction for the binding of benzoxaboroles to PBPs, optimisation of the pK_a of the boron may be important as optimisation of the non-covalent interactions of the sidechains. It may be difficult to distinguish the contributions of the two components, as any additional group will also contribute to the non-covalent interactions of the compound.

In the next chapter the possibility that the di-covalently bound benzoxaborole is acting as a transition state analogue in the transfer from one active serine to another is discussed. It appears that boronate compounds may have many uses in the inhibition and study of PBPs.

5.6 References

- 1 Richardson PG, Hideshima T, Anderson KC. Bortezomib (PS-341): A Novel, First-in-Class Proteasome Inhibitor for the Treatment of Multiple Myeloma and Other Cancers. *Cancer Control* 2003; **10**: 361–369.
- 2 Kane RC, Bross PF, Farrell AT, Pazdur R. Velcade[®]: U.S. FDA Approval for the Treatment of Multiple Myeloma Progressing on Prior Therapy. *The Oncologist* 2003; **8**: 508–513.
- 3 Lienhard GE, Koehler KA. 2-Phenylethaneboronic acid, a possible transition-state analog for chymotrypsin. *Biochemistry* 1971; **10**: 2477–2483.
- 4 Smoum R, Rubinstein A, Dembitsky VM, Srebnik M. Boron Containing Compounds as Protease Inhibitors. *Chem Rev* 2012; **112**: 4156–4220.
- 5 Hecker SJ, Reddy KR, Totrov M, Hirst GC, Lomovskaya O, Griffith DC *et al*. Discovery of a Cyclic Boronic Acid β -Lactamase Inhibitor (RPX7009) with Utility vs Class A Serine Carbapenemases. *J Med Chem* 2015; **58**: 3682–3692.
- 6 Lomovskaya O, Sun D, Rubio-Aparicio D, Nelson K, Tsivkovski R, Griffith DC *et*

- al.* Vaborbactam: Spectrum of Beta-Lactamase Inhibition and Impact of Resistance Mechanisms on Activity in Enterobacteriaceae. *Antimicrob Agents Chemother* 2017; **61**: e01443-17, e01443-17.
- 7 Tsivkovski R, Lomovskaya O. Biochemical Activity of Vaborbactam. *Antimicrob Agents Chemother* 2019; **64**: e01935-19, /aac/64/2/AAC.01935-19.atom.
- 8 Krajnc A, Brem J, Hinchliffe P, Calvopiña K, Panduwawala TD, Lang PA *et al.* Bicyclic Boronate VNRX-5133 Inhibits Metallo- and Serine- β -Lactamases. *J Med Chem* 2019; **62**: 8544–8556.
- 9 Liu B, Trout REL, Chu G-H, McGarry D, Jackson RW, Hamrick JC *et al.* Discovery of Taniborbactam (VNRX-5133): A Broad-Spectrum Serine- and Metallo- β -lactamase Inhibitor for Carbapenem-Resistant Bacterial Infections. *J Med Chem* 2020; **63**: 2789–2801.
- 10 Hamrick JC, Docquier J-D, Uehara T, Myers CL, Six DA, Chatwin CL *et al.* VNRX-5133 (Taniborbactam), a Broad-Spectrum Inhibitor of Serine- and Metallo- β -Lactamases, Restores Activity of Cefepime in *Enterobacterales* and *Pseudomonas aeruginosa*. *Antimicrob Agents Chemother* 2019; **64**: e01963-19, /aac/64/3/AAC.01963-19.atom.
- 11 Brem J, Cain R, Cahill S, McDonough MA, Clifton IJ, Jiménez-Castellanos J-C *et al.* Structural basis of metallo- β -lactamase, serine- β -lactamase and penicillin-binding protein inhibition by cyclic boronates. *Nat Commun* 2016; **7**: 12406.
- 12 Zervosen A, Bouillez A, Herman A, Amoroso A, Joris B, Sauvage E *et al.* Synthesis and evaluation of boronic acids as inhibitors of Penicillin Binding Proteins of classes A, B and C. *Bioorg Med Chem* 2012; **20**: 3915–3924.
- 13 Inglis SR, Zervosen A, Woon ECY, Gerards T, Teller N, Fischer DS *et al.* Synthesis and Evaluation of 3-(Dihydroxyboryl)benzoic Acids as D₁, D₂-Carboxypeptidase R39 Inhibitors. *J Med Chem* 2009; **52**: 6097–6106.
- 14 Contreras-Martel C, Amoroso A, Woon ECY, Zervosen A, Inglis S, Martins A *et al.* Structure-Guided Design of Cell Wall Biosynthesis Inhibitors That Overcome β -Lactam Resistance in *Staphylococcus aureus* (MRSA). *ACS Chem Biol* 2011; **6**: 943–951.
- 15 Woon ECY, Zervosen A, Sauvage E, Simmons KJ, Živec M, Inglis SR *et al.* Structure Guided Development of Potent Reversibly Binding Penicillin Binding Protein Inhibitors. *ACS Med Chem Lett* 2011; **2**: 219–223.
- 16 Zervosen A, Herman R, Kerff F, Herman A, Bouillez A, Prati F *et al.* Unexpected Tricovaleent Binding Mode of Boronic Acids within the Active Site of a Penicillin-Binding Protein. *J Am Chem Soc* 2011; **133**: 10839–10848.
- 17 Pechenov A, Stefanova ME, Nicholas RA, Peddi S, Gutheil WG. Potential Transition State Analogue Inhibitors for the Penicillin-Binding Proteins. *Biochemistry* 2003; **42**: 579–588.
- 18 Nicola G, Peddi S, Stefanova M, Nicholas RA, Gutheil WG, Davies C. Crystal Structure of *Escherichia coli* Penicillin-Binding Protein 5 Bound to a Tripeptide Boronic Acid Inhibitor: A Role for Ser-110 in Deacylation [†]. *Biochemistry* 2005; **44**: 8207–8217.
- 19 Dzhekieva L, Rocaboy M, Kerff F, Charlier P, Sauvage E, Pratt RF. Crystal Structure of a Complex between the Actinomadura R39 dd-Peptidase and a Peptidoglycan-mimetic Boronate Inhibitor: Interpretation of a Transition State Analogue in Terms of Catalytic Mechanism. *Biochemistry* 2010; **49**: 6411–6419.
- 20 Dzhekieva L, Kumar I, Pratt RF. Inhibition of Bacterial DD-Peptidases (Penicillin-Binding Proteins) in Membranes and in Vivo by Peptidoglycan-Mimetic Boronic Acids. *Biochemistry* 2012; **51**: 2804–2811.
- 21 Burns J, Daigle D, Chu G-H, Jackson RW, Hamrick J, Boyd SA *et al.* PENICILLIN-BINDING PROTEIN INHIBITORS (2018). .
- 22 Burns J, Daigle D, Chu G-H, Hamrick J, Lucas, M, Boyd SA *et al.* PENICILLIN-BINDING PROTEIN INHIBITORS (2018). .

- 23 Krajnc A, Lang PA, Panduwawala TD, Brem J, Schofield CJ. Will morphing boron-based inhibitors beat the β -lactamases? *Curr Opin Chem Biol* 2019; **50**: 101–110.
- 24 Groll M, Berkers CR, Ploegh HL, Ova H. Crystal Structure of the Boronic Acid-Based Proteasome Inhibitor Bortezomib in Complex with the Yeast 20S Proteasome. *Structure* 2006; **14**: 451–456.
- 25 Sharma N, Sharma D. An upcoming drug for onychomycosis: Tavaborole. *J Pharmacol Pharmacother* 2015; **6**: 236.
- 26 Rock FL, Mao W, Yaremchuk A, Tukalo M, Crepin T, Zhou H *et al*. An Antifungal Agent Inhibits an Aminoacyl-tRNA Synthetase by Trapping tRNA in the Editing Site. *Science* 2007; **316**: 1759–1761.
- 27 Transue TR, Gabel SA, London RE. NMR and Crystallographic Characterization of Adventitious Borate Binding by Trypsin. *Bioconjug Chem* 2006; **17**: 300–308.
- 28 Stoll VS, Eger BT, Hynes RC, Martichonok V, Jones JB, Pai EF. Differences in Binding Modes of Enantiomers of 1-Acetamido Boronic Acid Based Protease Inhibitors: Crystal Structures of γ -Chymotrypsin and Subtilisin Carlsberg Complexes ^{†,‡}. *Biochemistry* 1998; **37**: 451–462.
- 29 Martin JS, MacKenzie CJ, Fletcher D, Gilbert IH. Characterising covalent warhead reactivity. *Bioorg Med Chem* 2019; **27**: 2066–2074.
- 30 Lapa GB, Mirchink EP, Isakova EB, Preobrazhenskaya MN. Two approaches to the use of benzo[c][1,2]oxaboroles as active fragments for synthetic transformation of clarithromycin. *J Enzyme Inhib Med Chem* 2017; **32**: 452–456.
- 31 Hernandez V, Crépin T, Palencia A, Cusack S, Akama T, Baker SJ *et al*. Discovery of a Novel Class of Boron-Based Antibacterials with Activity against Gram-Negative Bacteria. *Antimicrob Agents Chemother* 2013; **57**: 1394–1403.
- 32 Hu Q-H, Liu R-J, Fang Z-P, Zhang J, Ding Y-Y, Tan M *et al*. Discovery of a potent benzoxaborole-based anti-pneumococcal agent targeting leucyl-tRNA synthetase. *Sci Rep* 2013; **3**: 2475.
- 33 Printsevskaya S, Reznikova M, Korolev A, Lapa G, Olsufyeva E, Preobrazhenskaya M *et al*. Synthesis and study of antibacterial activities of antibacterial glycopeptide antibiotics conjugated with benzoxaboroles. *Future Med Chem* 2013; **5**: 641–652.
- 34 Alam MA, Arora K, Gurrapu S, Jonnalagadda SK, Nelson GL, Kiprof P *et al*. Synthesis and evaluation of functionalized benzoboroxoles as potential anti-tuberculosis agents. *Tetrahedron* 2016; **72**: 3795–3801.
- 35 Kidd SL, Fowler E, Reinhardt T, Compton T, Mateu N, Newman H *et al*. Demonstration of the utility of DOS-derived fragment libraries for rapid hit derivatisation in a multidirectional fashion. *Chem Sci* 2020; **11**: 10792–10801.
- 36 Bellini D, Koekemoer L, Newman H, Dowson CG. Novel and Improved Crystal Structures of *H. influenzae*, *E. coli* and *P. aeruginosa* Penicillin-Binding Protein 3 (PBP3) and *N. gonorrhoeae* PBP2: Toward a Better Understanding of β -Lactam Target-Mediated Resistance. *J Mol Biol* 2019; **431**: 3501–3519.
- 37 Newman H, Krajnc A, Bellini D, Eyermann CJ, Boyle GA, Paterson NG *et al*. High-Throughput Crystallography Reveals Boron Containing Inhibitors of a Penicillin Binding Protein with Di- and Tri-covalent Binding Modes. *J Med Chem*; **Accepted**. doi:<https://doi.org/10.1021/acs.jmedchem.1c00717>.
- 38 Tickle IJ, Flensburg C, Keller P, Paciorek W, Sharff A, Vornrhein C *et al*. STARANISO. Global Phasing Ltd.: Cambridge, United Kingdom <http://staraniso.globalphasing.org/cgi-bin/staraniso.cgi>. Accessed 25/06/20
- 39 Vornrhein C, Flensburg C, Keller P, Sharff A, Smart O, Paciorek W *et al*. Data processing and analysis with the *autoPROC* toolbox. *Acta Crystallogr D Biol Crystallogr* 2011; **67**: 293–302.
- 40 McCoy AJ, Grosse-Kunstleve RW, Adams PD, Winn MD, Storoni LC, Read RJ. Phaser crystallographic software. *J Appl Crystallogr* 2007; **40**: 658–674.
- 41 Emsley P, Lohkamp B, Scott WG, Cowtan K. Features and development of

- Coot. *Acta Crystallogr D Biol Crystallogr* 2010; **66**: 486–501.
- 42 Vagin AA, Steiner RA, Lebedev AA, Potterton L, McNicholas S, Long F *et al*. *REFMAC 5* dictionary: organization of prior chemical knowledge and guidelines for its use. *Acta Crystallogr D Biol Crystallogr* 2004; **60**: 2184–2195.
 - 43 Winn MD, Ballard CC, Cowtan KD, Dodson EJ, Emsley P, Evans PR *et al*. Overview of the CCP 4 suite and current developments. *Acta Crystallogr D Biol Crystallogr* 2011; **67**: 235–242.
 - 44 Adams PD, Afonine PV, Bunkóczi G, Chen VB, Davis IW, Echols N *et al*. *PHENIX*: a comprehensive Python-based system for macromolecular structure solution. *Acta Crystallogr D Biol Crystallogr* 2010; **66**: 213–221.
 - 45 Smart OS, Womack TO, Sharff A, Flensburg C, Keller P, Paciorek W *et al*. *grade*. Global Phasing Ltd., 2011 <http://grade.globalphasing.org>. Accessed 07/04/21
 - 46 Williams CJ, Headd JJ, Moriarty NW, Prisant MG, Videau LL, Deis LN *et al*. MolProbity: More and better reference data for improved all-atom structure validation: PROTEIN SCIENCE.ORG. *Protein Sci* 2018; **27**: 293–315.
 - 47 McNicholas S, Potterton E, Wilson KS, Noble MEM. Presenting your structures: the CCP 4 *mg* molecular-graphics software. *Acta Crystallogr D Biol Crystallogr* 2011; **67**: 386–394.
 - 48 Shapiro AB, Gu R-F, Gao N, Livchak S, Thresher J. Continuous fluorescence anisotropy-based assay of BOCILLIN FL penicillin reaction with penicillin binding protein 3. *Anal Biochem* 2013; **439**: 37–43.
 - 49 Sacco MD, Kroeck KG, Kemp MT, Zhang X, Andrews LD, Chen Y. Influence of the α -Methoxy Group on the Reaction of Temocillin with *Pseudomonas aeruginosa* PBP3 and CTX-M-14 β -Lactamase. *Antimicrob Agents Chemother* 2019; **64**: e01473-19, /aac/64/1/AAC.01473-19.atom.
 - 50 Johnson KA. New standards for collecting and fitting steady state kinetic data. *Beilstein J Org Chem* 2019; **15**: 16–29.
 - 51 Adam M, Fraipont C, Rhazi N, Nguyen-Distèche M, Lakaye B, Frère JM *et al*. The bimodular G57-V577 polypeptide chain of the class B penicillin-binding protein 3 of *Escherichia coli* catalyzes peptide bond formation from thioesters and does not catalyze glycan chain polymerization from the lipid II intermediate. *J Bacteriol* 1997; **179**: 6005–6009.
 - 52 Jamin M, Damblon C, Millier S, Hakenbeck R, Frère JM. Penicillin-binding protein 2x of *Streptococcus pneumoniae*: enzymic activities and interactions with beta-lactams. *Biochem J* 1993; **292**: 735–741.
 - 53 Boes A, Olatunji S, Breukink E, Terrak M. Regulation of the Peptidoglycan Polymerase Activity of PBP1b by Antagonist Actions of the Core Divisome Proteins FtsBLQ and FtsN. *mBio* 2019; **10**. doi:10.1128/mBio.01912-18.
 - 54 De Meester F, Joris B, Reckinger G, Bellefroid-Bourguignon C, Frère J-M, Waley SG. Automated analysis of enzyme inactivation phenomena. *Biochem Pharmacol* 1987; **36**: 2393–2403.
 - 55 Graves-Woodward K, Pratt RF. Reaction of soluble penicillin-binding protein 2a of methicillin-resistant *Staphylococcus aureus* with β -lactams and acyclic substrates: kinetics in homogeneous solution. *Biochem J* 1998; **332**: 755–761.
 - 56 van Berkel SS, Nettleship JE, Leung IKH, Brem J, Choi H, Stuart DI *et al*. Binding of (5 S)-Penicilloic Acid to Penicillin Binding Protein 3. *ACS Chem Biol* 2013; **8**: 2112–2116.
 - 57 Zgurskaya HI, López CA, Gnanakaran S. Permeability Barrier of Gram-Negative Cell Envelopes and Approaches To Bypass It. *ACS Infect Dis* 2015; **1**: 512–522.
 - 58 Dougherty PF, Yotter DW, Matthews TR. Microdilution Transfer Plate Technique for Determining In Vitro Synergy of Antimicrobial Agents. *Antimicrob Agents Chemother* 1977; **11**: 225–228.
 - 59 Berthold MR, Cebron N, Dill F, Gabriel TR, Kötter T, Meinel T *et al*. KNIME - the Konstanz information miner: version 2.0 and beyond. *ACM SIGKDD Explor*

- News* 2009; **11**: 26–31.
- 60 Ashton M, Barnard J, Casset F, Charlton M, Downs G, Gorse D *et al*. Identification of Diverse Database Subsets using Property-Based and Fragment-Based Molecular Descriptions. *Quant Struct-Act Relatsh* 2002; **21**: 598–604.
 - 61 *RDKit: Open-source cheminformatics*; <http://www.rdkit.org>. Accessed 24/02/21.
 - 62 Wang R, Fu Y, Lai L. A New Atom-Additive Method for Calculating Partition Coefficients. *J Chem Inf Comput Sci* 1997; **37**: 615–621.
 - 63 Enamine Serine focused Covalent Fragments Library. Serine Focus. Covalent Fragn. 2020.
https://enamine.net/index.php?option=com_content&view=article&id=616&Itemid=720). Accessed 17/06/21.
 - 64 Congreve M, Carr R, Murray C, Jhoti H. A 'Rule of Three' for fragment-based lead discovery? *Drug Discov Today* 2003; **8**: 876–877.
 - 65 Lipinski CA, Lombardo F, Dominy BW, Feeney PJ. Experimental and computational approaches to estimate solubility and permeability in drug discovery and development settings. *Adv Drug Deliv Rev* 1997; **23**: 3–25.
 - 66 Alterio V, Cadoni R, Esposito D, Vullo D, Fiore AD, Monti SM *et al*. Benzoxaborole as a new chemotype for carbonic anhydrase inhibition. *Chem Commun* 2016; **52**: 11983–11986.
 - 67 Dave K, Palzkill T, Pratt RF. Neutral β -Lactams Inactivate High Molecular Mass Penicillin-Binding Proteins of Class B1, Including PBP2a of MRSA. *ACS Med Chem Lett* 2014; **5**: 154–157.
 - 68 Han S, Zaniewski RP, Marr ES, Lacey BM, Tomaras AP, Evdokimov A *et al*. Structural basis for effectiveness of siderophore-conjugated monocarbams against clinically relevant strains of *Pseudomonas aeruginosa*. *Proc Natl Acad Sci* 2010; **107**: 22002–22007.
 - 69 Gamrat JM, Mancini G, Burke SJ, Colandrea RC, Sadowski NR, Figula BC *et al*. Protection of the Benzoxaborole Moiety: Synthesis and Functionalization of Zwitterionic Benzoxaborole Complexes. *J Org Chem* 2018; **83**: 6193–6201.
 - 70 Krishnamoorthy G, Wolloscheck D, Weeks JW, Croft C, Rybenkov VV, Zgurskaya HI. Breaking the permeability barrier of *Escherichia coli* by controlled hyperporination of the outer membrane. *Antimicrob Agents Chemother* 2016; : AAC.01882-16.
 - 71 Dunbrack RL, Karplus M. Conformational analysis of the backbone-dependent rotamer preferences of protein sidechains. *Nat Struct Biol* 1994; **1**: 334–340.
 - 72 Cummings WM, Cox CH, Snyder HR. Arylboronic acids. Medium-size ring-containing boronic ester groups. *J Org Chem* 1969; **34**: 1669–1674.
 - 73 Vshyvenko S, Clapson ML, Suzuki I, Hall DG. Characterization of the Dynamic Equilibrium between Closed and Open Forms of the Benzoxaborole Pharmacophore. *ACS Med Chem Lett* 2016; **7**: 1097–1101.
 - 74 Paetzel M, Strynadka NCJ, Tschantz WR, Casareno R, Bullinger PR, Dalbey RE. Use of Site-directed Chemical Modification to Study an Essential Lysine in *Escherichia coli* Leader Peptidase. *J Biol Chem* 1997; **272**: 9994–10003.
 - 75 Arabshahi A, Frey PA. Standard Free Energy for the Hydrolysis of Adenylylated T4 DNA Ligase and the Apparent pK of Lysine 159. *J Biol Chem* 1999; **274**: 8586–8588.
 - 76 Bollenbach TJ, Mesecar AD, Nowak T. Role of Lysine 240 in the Mechanism of Yeast Pyruvate Kinase Catalysis. *Biochemistry* 1999; **38**: 9137–9145.
 - 77 Harris TK, Wu G, Massiah MA, Mildvan AS. Mutational, Kinetic, and NMR Studies of the Roles of Conserved Glutamate Residues and of Lysine-39 in the Mechanism of the MutT Pyrophosphohydrolase [†]. *Biochemistry* 2000; **39**: 1655–1674.
 - 78 Isom DG, Castaneda CA, Cannon BR, Garcia-Moreno E. B. Large shifts in pKa values of lysine residues buried inside a protein. *Proc Natl Acad Sci* 2011; **108**:

- 5260–5265.
- 79 Stefanova ME, Davies C, Nicholas RA, Gutheil WG. pH, inhibitor, and substrate specificity studies on *Escherichia coli* penicillin-binding protein 5. *Biochim Biophys Acta BBA - Protein Struct Mol Enzymol* 2002; **1597**: 292–300.
 - 80 Davies C, White SW, Nicholas RA. Crystal Structure of a Deacylation-defective Mutant of Penicillin-binding Protein 5 at 2.3-Å Resolution. *J Biol Chem* 2001; **276**: 616–623.
 - 81 Thomas B, Wang Y, Stein RL. Kinetic and Mechanistic Studies of Penicillin-Binding Protein 2x from *Streptococcus pneumoniae*. *Biochemistry* 2001; **40**: 15811–15823.
 - 82 McKinney DC, Zhou F, Eyermann CJ, Ferguson AD, Prince DB, Breen J *et al.* 4,5-Disubstituted 6-Aryloxy-1,3-dihydrobenzo[c][1,2]oxaboroles Are Broad-Spectrum Serine β -Lactamase Inhibitors. *ACS Infect Dis* 2015; **1**: 310–316.
 - 83 Catherwood AC, Lloyd AJ, Tod JA, Chauhan S, Slade SE, Walkowiak GP *et al.* Substrate and Stereochemical Control of Peptidoglycan Cross-Linking by Transpeptidation by *Escherichia coli* PBP1B. *J Am Chem Soc* 2020; **142**: 5034–5048.
 - 84 Adamczyk-Woźniak A, Borys KM, Sporyński A. Recent Developments in the Chemistry and Biological Applications of Benzoxaboroles. *Chem Rev* 2015; **115**: 5224–5247.
 - 85 Tomsho JW, Pal A, Hall DG, Benkovic SJ. Ring Structure and Aromatic Substituent Effects on the pK_a of the Benzoxaborole Pharmacophore. *ACS Med Chem Lett* 2012; **3**: 48–52.
 - 86 Akama T, Dong C, Virtucio C, Sullivan D, Zhou Y, Zhang Y-K *et al.* Linking Phenotype to Kinase: Identification of a Novel Benzoxaborole Hinge-Binding Motif for Kinase Inhibition and Development of High-Potency Rho Kinase Inhibitors. *J Pharmacol Exp Ther* 2013; **347**: 615–625.

Chapter 5.S. Supplemental Information for Chapter 5

5.S1 Fragments Screened

O=C(Nc1cccc(B(O)O)c1)C1CCCCO1
O=C(c1cc2c(c1)CCCC2)N1CC=C(B(O)O)CC1
OB(O)c1cccc2c(c1)OC(F)O2
CC1(C)OB(c2cnc(C3CC3)O2)OC1(C)C
O=C(O)c1cccc2c(c1)COB2O
CC1CCC(C)N(C(=O)c2cccc(B(O)O)c2)C1
CC[C@@H](Cc1cccc1)NC(=O)c1ccc2c(c1)B(O)OC2
CCN(C(=O)c1ccc2c(c1)B(O)OC2)[C@H]1CCOC(C)(C)C1
CC[C@@H](Cc1cccc1)NC(=O)c1ccc2c(c1)COB2O
CSCCCNC(=O)c1ccc(B(O)O)cc1
C[C@H](CC(=O)c1cccs1)NC(=O)c1ccc2c(c1)B(O)OC2
CCn1cccc1B1OC(C)(C)C(C)O1
O[B](O)c1cccc(c1)C(=O)NCCN1CCCC1
O[B](O)c1cccc(c1)-n1ccn1
CC(C)(C)OC(=O)NCc1cccc(c1)[B](O)O
O[B](O)c1cc(ccc1F)C(=O)NC1CCCC1
O[B](O)c1cccc(c1)-c1nnn[nH]1
COc1ccc(-c2cnc2)cc1B(O)O
Cc1cc(C)n(-c2cccc(B(O)O)c2)n1
O=C(O)c1ccc(B(O)O)cc1
O=C1ccccn1Cc1ccc(B(O)O)cc1
OB(O)c1cnn(-c2cccc(C(F)(F)F)c2)c1
CCC1(O)CCN(C(=O)c2ccc(B(O)O)c(F)c2)CC1
CCN(C(=O)c1cccc(B(O)O)c1)C1CCOC(C)(C)C1
CN(C)c1ncc(CNc2ccc3c(c2)B(O)OC(C)(C)C3)s1
O=S(=O)(c1ccccc1)N1CCC(B(O)O)C1
O=C(c1ccccc1)N1CCC(B(O)O)C1
OB(O)C1CCN(Cc2cnc(C3CCC3)nn2)C1
OB(O)C1=CCN(Cc2cnc(C3CCC3)nc2)CC1
OB(O)C1=CCN(Cc2cnc(C3CCC3)nn2)CC1
O=C(C1CCc2cc(F)ccc21)N1CC=C(B(O)O)CC1
OB(O)c1ccc(Cn2ccn2)c(F)c1
CC(=O)Nc1ccc(B2OC(C)(C)C(C)(C)O2)cn1
OB(O)c1ccc(C(F)(F)F)O1
O=c1[nH]cc(B(O)O)cc1F
Cc1nc(N)ccc1B1OC(C)(C)C(C)O1
CNc1ncc(B2OC(C)(C)C(C)O2)cn1
OB1OCc2cc(Cl)ccc21
COc1cc(OC)cc(B(O)O)c1
CC1(C)OB(C2=CCNCC2)OC1(C)C
CS(=O)(=O)Nc1ccc(B(O)O)cc1
COc1ncc(B2OC(C)(C)C(C)O2)cn1
CC1(C)OB(c2sc3c2OCCO3)OC1(C)C
CC1(C)OB(c2cnc(C(F)F)c2)OC1(C)C
CC1(C)OB(c2cnn2C2CCOCC2)OC1(C)C
Cc1ncc(B2OC(C)(C)C(C)O2)s1
OB(O)c1cnc(-n2ccn2)c1
CC1(C)OB([C@H]2C3CCN(CC3)S2(=O)=O)OC1(C)C
C[C@H]1OB(O)c2cc(CO)c(F)cc21
OB(O)c1ccc(OCc2cccn2)cc1
COc1ccc(C)cc1CC(=O)Nc1ccc2c(c1)B(O)OCC2
CC1(C)Cc2ccc(NC(=O)Cn3cnc4cccc43)cc2B(O)O1
CC1OCCC12CN(C(=O)c1ccc(B(O)O)cc1)CCO2
C[C@H](C#N)CNc1cccc1B(O)O
Cn1ncc(C2CC2)c1CN1CC=C(B(O)O)CC1
OB(O)c1cccc(OCN2CCCC2)c1
CCC1(O)CCN(C(=O)c2cc(B(O)O)ccc2F)CC1
O=C(NCC1CCC(O)C1)c1cc(B(O)O)ccc1F
C[C@H](O)(CCc1ccccc1)C(=O)Nc1ccc2c(c1)B(O)OCC2
CC1CCC(C)N(C(=O)c2ccc3c(c2)B(O)OC3)C1
O=C(NCC1CCC(O)C1)c1ccc(B(O)O)cc1
CC1(C)Cc2ccc(NC(=O)[C@H]3CCCCO3)cc2B(O)O1

O=C(c1ccnn1C1CCCC1)N1CCC(B(O)O)C1
Cc1cc2cn[nH]c2cc1B(O)O
OB(O)c1cccc(C2CC2)cc1Cl
O=C(O)c1ccc2c(c1)B(O)OC2
CCOC1CC(c2nc(-c3cccc(B(O)O)c3)no2)C1
CCN(C(=O)c1cc(B(O)O)ccc1F)C1CCOC(C)(C)C1
CN1CCN(C(=O)c2ccc3c(c2)B(O)OC3)C(C)C1=O
O=C(NCC1CCC(O)C1)c1cccc(B(O)O)c1
CC1(C)OB(c2cnn3ccncc23)OC1(C)C
CSCCCNC(=O)c1cc(B(O)O)ccc1F
CC1(C)OB(c2ccc(C(N)=O)s2)OC1(C)C
Cc1nn(C)cc1B1OC(C)(C)C(C)O1
O[B](O)c1cccc(c1)S(=O)(=O)N1CCCC1
Cl.O[B](O)c1cccc(c1)C(=O)Nc1nnn[nH]1
CC(C)(C)NC(=O)c1ccc(c(c1)[B](O)O)F
O[B](O)c1cccc(c1)S(=O)(=O)NCc1ccccc1
OCCNC(=O)c1cccc(c1)[B](O)O
OB(O)c1ccc(Cn2cnc2)cc1
O=C(O)c1cccc(B(O)O)c1
Cc1cc(C)n(-c2ccc(B(O)O)cc2)n1
OB(O)c1cnn(-c2ccc(C(F)(F)F)cc2)c1
Cc1ccc2[nH]c(C3CCCN3C(=O)c3cccc(B(O)O)c3)nc2c1
CC1CCC(C)N(C(=O)c2ccc(B(O)O)cc2)C1
CCOC1cc(CNc2ccc3c(c2)B(O)OCC3)ccc1OC
CCOCc1nc(-c2ccc(B(O)O)c2)no1
Cc1cc(C(=O)N2CCC(B(O)O)C2)ccn1
Cn1nnc2cc(CN3CC=C(B(O)O)CC3)ccc21
OB(O)C1=CCN(Cc2cc(-c3cccn3)n[nH]2)CC1
OB(O)C1=CCN(Cc2cc3cnc3o2)CC1
O=C(C1CCC(C2CC2)CC1)N1CC=C(B(O)O)CC1
OB(O)c1cc(F)ccc1OCc1cnc1
CC(C)OCc1cccc(B(O)O)c1
OB(O)c1cccc2c1OCCO2
Cc1ccc2ncccc2c1B(O)O
OB(O)c1ccc(O)nc1F
COc1ncc(C)c1B(O)O
OB1OCc2cc(F)ccc21
Cc1ncc(C)c1B1OC(C)(C)C(C)O1
CC1(C)OB(c2cnn([C@H]3CCCCO3)c2)OC1(C)C
OB(O)c1ccc2nncn2c1
CC1(C)OB(c2cnc(-n3cccn3)c2)OC1(C)C
CN(C)C(=O)c1cnc(B2OC(C)(C)C(C)O2)c1
CC(=O)n1ncc2ccc(B3OC(C)(C)C(C)O3)cc21
CC1(C)OB(c2cnn(-c3cccn3)c2)OC1(C)C
Nc1ccc(B(O)O)cn1
COc1cccc2cc(B(O)O)cc12
CC1(C)OB(c2cnc3c(c2)CC(=O)N3)OC1(C)C
COc1ncc1B1OC(C)(C)C(C)O1
O=C(O)C[C@H]1OB(O)c2ccccc21
Cc1cc(C)n([C@H](C)CC(=O)Nc2cccc(B(O)O)c2)n1
CC(C)(C)N1C[C@H](C(=O)Nc2ccc3c(c2)B(O)OCC3)CC1=O
CN1CCN(C(=O)c2ccc3c(c2)COB3O)C(C)C1=O
CC1(C)Cc2ccc(NCc3c[nH]nc3-c3cccn3)cc2B(O)O1
O=C(C1Cc2cccc(F)c2O1)N1CCC(B(O)O)C1
OB(O)[C@H]1CCN(Cc2cc3n(n2)CCCC3)C1
OB(O)c1cc2cccc(Cl)c2s1
CC1CCC(C)N(C(=O)c2cc(B(O)O)ccc2F)C1
O=C(CN1CSCC1=O)Nc1ccc2c(c1)B(O)OCC2
Cc2ccc(NC(=O)CN3CSCC3=O)cc2B(O)O1
C[C@H](C(=O)Nc1ccc2c(c1)B(O)OC(C)(C)C2)N1CCN(C)CC1
O=C(Nc1ccc2c(c1)B(O)OCC2)[C@H]1CCCCO1
CC1CCC(C)N(C(=O)c2ccc3c(c2)COB3O)C1

CCN(C(=O)c1ccc2c(c1)COB2O)[C@H]1CCOC(C)(C)C1
CC1(C)OB(c2cnn(-c3ccncc3)c2)OC1(C)C
CN(C)c1ncccc1C(=O)Nc1ccc2c(c1)B(O)OCC2
OB(O)C1=CCN(Cc2cc3c(cn2)OCO3)CC1
Cc1c[nH]nc1C(=O)Nc1ccc2c(c1)B(O)OC(C)(C)C2
C[C@H](C)(C(=O)c1cccs1)NC(=O)c1ccc2c(c1)COB2O
CC1(C)OB(c2cnn2[C@@H]2CCCCO2)OC1(C)C
O=S1(=O)CCCN1c1cccc(NCc2cccc(B(O)O)c2)c1
CCc1noc(CC)c1CNCC1ccc(B(O)O)cc1
Cn1nccc1B1OC(C)(C)C(C)O1
NC[C@@H]1OB(O)c2cccc21
OB(O)c1cc(F)ccc1OC[C@H]1CCOC1
CC(C)NC(=O)C(C)NCc1ccc(B(O)O)cc1
O=S1(=O)CCC2(CC1)CO2
Cc1cccc1CN1CCCN([C@H]2CCOC2=O)CC1
CC1CN(C2CCOC2=O)CCN1c1nccs1
Cc1nc(CN2CCCN(C3CC(C)OC3=O)CC2)no1
CCN1CCN(C2CCN(C3CC(C)OC3=O)CC2)C1=O
Cc1cc(C)n(CC2CCCCN2C2CC(C)OC2=O)n1
Cc1nn(C)c(Cl)c1C1CCCN1C1CCOC1=O
CC1CC(N2CCc3c(nc(C(C)C)n3C)C2)C(=O)O1
O=C1OCC[C@H]1Nc1ccc2c(c1)CCCO2
COc1cc(F)ccc1N1CCN([C@H]2CCOC2=O)CC1
O=C1OCC[C@H]1NC1c2cccc2-c2cccc21
Cc1ccc(N)cc1S(=O)(=O)F
CC1CC(NC2CCc3c2cnn3C(C)(C)C)C(=O)O1
CC(=O)N1CCN(C2CN(C3CCOC3=O)CC2C)CC1
CCC1CN(C2CC(C)OC2=O)CCS1
CC(=O)N(C)C1cccc(NC2CC(C)OC2=O)c1
N#C[C@H]1C[C@H]2C[C@H]1[C@H]1O[C@H]21
CC1CC(NC(=O)c2n[nH]c3cccc23)C(=O)O1
Cc1cc(NC2CC(C)OC2=O)nn1C
Cc1csc(NC(=O)N[C@H]2CC(C)(C)OC2=O)n1
Nn1cc(-c2cccc2)nc1S[C@H]1CCOC1=O
O=C1OCC2CN(Cc3cccc3)CC12
O=C1OCC12CCNCC2
Cc1nc2c([nH]1)CCC(C(=O)N1CC(C)(C)OC1=O)C2
Cc1cccc1C1CC1C(=O)N1CCCC12CCOC2=O
C[C@H]1CCOC(C2OC2(C)C)C1
Nc1nnc(S[C@H]2CCOC2=O)[nH]1
O=C1OCC[C@H]1N1C(=O)c2cccc2S1(=O)=O
CC1CC(N(C)Cc2nc3cccc3s2)C(=O)O1
CC1CC(N2CC=C(c3ccc(F)cc3)CC2)C(=O)O1
CCN1c(S[C@H]2CCOC2=O)nc2cccc2c1=O
CN(C(=O)Cn1ccc(=O)[nH]c1=O)[C@H]1CC(C)(C)OC1=O
O=C1CC(CG(=O)N2CC3C4CCC(C4)C3C2)CO1
O=C1OCC[C@H]1Sc1nnc(C2CCCC2)o1
O=C1CC[C@H](CN2CCc3[nH]c4ccc(F)cc4c3C2)O1
NC[C@H]1CC2(CCC2)C(=O)O1
O=C1C[C@H](NS(=O)(=O)c2csc3cccc23)CO1
Cc1nn(C(=O)N2CCOCC2)c(C)c1Cl
CC1CC(N2CCc3cccc32)C(=O)O1
N[C@H]1CC[C@H](CS(=O)(=O)F)C1
Cc1cc(O[C@H]2CCOC2=O)ccc1N
CN(Cc1cccc1OC(F)(F)F)C(=O)n1ccnc1
CN(C)S(=O)(=O)N1CCN([C@H]2CCOC2=O)CC1
O=C(NCc1ccc2c(c1)OCO2)n1ccnc1
CC(=O)Nc1cccc2c1CCN(C1CC(C)OC1=O)C2
Cc1cccc1C(=O)N1CCN(C2CC(C)OC2=O)CC1
O=C(NC1CCN([C@H]2CCOC2=O)CC1)c1cccs1
CCOc1nnc2c1CN([C@H]1CCOC1=O)CC2
O=C1OCCC1N1CCCC(CN2CCCCC2)C1
CC1CC(N(C)CC2CCCCC2)C(=O)O1
CC1(C)CC(NC2CCOC2=O)C(C)O1
CC1CC(N2CCCC(c3cc(C(N)=O)[nH]n3)C2)C(=O)O1
Cc1cccc(NC(=O)N[C@H]2C(=O)OCC2(C)C)n1
CN(Cc1ccc(F)cc1)[C@H]1CCOC1=O
O=C(NC12CC3CC(C3)C1)C2)n1ccnc1
O=C(N1CCC2CCCC2C1)n1ccnc1
CC1(C)OB(c2cnc3ccnn3c2)OC1(C)C
CSCCCNC(=O)c1cccc(B(O)O)c1
CN(C)c1ncccc1C(=O)Nc1ccc2c(c1)B(O)OC(C)(C)C2
OB(O)C1=CCN(Cc2cc3c(cn2)OCO3)CC1
CC(C)n1ncccc1CNc1ccc2c(c1)B(O)OC(C)(C)C2
Cc1cc(B2OC(C)(C)C(C)(C)O2)n([C@H]2CCCCO2)n1
O=S1(=O)CCCN1c1cccc(NCc2cccc(B(O)O)c2)c1
CCc1noc(CC)c1CNCC1cccc(B(O)O)c1
CC1(C)OB(c2ccc(CN)s2)OC1(C)C
NCC1OB(O)c2cccc21
OB(O)c1cc(F)ccc1OCC1CCOCC1
Cc1c(B2OC(C)(C)C(C)(C)O2)cnn1C
CC(C)NC(=O)C(C)NCc1cccc(B(O)O)c1
CC1CN(C2CCOC2=O)c2cccc21
Cc1ccc(N2CCCC(N(C)C3CCOC3=O)C2)nn1
Cc1noc(C(C)N2CCN(C3CCOC3=O)CC2)n1
CCc1nc2n(n1)CC(NC1CCOC1=O)CC2
O=C1OCCC1N1CCCC1Cn1cnn1
Cc1cnn(CC2CN(C3CC(C)OC3=O)CCO2)c1
O=C1OCC[C@H]1N1CC(n2cccc2)C1
CC(=O)N1CCCC1C1CCCN1C1CC(C)OC1=O
CC1CC(Nc2ccc3c(c2)CCCC(=O)N3)C(=O)O1
NC(=O)C1CCN([C@H]2CCOC2=O)CC1
COc1ccc(C2CC(C)N(C3CCOC3=O)C2)cc1
CC(C)c1csc(C2CCCN(C3CCOC3=O)C2)n1
CC(C)(C)c1n[nH]c(C2CN(C3CCOC3=O)CCO2)n1
CN(C)c1cccc(C2CCCN2C2CCOC2=O)c1
CC1CC(N2CCn3c(nnc3-c3cccc3)C2)C(=O)O1
CC1CC(N2CC(C)C2c2cccc2)C(=O)O1
O=C1OCC[C@H]1NS(=O)(=O)c1nc2ccsc2c1
O=C1CC[C@H](C(=O)NC2CCCCC2)O1
Clc1cccc(C[C@H]2CO2)c1
CC1(C)C[C@H](NC(=O)C2(c3cccc3F)CC2)C(=O)O1
Nn1c(S[C@H]2CCOC2=O)nn1-c1cccs1
Nc1nc(S[C@H]2CCOC2=O)nc2sccc12
Cc1ccn(CC[C@H]2CCOC2=O)c(=O)c1C#N
CCc1cccc1S(=O)(=O)N[C@H]1CCOC1=O
Cc1nc2c(n1C1CCN(C3CCOC3=O)C1)CCCC2
O=C1OCC[C@H]1n1nnc(-c2ccc(F)cc2)n1
Nc1nnc(S[C@H]2CCOC2=O)s1
O=C(O)CS[C@H]1CCOC1=O
NC(=O)N1CCc2cc(S(=O)(=O)F)ccc21
CC1(C)COC(=O)[C@H]1NC(=O)CN1CCCCC1=O
CC1CC(NS(=O)(=O)c2ccc3c(c2)OCO3)C(=O)O1
CN(C(=O)c1cc(C(N)=O)cs1)[C@H]1CC(C)(C)OC1=O
CCc1ccc2occ(C(=O)NC3CC(C)OC3=O)c2c1
COc1cccc([C@H]2CCCN2C(=O)n2ccne2)c1
CC1CC(N2CCC(c3c[nH]c4cccc34)CC2)C(=O)O1
Nc1ccnc1S(=O)(=O)F
O=C1OC[C@H]23CC[C@H](O2)[C@H](C(=O)O)[C@H]13
Cc1cc2nnc(C(=O)N3CCCC3)c2cc1C
CC1CC(NC(C)c2cccc2Cl)C(=O)O1
O=C1OCC[C@H]1N1CC=C(c2c[nH]c3cccc23)CC1
N#Cc1ccnc(N2CCN(C(=O)n3ccnc3)CC2)c1
Cc1ccc2[nH]c3c(c2c1)CN(C(=O)n1ccnc1)CC3
C[C@H](NC(=O)n1ccnc1)c1ccc(F)cc1
O=C1OCC[C@H]1Oc1nnc2cccc12
Cn1c(=O)c2c(ncn2[C@H]2CCOC2=O)n(C)c1=O
N#Cc1ccnc1N1CCCN([C@H]2CCOC2=O)CC1
CC1CC(Sc2nnc(-c3cccc3)n2C)C(=O)O1
O=C1OCC[C@H]1N1CC(Cc2n[nH]c2)CC1
NC1CCN([C@H]2CCOC2=O)CC1
CC1CC(NCC2CN(C)CCO2)C(=O)O1
CC1CC(N2CCOC(C)C2)C(=O)O1
CC1CC(N2CCCC(c3ccn[nH]3)C2)C(=O)O1
CC1CC(NC(=O)Nc2ccc(F)cn2)C(=O)O1
CC1(C)C[C@H](C)(NCc2cccc(F)c2)C(=O)O1
CN(C)CCNC(=O)c1cccc(c1)[B](O)O

Table 5.S1. Fragments screened by crystallography. Compounds (in SMILES format) in red were identified as hits (Figure 5.2, Table 5.2).

5.S2 Crystallography Statistics

Dataset	PaPBP3:1 PDB Code: 7ATM	PaPBP3:2 PDB Code: 7ATO	PaPBP3:3 PDB Code: 7ATW	PaPBP3:4 PDB Code: 7ATX	PaPBP3:8 PDB Code: 7AU0
Beamline	DLS I03	DLS I03	DLS I03	DLS I03	DLS I04-1
Wavelength	0.97624	0.97934	0.97934	0.97934	0.91587
Resolution range (Å)	1.58 –59.82 (1.58 -1.72)	1.59 - 61.11 (1.59 -1.71)	1.44 - 60.25 (1.44 - 1.59)	1.77 – 60.88 (1.77– 1.88)	2.17- 60.45 (2.17 - 2.21)
Space group	P 21 21 21	P 21 21 21	P 21 21 21	P 21 21 21	P 21 21 21
Unit cell	69.85 80.95 88.80 90 90 90	68.25 83.16 90.12 90 90 90	69.30 82.24 88.52 90 90 90	68.92, 83.03, 89.53 90 90 90	68.575 82.676 88.616 90 90 90
Unique reflections	53811	53748	67983	44742	27129
Multiplicity	8.7 (8.2)	7.4 (7.4)	7.1 (6.0)	7.3 (7.6)	8.8 (8.6)
Completeness (%) ^a	95.3 (62.9)	95.5 (65.4)	95.7 (67.6)	95.5 (52.2)	99.9 (99.9)
Mean I/sigI	15.8 (1.5)	15.4 (1.4)	18.0 (1.8)	16.4 (1.2)	8.2 (1.0)
R _{meas}	0.069 (1.51)	0.064 (1.426)	0.048 (0.952)	0.056 (1.683)	0.201 (2.816)
CC _{1/2}	1.0 (0.5)	1.0 (0.6)	1.0 (0.7)	1.0 (0.5)	1.0 (0.5)
R-work	0.1906	0.1498	0.1407	0.2088	0.1985
R-free	0.2246	0.2343	0.2010	0.2645	0.2619
Number of non-	3926	4133	4062	3982	3846
macromolecules	3669	3866	3826	3809	3685
ligands	22	21	30	21	23
solvent	235	246	206	152	138
RMS(bonds)	0.02	503	0.02	497	0.02
RMS(angles)	1.82	0.016	2	0.014	1.93
Ramachandran outliers (%)	0	1.98	0	1.86	0.42
Rotamer outliers	1.03	0.2	0.74	0	2.34
Average B-factor	35.64	2.22	36.6	3.24	54.3
macromolecules	35.45	44.11	36.24	53.61	54.54
ligands	40.59	44.07	55.86	53.73	63.14
solvent	38.11	35.89	40.31	52.91	46.39

Dataset	PaBPB3:13 PDB Code: 7AU1	PaBPB3:14 PDB Code: 7AU8	PaBPB3:15 PDB Code: 7AU9	PaBPB3:16 PDB Code: 7AUB	PaBPB3: Vaborbactam PDB Code: 7AUH
Beamline	DLS I04-1	DLS I04-1	DLS I04-1	DLS I03	DLS I04
Wavelength	0.91587	0.91587	0.91587	0.97625	0.97950
Resolution range (Å)	1.36 – 60.04 (1.36 - 1.49)	1.79 – 60.57 (1.79 – 1.97)	2.14 - 60.45 (2.14 – 2.34)	1.91 - 60.72 (1.91 – 1.94)	2.01 – 61.13 (2.01 – 2.22)
Space group	P 21 21 21	P 21 21 21	P 21 21 21	P 21 21 21	P 21 21 21
Unit cell	68.038 81.925 88.241 90 90 90	68.996 82.871 88.735 90 90 90	68.700 82.724 88.538 90 90 90	69.256 82.977 89.089 90 90 90	68.175 83.659 89.530 90 90 90
Unique reflections	69775	35335	21028	40602	25128
Multiplicity	8.1 (5.7)	9.1 (12.0)	8.6 (7.8)	7.2 (6.4)	8.5 (6.7)
Completeness (%) ^a	91.7 (62.5)	94.9 (65.1)	94.1 (67.2)	99.7 (98.3)	94.0 (62.9)
Mean I/sigI	15.1 (1.6)	16.7 (1.5)	12.9 (1.6)	16.7 (0.9)	15.5 (1.5)
Rmeas	0.077 (0.935)	0.074 (1.613)	0.129 (1.404)	0.058 (1.801)	0.079 (1.127)
CC _{1/2}	1.0 (0.7)	1.0 (0.7)	1.0 (0.6)	1.0 (0.4)	1.0 (0.7)
R-work	0.1445	0.1969	0.1919	0.1985	0.2131
R-free	0.2033	0.2567	0.2743	0.2456	0.2820
Number of non-hydrogen atoms	4508	3999	3871	3829	4026
macromolecules	4009	3754	3739	3657	3863
ligands	91	27	32	21	26
solvent	408	218	100	151	137
RMS(bonds)	0.02	0.014	0.01	0.01	0.015
RMS(angles)	2.11	1.82	1.89	1.83	1.92
Ramachandran outliers (%)	0	0	0.83	0.21	0.4
Rotamer outliers	1.16	2.8	3.84	1.83	2.48
Average B-factor	22.25	47.55	52.13	55.72	51.3
macromolecules	20.84	47.8	52.37	55.95	51.56
ligands	37	47.21	55.78	59.02	48.35
solvent	32.82	43.24	41.79	49.75	42.82

Table 5.S2. Crystallography Statistics. Values for the highest resolution shell are given in parentheses. ^aAll data, except structures PaBPB3:8 and PaBPB3:16, were processed using STARANISO (Global Phasing) and the ellipsoidal completeness is given ^{1,2}. PaBPB3:8 and PaBPB3:16 were processed with autoPROC (Global Phasing) ³, and the value given is the spherical completeness.

Structure	Core	Binding Mode	pH
PaPBP3:1	Phenylboronic acid	Tri-covalent	8
PaPBP3:2	Phenylboronic acid	Tri-covalent	8
PaPBP3:3	Benzoxaborole	Di-covalent	6
PaPBP3:4	Benzoxaborole	Di-covalent	8
PaPBP3:8	Benzoxaborole	Di-covalent	6
PaPBP3:13	Benzoxaborole with 3-carboxylic acid group	Di-covalent	6
PaPBP3:14	Benzoxaborole with 3-carboxylic acid group	Di-covalent	8
PaPBP3:15	Benzoxaborole	Di-covalent	6
PaPBP3:16	Benzoxaborole with 3-carboxylic acid group	Di-covalent	6
PaPBP3: Vaborbactam	Monocyclic, 6-membered boron-containing ring	Mono-covalent	8

Table 5.S3. PaPBP3 crystal pH. Different pHs were used when growing and soaking each ligand into PaPBP3 crystals. The pH that gave the most complete density around the ligand was selected for analysis and deposition. Good quality data was collected at both pHs. Based on these data, pH does not appear to correlate with the binding mode observed.

5.S3 Further Crystallography Views

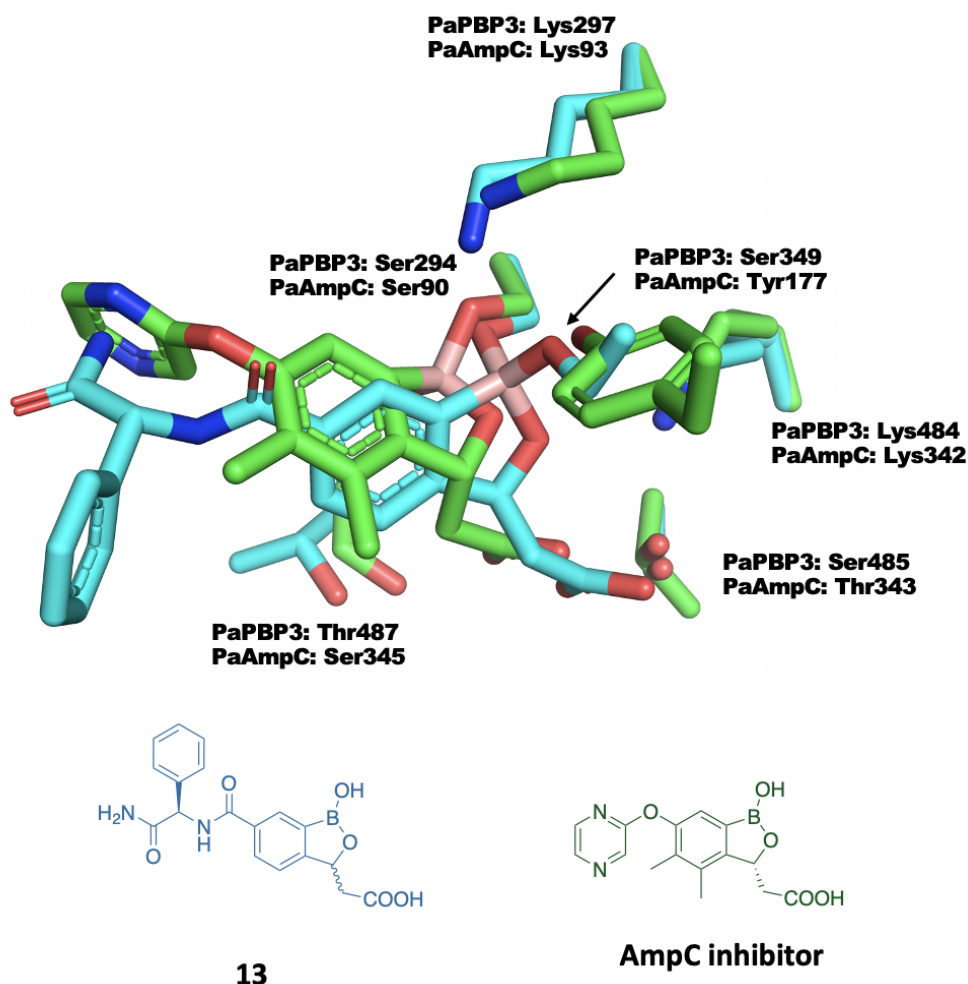


Figure 5.S1. Benzoxaboroles engage β -lactamases (AmpC) and PaBPB3 differently. Selected residues from crystal structures of *P. aeruginosa* AmpC and PaBPB3. The C α carbons of residues of the **SXXK**, **SXN** and **K(S/T)G** motifs (residues 294/90, 297/93, 349/177 and 484/342 in PaBPB3/PaAmpC respectively) of the PaBPB3:**13** complex (cyan) and the PaAmpC:**benzoxaborole** complex (PDB: 4WYY⁴). In AmpC the benzoxaborole is mono-covalently reacted. The PaAmpC benzoxaborole is rotated by $\sim 50^\circ$ (through its long axis) relative to its position in the PaBPB3 crystal structure which is associated with attack of the benzoxaborole on the other face. The C-3 acid group is positioned similarly in both complexes. Only one of the two alternate conformations of the side chain of PaBPB3 Lys297 is shown for clarity.

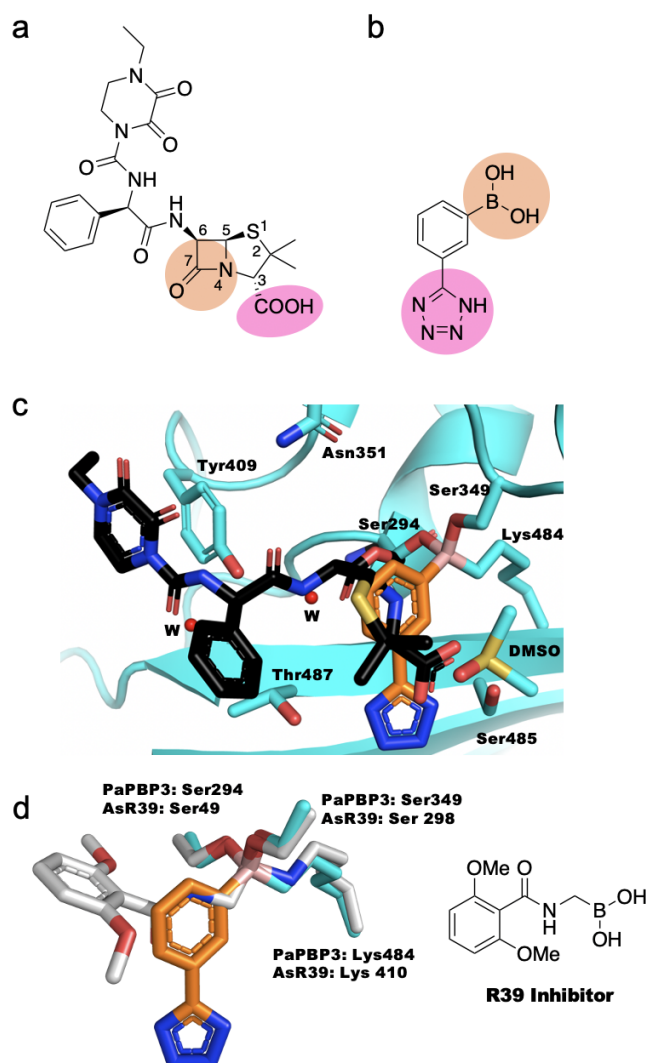


Figure 5.S2. Comparison of the interactions of reacted piperacillin and 1 with PaBPB3. Crystal structures of PaBPB3 with (a) reacted piperacillin and (b) 1 are shown with serine-binding groups coloured in orange and groups engaging the acid binding pocket shown in pink. (c) Active site of PaBPB3:1 (orange and cyan), with the molecule of reacted piperacillin overlaid (black, PDB code: 6R3X⁵). A molecule of DMSO found in the active site of PaBPB3:1 is shown, as well as certain water molecules (w). The right hand water molecule occupies the oxyanion hole. (d) Comparison of the interactions of residues of PaBPB3 and residues of *Actinomadura* sp. R39 (AsR39) with boronates 1 and an R39 inhibitor from Zervosen *et al.*⁶. All three residues (294/49, 349/298 and 484/410 in PaBPB3/AsR39 respectively) have similar conformations as they engage the boron atom.

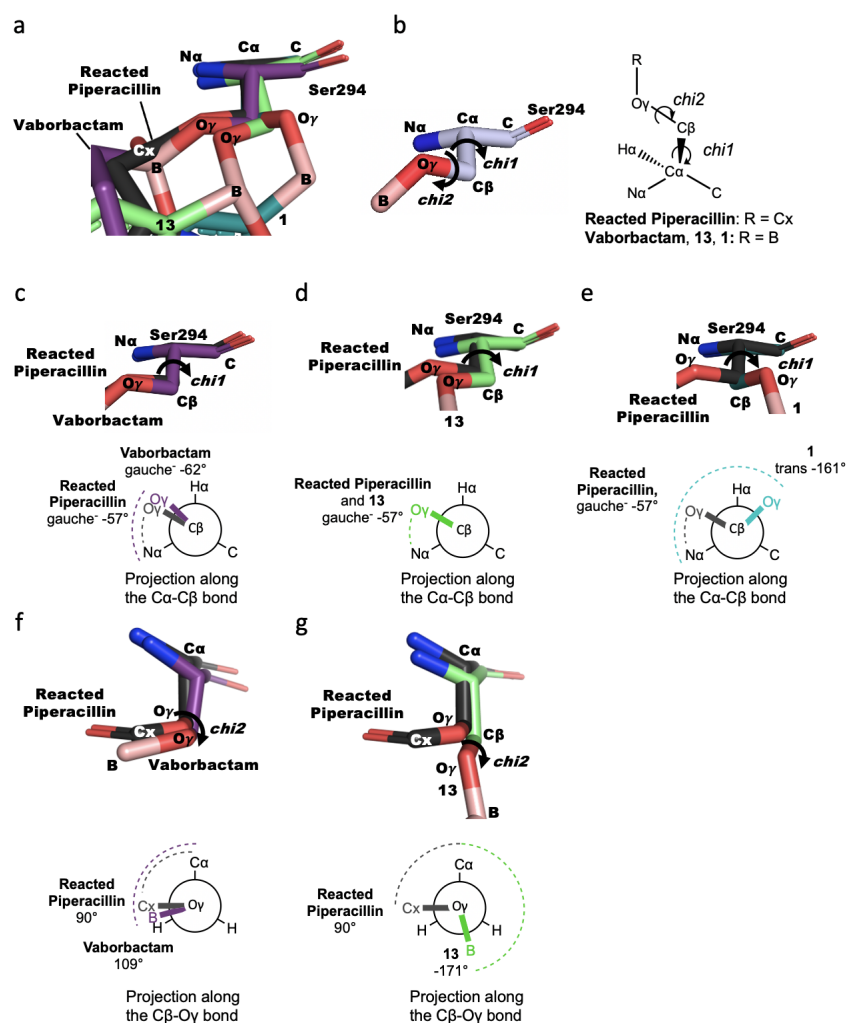


Figure 5.S3. Crystal structure views and Newman projections of Ser294 of PaPBP3 reacted with boron-containing inhibitors and piperacillin. (a) Enlarged view of Figure 5.10. Overlay of Ser294 of PaPBP3 reacted to boron-containing compounds (**1**, **13** and **Vaborbactam**) and piperacillin (PDB: 6R3X)⁵. Residues Ser349 and Lys484 are not shown in any of these figures. The position of boron within the active site correlates with changes in the Ser294 χ_1 and χ_2 angles. (b) Atoms and side chain angles of Ser294. (c-g) Structure views and Newman projections aligned along the Ser294 Ca-C β bond (c-e) and the Ser294 C β -O γ bond (f and g) for each of the boron-containing compounds compared to the piperacillin-reacted structure (black): vaborbactam (c and f), **13** (d and g), **1** (e). χ_1 dihedral angles are defined relative to the Ser294 Na, χ_2 dihedral angles are defined relative to the Ser294 Ca. Mono-covalent structures (vaborbactam and β -lactams) and di-covalent structures (benzoxaboroles) are differentiated by their Ser294 χ_2 angles but have similar (gauche $^-$) Ser294 χ_1 angles. Tri-covalent structures (phenyl boronic acids **1** and **2** and previous observations ⁶) have trans serine χ_1 angles.

5.S4 Computational Chemistry

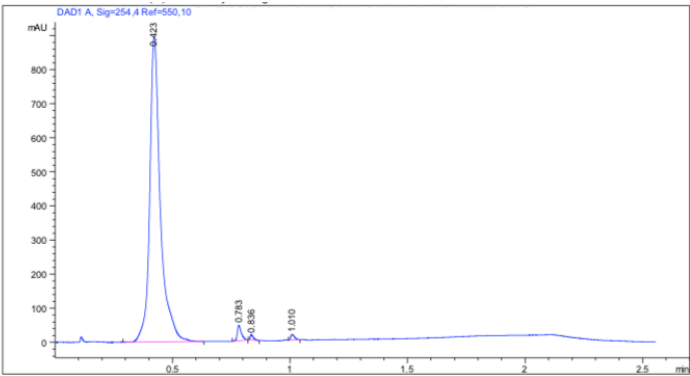
Computational docking of boronates was performed by Charles Eyermann (University of Cape Town). The protocol is reproduced here, with permission.

The benzoxaborole di-covalent binding mode of compound **3** in complex with PaBPB3 was used as a template for modelling benzoxaborole design ideas. Given the $\beta 5$ - $\alpha 11$ loop was not defined in the PaBPB3: **3** structure (PDB: 7ATX), presumably due to its inability to engage the residues on the $\beta 5$ - $\alpha 11$ loop, a model of **3** bound to the PaBPB3 structure as observed in the piperacillin-reacted PaBPB3 structure (PDB: 6R3X ⁵) was developed. All modelling studies were performed using the Schrodinger Suite of programs (Schrodinger LLC, New York). Benzoxaborole design ideas which incorporate the key binding interactions between reacted piperacillin and PaPB3 were built by modifying compound **3** using Schrodinger's 3D Builder tool. All designs, including compound **11**, were docked into PaBPB3 using the Glide SP software. Glide SP docking calculations were performed on a noncovalently bound ligand where the oxaborole portion of the benzoxaborole was deleted and the remaining phenyl group was constrained to the position observed in PaBPB3:**3**. Hydrogen-bond constraints to Tyr328, Asn351 and Arg489 were applied in the Glide SP docking. The Glide docking poses of the inhibitor were then reconstituted to a complete covalently bound benzoxaborole and the inhibitor and PaBPB3 residues within 6 Å of the inhibitor were then minimized using Prime. The only explicit water included in the minimization calculations was a crystallographically observed (in PaBPB3:**3**) water that hydrogen bonds to the backbone NHs of Ser294 and Thr487 (**w** in Figure 5.4). The minimizations were performed using the OPLS2005 force field, the variable-dielectric generalized Born solvation model for water, a dielectric constant of 80, and 40 iterations of 200 steps each.

5.S5 LC-MS traces

Compound

5



=====
Area Percent Report
=====

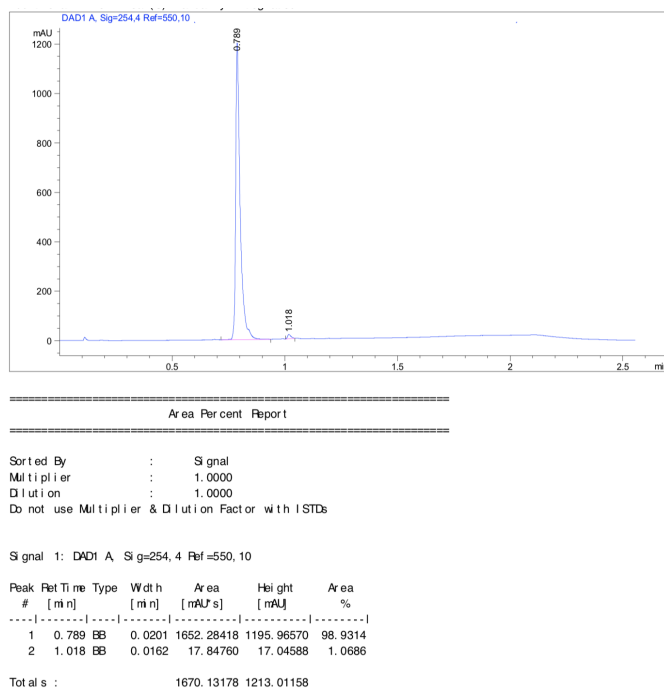
Sorted By : Signal
Multiplier : 1.0000
Dilution : 1.0000
Do not use Multiplier & Dilution Factor with ISTDs

Signal 1: DAD1 A, Sig=254.4 Ref=550.10

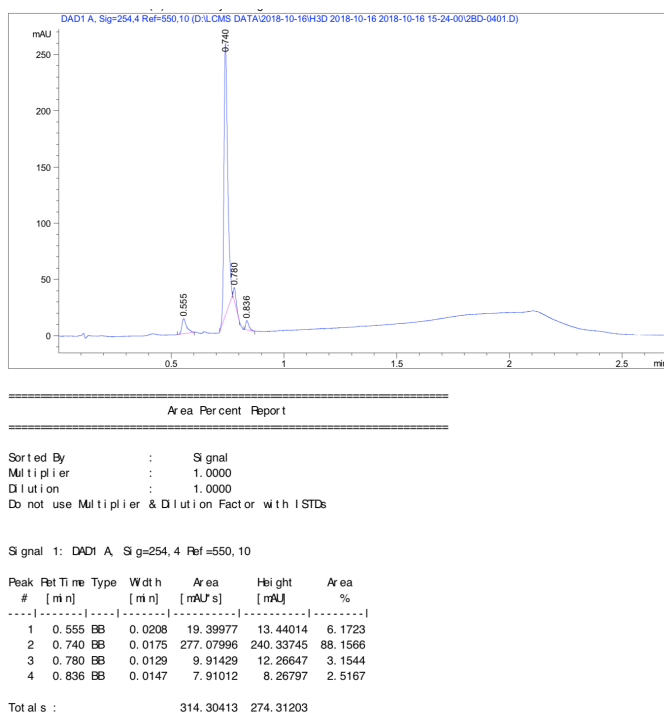
Peak #	Ret Time [min]	Type	Width [min]	Area [mAU*s]	Height [mAU]	Area %
1	0.423	BB	0.0462	2809.03638	893.39703	96.9137
2	0.783	BB	0.0176	55.13561	45.46098	1.9022
3	0.836	BB	0.0150	15.39992	15.64933	0.5313
4	1.010	BB	0.0174	18.92163	16.47529	0.6528

Totals : 2898.49354 970.98263

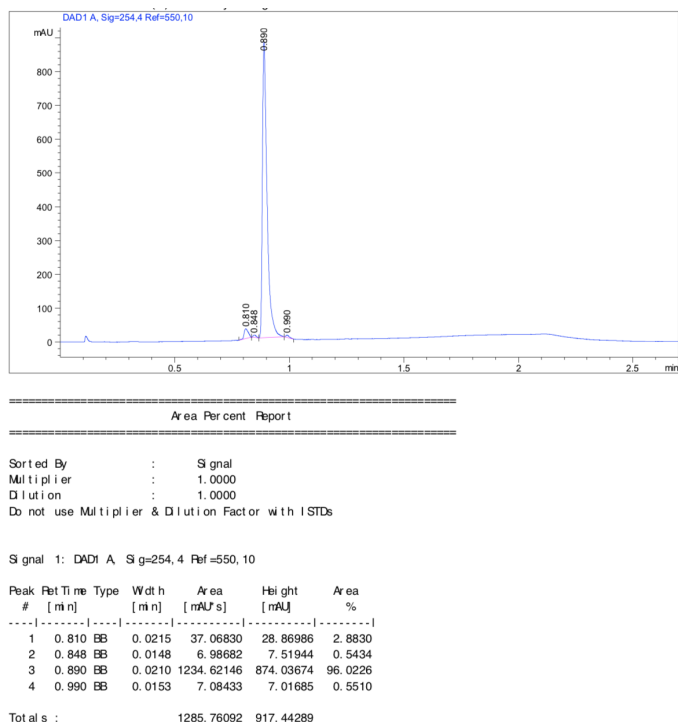
6



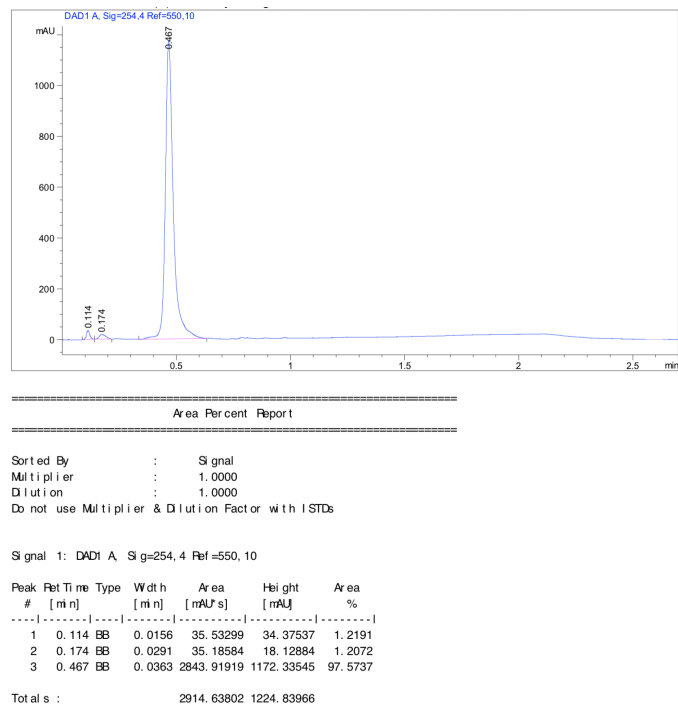
7



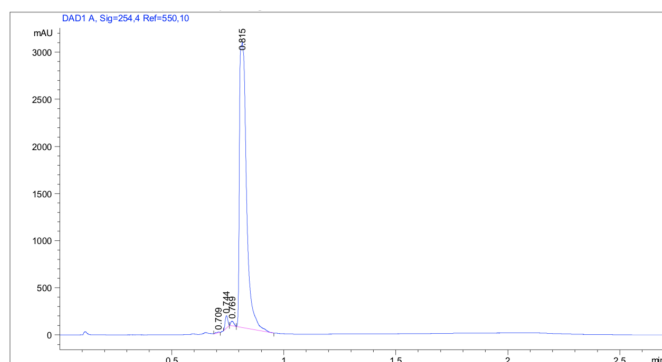
8



9



10



Area Percent Report

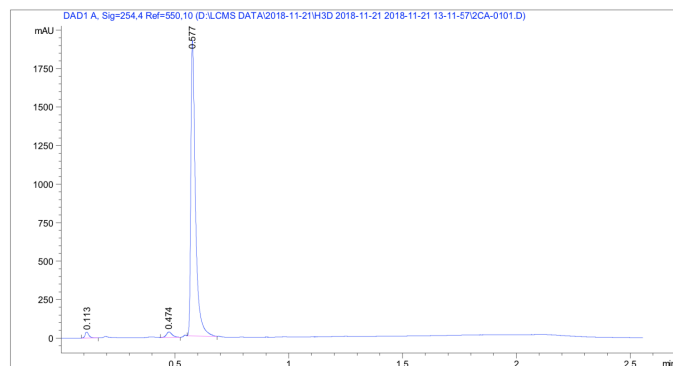
Sorted By : Signal
Multiplier : 1.0000
Dilution : 1.0000
Do not use Multiplier & Dilution Factor with ISTDs

Signal 1: DAD1 A, Sig=254.4 Ref=550.10

Peak #	Ret Time [min]	Type	Width [min]	Area [mAU s]	Height [mAU]	Area %
1	0.709	BB	0.0167	9.87181	8.08875	0.1470
2	0.744	BB	0.0127	104.87284	132.30966	1.5812
3	0.769	BB	0.0164	47.70490	48.78843	0.7101
4	0.815	BB	0.0303	6555.15283	3020.34473	97.5817

Totals : 6717.60238 3209.51157

11



Area Percent Report

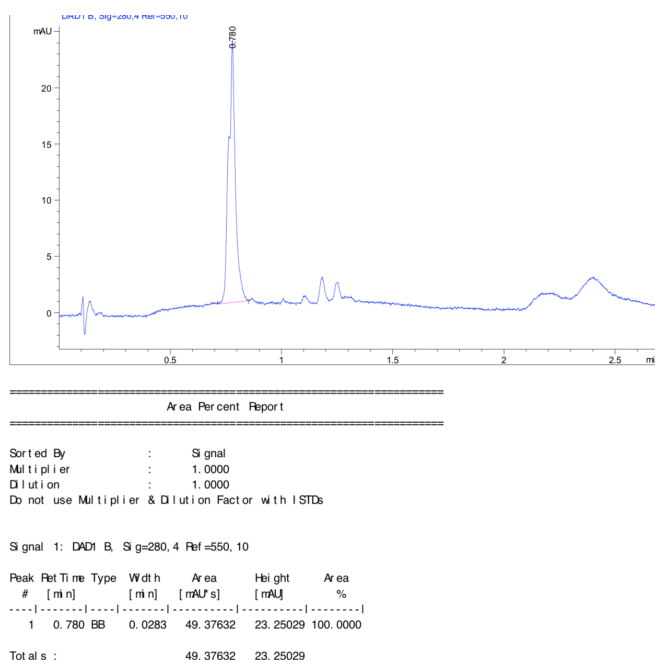
Sorted By : Signal
Multiplier : 1.0000
Dilution : 1.0000
Do not use Multiplier & Dilution Factor with ISTDs

Signal 1: DAD1 A, Sig=254.4 Ref=550.10

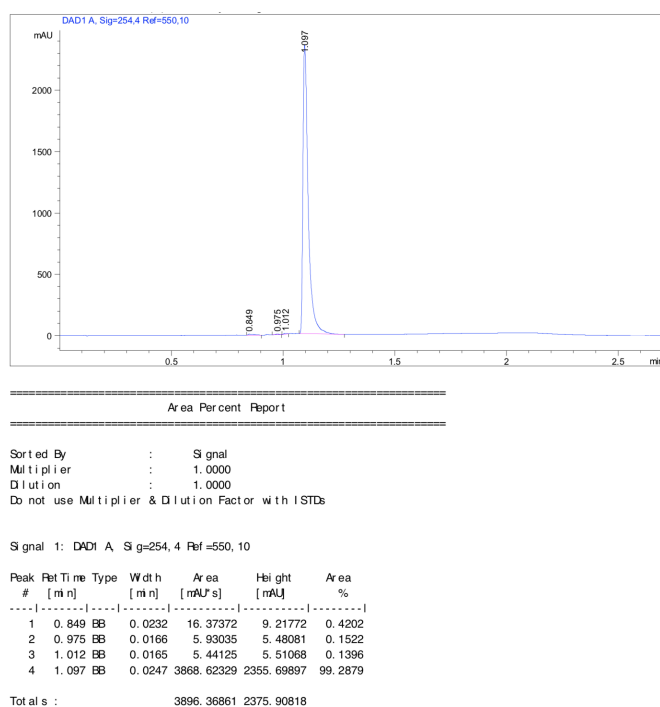
Peak #	Ret Time [min]	Type	Width [min]	Area [mAU s]	Height [mAU]	Area %
1	0.113	BB	0.0174	43.70873	38.08951	1.5636
2	0.474	BB	0.0254	61.48521	35.98430	2.1995
3	0.577	BB	0.0209	2690.25928	1912.42139	96.2370

Totals : 2795.45322 1986.49519

12



15



5.S6 References

- (1) Dong, H.; Zhang, Z.; Tang, X.; Paterson, N. G.; Dong, C. Structural and Functional Insights into the Lipopolysaccharide ABC Transporter LptB2FG. *Nat. Commun.* **2017**, *8* (1), 222. <https://doi.org/10.1038/s41467-017-00273-5>.
- (2) Tickle, I. J.; Flensburg, C.; Keller, P.; Paciorek, W.; Sharff, A.; Vonrhein, C.; Bricogne, G. *STARAN/ISO*; Global Phasing Ltd.: Cambridge, United Kingdom.
- (3) Vonrhein, C.; Flensburg, C.; Keller, P.; Sharff, A.; Smart, O.; Paciorek, W.; Womack, T.; Bricogne, G. Data Processing and Analysis with the *AutoPROC* Toolbox. *Acta Crystallogr. D Biol. Crystallogr.* **2011**, *67* (4), 293–302. <https://doi.org/10.1107/S0907444911007773>.
- (4) McKinney, D. C.; Zhou, F.; Eyermann, C. J.; Ferguson, A. D.; Prince, D. B.; Breen, J.; Jacobbe, R. A.; Lahiri, S.; Verheijen, J. C. 4,5-Disubstituted 6-Aryloxy-1,3-Dihydrobenzo[*c*] [1,2]Oxaboroles Are Broad-Spectrum Serine β -Lactamase Inhibitors. *ACS Infect. Dis.* **2015**, *1* (7), 310–316. <https://doi.org/10.1021/acsinfecdis.5b00031>.
- (5) Bellini, D.; Koekemoer, L.; Newman, H.; Dowson, C. G. Novel and Improved Crystal Structures of *H. influenzae*, *E. coli* and *P. aeruginosa* Penicillin-Binding Protein 3 (PBP3) and *N. gonorrhoeae* PBP2: Toward a Better Understanding of β -Lactam Target-Mediated Resistance. *J. Mol. Biol.* **2019**, *431* (18), 3501–3519. <https://doi.org/10.1016/j.jmb.2019.07.010>.
- (6) Zervosen, A.; Herman, R.; Kerff, F.; Herman, A.; Bouillez, A.; Prati, F.; Pratt, R. F.; Frère, J.-M.; Joris, B.; Luxen, A.; Charlier, P.; Sauvage, E. Unexpected Tricovaleent Binding Mode of Boronic Acids within the Active Site of a Penicillin-Binding Protein. *J. Am. Chem. Soc.* **2011**, *133* (28), 10839–10848. <https://doi.org/10.1021/ja200696y>.
- (7) Han, S.; Zaniewski, R. P.; Marr, E. S.; Lacey, B. M.; Tomaras, A. P.; Evdokimov, A.; Miller, J. R.; Shanmugasundaram, V. Structural Basis for Effectiveness of Siderophore-Conjugated Monocarbams against Clinically Relevant Strains of *Pseudomonas aeruginosa*. *Proc. Natl. Acad. Sci.* **2010**, *107* (51), 22002–22007. <https://doi.org/10.1073/pnas.1013092107>.

Chapter 6. Double Reaction of Nitrocefin with PBP3

Chapter 6.S (p268-274) contains additional information referred to in this chapter

6.1 Introduction

Nitrocefin (Figure 6.1) was initially studied as an antibiotic compound, but whilst it was found to have antimicrobial effects against some species, (e.g. 0.05 µg/ml against non-β-lactamase producing *S. aureus*)^{1,2}, its value was recognised as an agent for detecting β-lactamase producing organisms²; in the presence of β-lactamases, the colour changes from yellow to dark red. Its chromogenic properties have been used to study the kinetics of purified β-lactamases³⁻⁹ and a few PBPs¹⁰⁻¹⁵, but to my knowledge it has only been used in gram-negative class B PBPs to obtain simple IC₅₀s^{16,17}. Whilst undertaking structural characterisation of the reaction of nitrocefin with PaPBP3 mutants, a crystal structure in which two nitrocefin molecules were bound was identified; this work covers attempts to understand this complex.

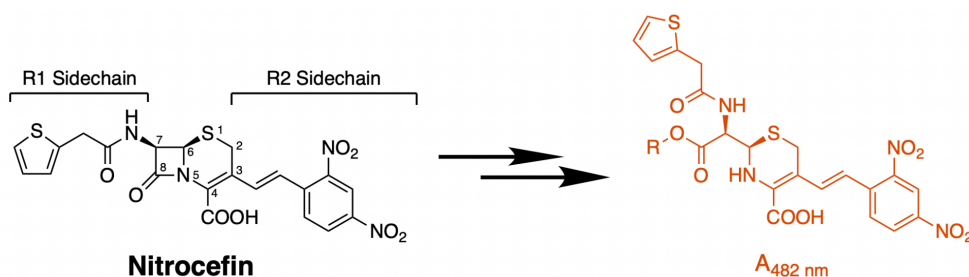
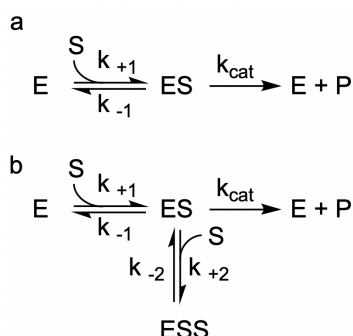


Figure 6.1. Chemical structure of nitrocefin. Atoms of the cephalosporin core and side chains are labelled. Nitrocefin molecular mass is 516.5 Da. On the right hand side, the R = the enzyme (linked via serine) when the nitrocefin has formed an adduct or R = H if the molecule is deacylated and in solution.

6.1.1 Simple Saturation and Substrate Inhibition Kinetics



Scheme 6.1. Schemes of the simple reaction pathway (a) and the substrate inhibition pathway (b). Where *E*: enzyme; *S*: substrate; *ES*: enzyme:substrate complex with one substrate bound; *P*: product; *ESS*: enzyme:substrate complex with two substrates bound. Rate constants (k_{+1} , k_{-1} , k_{cat} , k_{+2} , and k_{-2}) are shown for their respective steps. (b) This is a simple substrate inhibition scheme in which the second substrate can only bind to the *ES* complex and the *ESS* complex does not yield a product directly (see section 6.4.4).

The kinetic constants of many bimolecular enzymatic reactions can be found by measuring the steady state initial rate of reaction at varying substrate concentrations to find a “substrate concentration graph”. The substrate concentration graphs of many enzymes can be fitted to a “Briggs-Haldane” kinetic model, where the initial reaction velocity (*v*) increases hyperbolically with substrate concentration (*[S]*), scaled by two constants: the maximum reaction velocity (V_{max}) and the constant K_M (equation 6.1, Scheme 6.1a). This is termed simple saturation kinetics as the dependence of the rate of reaction on concentration of substrate follows a single phase, saturating at V_{max} . This model assumes: steady state kinetics (where the concentration of intermediate *ES* is constant throughout the reaction); that *[S]* is in great excess of the enzyme concentration; and that the rate limiting step is k_{cat} (Scheme 6.1, equation 6.S7) ^{18–22}.

$$v = \frac{V_{max} [S]}{K_M + [S]} \quad (6.1)$$

In some enzymes ^{23,24}, a non-hyperbolic relationship is observed with increasing substrate concentration (Figure 6.2), where there is a maximum rate attained at a given substrate concentration, above which, it declines. In cases where such substrate inhibition is observed, an extra term $(1 + [S]/K_{SI})$ can be included to account for the decrease (equation 6.2) ²¹:

$$v = \frac{V_{max} [S]}{K_M + [S] \left(1 + \frac{[S]}{K_{SI}}\right)} \quad (6.2)$$

The new term is a consequence of the ability of the *ES* complex to combine with substrate to form *ESS* (Scheme 6.1b). K_{SI} is the dissociation constant for complex *ESS* (equation 6.S6). Rearrangement of equation 6.2 makes it plain that the initial velocity at a given concentration of substrate is a weighted reduction of V_{max} (scaled by the values of K_M and K_{SI})²¹.

$$v = \frac{V_{max}}{1 + \frac{K_M}{[S]} + \frac{[S]}{K_{SI}}} \quad (6.3)$$

Equation 6.1 can be considered a case of equation 6.2 where K_{SI} is infinite, meaning $[S]/K_{SI}$ approaches zero and the term is ignored. Simulations with various arbitrary values of K_M , K_{SI} and V_{max} are shown in Figure 6.2. Derivation of equation 6.3 from Scheme 6.1b is shown in Chapter 6.S. The Briggs-Haldane and substrate inhibition models (Scheme 6.1) were used to fit the kinetic curves of the reaction various class B PBPs with nitrocefin.

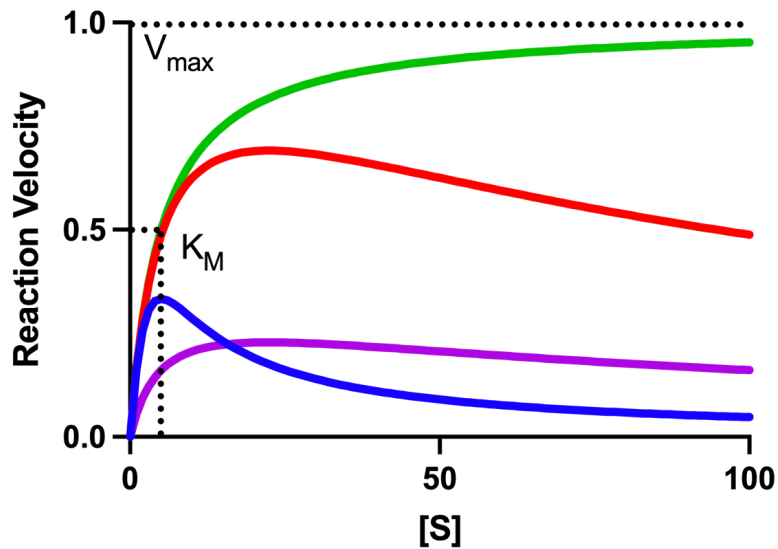


Figure 6.2. Simulations of substrate inhibition kinetics by plotting equation 6.3 with different values of K_{SI} and V_{max} . Green: Simple saturation kinetics, $K_{SI} = \infty$, $V_{max} = 1$; Red: Weak substrate inhibition, $K_{SI} = 100$, $V_{max} = 1$; Blue: strong substrate inhibition, $K_{SI} = 10$, $V_{max} = 1$; Purple: Substrate inhibition with lower V_{max} : $K_{SI} = 100$, $V_{max} = 0.33$. In all examples $K_M = 5$. Arbitrary units of concentration for substrate and arbitrary reciprocal time units for velocity. The values of $K_M = 5$ and $V_{max} = 1$ are shown with dotted lines. For substrate inhibition, the maximal velocity observed occurs at the geometric mean of K_M and K_{SI} ($\sqrt{K_M \cdot K_{SI}}$). V_{max} can no longer be reached experimentally (red and blue lines) because one of either $K_M/[S]$ or $[S]/K_{SI}$ will always be large in the denominator.

6.2 Methods

6.2.1 Protein Expression and Purification

PBP3 from *A. baumannii* (AbPBP3) and *E. coli* (EcPBP3) were cloned by D. Bellini and purified by J. Todd. All the proteins have both the C- and N-terminal domains, but were solubilised by the removal of the single transmembrane helix (the first ~50 residues²⁵). Plasmids containing the genes for each of the proteins: wild type *P. aeruginosa* PBP (PaPBP3_{wt}), PaPBP3_{S294A}, PaPBP3_{S349A} and PaPBP3_{Y409A} were a kind gift from D. Bellini. All plasmids were pET47b vector-based with kanamycin resistance and N-terminal 6xHis-tag.

Chemically competent *E. coli* BL21-DE3 cells (50 µL) were inoculated with 2 µL of plasmid and incubated on ice for 30 minutes. Heat shock (42 °C for 45 seconds) was then performed before further incubation on ice (5 minutes). 400 µL of SOC media (2% (w/v) tryptone, 0.5% (w/v) yeast extract, 10 mM NaCl, 2.5 mM KCl, 10 mM MgCl₂, 10 mM MgSO₄, 20 mM glucose) was added and the bacteria were allowed to grow (37 °C, 1 hour, 180 rpm shaking). This inoculum (100 µL) was then spread onto agar plates containing kanamycin (50 µg/mL) and grown overnight (37 °C). A single colony from the plate was picked and used to inoculate lysogeny broth (LB) containing kanamycin at 50 µg/ml, which was then allowed to grow as a starter culture overnight (37 °C, 180 rpm shaking). The following day, 3 x 1 L of LB (containing kanamycin at 50 µg/mL) were inoculated each with 10 mL of the overnight culture and allowed to grow to an optical density ($A_{600\text{ nm}}$) of 0.6 in baffled flasks (37 °C, 180 rpm shaking). The cultures were then cooled to 20 °C and induced with 1 mM of Isopropyl β-D-1-thiogalactopyranoside (IPTG) and allowed to express protein overnight (20 °C, 180 rpm shaking).

The next day, cells were pelleted at 9,000 x g in a Beckman JLA 8.1000 rotor for 20 minutes at 4 °C. The cell pellet was resuspended in lysis buffer (20 mM Sodium Phosphate pH 8, 500 mM NaCl, 20 mM imidazole (binding buffer), supplemented with 5 mg/ml lysozyme and 5 mg/ml bovine DNase) and then lysed by ultrasonication (10 x (30 s bursts interspersed by a 30 s pause on ice), using a Bandelin Electronic sonicator. Centrifugation (30,000 x g for 30 minutes at 4 °C in a Beckman JA 25.50 rotor) was used to remove cell debris. All subsequent chromatographic steps were performed at room temperature, flow rate 3 ml/min:

the supernatant was loaded onto a 5 ml HisTrap FF Crude column (Cytiva). Subsequently the column was washed with binding buffer (25 mL) supplemented with 10% (w/v) glycerol. An ÄKTA FPLC system (Cytiva) was equilibrated in binding buffer + 10 % (w/v) glycerol and then eluted with a gradient of 10 % to 100 % of elution buffer (20 mM Sodium Phosphate pH 8, 500 mM NaCl, 500 mM imidazole, 10 % (w/v) glycerol) across the column, which eluted the protein (which have an N-terminal his-tag). Dialysis was used to exchange the protein into a storage buffer (20 mM Sodium Phosphate pH 8, 500 mM NaCl, 20 % (w/v) glycerol) then the protein was aliquoted and frozen at -20 °C. Protein concentration was determined by absorbance at 280 nm on a NanoDrop (Thermo Scientific) using a calculated extinction coefficient from ProtParam²⁶. Purity (> 95%) was confirmed by gel electrophoresis and mass spectrometry.

6.2.2 Kinetics Assays

Measurements were carried out at 30 °C in triplicate using a Hellma micro quartz cuvette (1 cm pathlength) in a Cary 100 UV/vis spectrophotometer (Agilent). Data was acquired every 0.1 s. Nitrocefin (Abcam) or CENTA ((6*R*,7*R*)-3-(((3-carboxy-4-nitrophenyl)thio)methyl)-8-oxo-7-(2-(thiophen-2-yl)acetamido)-5-thia-1-azabicyclo[4.2.0]oct-2-ene-2-carboxylic acid, Calbiochem) in a buffer of 50 mM *bis*-Tris propane (Merck) pH 8.5, 75 mM NaCl, 1 % (v/v) DMSO (Merck) was added to the cuvette before the protein (in the same buffer) was added to initiate the reaction. The final volume in the cuvette was 200 µL. The initial rate immediately after mixing was found using the spectrophotometer's software. A dead time of ~ 10 s occurred whilst the substrates were mixed and the measurement initiated. The background turnover due to the spontaneous hydrolysis of nitrocefin or CENTA was measured alongside the experiment and subtracted from the rate. Reactions with nitrocefin were followed at 482 nm ($\epsilon_{1\text{ cm}, 482\text{ nm}} = 17,400\text{ M}^{-1}\cdot\text{cm}^{-1}$)¹⁰ and reactions with CENTA were followed at 405 nm ($\epsilon_{1\text{ cm}, 405\text{ nm}} = 6,400\text{ M}^{-1}\cdot\text{cm}^{-1}$)³. The specific rates (reaction velocity divided by the concentration of enzyme (equation 6.S3)) were fitted to either Equation 6.3 or Equation 6.1 using non-linear regression in Prism 9 (GraphPad Software), and the best fit parameters are reported alongside the standard errors of the mean found by the software.

The protein concentration for each reaction used was chosen such that the turnover rate was at least 10-fold higher than the background nitrocefin turnover rate. For reactions with nitrocefin, the protein concentrations were: PaPBP3_{wt}: 0.4 µM;

PaPBP3_{S349A}: 2.4 μ M; PaPBP3_{Y409A}: 2.4 μ M; AbPBP3: 0.8 μ M; EcPBP3: 1.8 μ M. For the reaction with CENTA, 0.8 μ M of PaPBP3_{wt} was used. For PaPBP3_{S294A}, conditions for steady state turnover at a sufficient rate were not identified (up to 10 μ M was tested) .

The upper limits for concentrations of substrates were determined by the solubility of the substrate. Partial solubility was observed >500 μ M of nitrocefin and >1 mM of CENTA. ~ 2 fold less than this was used to ensure insolubility was not causing the observed effects. The lowest concentration of nitrocefin tested was always > 10 fold higher than the protein concentration.

6.2.3 BOCILLIN FL Stained Gels

7.5 μ g of each protein was reacted with 1 μ M of BOCILLIN FL for 20 minutes in a buffer of 50 mM *bis*-Tris propane (Merck) pH 8.5, 75 mM NaCl, 1 % (v/v) DMSO, before the reaction was terminated by the addition of SDS loading dye (16.7 mM Tris pH 8.8, 0.67 % (w/v) SDS, 6.7 % (v/v) glycerol and 0.005% (w/v) bromophenol blue, 10 mM DTT). The samples (0.75 μ g) were loaded into Mini-PROTEAN TGX Precast 4-20 % gels (Bio-Rad) along with a Color Prestained Protein Standard ladder (New England Biolabs). Electrophoresis was carried out at 140 V for 50 minutes in 25 mM Tris pH 8.3, 190 mM glycine and 0.1 % (w/v) SDS. The gels were rinsed in water then imaged by a Typhoon FLA 9500 (Cytiva) imager with a 473 nm excitation laser and a 510 nm emission filter (LPB (510LP)). The gels were then stained with coomassie dye (Instant Blue, Exedon) and imaged by white light transillumination in a GeneSnap G:Box Gel Doc (Syngene).

6.2.4 Denaturing Mass Spectrometry

Denaturing mass spectrometry was carried out on a RapidFire RF365 high throughput sampling robot connected to a 6550 QTOF, by collaboration with the University of Oxford (C. Schofield group): with thanks to Dr. A. Krajnc and Dr A. Tumber. 1 μ M of protein was reacted with 10 μ M of nitrocefin in 50mM sodium phosphate, pH 7.5 buffer and the mass spectra recorded in positive mode. Full methods will be published in a forthcoming publication (*in preparation*).

Methods investigated for tryptic digest mass spectrometry are given in section 6.S3.

Methods for the crystallography (Carried out by D. Bellini) are given in section 6.S4.

6.3 Results

6.3.1 Crystal Structures

During analysis of crystallographic data of β -lactams reacted with *P. aeruginosa* PBP3 (PaPBP3), the double binding of nitrocefin to a Y409A substitution mutant of PaPBP3 (PaPBP3_{Y409A}) was unexpectedly observed (Figure 6.3). In contrast, only a single nitrocefin is observed in the crystal structure with the wild type protein (PaPBP3_{wt}) (Figure 6.4). This is a novel configuration for a PBP: β -lactam complex. The Y409A mutant was originally of interest as Tyr409 is one of the only active site residues (outside of the flexible loop regions, see Chapter 4) with significant conformational flexibility (Figure 6.S1).

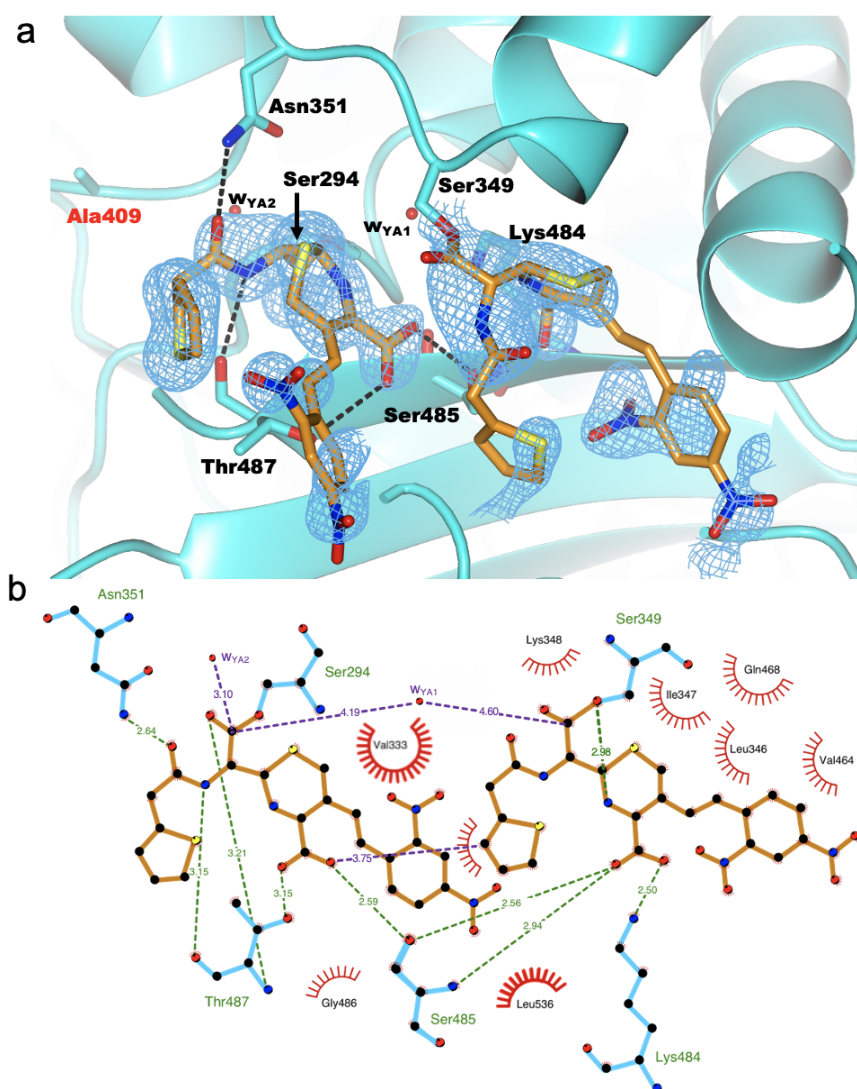


Figure 6.3. Crystal structure of nitrocefin-reacted PaBPB_{Y409A}. Nitrocefin reacts separately with Ser294 and Ser349 in the PaBPB_{Y409A} structure. (a) Neighbouring residues are shown in sticks and are labelled. Hydrogen bonds (black dashed lines) are shown from the nitrocefin ligands to nearby residues. Two waters (w_{YA1} and w_{YA2}) are found in the active site. Composite omit maps (contoured at 1 σ) are shown around the nitrocefin ligands. A comparison of the active sites of both structures is shown in Figure 6.4. (b) LigPlot 2D representation of the active site²⁷, showing polar (green dashed lines) and non-polar interactions (red arcs) of the two reacted nitrocefin molecules (orange). The shortest distance between the two molecules (3.75 Å) and the distance from w_{YA1} and w_{YA2} to the β -lactam-derived carbonyl carbons are shown with purple dashed lines.

The PaBPB_{Y409A} crystal structure does not have complete coverage of the ligand; in particular the flexible nitrophenyl-containing side chain, R2 (Figure 6.1), has only very weak density in both observations within the PaBPB_{Y409A} structure (Figure 6.3), as well as in the single nitrocefin-reacted PaBPB_{3wt} structure (6.S2). This is consistent with another report of nitrocefin bound to a PBP from the actinobacterium

Actinomadura in the PDB (PDB: 1W8Y ²⁸), although the nitrophenyl was fully resolved in two other PBP-nitrocefins complexes (PDB: 2UWX ¹⁴ and 1MWS ²⁹). Double binding of nitrocefins was not observed in any of these structures.

The “second” (novel) molecule of nitrocefins reacts with the side chain γ -OH of Ser349, to form an analogous acyl-enzyme complex to the β -lactam adduct of the canonical Ser294 side chain. The second nitrocefins extends into the active site cleft to the right of the first (Figure 6.3) and significantly disrupts the conformation of the α 10- β 3 loop (Figure 6.4), preventing it from being resolved in the crystal structure. The second nitrocefins makes hydrogen bonds with Ser485 and Lys484 via its C-4 acid group, but no other polar interactions to active site residues. The two reacted nitrocefins molecules make no direct interactions to one another and at their closest they are 3.75 Å apart (Figure 6.3b).

In the two nitrocefins-reacted structures (PaPBP3_{wt} and PaPBP3_{Y409A}) Ser349 is observed in three different conformations, with two alternate conformations seen in the PaPBP3_{wt}:nitrocefins complex (Figure 6.4c). Ser349 faces out of the active site (in a *gauche*⁺ conformation) when reacted with nitrocefins, in contrast to its inward conformation (*trans*) when reacting with boronate compounds (Chapter 5) (Figure 6.4d). Figure 6.4c-g shows a comparison of the position of Ser349 in both of the nitrocefins-reacted structures as well as in the PaPBP3:**13** and PaPBP3:piperacillin complexes.

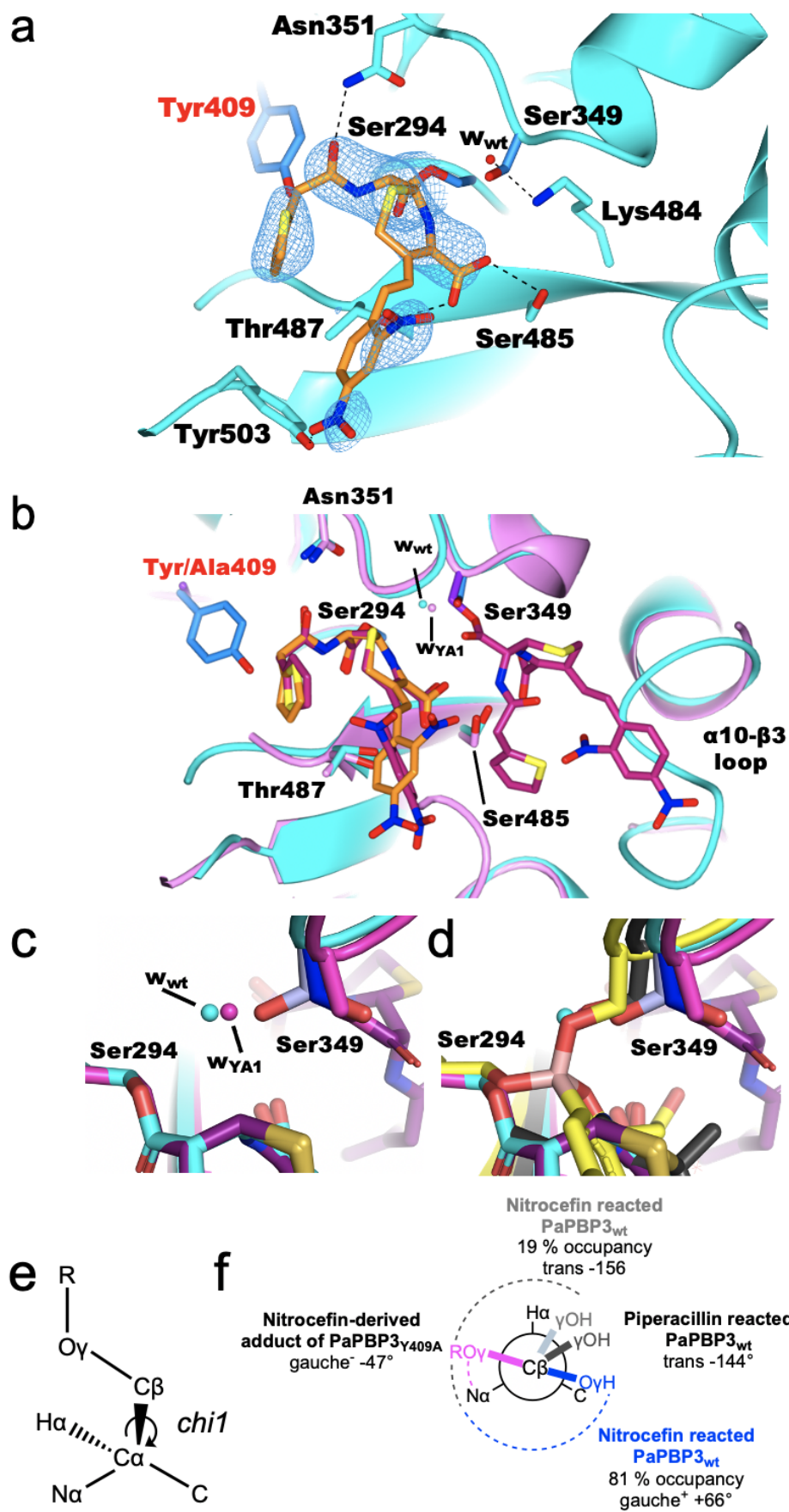


Figure 6.4. Electron density of nitrocefin-reacted PaBPB3_{wt} (a) and comparison of the active sites of crystal structures of PaBPB3_{wt} and PaBPB3_{Y409A} reacted with nitrocefin (b), including the positions of serine residues (c-f). The PaBPB3_{wt} protein structure is coloured in cyan and the reacted nitrocefin ligands coloured orange. The PaBPB3_{Y409A} protein structure (b) is coloured in pink and the reacted nitrocefin ligands coloured purple. Nitrocefin reacts with Ser294 in the PaBPB3_{wt} structure, and with Ser294 and Ser349 (separately) in the PaBPB3_{Y409A} structure. Neighbouring residues are shown in sticks and are labelled. Hydrogen bonds (black dashed lines) are shown from the nitrocefin ligands to nearby residues. Residues Ser294, Ser349 and Tyr409/Ala409 are shown in darker blue in the PaBPB3_{wt} structure and purple in the PaBPB3_{Y409A} structure. In the PaBPB3_{wt} structure, only one of the two alternate conformations of Ser349 is shown. A water (w_{wt} and w_{YA1} for the structures with PaBPB3_{wt} and PaBPB3_{Y409A} respectively) is shown positioned similarly in the active site of both structures. (c) The position of Ser294 is similar in the PaBPB3_{wt} (cyan) and PaBPB3_{Y409A} (pink) nitrocefin-reacted structures, but Ser349 can rotate. In the PaBPB3_{wt} structure, two conformations of Ser349 were observed with occupancies of: 19 % (pale blue) and 81 % (dark blue). A water (w_{wt} , occupancy: 81 %) is found close to the serine when Ser349 is in the outwards (dark blue) conformation. In the PaBPB3_{Y409A} structure a water (w_{YA1}) sits in a similar position. (d) Comparison of the position of both serine residues with other PaBPB3 structures: PaBPB3:13 (yellow, see Chapter 5) and PaBPB3:piperacillin (black, PDB: 6R3X²⁵). There is a difference of 1.3 Å between the position of the C α of Ser349 of the PaBPB3:13 complex and that of the PaBPB3_{wt}:nitrocefin structure. (e) Serine atom and dihedral bond angle labelling. (f) The *chi1* bond angles of Ser349 of the PaBPB3_{wt} and PaBPB3_{Y409A} nitrocefin reacted structures, compared to the piperacillin reacted structure. Ser349 is unreacted in PaBPB3_{wt} structures, but reacted with nitrocefin in the PaBPB3_{Y409A} structure. Dihedral bond angles are measured relative to the serine N α atom.

6.3.2 Substrate Inhibition Kinetics

6.3.2.2 Nitrocefin Turnover by gram-negative class B PBPs

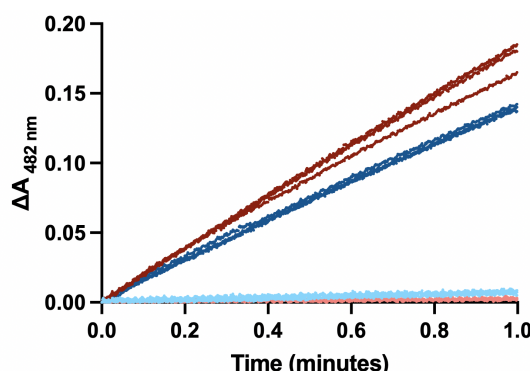


Figure 6.5. Change in absorbance at 482 nm due to nitrocefin turnover. Individual readings each of the 3 repeats are plotted as dots. The PaBPB3_{wt}-catalysed turnover rate (dark colours) is compared to the background turnover rate (light colours): nitrocefin at 48 μ M (red and pink) and nitrocefin at 160 μ M (blue and cyan).

Nitrocefin turnover can be observed by measuring the change in absorbance at 482 nm ($A_{482\text{nm}}$)¹⁰ (Figure 6.5). After acylation by a PBP, the red cephalosporic acid produced is strongly shifted from the yellow nitrocefin ($\lambda_{\text{max}} = 390 \text{ nm}$)³⁰ (Figure 1.5). Measuring the rate of nitrocefin turnover at several concentrations (8-200 μM of nitrocefin) revealed that several of the enzymes investigated (PaPBP3_{wt}, AbPBP3, EcPBP3) appear to have substrate inhibition kinetics (Figure 6.6 and Table 6.1). The PaPBP3_{Y409A} protein had a highly attenuated turnover rate (~40-fold reduction in k_{cat} , compared to PaPBP3_{wt}) and appeared to show simple saturation kinetics. To probe the role of Ser349 in the putative substrate inhibition mechanism, a S349A mutant (PaPBP3_{S349A}) was produced. The PaPBP3_{S349A} has very different kinetics to the wild type protein: the K_M was ~ 8-fold higher and the $k_{\text{cat}} > 10$ -fold lower. A mutant of the active site serine: Ser294 (PaPBP3_{Ser294}) showed insignificant turnover compared to the background turnover rate under the conditions tested.

To test the generality of the substrate inhibition, the nitrocefin turnover kinetics of class B PBPs from two other gram-negative species were investigated: *A. baumannii* PBP3 (AbPBP3) and *E. coli* PBP3 (EcPBP3). AbPBP3 and EcPBP3 have slower turnover (8-fold and 20-fold lower respectively) than PaPBP3, but appear to have substrate inhibition kinetics. For EcPBP3, the K_M was too low to be determined (<15 fold above the protein concentration) and the shallow negative gradient of the right hand portion of the graph (Figure 6.6c; $-1.4 \times 10^{-3} \text{ min}^{-1} \cdot \mu\text{M}^{-1}$ compared to $-44.6 \times 10^{-3} \text{ min}^{-1} \cdot \mu\text{M}^{-1}$ for PaPBP3_{wt}) also makes it impossible to define the K_{SI} of the interaction accurately.

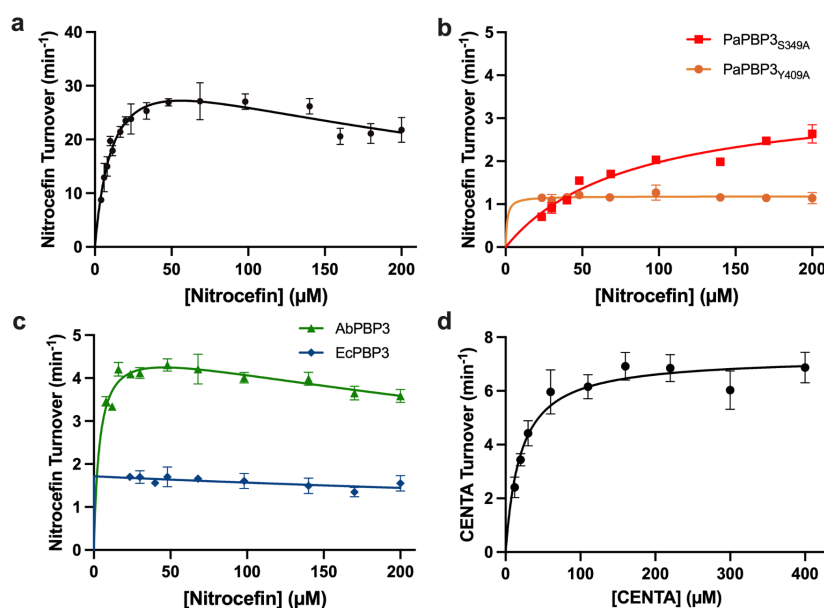


Figure 6.6. The kinetics of nitrocefin and CENTA turnover by PBPs. (a-d) Substrate concentration nitrocefin turnover graphs in the presence of: (a) PaPBP3_{wt} (protein concentration: 0.4 μM); (b) PaPBP3_{S349A} (red, squares) and PaPBP3_{Y409A} (orange, circles) (both: 2.4 μM); (c) AbPBP3 (green, triangles, 0.8 μM), EcPBP3 (blue, diamonds, 1.8 μM). (d) CENTA turnover rates with PaPBP3_{wt} (PBP concentration: 0.8 μM). Data points were fitted using non-linear regression (solid line) in Prism 9 for Mac OS (Graphpad) to equation 6.2 (a and c) or equation 6.1 (b and d). The best fit parameters are shown in Table 6.1. For all graphs, standard deviation of 3 points is shown for each point.

Substrate	Protein	Model ^a	k_{cat} (min ⁻¹) ^b	K_M (μM) ^b	K_{SI} (μM) ^b
Nitrocefin	PaPBP3 _{wt}	SI	39.0 ± 2.5	12.1 ± 1.7	259.1 ± 49.1
	PaPBP3 _{S294A}	ND	- ^c	-	-
	PaPBP3 _{S349A}	SS	3.6 ± 0.2	81.3 ± 10.2	-
	PaPBP3 _{Y409A}	SS	1.2 ± 0.03	<24 ^d	-
	AbPBP3	SI	5.0 ± 0.2	3.8 ± 0.7	552.9 ± 107.5
	EcPBP3	SI	1.7 ± 0.2	<24 ^d	>200 ^e
CENTA	PaPBP3 _{wt}	SS	7.3 ± 0.2	20.0 ± 2.9	-

Table 6.1. Kinetics of nitrocefin and CENTA turnover. ^aModels- SI: substrate inhibition, fitted with equation 6.2; ND: constants could not be determined under the conditions tested; SS: simple saturation, fitted with equation 6.1. Substrate concentration curves for SI and SS models are shown in Figure 6.6. ^bErrors are standard errors of the mean calculated by Prism 9. ^cConditions for nitrocefin turnover were not identified. ^d K_M is lower than the lowest concentration of nitrocefin tested. ^e K_{SI} is not determinable with confidence from the data collected.

6.3.2.3 CENTA turnover by PaPBP3

To determine whether substrate inhibition is observed with other β -lactams, turnover of another chromogenic cephalosporin, CENTA^{1,3} (12 - 400 nM) was investigated. Upon reaction, CENTA loses a leaving group, which leads to the change in absorbance³ (Figure 1.5). Unlike nitrocefin, this appears to have simple saturation kinetics when reacting with PaPBP3 (Figure 6.6d and Table 6.1).

6.3.3 Reactions with BOCILLIN FL

The ability of the PBPs to bind BOCILLIN FL was investigated with gel electrophoresis (Table 1.2). All proteins except PaPBP3_{S294A} and PaPBP3_{S349A} were able to react with BOCILLIN FL under the conditions tested (Figure 6.7).

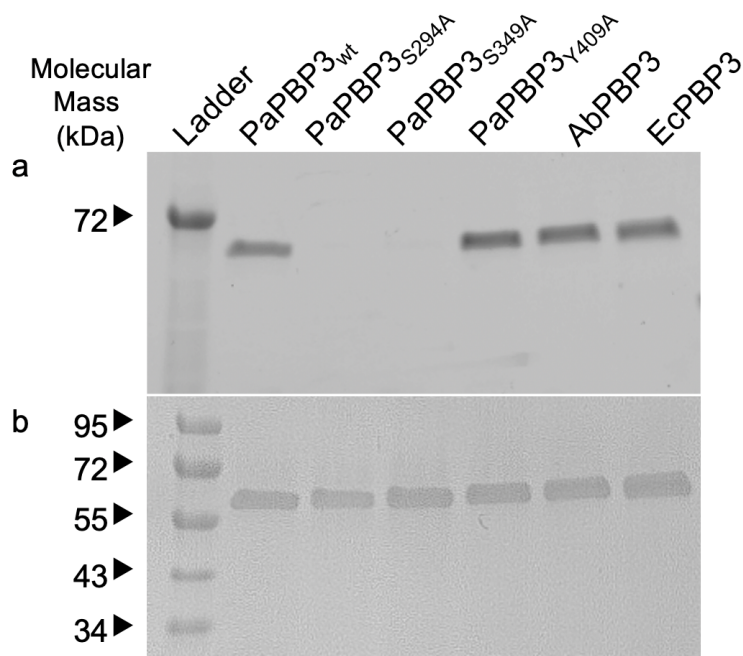


Figure 6.7. BOCILLIN FL (a) and coomassie (b) staining of an SDS-PAGE gel. (a) BOCILLIN FL (1 μ M) was reacted with each PBP (7.5 μ g) for 20 minutes before the reaction was terminated by the addition of SDS. Fluorescence was measured using a Typhoon FLA 9000. The ladder has a fluorescent marker protein at 72 kDa. (b) Coomassie staining was carried out on the same gel after the fluorescence was measured. Gel representative of 2 replicates.

6.3.4 Denaturing Mass Spectrometry

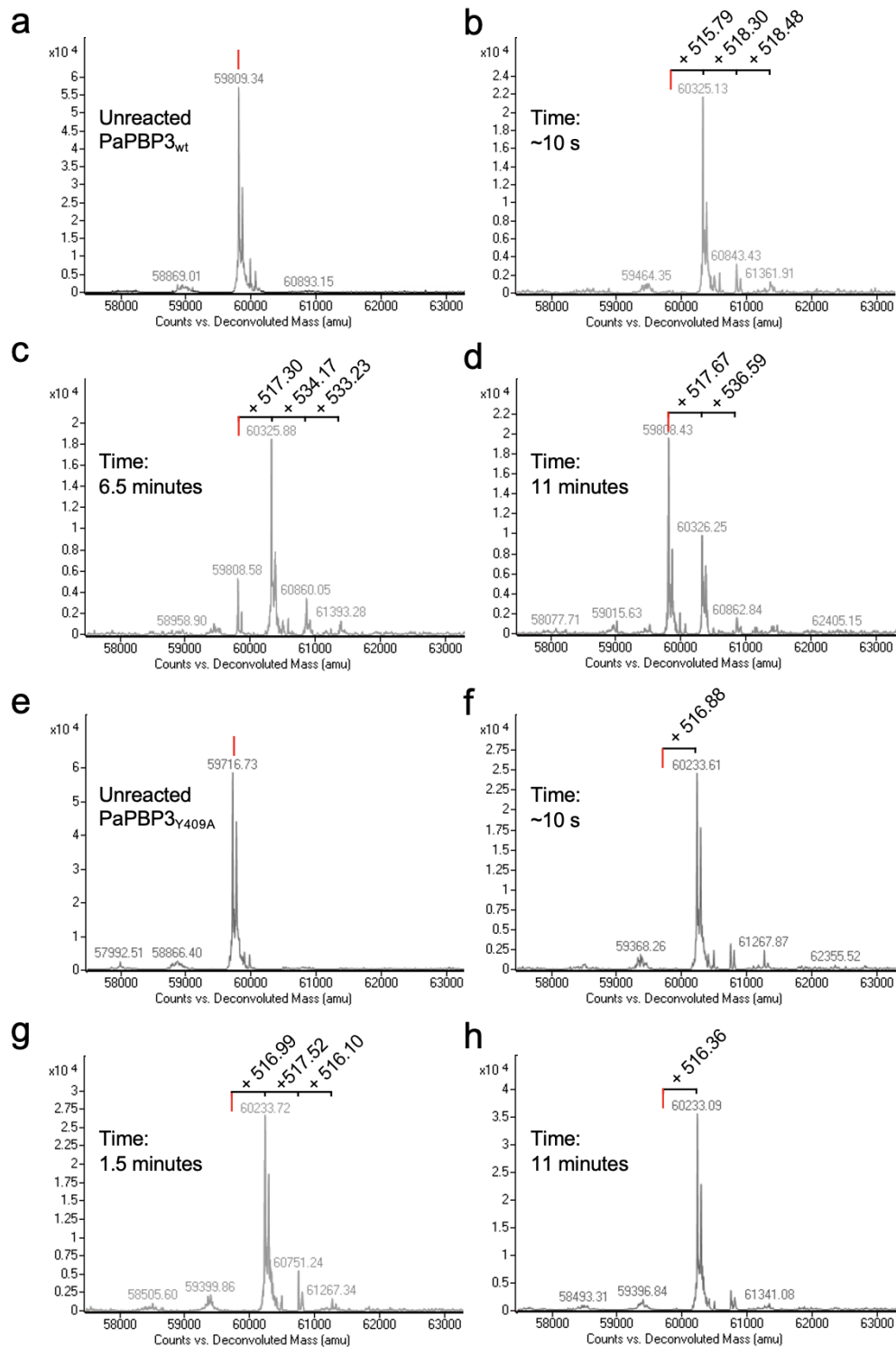


Figure 6.8. Denaturing mass spectrometry of the reaction of PaBPB3_{wt} (a-d) and PaBPB3_{Y409A} (e-h) with nitrocefin. Deconvoluted mass spectra show masses corresponding to the *apo* protein ion for (a) PaBPB3_{wt}, predicted mass

(from sequence): 59809.29 Da, observed 59809.34 Da and (e) PaPBP3_{Y409A}, predicted mass: 59717.19 Da, 5916.73 Da. A red line indicates the position of the *apo* protein with additional peaks corresponding to adducts of nitrocefin (expected incremental Δ mass: 516.50 Da). Significant peaks are labelled and the differences between peaks are given in daltons. Reaction time courses were measured by sampling from the same reaction at multiple time points. The instrument dead time was ~ 10 s, preventing measurement of the reaction before this time. For both proteins, a PBP-nitrocefin complex was formed within 10 s (b and f). For PaPBP3_{wt} (a-d), sufficient nitrocefin (initial concentration: 10 μ M) was turned over by 6.5 minutes to observe a mass corresponding to *apo* protein (c), which was the major ion after 11 minutes (d). For PaPBP3_{Y409A}, the reaction velocity is presumably too slow (Table 6.1) to fully turnover the nitrocefin so the *apo* protein mass was not observed after 11 minutes. A mass corresponding to the reaction of two nitrocefin molecules ($n = 2$) with the PaPBP3_{Y409A} (observed: 60751.24, expected: 60749.73 Da) is large relative to the major ion after 1.5 minutes of reaction (g) but has reduced abundance after 11 minutes (h).

Mass spectra of the wild type and three active site mutants of PaPBP3 (Figure 6.8 and Figure 6.9) reacting with nitrocefin were recorded under denaturing conditions. PaPBP3_{wt} and PaPBP3_{Y409A} react rapidly (<10 s) and completely (i.e. no *apo* protein mass is observed in Figure 6.8b or d) with nitrocefin to produce an ion corresponding to a singly reacted nitrocefin molecule (i.e. $(\text{PBP3} + nS)^+$, where S is nitrocefin and $n = 1$). For PaPBP3_{wt} it appears little nitrocefin remains after 11 minutes as the *apo* protein ion is once again observed. The lower rate of nitrocefin turnover recorded in absorbance assays for PaPBP3_{Y409A} is reflected in the lack of reformation of the *apo* ion after 11 minutes (Figure 6.8h) with this mutant.

The mass spectral analysis of each protein reacting with nitrocefin shows a mass corresponding to the adduct of two or more molecules of nitrocefin (i.e. $(\text{PBP3} + nS)^+$, where $n \geq 1$). The presence of additional adducts is particularly clear in the PaPBP3_{S294A} spectra (Figure 6.9a), where they appear up to $(\text{PBP3} + 3S)^+$, with each subsequent adduct (increasing values of n) having progressively lower abundance. It is possible these adducts correspond to nonspecific interactions of protein and ligand³¹, as masses corresponding to $(\text{PBP3} + 2S)^+$ are not anticipated in the Ser294 and Ser349 mutants and they appear at roughly constant abundance ($< 0.3 \times 10^4$) in all mass spectra (Figure 6.8 and Figure 6.9).

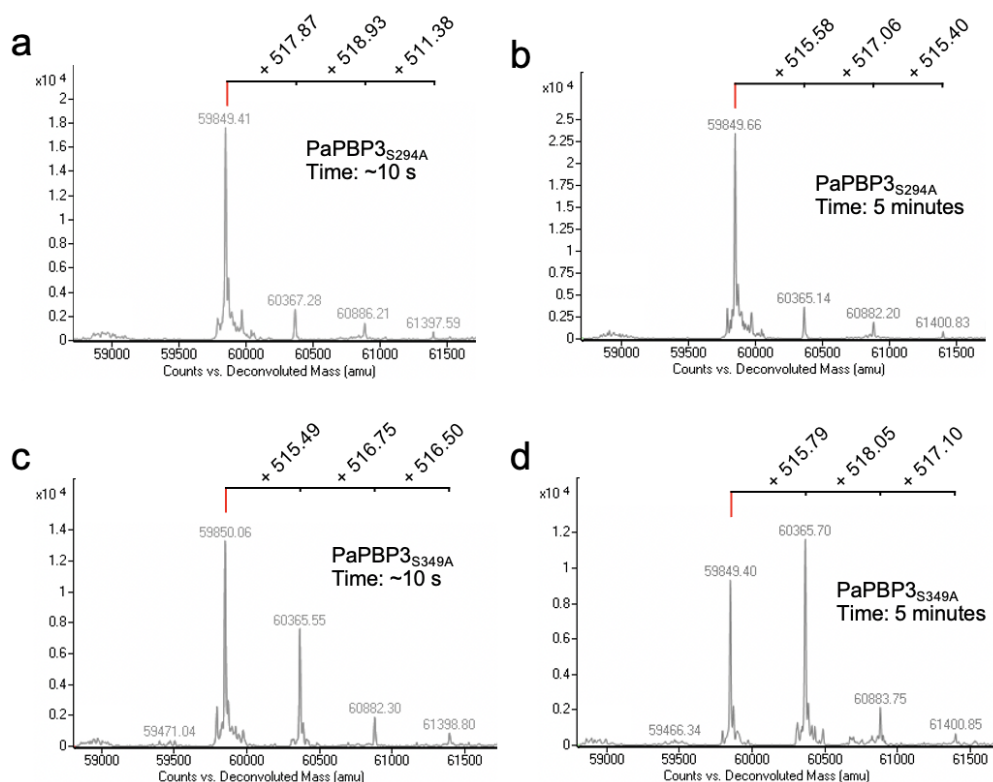


Figure 6.9. Denaturing mass spectrometry of the reaction of PaBPB3_{S294A} (a and b) and PaBPB3_{S349A} (c and d) with nitrocefin. Both proteins were reacted with nitrocefin and their mass spectra were recorded after ~10 seconds (a and c) and 5 minutes (b and d). Significant peaks are labelled and the differences between peaks are given in daltons. The red line indicates the position of the *apo* protein, confirmed by a spectra of the unreacted protein. Both proteins have an expected mass of 59793.29 Da, but the observed *apo* protein mass is ~59849 for both proteins, a difference of ~56, which in the absence of detectable amino acid substitutions may correspond to an adduct of an ⁵⁶Fe ion possibly at the His-tag: further work is needed to confirm this. Additional masses corresponding to adducts of up to 3 nitrocefin molecules ($n = 3$) are observed in the spectra with both proteins, after both 10 s and 5 minutes.

The PaBPB3_{Y409A} mass spectrum (Figure 6.8g) has a relatively large (PBP3 + 2S)⁺ peak after 1.5 minutes, which is not seen after 11 minutes (Figure 6.8g). This may correspond to a specific interaction of nitrocefin with Ser349 in the active site. However, the presence of apparently nonspecific (PBP3 + n S)⁺ ions makes it difficult to assign the specific (PBP3 + 2S)⁺ with confidence.

6.3.5 Tryptic Digest Mass Spectrometry

Analysis of a PBP-nitrocefin complex by tryptic digest mass spectrometry could be used to confirm the binding site(s) of nitrocefin within the protein. The addition of the mass of the nitrocefin-derived adduct should be detectable by liquid chromatography coupled to mass spectrometry analysis (LC-MS/MS)³². This method has previously been used to detect the β -lactam binding site of β -lactamases^{33,34}. Disappointingly, it was not possible to identify the site of nitrocefin reaction by tryptic mass spectrometric digest, despite several attempts (Table 6.2, section 6.S3). Peptides covering almost all of the protein were found but none were shown to have the nitrocefin-derived adduct (Table 6.2). This result is consistent with a previous unsuccessful attempt (using a similar method) by researchers at Eli Lilly to identify the catalytic residues of MRSA PBP2a which interact with nitrocefin

13.

Trial	Protein	Amount of PBP digested	Compound	Reaction Conditions	Unfolding Conditions	Trypsin Digest ^a	Protocol	Coverage ^b	Adduct
A	PaPBP3 _{Y409A} , PaPBP3 _{wt} , AbPBP3	100 μ g	Ceftazidime and Nitrocefin, 100 μ M	5 minutes, rt	8 M Urea	Overnight, 1:50	I	70%: Ser294 but no Ser349 coverage	No
B	PaPBP3 _{Y409A}	20 μ g	Nitrocefin, 100 μ M	5 minutes, rt	8 M Urea	4 hours, 1:20	I	83%	No
C	PaPBP3 _{Y409A}	20 μ g	Nitrocefin, 10 μ M	2 minutes, rt	99 °C 5 minutes heat shock.	4 hours, 1:20	II	96%	No
D	PaPBP3 _{Y409A}	5 μ g	Nitrocefin, 100 μ M	3 minutes, rt	99 °C 5 minutes heat shock.	4 hours, 1:20	II	58% Ser294 but no Ser349 coverage	No
E	PaPBP3 _{wt}	60 μ g	Nitrocefin, 1 mM	5 minutes, rt	SDS	4 hours, 1:20	III	97%	No

Table 6.2. Screens to identify tryptic digestion mass spectrometry conditions for stable adduction. ^aTime exposed to trypsin and protein:trypsin ratio given.

^bCoverage is the percentage of the peptide sequence observed by mass spectrometry. rt: room temperature; SDS: sodium dodecyl sulphate.

6.4 Discussion

6.4.1 Structural Analysis

The crystallographic observation of two molecules of a β -lactam acylating the active site of a PBP is, to my knowledge, without precedent amongst the many reported PBP: β -lactam crystal structures. The density around the “second” nitrocefins reacting with Ser349 is not complete in the PaPBP3_{Y409A} structure, but there is sufficient density around the core of the compound to be confident of its presence. The R1 and R2 side chains (Figure 6.1) of the “second” nitrocefin that reacts with PaPBP3_{Y409A} as well as the nitrocefin in the PaPBP3_{wt} structure are poorly defined by the electron density, likely due to their flexibility (they make few direct hydrogen bonds, Figure 6.3). The position of the R2 side chain of the “second” nitrocefin reacted with PaPBP3_{Y409A} is particularly ambiguous. It is modelled extending into a region normally occupied by the α 10- β 3 loop of the protein. Like the side chain, the α 10- β 3 loop lacks clear density and its conformation is very poorly resolved. It appears that in the presence of the second nitrocefin the conformation of the loop is disrupted, increasing its flexibility, and preventing its resolution. This disruption has analogy with the dynamic conformations of the α 10- β 3 loop observed when various novel boronate compounds bind to PaPBP3 (Chapters 4 and 5). The α 10- β 3 loop of the PaPBP3_{wt}:nitrocefin structure is fully resolved.

In neither the PaPBP3_{wt} nor the PaPBP3_{Y409A} nitrocefin-reacted structure is the β 5- α 11 loop resolved (residues 530-536 and 531-534 respectively are missing). This is consistent with the structures of PaPBP3:boronate complexes, many of which lack electron density for this loop (Chapter 5). The nitrophenyl group of the R2 sidechain of the Ser294-reacting nitrocefin is located in a similar position to the hydrophobic wall residues Tyr532 and Phe533³⁵ of the PaPBP3:piperacillin complex (PDB: 6R3X²⁵), which may prevent the β 5- α 11 loop from entering the “closed” conformation (Chapter 4).

The crystallography data was collected after soaking crystals with 10 mM of nitrocefin for 60 minutes. This concentration is many fold higher than the concentrations used in the assays or mass spectrometry. Soaking (where a high concentration of the compound is added to a pre-grown crystal) was used to add nitrocefin to PaPBP3. This means that the reaction did not occur in solution but in

the crystal phase of the protein (which also has a much higher concentration than in solution), which may affect the kinetics. It is possible that the observation of nitrocefin bound to Ser349 is a crystallographic artefact, but the lack of the second nitrocefin in the wild type structure or at the various other solvent-exposed serines within the protein indicates specificity of the reaction.

6.4.2 Nitrocefin Kinetics

The PaBPB3_{wt} nitrocefin turnover rates are much faster than values reported for PaBPB3_{wt} turnover of other β -lactams (e.g. meropenem turnover (the rate limiting deacylation step) is just 0.02 min^{-1})³⁶, but still much slower than nitrocefin turnover rates by β -lactamases (e.g. TEM-1 can turnover nitrocefin at rates of $> 4 \times 10^4 \text{ min}^{-1}$: more than one thousand fold faster than PaBPB3)³⁷. Comparison between PaBPB3_{wt}, AbBPB3 and EcBPB3, show significant differences in their behaviour, despite their structural and sequence similarities (Figure 1.3). Catalytic fine tuning as a result of small differences in the spatial geometry of the active site and/or non-conserved residues may cause the variance in the behaviour of these proteins. Although weak, there does appear to be substrate inhibition in AbBPB3 and possibly in EcBPB3, which suggests conservation of the substrate inhibition mechanism between species.

The differences in the K_M and k_{cat} of CENTA and nitrocefin for PaBPB3_{wt} are consistent with other reports which show that substrate specificity for CENTA and nitrocefin varies between enzymes³. The apparent lack of substrate inhibition (under the conditions tested) in CENTA is interesting and suggests that the mechanism may have some specificity to nitrocefin. CENTA has a 3-position leaving group³ but nitrocefin does not, which may be important. Unfortunately, studies (using similar techniques) with other β -lactams are experimentally challenging in PBPs due to their low turnover rates and their generally small extinction coefficients (typically $< 1000 \text{ M}^{-1} \cdot \text{cm}^{-1}$)³⁸, which would necessitate very high protein concentrations to get measurable signals.

6.4.3 β -lactam Kinetics Beyond Gram-Negative Class B PBPs

Other HMM PBPs have been investigated for their reactions with nitrocefin: *S. aureus* PBP2a³⁹, *Streptococcus pneumoniae* PBP1b¹⁴ and PBP2b¹² and *E. coli*

PBP1b¹⁰. For each of these proteins, the nitrocefin turnover rate was either not measured or $< 0.03 \text{ min}^{-1}$. For *S. pneumoniae* PBP2b, mutations in a clinical strain were shown weakly to increase the rate of deacylation (Chapter 4)¹²; Interestingly, Page describes EcPBP1b as having biphasic kinetics and greater-than-stoichiometric acylation of the protein¹⁰. After several enzyme turnovers the formation of a “new inhibited species” was observed which slows the turnover. The new species was attributed to a conformational change within the protein¹⁰, but the formation of a doubly acylated EcPBP1b is also consistent with these observations.

Examples across all classes of serine β -lactamase (class A, C, and D) have shown non-stoichiometric burst kinetics for the reaction of β -lactamase with many different β -lactams tested^{4,7,8,40–42}. This behaviour is typically described as “substrate-induced inactivation”⁴² and not substrate inhibition: that is to say the transition to the less active form is a consequence of interaction with β -lactam substrates, but does not appear to be substrate concentration dependent. Waley suggested that the inactivation is the result of branching at the level of the *ES* complex to a less active form⁴², a mechanism that is similar to the model shown in Scheme 6.1b, but without the molecule of substrate required for the transition from *ES* to *ESS*.

6.4.4 Kinetics Models

Considering first only the reaction of a single nitrocefin with PBP3, the kinetic scheme (Scheme 6.1a) used to fit the data to Briggs-Haldane steady state models is a simplification of the scheme presented in Scheme 1.2. It is expected nitrocefin will pass through both of the complexes described (*E·I* and *EI*) during a turnover cycle, however the kinetic model reduces the two catalytic reactions (covalent bond formation and bond hydrolysis) to a single term: k_{cat} , effectively ignoring the *EI* complex⁴³. The magnitude of k_{cat} will be limited by the slowest of the two steps. Additionally, K_M also includes the k_{cat} term (equation 6.S5), which means that mutants affecting k_{cat} also affect K_M . Therefore within the context of a system obeying steady-state kinetics, it is not correct to say that the increase in K_M measured with PaPBP3_{S349A} is solely due to the change in affinity of the protein for nitrocefin: there is also a change in catalytic rate⁴⁴.

In addition to the simplifications present in kinetic model for Brigg-Haldane steady state nitrocefin turnover, the kinetic model of substrate inhibition (Scheme 6.1b)

makes a number of assumptions. It assumes that: (I) the “second” molecule of nitrocefin can only bind to the *ES* complex; (II) *ESS* is unproductive (or nitrocefin turnover from *ES* is so much faster than turnover from *ESS* that the *ESS* complex appears to be unproductive); (III) *ES* is in rapid equilibrium with *ESS* (necessary for the validity of equation 6.S2).

More complex kinetic models can be designed in which the *ESS* complex is productive (Scheme 6.S1a) or in which the “second” nitrocefin can bind to both *E* and *ES* (Scheme 6.S1b). Fitting of the rate equation to the former model (Scheme 6.S1c) to the data for PaBPB3_{wt} (Figure 6.6a) was attempted. An equivalent fit of the data was achieved, but several of the parameters were indeterminate, indicating that the model is too complex for the data. Therefore the simplest possible model for substrate inhibition (Scheme 6.1 and equation 6.3) was chosen for analysis of the data. This model may be sufficient given that K_{Si} is so much larger than K_M (almost 7 fold for PaBPB3_{wt}), so the fraction of enzyme in the doubly-bound form (i.e. $ESS/(E + ES + ESS)$) is small at the concentrations tested and the reactions of *ESS* make little contribution to the overall rate.

Unlike the kinetics experiments, both denaturing mass spectrometry and the BOCILLIN FL stained gel only measure the *EI* complex as the non-covalent *E·I* complex is lost due to the denaturing process. These techniques compared to the kinetics are making orthogonal observations of the same processes but both techniques here are only used qualitatively.

6.4.5 S294A and S349A Mutants

Alanine substitution of two serines in the active site: Ser294 (**SXXK**) and Ser349 (**SXN**) have differing effects. S294A leads to a complete loss of kinetic activity, consistent with the importance of this residue for catalysis. The mass spectrometry for PaBPB3_{S294A} (Figure 6.9a and b) shows little nitrocefin reaction beyond the rapid formation of apparently nonspecific nitrocefin adducts (see below). It therefore appears that this mutant is unable to acylate nitrocefin.

In contrast, the S349A substitution leads to an increase in K_M and decrease in k_{cat} . The k_{cat}/K_M for PaBPB3_{S349A} is $0.044 \mu\text{M}^{-1} \cdot \text{min}^{-1}$: 73 fold lower than the value for PaBPB3_{wt} ($3.22 \mu\text{M}^{-1} \cdot \text{min}^{-1}$), indicating the mutation has a significant effect on the

catalytic activity of the protein. Substrate inhibition is not observed in PaPBP3_{S349A}, which is consistent with S349A being the binding site for the second (inhibition-causing) molecule of nitrocefin. However, nitrocefin insolubility prevents measurement of turnover at higher nitrocefin concentrations, so it is not possible to confirm a lack of substrate inhibition: ideally values closer to k_{cat} should be observed.

The mass spectrometry of PaPBP3_{S349A} shows (unlike PaPBP3_{wt}) that the majority of the protein remained unligated after 10 s of reaction (Figure 6.9c), which may indicate this mutation is reducing the rate of acylation. Consistent with this, is the lack of (or slow) reaction with BOCILLIN FL, which could be due to a slow acylation rate.

The equivalent serine in Class A β -lactamases (Ser130) is hypothesised to assist in the β -lactam bond cleavage during acylation by hydrogen bonding to nitrogen and donating a proton^{45–47}, so it may have an analogous role in HMM PBP. The effect of S349A mutation on the rate of catalysis is within values reported for the analogous substitution in other proteins: S130A substitution in a class A β -lactamase (*Streptomyces albus* G β -lactamase) led to a 10 fold decrease in the k_{cat}/K_M for nitrocefin⁴⁸; S110A substitution in *E. coli* PBP5 (a LMM carboxypeptidase) decreased both acylation (83-fold vs wild type) and deacylation (8 fold vs wild type) of benzylpenicillin⁴⁹.

6.4.6 The Tyr409Ala Mutant

Steady state kinetic analysis shows that the Y409A substitution mutation leads to an almost 40-fold decrease in the nitrocefin k_{cat} compared to PaPBP3_{wt} ($39.0 \pm 2.5 \text{ min}^{-1}$ and $1.2 \pm 0.03 \text{ min}^{-1}$ for PaPBP3_{wt} and PaPBP3_{Y409A} respectively), whilst the K_M appears to remain low (<24 μM for both proteins). Furthermore, mass spectrometry shows the mutation does not prevent the rapid (< 10 s) acylation of the protein (Figure 6.8f). The kinetics of PaPBP3_{Y409A} were modelled with Briggs-Haldane kinetics (Equation 6.1), as opposed to substrate inhibition kinetics (Equation 6.3). However, this does not necessarily mean that substrate inhibition is not occurring, as the large reduction in the k_{cat} makes the absolute decrease in velocity at higher nitrocefin concentrations smaller (Figure 6.2), and therefore harder to measure with

certainty. Alternatively, the mutation might increase the value of K_{SI} to such an extent as to render it practically impossible to demonstrate substrate inhibition. The role of Tyr409 in the active site may be that it helps to position a water near to Ser294 for catalysis of the β -lactam-derived acyl bond. In the piperacillin-reacted PaBPB3 structure (PDB: 6R3X²⁵), a water is hydrogen bonded to Tyr409 as well as the β -lactam-derived carbonyl (Figure 6.10). In the PaBPB3_{Y409A}:nitrocefim structure the water is still present, but it is displaced slightly (0.3 Å) away from the β -lactam-derived carbonyl with concurrent loss of hydrogen bonds to Asn351. This could result in the decreased catalysis rate observed (Table 6.1). Curiously, in the PaBPB3_{wt}:nitrocefim this water is not observed, perhaps due to the structure's lower resolution (2.53 Å compared to 1.99 Å in the PaBPB3_{wt} and PaBPB3_{Y409A} nitrocefim-reacted structures respectively).

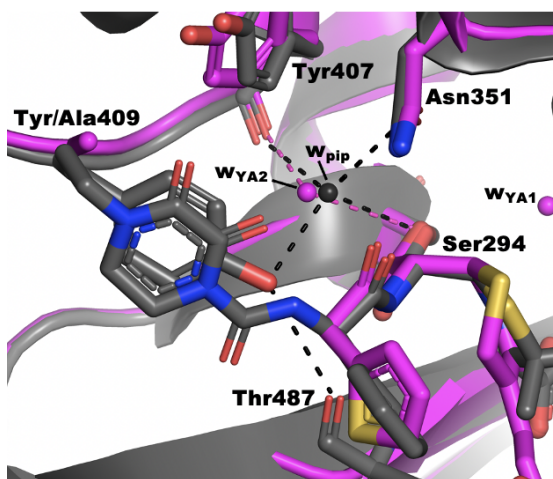


Figure 6.10. Waters near to the active site serine. Crystal structures of PaBPB3_{Y409A}:nitrocefim (pink) and PaBPB3_{wt}:piperacillin (black, PDB: 6R3X²⁵) complexes show a water (labelled **w_{YA2}** and **w_{pip}** respectively in the two structures). Hydrogen bonds are formed from **w_{pip}** to Ser294, Asn351, Tyr407 and Thr487, whereas **w_{YA2}** only hydrogen bonds to Ser294 and Tyr407. The water is displaced away from Ser294 in the PaBPB3_{Y409A}:nitrocefim complex: the distance from **w_{YA2}** to the β -lactam derived carbonyl carbon is 3.1 Å but the equivalent distance in the PaBPB3_{wt}:piperacillin is 2.7 Å. The distance from the water to the δ O of Asn351 increases from 3.0 Å in the PaBPB3_{wt}:piperacillin structures to 3.7 Å in the PaBPB3_{Y409A}:nitrocefim structure, with the associated loss of a hydrogen bond. The water **w_{YA1}** is also shown to the right of Ser294. A hydrogen bond between Tyr409 and Thr487 is shown.

6.4.7 Mass Spectrometry

Assuming uniform efficiency of ionisation of species, denaturing mass spectrometry of nitrocefin-reacted proteins creates a snapshot of the solution state of covalent complexes at a given time point. After denaturing the protein, only covalent adducts should remain, with non-covalent interactions dissociated. The results presented here appear to show that for PaPBP3_{wt}, PaPBP3_{S349A}, PaPBP3_{Y409A} a single nitrocefin-derived acyl-enzyme complex is formed as a major ion, whilst additional adducts of $n \geq 1$ are formed non-specifically. The adducts are designated to be non-specific from their presence in the catalytically inactive PaPBP3_{S294A}, their consistent low abundance and apparent high affinity (they are formed in <10 s). Investigation of comparable adducts in other proteins concluded that they form as the results of a random chemical process during the gas phase of the electrospray technique^{31,50}. Work to improve the quality of the mass spectra is ongoing. The use of a reference protein to measure only the non-specific portion of the interaction⁵⁰ or increasing concentration of salt ions to suppress non-specific interactions³¹ may be effective.

Alternatively, the non-specific adducts could be the result of the reaction of relatively reactive nitrocefin with solvent-exposed serines outside the active site. Adducts to other serines (i.e. not Ser294 or Ser349) are not observed crystallographically, but could occur in solution or be unobservable due to high mobility. Non-specific adducts such as these could provide an explanation for the observations of high affinity, irreversible interactions seen between nitrocefin and PaPBP3 in SPR experiments (Figure 2.11).

The mass spectrometry did not provide strong evidence of specific double binding of nitrocefin to PaPBP3. For PaPBP3_{Y409A}, a (PBP3 + 2S)⁺ ion was observed to form and decay (Figure 6.8e-h), although its abundance is too low to be sure of its specificity. Increasing the ligand concentration may increase the abundance of the doubly bound ion. Ideally concentrations above the kinetically determined K_{SI} (> 260 μ M) should be used for the mass spectrometry experiments but this is experimentally limited (to ~ 100 fold above protein concentration) by ion suppression which increases with ligand concentration⁵⁰.

6.4.8 Hypotheses on the Observation of Two Nitrocefin Molecules

One possibility for the presence of the two molecules of nitrocefin in the PaPBP3_{Y409A} structure proposes that the 'second' nitrocefin is able to react with Ser349 due to the slow nitrocefin catalysis of PaPBP3_{Y409A}. The structures of di-covalently reacted benzoxaboroles (e.g. Figure 5.6, Chapter 5) may offer a potential mechanism for this. Mono-covalently reacting boronates have previously been described as transition state mimics of β -lactam acylation^{16,51}; speculatively, di-covalently reacting boronates could be transition state mimics of nucleophilic attack on the Ser294 acyl-enzyme complex by Ser349, the result of which is the observed Ser349:nitrocefin complex (Figure 6.11). The di-covalent benzoxaborole crystal structures demonstrate that the two serine residues are sufficiently close and that the necessary reorientation of Ser294 is possible by rotation of *chi1* and *chi2* angles (Figure 5.10). This pathway may become dominant in PaPBP3_{Y409A} as the nucleophilic water **w_{YA2}** is displaced and becomes less reactive (Figure 6.10), leaving Ser349 as the most reactive nucleophile. An analogous mechanism in which the equivalent 'second' serine attacks an acylated catalytic site serine was proposed to explain a structure in which two serines are bonded to two different species following reaction of SHV-1 with tazobactam⁵².

Alternatively, the double reaction with nitrocefin may be an indirect consequence of the Y409A substitution. The substitution may have a similar effect to clinical mutations described in Chapter 4 (to my knowledge, mutations at position 409, or equivalent in other species, have not been identified in any clinical mutations). For example, this could be mediated via the loss of interactions of Tyr409 with backbone carbonyl of Thr487 on the β 3 strand (Figure 6.10, 6.S1). Changes to the β 3 strand could lead to a rearrangement of the α 10- β 3 loop, which opens up to allow nitrocefin to reach and react with Ser349.

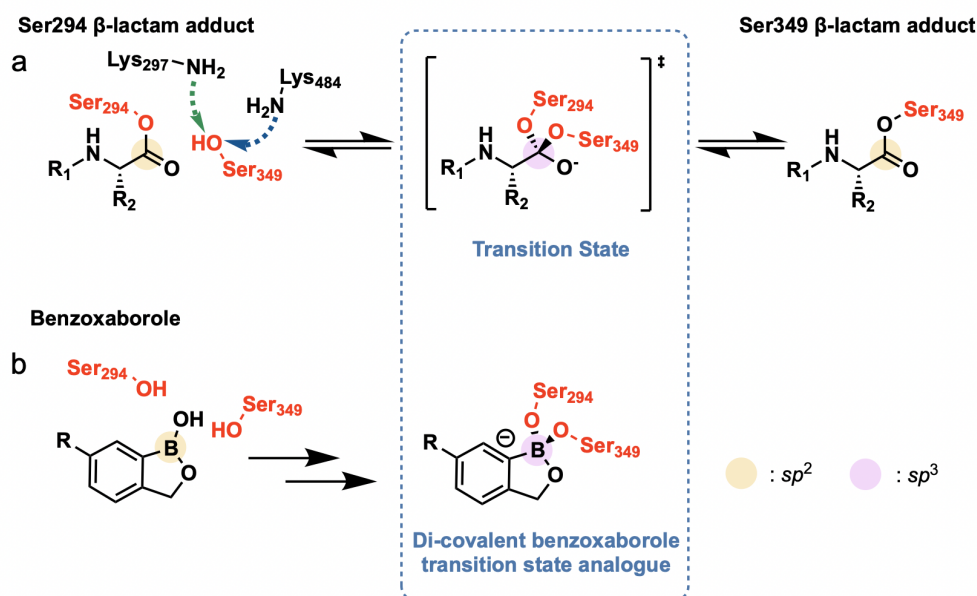


Figure 6.11. Di-covalently binding benzoxaboroles may mimic a transition state in a nitrocefin serine transfer mechanism. (a) A Ser294 nitrocefin adduct is first formed by the classical β -lactam reaction (e.g. Figure 1.2). After reorientation of the serine side chain and its β -lactam-derived adduct, nucleophilic attack by Ser349 of the β -lactam-derived carbonyl carbon can occur. Either Lys297 or Lys484 could act as the general base for the activation of Ser349 (shown with green or blue dashed arrows respectively). The result of the nucleophilic substitution is the transfer of the nitrocefin adduct from Ser294 to Ser349. (b) The transition state in this reaction is analogous to the di-covalent benzoxaborole complex (e.g. Figure 5.6).

Presently there is insufficient evidence to confidently determine the mechanism that leads to the formation of the doubly acylated complex. Nucleophilic attack by Ser349 (necessary in both mechanisms) will likely require activation by a general base, most likely either neutral Lys297 or Lys484 (green and blue arrows respectively in Figure 6.11). The general base mechanism is analogous to the acylation mechanism proposed in other penicillin reactive enzymes where Lys297 (or equivalent) activates Ser294 (or equivalent) for nucleophilic attack on the β -lactam ring^{45,46,53–56}.

However, it cannot be discounted that the complex may solely have arisen as the result of a crystallographic artefact in the PaBPB3_{Y409A}.

6.4.9 Future Work

Further work is required to fully characterise the doubly reacted PBP3 structure. Evidence for such a complex in solution remains ambiguous. Further kinetic experiments are required to establish the link between the crystallographic species and the substrate inhibition observed. The use of pre-steady state kinetics may provide insight into the rate constants for individual steps, as has been applied to study substrate-induced inactivation in β -lactamases^{42,57}. Kinetic studies at a range of pHs could be used to determine the pK_a of residues involved in catalysis^{6,54,58,59}. In particular it would be of interest to see if the degree of substrate inhibition is affected by pH, as it may be possible to distinguish reaction at the two serines by their pH profiles. In general, the catalytic mechanisms of residues in the HMM PBP active site⁵⁹ have been understudied compared to LMM PBPs or β -lactamases so further work may have a wider benefit.

Substitutions of Lys297 and Lys484 may be interesting to investigate. Whichever residue serves as a general base to Ser349, its mutation should slow or prevent nucleophilic attack by Ser349. To probe the role of Tyr409, further substitution of the position may be valuable. For example, substitution with hydrophilic phenylalanine or acidic glutamic acid may affect the behaviour of water w_{YA2} and perhaps affect double acylation.

Optimisations of the conditions for conducting denaturing mass spectrometry experiments may lead to clearer evidence of the doubly reacted species in solution. Mass spectrometry could be used to investigate whether other β -lactams are able to doubly react with PBPs, since this is challenging spectrophotometrically for non-chromogenic compounds. Once conditions have been established for the denaturing mass spectrometry, they may be applied to improve the quality of the tryptic digest mass spectrometry data to allow confirmation of double binding by this method.

Finally the penamaldate assay, once used to establish the stoichiometric binding of β -lactams to β -lactamases^{44,60,61}, could be used to independently establish the reaction stoichiometry, although $HgCl_2$ is toxic, presenting an experimental challenge.

6.5 Conclusion

This work focuses on initial efforts to understand the observation of double reaction of an active site mutant of PaPBP3 with the chromogenic β -lactam nitrocefin. Steady state turnover of nitrocefin by PaPBP3_{wt} and several active site mutants was carried out which showed substrate inhibition, a behaviour consistent with the binding of a second molecule of substrate. Substrate inhibition was observed in other class B PBPs from related species. Mass spectrometry of nitrocefin-reacted proteins shows turnover of the substrate, but does not provide firm evidence of doubly-reacted proteins. Tryptic digest mass spectrometry was unsuccessful and nitrocefin adducts could not be recorded. For now, caution must be taken when interpreting this interesting observation as a biologically relevant phenomenon. This effect may be limited to nitrocefin, which appears to have an unusually high turnover rate compared to other β -lactams³⁶. Nitrocefin (but not imipenem) has been reported to bind reversibly to the active site of a L,D-transpeptidase from *Enterococcus faecium*: a peptidoglycan cross-linking enzyme structurally unrelated to PBPs⁶². Nitrocefin itself then may be a unique β -lactam, capable of reacting in unique ways. If this behaviour can be better understood (perhaps with further insight from boronate binding), it may be possible to design a novel generation of inhibitors which exploit reactions at both Ser294 and Ser349, similarly to the reactions of e.g. clavulanic acid and tazobactam with β -lactamases^{52,63–65}.

6.6 References

- (1) Jones, R. N.; Wilson, H. W.; Novick, W. J.; Barry, A. L.; Thornsberry, C. In Vitro Evaluation of CENTA, a New Beta-Lactamase-Susceptible Chromogenic Cephalosporin Reagent. *J. Clin. Microbiol.* **1982**, *15* (5), 954–958.
- (2) O’Callaghan, C. H.; Morris, A.; Kirby, S. M.; Shingler, A. H. Novel Method for Detection of β -Lactamases by Using a Chromogenic Cephalosporin Substrate. *Antimicrob. Agents Chemother.* **1972**, *1* (4), 283–288. <https://doi.org/10.1128/AAC.1.4.283>.
- (3) Bebrone, C.; Moali, C.; Mahy, F.; Rival, S.; Docquier, J. D.; Rossolini, G. M.; Fastrez, J.; Pratt, R. F.; Frère, J.-M.; Galleni, M. CENTA as a Chromogenic Substrate for Studying β -Lactamases. *Antimicrob. Agents Chemother.* **2001**, *45* (6), 1868–1871. <https://doi.org/10.1128/AAC.45.6.1868-1871.2001>.
- (4) Ledent, P.; Frère, J. M. Substrate-Induced Inactivation of the OXA2 Beta-Lactamase. *Biochem. J.* **1993**, *295* (Pt 3), 871–878. <https://doi.org/10.1042/bj2950871>.
- (5) Thornewell, S. J.; Waley, S. G. Site-Directed Mutagenesis and Substrate-Induced Inactivation of β -Lactamase I. *Biochem. J.* **1992**, *288* (3), 1045–1051. <https://doi.org/10.1042/bj2881045>.
- (6) Chow, C.; Xu, H.; Blanchard, J. S. Kinetic Characterization of Hydrolysis of

- Nitrocefin, Cefoxitin, and Meropenem by β -Lactamase from *Mycobacterium Tuberculosis*. *Biochemistry* **2013**, 52 (23), 4097–4104. <https://doi.org/10.1021/bi400177y>.
- (7) Citri, N.; Samuni, A.; Zyk, N. Acquisition of Substrate-Specific Parameters during the Catalytic Reaction of Penicillinase. *Proc. Natl. Acad. Sci. U. S. A.* **1976**, 73 (4), 1048–1052.
 - (8) Frère, J.-M. Interaction between Serine β -Lactamases and Class a Substrates: A Kinetic Analysis and a Reaction Pathway Hypothesis. *Biochem. Pharmacol.* **1981**, 30 (6), 549–552. [https://doi.org/10.1016/0006-2952\(81\)90124-6](https://doi.org/10.1016/0006-2952(81)90124-6).
 - (9) Lietz, E. J.; Truher, H.; Kahn, D.; Hokenson, M. J.; Fink, A. L. Lysine-73 Is Involved in the Acylation and Deacylation of β -Lactamase. *Biochemistry* **2000**, 39 (17), 4971–4981. <https://doi.org/10.1021/bi992681k>.
 - (10) Page, M. G. P. The Reaction of Cephalosporins with Penicillin-Binding Protein Lby from Escherichia Coli. *Biochim. Biophys. Acta BBA - Protein Struct. Mol. Enzymol.* **1994**, 1205 (2), 199–206. [https://doi.org/10.1016/0167-4838\(94\)90234-8](https://doi.org/10.1016/0167-4838(94)90234-8).
 - (11) Graves-Woodward, K.; Pratt, R. F. Reaction of Soluble Penicillin-Binding Protein 2a of Methicillin-Resistant Staphylococcus Aureus with β -Lactams and Acyclic Substrates: Kinetics in Homogeneous Solution. *Biochem. J.* **1998**, 332 (3), 755–761. <https://doi.org/10.1042/bj3320755>.
 - (12) Calvez, P.; Breukink, E.; Roper, D. I.; Dib, M.; Contreras-Martel, C.; Zapun, A. Substitutions in PBP2b from β -Lactam-Resistant Streptococcus Pneumoniae Have Different Effects on Enzymatic Activity and Drug Reactivity. *J. Biol. Chem.* **2017**, 292 (7), 2854–2865. <https://doi.org/10.1074/jbc.M116.764696>.
 - (13) Roychoudhury, S.; Kaiser, R. E.; Brems, D. N.; Yeh, W. K. Specific Interaction between Beta-Lactams and Soluble Penicillin-Binding Protein 2a from Methicillin-Resistant Staphylococcus Aureus: Development of a Chromogenic Assay. *Antimicrob. Agents Chemother.* **1996**, 40 (9), 2075–2079. <https://doi.org/10.1128/AAC.40.9.2075>.
 - (14) Macheboeuf, P.; Guilmi, A. M. D.; Job, V.; Vernet, T.; Dideberg, O.; Dessen, A. Active Site Restructuring Regulates Ligand Recognition in Class A Penicillin-Binding Proteins. *Proc. Natl. Acad. Sci.* **2005**, 102 (3), 577–582. <https://doi.org/10.1073/pnas.0407186102>.
 - (15) Lovering, A. L.; Gretes, M. C.; Safadi, S. S.; Danel, F.; de Castro, L.; Page, M. G. P.; Strynadka, N. C. J. Structural Insights into the Anti-Methicillin-Resistant Staphylococcus Aureus (MRSA) Activity of Ceftobiprole. *J. Biol. Chem.* **2012**, 287 (38), 32096–32102. <https://doi.org/10.1074/jbc.M112.355644>.
 - (16) Brem, J.; Cain, R.; Cahill, S.; McDonough, M. A.; Clifton, I. J.; Jiménez-Castellanos, J.-C.; Avison, M. B.; Spencer, J.; Fishwick, C. W. G.; Schofield, C. J. Structural Basis of Metallo- β -Lactamase, Serine- β -Lactamase and Penicillin-Binding Protein Inhibition by Cyclic Boronates. *Nat. Commun.* **2016**, 7 (1), 12406. <https://doi.org/10.1038/ncomms12406>.
 - (17) van Berkel, S. S.; Nettleship, J. E.; Leung, I. K. H.; Brem, J.; Choi, H.; Stuart, D. I.; Claridge, T. D. W.; McDonough, M. A.; Owens, R. J.; Ren, J.; Schofield, C. J. Binding of (5 S)-Penicilloic Acid to Penicillin Binding Protein 3. *ACS Chem. Biol.* **2013**, 8 (10), 2112–2116. <https://doi.org/10.1021/cb400200h>.
 - (18) Briggs, G. E.; Haldane, J. B. S. A Note on the Kinetics of Enzyme Action. *Biochem. J.* **1925**, 19 (2), 338–339. <https://doi.org/10.1042/bj0190338>.
 - (19) Johnson, K. A.; Goody, R. S. The Original Michaelis Constant: Translation of the 1913 Michaelis–Menten Paper. *Biochemistry* **2011**, 50 (39), 8264–8269. <https://doi.org/10.1021/bi201284u>.
 - (20) Henri, V. *Lois Générales de l'action Des Diastases*; Librairie Scientifique A. Hermann, 1903.
 - (21) Copeland, R. A. *Enzymes: A Practical Introduction to Structure, Mechanism,*

- and *Data Analysis*, 2nd ed.; Wiley: New York, 2000.
- (22) Dixon, M.; Webb, E. C. *Enzymes*, 3. ed., (completely rev.); Longman: London, 1979.
 - (23) Kaiser, P. M. Substrate Inhibition as a Problem of Non-Linear Steady State Kinetics with Monomeric Enzymes. *J. Mol. Catal.* **1980**, 8 (4), 431–442. [https://doi.org/10.1016/0304-5102\(80\)80082-4](https://doi.org/10.1016/0304-5102(80)80082-4).
 - (24) Reed, M. C.; Lieb, A.; Nijhout, H. F. The Biological Significance of Substrate Inhibition: A Mechanism with Diverse Functions. *BioEssays* **2010**, 32 (5), 422–429. <https://doi.org/10.1002/bies.200900167>.
 - (25) Bellini, D.; Koekemoer, L.; Newman, H.; Dowson, C. G. Novel and Improved Crystal Structures of *H. influenzae*, *E. coli* and *P. aeruginosa* Penicillin-Binding Protein 3 (PBP3) and *N. gonorrhoeae* PBP2: Toward a Better Understanding of β -Lactam Target-Mediated Resistance. *J. Mol. Biol.* **2019**, 431 (18), 3501–3519. <https://doi.org/10.1016/j.jmb.2019.07.010>.
 - (26) Gasteiger, E.; Hoogland, C.; Gattiker, A.; Duvaud, S.; Wilkins, M. R.; Appel, R. D.; Bairoch, A. Protein Identification and Analysis Tools on the ExPASy Server. In *The Proteomics Protocols Handbook*; Walker, J. M., Ed.; Humana Press: Totowa, NJ, 2005; pp 571–607. <https://doi.org/10.1385/1-59259-890-0:571>.
 - (27) Wallace, A. C.; Laskowski, R. A.; Thornton, J. M. LIGPLOT: A Program to Generate Schematic Diagrams of Protein-Ligand Interactions. *Protein Eng.* **1995**, 8 (2), 127–134. <https://doi.org/10.1093/protein/8.2.127>.
 - (28) Woon, E. C. Y.; Zervosen, A.; Sauvage, E.; Simmons, K. J.; Živec, M.; Inglis, S. R.; Fishwick, C. W. G.; Gobec, S.; Charlier, P.; Luxen, A.; Schofield, C. J. Structure Guided Development of Potent Reversibly Binding Penicillin Binding Protein Inhibitors. *ACS Med. Chem. Lett.* **2011**, 2 (3), 219–223. <https://doi.org/10.1021/ml100260x>.
 - (29) Lim, D.; Strynadka, N. C. J. Structural Basis for the β Lactam Resistance of PBP2a from Methicillin-Resistant Staphylococcus Aureus. *Nat. Struct. Biol.* **2002**. <https://doi.org/10.1038/nsb858>.
 - (30) Lisa, M.-N.; Morán-Barrio, J.; Guindón, M.-F.; Vila, A. J. Probing the Role of Met221 in the Unusual Metallo- β -Lactamase GOB-18. *Inorg. Chem.* **2012**, 51 (22), 12419–12425. <https://doi.org/10.1021/ic301801h>.
 - (31) Wang, W.; Kitova, E. N.; Klassen, J. S. Nonspecific Protein–Carbohydrate Complexes Produced by Nano electrospray Ionization. Factors Influencing Their Formation and Stability. *Anal. Chem.* **2005**, 77 (10), 3060–3071. <https://doi.org/10.1021/ac048433y>.
 - (32) Goodman, J. K.; Zampronio, C. G.; Jones, A. M. E.; Hernandez-Fernaund, J. R. Updates of the In-Gel Digestion Method for Protein Analysis by Mass Spectrometry. *PROTEOMICS* **2018**, 18 (23), 1800236. <https://doi.org/10.1002/pmic.201800236>.
 - (33) Tan, A. K.; Fink, A. L. Identification of the Site of Covalent Attachment of Nafcillin, a Reversible Suicide Inhibitor of Beta-Lactamase. *Biochem. J.* **1992**, 281 (Pt 1), 191–196.
 - (34) Roach, P. L.; Baldwin, J. E.; Aplin, R. T.; Robinson, C. V.; Schofield, C. J. Peptide Mapping of the Active Site of Bacillus Cereus β -Lactamase I by the Use of High Pressure Liquid Chromatography Coupled to Electrospray Ionisation Mass Spectrometry. *J Chem Soc Chem Commun* **1994**, No. 7, 849–850. <https://doi.org/10.1039/C39940000849>.
 - (35) Han, S.; Zaniewski, R. P.; Marr, E. S.; Lacey, B. M.; Tomaras, A. P.; Evdokimov, A.; Miller, J. R.; Shanmugasundaram, V. Structural Basis for Effectiveness of Siderophore-Conjugated Monocarbams against Clinically Relevant Strains of Pseudomonas Aeruginosa. *Proc. Natl. Acad. Sci.* **2010**, 107 (51), 22002–22007. <https://doi.org/10.1073/pnas.1013092107>.
 - (36) Shapiro, A. B.; Gu, R.-F.; Gao, N.; Livchak, S.; Thresher, J. Continuous

- Fluorescence Anisotropy-Based Assay of BOCILLIN FL Penicillin Reaction with Penicillin Binding Protein 3. *Anal. Biochem.* **2013**, *439* (1), 37–43. <https://doi.org/10.1016/j.ab.2013.04.009>.
- (37) Stojanoski, V.; Chow, D.-C.; Hu, L.; Sankaran, B.; Gilbert, H. F.; Prasad, B. V. V.; Palzkill, T. A Triple Mutant in the Ω -Loop of TEM-1 β -Lactamase Changes the Substrate Profile via a Large Conformational Change and an Altered General Base for Catalysis. *J. Biol. Chem.* **2015**, *290* (16), 10382–10394. <https://doi.org/10.1074/jbc.M114.633438>.
- (38) Waley, S. G. A Spectrophotometric Assay of β -Lactamase Action on Penicillins. *Biochem. J.* **1974**, *139* (3), 789–790. <https://doi.org/10.1042/bj1390789>.
- (39) Otero, L. H.; Rojas-Altuve, A.; Llarrull, L. I.; Carrasco-López, C.; Kumarasiri, M.; Lastochkin, E.; Fishovitz, J.; Dawley, M.; Hesek, D.; Lee, M.; Johnson, J. W.; Fisher, J. F.; Chang, M.; Mobashery, S.; Hermoso, J. A. How Allosteric Control of Staphylococcus Aureus Penicillin Binding Protein 2a Enables Methicillin Resistance and Physiological Function. *Proc. Natl. Acad. Sci. U. S. A.* **2013**, *110* (42), 16808–16813. <https://doi.org/10.1073/pnas.1300118110>.
- (40) Danel, F.; Frère, J.-M.; Livermore, D. M. Evidence of Dimerisation among Class D β -Lactamases: Kinetics of OXA-14 β -Lactamase. *Biochim. Biophys. Acta BBA - Protein Struct. Mol. Enzymol.* **2001**, *1546* (1), 132–142. [https://doi.org/10.1016/S0167-4838\(01\)00133-9](https://doi.org/10.1016/S0167-4838(01)00133-9).
- (41) Page, M. G. P. The Kinetics of Non-Stoichiometric Bursts of β -Lactam Hydrolysis Catalysed by Class C β -Lactamases. *J. Biochem. (Tokyo)* **1993**, *295*, 295–304.
- (42) Waley, S. G. The Kinetics of Substrate-Induced Inactivation. *Biochem. J.* **1991**, *279* (1), 87–94. <https://doi.org/10.1042/bj2790087>.
- (43) Ghuysen, J. M.; Frère, J. M.; Leyh-Bouille, M.; Nguyen-Distèche, M.; Coyette, J. Active-Site-Serine D-Alanyl-D-Alanine-Cleaving-Peptidase-Catalysed Acyl-Transfer Reactions. Procedures for Studying the Penicillin-Binding Proteins of Bacterial Plasma Membranes. *Biochem. J.* **1986**, *235* (1), 159–165. <https://doi.org/10.1042/bj2350159>.
- (44) Waley, S. G. SS-Lactamase: Mechanism of Action. In *The Chemistry of β -Lactams*; Page, M. I., Ed.; Springer Netherlands: Dordrecht, 1992; pp 198–228. https://doi.org/10.1007/978-94-011-2928-2_6.
- (45) Chen, Y.; Bonnet, R.; Shoichet, B. K. The Acylation Mechanism of CTX-M β -Lactamase at 0.88 Å Resolution. *J. Am. Chem. Soc.* **2007**, *129* (17), 5378–5380. <https://doi.org/10.1021/ja0712064>.
- (46) Strynadka, N. C. J.; Adachi, H.; Jensen, S. E.; Johns, K.; Sielecki, A.; Betzel, C.; Sutoh, K.; James, M. N. G. Molecular Structure of the Acyl-Enzyme Intermediate in β -Lactam Hydrolysis at 1.7 Å Resolution. *Nature* **1992**, *359* (6397), 700–705. <https://doi.org/10.1038/359700a0>.
- (47) Wladkowski, B. D.; Chenoweth, S. A.; Sanders, J. N.; Krauss, M.; Stevens, W. J. Acylation of β -Lactams by Class A β -Lactamase: An *Ab Initio* Theoretical Study on the Effects of the Oxy-Anion Hole. *J. Am. Chem. Soc.* **1997**, *119* (27), 6423–6431. <https://doi.org/10.1021/ja963678g>.
- (48) Jacob, F.; Joris, B.; Lepage, S.; Dusart, J.; Frère, J. M. Role of the Conserved Amino Acids of the 'SDN' Loop (Ser130, Asp131 and Asn132) in a Class A β -Lactamase Studied by Site-Directed Mutagenesis. *Biochem. J.* **1990**, *271* (2), 399–406. <https://doi.org/10.1042/bj2710399>.
- (49) van der Linden, M. P. G.; de Haan, L.; Dideberg, O.; Keck, W. Site-Directed Mutagenesis of Proposed Active-Site Residues of Penicillin-Binding Protein 5 from Escherichia Coli. *Biochem. J.* **1994**, *303* (2), 357–362. <https://doi.org/10.1042/bj3030357>.
- (50) Sun, N.; Soya, N.; Kitova, E. N.; Klassen, J. S. Nonspecific Interactions Between Proteins and Charged Biomolecules in Electrospray Ionization Mass

- Spectrometry. *J. Am. Soc. Mass Spectrom.* **2010**, *21* (3), 472–481. <https://doi.org/10.1016/j.jasms.2009.12.002>.
- (51) Krajnc, A.; Lang, P. A.; Panduwawala, T. D.; Brem, J.; Schofield, C. J. Will Morphing Boron-Based Inhibitors Beat the β -Lactamases? *Curr. Opin. Chem. Biol.* **2019**, *50*, 101–110. <https://doi.org/10.1016/j.cbpa.2019.03.001>.
 - (52) Kuzin, A. P.; Nukaga, M.; Nukaga, Y.; Hujer, A.; Bonomo, R. A.; Knox, J. R. Inhibition of the SHV-1 β -Lactamase by Sulfones: Crystallographic Observation of Two Reaction Intermediates with Tazobactam ^{†,‡}. *Biochemistry* **2001**, *40* (6), 1861–1866. <https://doi.org/10.1021/bi0022745>.
 - (53) Hargis, J. C.; White, J. K.; Chen, Y.; Woodcock, H. L. Can Molecular Dynamics and QM/MM Solve the Penicillin Binding Protein Protonation Puzzle? *J. Chem. Inf. Model.* **2014**, *54* (5), 1412–1424. <https://doi.org/10.1021/ci5000517>.
 - (54) Stefanova, M. E.; Davies, C.; Nicholas, R. A.; Gutheil, W. G. PH, Inhibitor, and Substrate Specificity Studies on Escherichia Coli Penicillin-Binding Protein 5. *Biochim. Biophys. Acta BBA - Protein Struct. Mol. Enzymol.* **2002**, *1597* (2), 292–300. [https://doi.org/10.1016/S0167-4838\(02\)00311-4](https://doi.org/10.1016/S0167-4838(02)00311-4).
 - (55) Davies, C.; White, S. W.; Nicholas, R. A. Crystal Structure of a Deacylation-Defective Mutant of Penicillin-Binding Protein 5 at 2.3-Å Resolution. *J. Biol. Chem.* **2001**, *276* (1), 616–623. <https://doi.org/10.1074/jbc.M004471200>.
 - (56) Vandavasi, V. G.; Langan, P. S.; Weiss, K. L.; Parks, J. M.; Cooper, J. B.; Ginell, S. L.; Coates, L. Active-Site Protonation States in an Acyl-Enzyme Intermediate of a Class A β -Lactamase with a Monobactam Substrate. *Antimicrob. Agents Chemother.* **2017**, *61* (1), e01636-16, e01636-16. <https://doi.org/10.1128/AAC.01636-16>.
 - (57) Johnson, K. A. Transient-State Kinetic Analysis of Enzyme Reaction Pathways. In *The Enzymes*; Elsevier Science, 1992; Vol. XX, pp 2–60.
 - (58) Zhang, W.; Shi, Q.; Meroueh, S. O.; Vakulenko, S. B.; Mobashery, S. Catalytic Mechanism of Penicillin-Binding Protein 5 of *Escherichia Coli*. *Biochemistry* **2007**, *46* (35), 10113–10121. <https://doi.org/10.1021/bi700777x>.
 - (59) Thomas, B.; Wang, Y.; Stein, R. L. Kinetic and Mechanistic Studies of Penicillin-Binding Protein 2x from *Streptococcus Pneumoniae*. *Biochemistry* **2001**, *40* (51), 15811–15823. <https://doi.org/10.1021/bi011368r>.
 - (60) Martin, M. T.; Waley, S. G. Kinetic Characterization of the Acyl-Enzyme Mechanism for β -Lactamase I. *Biochem. J.* **1988**, *254* (3), 923–925. <https://doi.org/10.1042/bj2540923>.
 - (61) Levine, B. B. N(α -D-Penicilloyl) Amines as Univalent Hapten Inhibitors of Antibody-Dependent Allergic Reactions to Penicillin. *J. Med. Pharm. Chem.* **1962**, *5* (5), 1025–1034. <https://doi.org/10.1021/jm01240a016>.
 - (62) Edoo, Z.; Arthur, M.; Hugonnet, J.-E. Reversible Inactivation of a Peptidoglycan Transpeptidase by a β -Lactam Antibiotic Mediated by β -Lactam-Ring Recyclization in the Enzyme Active Site. *Sci. Rep.* **2017**, *7* (1), 9136. <https://doi.org/10.1038/s41598-017-09341-8>.
 - (63) Bush, K. Past and Present Perspectives on β -Lactamases. *Antimicrob. Agents Chemother.* **2018**, *62* (10), e01076-18, /aac/62/10/e01076-18.atom. <https://doi.org/10.1128/AAC.01076-18>.
 - (64) Helfand, M. S.; Totir, M. A.; Carey, M. P.; Hujer, A. M.; Bonomo, R. A.; Carey, P. R. Following the Reactions of Mechanism-Based Inhibitors with β -Lactamase by Raman Crystallography [†]. *Biochemistry* **2003**, *42* (46), 13386–13392. <https://doi.org/10.1021/bi035716w>.
 - (65) Charnas, R. L.; Fisher, J.; Knowles, J. R. Chemical Studies on the Inactivation of Escherichia Coli RTEM β -Lactamase by Clavulanic Acid. *Biochemistry* **1978**, *17* (11), 2185–2189. <https://doi.org/10.1021/bi00604a0>

Chapter 6.S. Supplemental Information for Chapter 6

6.S1 Structural Views

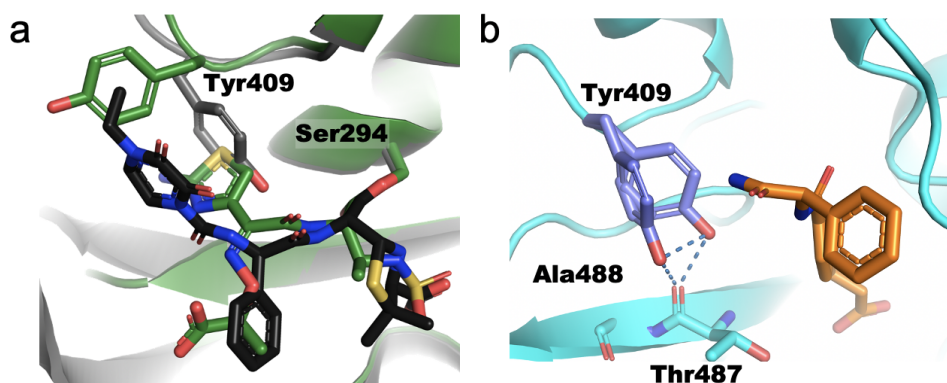


Figure 6.S1. Tyr409 conformational flexibility in PaPBP3. (a) Comparison of the PaPBP3:aztreonam (green, PDB: 3PBS¹) and PaPBP3:piperacillin (black, PDB: 6R3X²) crystal structures. Tyr409 is pointed towards the active site serine in the piperacillin-reacted structure, but faces outwards in the aztreonam-reacted structure. (b) Structure of PaPBP3:13 (see Chapter 5) which has two alternate conformations for Tyr409. Occupancies were determined by occupancy refinement in Phenix³ as 58 % and 42 % for the left and right tyrosine respectively. Both conformations form a hydrogen bond with the Thr487 backbone carbonyl. See also Figure 5.6.

6.S2 Kinetics

6.S2.1 Derivation of Equation 6.3

The substrate inhibition equation (equation 6.3) is derived by treating the scheme shown in Scheme 6.1b with the steady state method (derivation modified from ⁴).

$[ES]$ is assumed to be constant throughout the reaction. This produces three equations. The first is the equilibria of the production (right hand side) and destruction (left hand side) of $[ES]$:

$$k_{+1} \cdot [S] \cdot ([E] - [ES] - [ESS]) + k_{-2} \cdot [ESS] = (k_{-1} + k_{cat} + k_{+2} \cdot [S]) \cdot [ES] \quad (6.S1)$$

The second corresponds to the equilibrium between ES and ESS :

$$k_{+2} \cdot [S] \cdot [ES] = k_{-2} \cdot [ESS] \quad (6.S2)$$

The third is the uses the assumption that the rate (v) is limited by the k_{cat} (i.e. $k_{cat} \ll k_{+1}$):

$$v = k_{cat} \cdot [ES] \quad (6.S3)$$

These simultaneous equations can then be combined and simplified to express the rate in terms of the $[E]$, $[S]$ and the rate constants.

$$v = \frac{k_{cat} \cdot [E]}{1 + \frac{k_{-1} + k_{cat}}{k_{+1}[S]} + \frac{[S] \cdot k_{+2}}{k_{-2}}} \quad (6.S4)$$

Finally we substitute the rate constants for the constant K_M (equation 6.S5) and the substrate inhibition constant (K_{SI} , equation 6.S6) and use the expression for V_{max} (equation 6.S7) to eliminate the $[E]$ term, yielding equation 6.3:

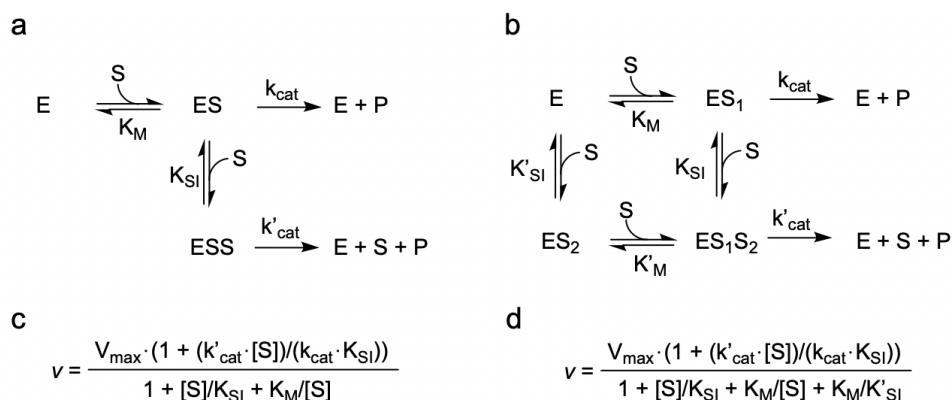
$$K_M = \frac{k_{-1} + k_{cat}}{k_{+1}} \quad (6.S5)$$

$$K_{SI} = \frac{k_{-2}}{k_{+2}} \quad (6.S6)$$

$$V_{max} = k_{cat} \cdot [E] \quad (6.S7)$$

$$v = \frac{V_{max}}{1 + \frac{K_M}{[S]} + \frac{[S]}{K_{SI}}} \quad (6.3)$$

6.S2.2 More Complex Models



Scheme 6.S1 Alternative schemes (a-b) and rate equations (c-d) for substrate inhibition. (a and c) A model that includes turnover of *ESS* but like Scheme 6.1 only permits the binding of the second nitrocefin to the *ES* complex; (b and d) a model in which two binding sites can each independently bind a molecule of substrate (in either order), with turnover permitted from the doubly- or singly-reacted species. Schemes and rate equations modified from Yoshino *et al.*⁵.

6.S3 Tryptic Digest Mass Spectrometry

6.S3.1 Sample Preparation Methods

6.S3.1.1 Protocol I

Filter-Aided Sample Preparation⁶

The reaction with nitrocefin was conducted at room temperature (Trial **A** buffer: 500 mM NaCl, 10mM sodium phosphate, pH 8, Trial **B** buffer: 300mM ammonium bicarbonate (ABC)) in a volume of 100 μ l (Trial **A**) or 50 μ l (Trial **B**), and then terminated by the addition of 8 M urea (400 μ l). The sample was added to a protein spin column (0.5 mL, 10 kDa molecular weight cutoff, Amicon Ultra) and centrifuged at 8000 x g for 20 minutes. The sample was then buffer exchanged into 50mM ABC by the sequential addition of ABC (400 μ l) then centrifugation to reduce the volume, three times in total. Trypsin (sequencing grade, Promega) was then added and digestion allowed to proceed at room temperature: Trial **A**: 2 μ g trypsin added, digestion overnight; Trial **B**: 1 μ g trypsin added, digestion for 4 hours. After the digestion, the peptides were eluted by centrifugation through a spin column (8000 x

g, 20 minutes), then the spin column was additionally washed with 400 µl of water and centrifuged (8000 x g, 20 minutes). Both the elution and the washes were concentrated by SpeedyVac vacuum concentrator (30 °C, Thermofisher Scientific) until dry, then resuspended in a solution of 2% (v/v) acetonitrile, 0.1% (v/v) trifluoroacetic acid (TFA) in water.

C₁₈ StageTip

To ensure sample purity before MS, the sample was purified by C₁₈ fractionation in a “StageTip” (a pipette tip fitted with a filter in an adapter above an eppendorf tube). The StageTip was conditioned by applying the following solutions in order (each 50 µl) and then centrifuging at 2000 rpm: methanol then acetonitrile, then a solution of 2 % (v/v) acetonitrile, 0.1 % (v/v) TFA in water. The sample (150 µl) was then loaded onto the StageTip and centrifuged (15 minutes, 2000 rpm), then washed with first 1 % (v/v) TFA in ethyl acetate and centrifuged (50 µl, 4 minutes, 2000 rpm) then 2 % (v/v) acetonitrile, 0.1% (v/v) TFA in water and centrifuged (50 µl, 4 minutes, 2000 rpm). The peptides were then eluted in 80 % (v/v) acetonitrile in water before being concentrated to a dry powder by vacuum concentration. Peptides were stored at -20 °C, until they were ready to be run on the mass spectrometer (6.S3.2). Before analysis they were resuspended in 2 % (v/v) acetonitrile, 0.1 % (v/v) TFA in water (with 10 minutes ultrasonication to ensure solvation).

6.S3.1.2 Protocol II

Due to concerns about the long time taken to conduct the washing steps in Protocol I and III, Protocol II was designed to have minimal washing but required the sample to be pure to avoid contaminating the MS chromatography columns or machine itself.

To remove sodium chloride from the storage buffer of the protein, the protein was first dialysed into 300mM ammonium acetate (pH 8) and the nitrocefin was added (see Table 6.2 for reaction conditions). After heat shock (5 minutes, 99 °C), the sample was quickly cooled on ice, then trypsin was added (Trial **C**: 1 µg; Trial **D**: 0.25 µg;) and peptide digestion proceeded at room temperature for 4 hours. The sample was then concentrated by vacuum concentration to a dry mass, then stored at -20 °C until the sample was ready to be analysed (6.S3.2), at which time it was resuspended in 2 % (v/v) acetonitrile, 0.1 % (v/v) TFA in water (Trial **C**) or water (Trial **D**) and sonicated for 10 minutes.

6.S3.1.3 Protocol III (in-gel digest)

The reaction with nitrocefin was carried out at room temperature (50 µl reaction volume, buffer: 500 mM NaCl, 10 mM sodium phosphate, pH 8), then the reaction was terminated by unfolding the protein in SDS (8 % (w/v)). The sample was loaded onto a precast TruPAGE polyacrylamide gel (Merck) and run at 150 V for 40 minutes in 25 mM Tris pH 8.3, 190 mM glycine and 0.1% (w/v) SDS. The gel was stained for 10 minutes with coomassie dye (Instant Blue, Exedeeon) to allow the bands to be visualised. The protein-containing band was cut out of the gel and then cut into 4 mm slices and washed with a destaining buffer (50 % (v/v) ethanol, 50mM ABC, 3 x 40 µl) until the colour was lost. The gel fragments were dehydrated in ethanol for 5 minutes whilst shaking then trypsin (50 ng in 30 µl of 50 mM ABC) was added and the sample was digested for 4 hours at room temperature. After digestion, the buffer around the gel was collected and the gel fragments were washed with 3 x 20 µl of 25 % (v/v) acetonitrile, 5 % (v/v) formic acid in water with sonication (10 minutes) to extract all peptides. The peptide extractions were concentrated by vacuum concentration and stored at -20 °C until they were ready to be run on the mass spectrometer (6.S3.2). Before analysis, they were resuspended in 2 % (v/v) acetonitrile, 0.1 % (v/v) TFA in water and ultrasonicated for 10 minutes.

6.S3.2 Proteomic Mass Spectrometry Methods

An analysis was performed by LC-MS/MS on a Ultimate 3000-RSLCnano system (Dionex) coupled to an Orbitrap-Fusion Mass Spectrometer (Thermo-Scientific) as previously described ⁷. Data was analysed by MaxQuant software ⁸ against the known sample sequence and the *E. coli* database. Peptide sequences were assigned to the MS/MS spectra. Acylation by the nitrocefin (516.04 ± 0.5 Da, serine residues), methionine oxidation (15.99 ± 0.5 Da, methionine residues) and acetylation (42.01 ± 0.5 Da, peptide N-terminus) were treated as a variable modifications. Data was viewed in Scaffold4 (Proteome Software).

6.S4 Protein Crystallography Methods

Crystallography was carried out by D. Bellini.

Crystallisation and structure solution of nitrocefin:PaPBP3 adducts. Diffraction quality crystals of PaPBP3_{wt} and its PaPBP3_{Y409A} were obtained at 294 K using the hanging drop vapour diffusion method from mixing equal volumes of protein with a precipitant solution made up of 25%(w/v) polyethylene glycol 3350, 0.1M Bis-Tris propane, 1 % (w/v) protamine sulphate, pH 8⁹. Crystals were cryoprotected with 20 % (v/v) glycerol prior to flash-cooling in liquid nitrogen. Nitrocefin-protein complexes were obtained by soaking crystals with 10 mM compound for 60 minutes. Diffraction data were collected on Diamond beamlines I03 and I04. Structures were phased using molecular replacement with MrBump¹⁰. All data were processed using Dials¹¹. Manual building and ligand fitting was performed with COOT¹². Structures were refined with REFMAC5¹³ and validated with MolProb¹⁴. The structures are available online: PDB codes 6HR6 (nitrocefin-reacted PaPBP3_{wt}) and 6HR9 (nitrocefin-reacted PaPBP3_{Y409A}).

6.S5 References

- (1) Han, S.; Zaniwski, R. P.; Marr, E. S.; Lacey, B. M.; Tomaras, A. P.; Evdokimov, A.; Miller, J. R.; Shanmugasundaram, V. Structural Basis for Effectiveness of Siderophore-Conjugated Monocarbams against Clinically Relevant Strains of *Pseudomonas aeruginosa*. *Proc. Natl. Acad. Sci.* **2010**, *107* (51), 22002–22007. <https://doi.org/10.1073/pnas.1013092107>.
- (2) Bellini, D.; Koekemoer, L.; Newman, H.; Dowson, C. G. Novel and Improved Crystal Structures of *H. influenzae*, *E. coli* and *P. aeruginosa* Penicillin-Binding Protein 3 (PBP3) and *N. gonorrhoeae* PBP2: Toward a Better Understanding of β -Lactam Target-Mediated Resistance. *J. Mol. Biol.* **2019**, *431* (18), 3501–3519. <https://doi.org/10.1016/j.jmb.2019.07.010>.
- (3) Adams, P. D.; Afonine, P. V.; Bunkóczi, G.; Chen, V. B.; Davis, I. W.; Echols, N.; Headd, J. J.; Hung, L.-W.; Kapral, G. J.; Grosse-Kunstleve, R. W.; McCoy, A. J.; Moriarty, N. W.; Oeffner, R.; Read, R. J.; Richardson, D. C.; Richardson, J. S.; Terwilliger, T. C.; Zwart, P. H. PHENIX: A Comprehensive Python-Based System for Macromolecular Structure Solution. *Acta Crystallogr. D Biol. Crystallogr.* **2010**, *66* (2), 213–221. <https://doi.org/10.1107/S0907444909052925>.
- (4) Dixon, M.; Webb, E. C. *Enzymes*, 3. ed., (completely rev.); Longman: London, 1979.
- (5) Yoshino, M.; Murakami, K. Analysis of the Substrate Inhibition of Complete and Partial Types. *SpringerPlus* **2015**, *4* (1), 292. <https://doi.org/10.1186/s40064-015-1082-8>.
- (6) Wiśniewski, J. R.; Zougman, A.; Nagaraj, N.; Mann, M. Universal Sample Preparation Method for Proteome Analysis. *Nat. Methods* **2009**, *6* (5), 359–362. <https://doi.org/10.1038/nmeth.1322>.
- (7) Goodman, J. K.; Zamprano, C. G.; Jones, A. M. E.; Hernandez-Fernaund, J. R. Updates of the In-Gel Digestion Method for Protein Analysis by Mass Spectrometry. *PROTEOMICS* **2018**, *18* (23), 1800236. <https://doi.org/10.1002/pmic.201800236>.
- (8) Tyanova, S.; Temu, T.; Cox, J. The MaxQuant Computational Platform for Mass Spectrometry-Based Shotgun Proteomics. *Nat. Protoc.* **2016**, *11* (12),

- 2301–2319. <https://doi.org/10.1038/nprot.2016.136>.
- (9) Sainsbury, S.; Bird, L.; Rao, V.; Shepherd, S. M.; Stuart, D. I.; Hunter, W. N.; Owens, R. J.; Ren, J. Crystal Structures of Penicillin-Binding Protein 3 from *Pseudomonas aeruginosa*: Comparison of Native and Antibiotic-Bound Forms. *J. Mol. Biol.* **2011**, *405* (1), 173–184. <https://doi.org/10.1016/j.jmb.2010.10.024>.
 - (10) Keegan, R. M.; Winn, M. D. *MrBUMP*: An Automated Pipeline for Molecular Replacement. *Acta Crystallogr. D Biol. Crystallogr.* **2008**, *64* (1), 119–124. <https://doi.org/10.1107/S0907444907037195>.
 - (11) Winter, G.; Waterman, D. G.; Parkhurst, J. M.; Brewster, A. S.; Gildea, R. J.; Gerstel, M.; Fuentes-Montero, L.; Vollmar, M.; Michels-Clark, T.; Young, I. D.; Sauter, N. K.; Evans, G. *DIALS*: Implementation and Evaluation of a New Integration Package. *Acta Crystallogr. Sect. Struct. Biol.* **2018**, *74* (2), 85–97. <https://doi.org/10.1107/S2059798317017235>.
 - (12) Emsley, P.; Lohkamp, B.; Scott, W. G.; Cowtan, K. Features and Development of *Coot*. *Acta Crystallogr. D Biol. Crystallogr.* **2010**, *66* (4), 486–501. <https://doi.org/10.1107/S0907444910007493>.
 - (13) Vagin, A. A.; Steiner, R. A.; Lebedev, A. A.; Potterton, L.; McNicholas, S.; Long, F.; Murshudov, G. N. *REFMAC 5* Dictionary: Organization of Prior Chemical Knowledge and Guidelines for Its Use. *Acta Crystallogr. D Biol. Crystallogr.* **2004**, *60* (12), 2184–2195. <https://doi.org/10.1107/S0907444904023510>.
 - (14) Williams, C. J.; Headd, J. J.; Moriarty, N. W.; Prisant, M. G.; Videau, L. L.; Deis, L. N.; Verma, V.; Keedy, D. A.; Hintze, B. J.; Chen, V. B.; Jain, S.; Lewis, S. M.; Arendall, W. B.; Snoeyink, J.; Adams, P. D.; Lovell, S. C.; Richardson, J. S.; Richardson, D. C. MolProbity: More and Better Reference Data for Improved All-Atom Structure Validation: PROTEIN SCIENCE.ORG. *Protein Sci.* **2018**, *27* (1), 293–315. <https://doi.org/10.1002/pro.3330>.

Chapter 7. Concluding Remarks

Antimicrobial resistance will be one of the greatest healthcare challenges of the coming decades and loss of these clinical fire extinguishers could lead to the deaths of millions. But tackling this challenge is made more difficult by intertwining socio-economic and scientific hurdles as well as the need for broad engagement with the necessary solutions. The intractability of the problem and a lack of profitability of antimicrobial research has led to decades of neglect that only recently is being properly addressed. As progressive resistance makes current antimicrobials ineffective, new therapies must be discovered and approved to replace them. The challenges of antimicrobial resistance are perennial and will necessitate continued and ongoing research. Originality in the mode of action of new inhibitors is desirable, and new methods, including those discussed here, are needed in the search for this novelty.

The case of β -lactams is emblematic of the crisis in antimicrobial discovery: PBPs are a well-established and effective target, but no novel inhibitors have been approved since aztreonam in the 1980s. This is not without attempts; over the last 20 years, numerous academic groups and some pharmaceutical companies have published research reporting non- β -lactam PBP inhibitors but none of these compounds even approach the efficacy of β -lactams. This perhaps indicates how challenging this task is and once again underlines how well β -lactams are adapted for PBP inhibition. Boron based inhibitors (e.g. vaborbactam) have proven their efficacy against β -lactamases, but PBP-targeting boronates have yet to be realised as antimicrobials, for reasons that remain elusive.

Our fragment screen of serine covalent inhibitors found for the first time that boronates could bind to a high molecular mass PBP in di- or tri-covalent binding modes (depending on the warhead). Whilst the present on-target affinity is modest, further optimisation of derivatives (facilitated by 10 new structures of PBP:boronate complexes) may allow for improved antimicrobial activity. Utilisation of novel assays which employ natural substrates may allow better assessment of the ability of the compounds to inhibit the physiological functions of PBPs. This could lead to compounds with better in vitro efficacy.

The proposed role of boronates as transition state inhibitors of the reactions of PBPs with their substrates may be extended to explain the novel observation of two molecules of nitrocefin in the active site. Which I hypothesise may occur as the result of the transfer of the nitrocefin adduct from one active site serine to another. Whatever the mechanism, observation of the two nitrocefin molecules in the active site of mutant PBP3 is interesting and development of the observation could yield new inhibitors which exploit this phenomenon.

It is possible that non- β -lactam inhibitors will catalyse the further propagation of target-mediated resistance as β -lactamases become ineffective. In PBPs from gram-pathogens, the mechanisms underlying target-mediated resistance are not well understood but the frequent occurrence of clinical mutations in flexible loops adjacent to the active site suggests the loops have a role to play. Boronate compounds complexed to PBP3 show that signals can be transmitted between the active site and loops not in direct contact with the compound, perhaps by a network of interacting amino acids.

Finally this thesis has explored two tools to aid in drug discovery. A robotic liquid handling system has been utilised for antimicrobial screens which will find use in routine screening, aiding drug discovery. Attempts to characterise the interactions of PBP3 using a surface plasmon resonance, which had previously never been reported, were ultimately unsuccessful. One of the problems preventing development of the system was a lack of high affinity, reversibly binding compounds to act as a positive control. The outlook for finding such inhibitors is positive but further understanding of the protein and of inhibitors is required.

Appendix: Publications by the Author

Bellini D*, Koekemoer L*, [Newman H](#)*, Dowson CG. Novel and Improved Crystal Structures of H. influenzae, E. coli and P. aeruginosa Penicillin-Binding Protein 3 (PBP3) and N. gonorrhoeae PBP2: Toward a Better Understanding of β -Lactam Target-Mediated Resistance. J Mol Biol. 2019 Aug 23;431(18):3501–19. **Joint first authors*

This work formed the basis for Chapter 4 and is summarised in section 4.1.

Kidd SL, Fowler E, Reinhardt T, Compton T, Mateu N, [Newman H](#), et al. Demonstration of the utility of DOS-derived fragment libraries for rapid hit derivatisation in a multidirectional fashion. Chem Sci. 2020 Oct 14;11(39):10792–801.

The author contributed structural activity relationship input to this work, discussed in section 1.3.3 and published two crystal structures (PDB: 6Y6U and 6Y6Z)

[Newman H](#), Krajnc A, Bellini D, Eyermann CJ, Boyle GA, Paterson NG, et al. High-Throughput Crystallography Reveals Boron Containing Inhibitors of a Penicillin Binding Protein with Di- and Tri-covalent Binding Modes. J Med Chem. *Accepted.*

Chapter 5 was modified and submitted for publication: it was accepted, reviewed, revised and is currently returned to the reviewers for their approval (as of 11th June 2021). As part of this, 10 crystal structures (5.S2) were published on the PDB.

As this is not yet publicly available, the supporting information is also included.